

## **Appendix A**

### **Materials Degradation Modes and their Prediction**

"He that will not apply new remedies must expect new evils; for time is a great innovator,"  
from *Essays II Of Innovations*, Sir Francis Bacon (1561-1626)

"No sooner knew the reason, but they sought the remedy," from *As You Like It*, Shake-  
speare (1564-1616)



## Contents

	<u>Page</u>
A.1 Introduction .....	A-1
A.2 Materials of Construction .....	A-2
A.3 Corrosion Basics .....	A-7
A.4 Description of Degradation Modes and their Predictability in LWRs .....	A-13
A.5 References .....	A-46

## List of Tables

	<u>Page</u>
Table A.1 Compositions of Carbon & Low Alloy Steels Used in LWR Pressure Vessels & Piping (wt. %) .....	2
Table A. 2 Compositions of Some Stainless Steels Commonly Used in LWRs (wt. %). ....	3
Table A. 3 Compositions of Cast Stainless Steels used in LWRs (wt. %) .....	3
Table A. 4 Compositions of Nickel base alloys used in LWRs (wt. %). ....	5
Table A. 5 Expected Alloy/Degradation Mode Combinations for PWRs .....	6

## List of Figures

	<u>Page</u>
Figure A.1 Pourbaix diagram for the iron- water system at 25°C, Activities of dissolved species of 10 <sup>-6</sup> gm-equivalents/L [7].....	8
Figure A.2 Superimposition of Cr(OH) <sub>3</sub> stability region onto the Pourbaix diagram for the iron- water system at 25°C and activities of dissolved species of 10 <sup>-6</sup> gm-equivalents/L. [4; adapted from 7].....	9
Figure A.3. Oxidation and reduction reactions occurring on adjacent areas of surface [4].....	10
Figure A.4 Schematic “Evans” diagram indicating the equilibration of the oxidation and reduction rates for the dissolution of zinc in 1N HCl solution, and the associated “corrosion current, ( <i>i</i> <sub>corr</sub> )” and “corrosion potential, ( <i>E</i> <sub>corr</sub> )”. [4].....	11
Figure A.5 Schematic oxidation current density vs. electrode potential diagrams, indicating, for the oxidation reactions, transitions from activation control, to onset of passivation, to oxide break down due to transpassivity or pitting. [4].....	12
Figure A.6 Superposition of the reduction kinetics for dissolved oxygen on the metal oxidation rates from Figure A.5. In this case the reduction kinetics may be limited by the supply of oxygen to the reacting surface. [4] .....	13
Figure A.7 Corrosion of mild steel and solubility of magnetite at 300°C showing corrosion rate laws [9].....	14
Figure A.8. Relationship between the corrosion rate of carbon and low alloy steels in various acidified boric acid solutions as a function of temperature. [15] .....	18
Figure A.9. Schematic of two-layer oxide structure on carbon steel in high temperature water. [16].....	19
Figure A.10. Effect of temperature on the flow accelerated corrosion rate of carbon steel in deoxygenated ammoniated water. [20].....	21
Figure A.11. Flow-accelerated corrosion data for condensate and moisturizer separator reheater drain systems in four BWR plants as a function of the local dissolved oxygen contents [Appendix B.10].....	21
Figure A.12. Schematic of crevice in aerated solution, indicating the separation of the metal oxidation and oxygen reduction sites, and the consequent changes in pH and anionic concentrations.....	23
Figure A.13. Schematic of crevice formed at PWR steam generator tube/carbon steel tube-support, together with the phenomena that give rise to the localized corrosion. [23] .....	24
Figure A.14. Pitting, shown by the solid lines, and corrosion potential, ( <i>E</i> <sub>c</sub> ), shown by the dashed lines, for Alloy 600 in water containing chloride anions as a function of temperature. [26, 27].....	26

Figure A.15. Observed and theoretical crack propagation rate vs. crack tip strain rate relationships for sensitized 304 stainless steel in oxygenated water at 288°C. ....	29
Figure A.16. Conjoint material, stress and environment requirements for stress corrosion cracking [36]. ....	29
Figure A.17. IGSCC in a 400 mm(16 ins.) diameter welded Type 304 pipe exposed to oxygenated water at 288°C. Note propagation adjacent to the weld heat affected zone, in a region associated with maximum grain boundary chromium depletion and weld residual tensile stress [37] .....	31
Figure A.18. Schematic of the crack enclave and the relevant phenomena associated with the slip oxidation mechanism of crack advance. ....	32
Figure A.19. Observed and predicted dependency between crack propagation rate for sensitized stainless steel and corrosion potential. [34,35] .....	32
Figure A.20. Predicted response of defected piping for defined changes in water chemistry in BWR plant. [35] .....	34
Figure A.21. Effect of oxygen and chloride concentration on the SCC of austenitic stainless steels in water 250-350°C, together with the oxygen/chloride ranges in BWR and PWR environments. [38] .....	35
Figure A.22. Regions in the PWR Primary Reactor Coolant System where PWSCC of nickel base alloys have been observed. ....	36
Figure A.23. Schematic diagram illustrating the locus of an axial PWSCC crack front in the Alloy 82/182 weld between dissimilar alloy carbon and stainless steel components. ....	36
Figure A.24. Calculated change in crack depth in irradiated stainless steel as a function of fluence (e.g., time) due to specified changes in residual stress and degree of grain boundary sensitization. [see Appendix B.2] .....	38
Figure A.25. (a) Predicted [45] and observed [46] strain amplitude versus cycles to crack initiation relationships for unnotched carbon steel in 288°C, 8 ppm oxygenated water with strain applied at different rates. (b) Predicted [45] and observed [46,47] strain amplitude versus cycles to crack initiation relationships for unnotched carbon and low alloy steels in 288°C water, under the worst combination of material and environmental conditions. ....	42

## A.1 Introduction

In order to satisfy the objective of this Proactive Material Degradation Assessment it is necessary that, as Sir Francis Bacon and Shakespeare recognized, the various modes of degradation (e.g., stress corrosion cracking, crevice corrosion, thermal embrittlement, etc.) be defined and, in order to be proactive, there should be quantitative life-prediction capabilities for each of them. Some of the challenges to having an adequate prediction capability were discussed in Section 2.4, with examples taken specifically for the case of stress corrosion cracking. In this Appendix, a wider range of materials degradation modes are described, together with a brief description of the mechanisms and system parameters that control the extent of degradation. This information serves as an introduction to more extensive discussions in the topical reports given in Appendix B. These latter discussions outline the dependency of the various degradation modes on specific system parameters, and thereby lay the background behind the panelists' susceptibility, confidence, and knowledge scoring of degradation in the various Light Water Reactor (LWR) systems.

Since many of the degradation modes involve corrosion, a brief primer is included in Appendix A on corrosion basics so as to orient the reader to phraseology and concepts. The materials and degradation modes considered in the following sections in Appendix A are:

- A.2 Materials of Construction
- A.3 Corrosion Basics
- A.4 Description of Degradation Modes and their Predictability in LWRs
  - A.4.1 "Uniform" Corrosion
    - General Corrosion
    - Boric Acid Corrosion
    - Flow-Accelerated Corrosion and Erosion-Corrosion
  - A.4.2 Localized Corrosion
    - Crevice Corrosion
    - Pitting Corrosion
    - Galvanic Corrosion
    - Microbiologically-influenced Corrosion (MIC)
    - Environmentally Assisted Cracking
      - Intergranular Stress Corrosion Cracking (IGSCC)
      - Transgranular Stress Corrosion Cracking (TGSCC)
      - Primary Water Stress Corrosion Cracking (PWSCC)
      - Irradiation Assisted Stress Corrosion Cracking (IASCC)
      - Low-temperature Crack Propagation (LTCP)
  - A.4.3 Under-clad Cracking and Clad Disbonding
  - A.4.4 Fatigue
  - A.4.5 Loss of Fracture Resistance
    - Irradiation Effects
      - Neutron Embrittlement
      - Void Swelling Effects
    - Thermal Aging

## A.2 Materials of Construction

As detailed in Tables A.1-A.4, which are excerpted from the appropriate sections in Appendix B, there is a large variety of metallic materials used in the fabrication of PWR and BWR pressure boundary and internal components that include the following combinations:

1. *Reactor Coolant Piping and Fittings* – carbon steel, low-alloy steel, cast and wrought stainless steels and various weld materials depending on the parent material used.
2. *Reactor Pressure Vessel and PWR Pressurizer Vessel* - low-alloy steel, stainless steel cladding, wrought nickel-base penetrations and various weld materials.
3. *Reactor Internals* – cast and wrought austenitic stainless steels, nickel-base alloys, and their associated weld metals.
4. *PWR Steam Generator* – low alloy and carbon steels, stainless steel cladding, nickel-base alloys, and various weld materials.
5. *Pumps* – cast and wrought austenitic stainless steels for pressure boundary materials; various high alloy steels for bolting and austenitic or martensitic stainless steels for pump shafts and other internal components.

**Table A.1 Compositions of Carbon & Low Alloy Steels Used in LWR Pressure Vessels and Piping (wt. %)**

	A533-B	A508-2	A508-3	A333-6	A516
<b>Carbon (max)</b>	0.25	0.27	0.25	0.30	0.28
<b>Manganese</b>	1.15 – 1.50	0.5 – 1.00	1.20 – 1.50	0.29- 1.06	0.60 – 1.20
<b>Phosphorus (max)</b>	0.035	0.025	0.025	0.025	0.035
<b>Sulfur (max)</b>	0.035	0.025	0.025	0.025	0.035
<b>Silicon</b>	0.15 – 0.40	0.15 – 0.40	0.15 – 0.40	≤0.10	0.15 – 0.40
<b>Nickel</b>	0.40 – 0.70	0.50 – 1.00	0.40 – 1.00		
<b>Chromium</b>		0.25 – 0.45	≤0.25		
<b>Molybdenum</b>	0.45 – 0.60	0.55 – 0.70	0.45 – 0.60		
<b>Vanadium</b>		≤0.05	≤0.05		



**Table A. 2 Compositions of Some Stainless Steels Commonly Used in LWRs (wt. %)**

	Type 304L	Type 316	Type 321	Type 347	Type 308L	Type 309L	A-286	17-4PH
Carbon (max)	0.03	0.08	0.08	0.08	0.03	0.03	0.08	0.07
Manganese(max)	2.0	2.0	2.0	2.0	2.0	2.0	2.0	1.00
Silicon (max)	1.0	1.0	1.0	1.0	1.0	1.0	1.0	1.00
Chromium	18-20	16-18	17-19	17-19	19-21	22-24	12-15	15-17.5
Nickel	8-12	10-14	9-12	9-13	10-12	12-15	24-27	3.0-5.0
Molybdenum		2.0-3.0					1.00-1.50	
Phosphorus (max)	0.045	0.045	0.045	0.045	0.045	0.045	0.040	0.040
Sulfur (max)	0.030	0.030	0.030	0.030	0.030	0.030	0.030	0.030
Other elements			Ti >5C	Nb+Ta >10C			Ti 1.55-2.00 Al ≤0.35 V 0.10-0.50	Cu 3.0-5.0 Nb+Ta 0.15-0.45

**Table A. 3 Compositions of Cast Stainless Steels used in LWRs (wt. %)**

	CF-3	CF-3A	CF-8	CF-8A	CF-8M
Carbon (max)	0.03	0.03	0.08	0.08	0.08
Manganese (max)	1.50	1.50	1.50	1.50	1.50
Silicon (max)	2.00	2.00	2.00	2.00	1.50
Sulfur (max)	0.040	0.040	0.040	0.040	0.040
Phosphorus (max)	0.040	0.040	0.040	0.040	0.040
Chromium	17.0-21.0	17.0-21.0	18.0-21.0	18.0-21.0	18.0-21.0
Nickel	8.0-12.0	8.0-12.0	8.0-11.0	8.0-11.0	9.0-12.0
Molybdenum (max)	0.50	0.50	0.50	0.50	2.0-3.0

All of the above materials are potentially susceptible to one or more degradation modes, depending upon the combinations of material and service conditions. Some of these combinations for PWRs are indicated in Table A.5 as an example of the range of degradation modes and how their emergence changes between one system and another. For example, alloys, which may potentially degrade by a given mode in a given system, are shaded in Table A.5 (with no judgment being made as to the extent of the degradation). The environmental conditions shown in the Table have been chosen to represent the range of chemistry and temperature conditions in various PWR systems (e.g., Reactor Coolant System, both primary and secondary; Emergency Core Coolant System (ECCS); Service Water; etc). Although stress corrosion (SCC) and fatigue (FAT) are possible for the majority of the chosen environment/material combinations, other degradation modes will change with different system conditions. For instance, microbiologically-induced-corrosion (MIC) will not be an issue in the higher temperature borated RCS, since the microbes cannot survive under these conditions, but MIC may be an issue in the lower temperature systems, such as parts of ECCS, and especially in those reactor systems that are not borated, such as the component coolant and service water systems. Ranges in temperature are shown in some of the system examples, and this will give rise to a range in degradation susceptibilities within that system since most of the degradation modes are temperature activated to different degrees. It is the objective of the PMDA project to assess the extent to which these susceptibilities may vary due to temperature, material condition, etc. for each component within the various subsystems (and to assess whether there is sufficient knowledge to predict and mitigate this degradation). It should also be noted in Table A.5 that many of the alloy/degradation mode combinations are shown blank; indicating that although there may be a possibility of degradation, its likelihood of occurrence is small. The rationale for such judgments is either the fact that that particular combination (marked with an X) does not occur (e.g., there are no Alloy 82/182 welds in the highly irradiated core region, so irradiation induced creep is unlikely), or there are mechanistic reasons to judge that the likelihood of degradation is low; this latter aspect is covered in Section A.4 of this Appendix.

**Table A. 4 Compositions of Nickel base alloys used in LWRs (wt. %)**

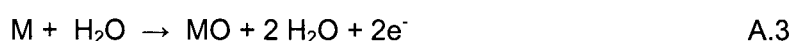
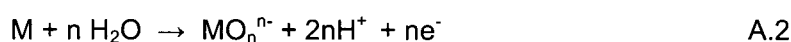
	<b>Alloy 600</b>	<b>Alloy 182</b>	<b>Alloy 82</b>	<b>Alloy 690</b>	<b>Alloy 152</b>	<b>Alloy 52</b>	<b>Alloy 800</b>	<b>Alloy X750</b>	<b>Alloy 718</b>
<b>Nickel</b>	>72.0	Bal.	Bal.	>58.0	Bal.	Bal.	30-35	>70.0	50-55
<b>Chromium</b>	14-17	13-17	18-22	28-31	28-31.5	28-31.5	19-23	14-17	17-21
<b>Iron</b>	6-10	≤10.0	≤3.00	7-11	8-12	8-12	>39.5	5-9	Bal.
<b>Titanium</b>		≤1.0	≤0.75		≤0.50	≤1.0	0.15-0.60	2.25-2.75	0.65-1.15
<b>Aluminum</b>						≤1.10	0.15-0.60	0.4-1.0	0.2-0.8
<b>Niobium plus Tantalum</b>		1.0-2.5	2.0-3.0		1.2-2.2	≤0.10		0.7-1.2	4.75-5.50
<b>Molybdenum</b>					≤0.50	≤0.05			2.8-3.3
<b>Carbon (max)</b>	0.05	0.10	0.10	0.04	0.045	0.040	0.10	0.08	0.08
<b>Manganese</b>	≤1.0	5.0-9.5	2.5-3.5	≤0.50	≤5.0	≤1.0	≤1.50	≤1.0	≤0.35
<b>Sulfur</b>	≤0.015	≤0.015	≤0.015	≤0.015	≤0.008	≤0.008	≤0.015	≤0.010	≤0.010
<b>Phosphorus</b>		≤0.030	≤0.030		≤0.020	≤0.020			
<b>Silicon</b>	≤0.5	≤1.0	≤0.50	≤0.50	≤0.65	≤0.50	≤1.0	≤0.5	≤0.35
<b>Copper</b>	≤0.5	≤0.50	≤0.50	≤0.5	≤0.50	≤0.30	≤0.75	≤0.5	≤0.30
<b>Cobalt</b>	≤0.10	≤0.12	≤0.10	≤0.10	≤0.020	≤0.020			

**Table A. 5 Expected Alloy/Degradation Mode Combinations for PWRs** (GC=General Corrosion; BAC=Boric Acid Corrosion; FAC= Flow Accelerated Corrosion; CREV= Crevice Corrosion; PIT=Pitting; GALV=Galvanic Attack; SCC=Stress Corrosion Cracking; MIC= Microbiologically-Induced Corrosion; FAT= Fatigue)

Alloy System	"General Corrosion"			"Localized Corrosion"					"Mechanical"			
	GC	BAC	FAC	CREV	PIT	GALV	SCC	MIC	FAT	Therm. Emb.	Irrad Emb	Irrad Creep
<b>Reactor Coolant System, 550-650 F, PWR Primary and Secondary Water</b>												
Low Alloy & Carbon Steel												
Wrought Stainless Steel, 304/316												
Stainless Steel Welds 308/309												
Cast Stainless Steel CF8/CF8M											X	X
Alloy 600 Nozzles, Safe-ends, SGTubes											X	X
Alloy 82/182 Welds											X	X
<b>Main Feedwater, 250-450F, Demin Water, pH 9-10</b>												
Carbon Steel Piping												
Alloy 690 Forging												
<b>Main Steam Line, 445-530F, Steam</b>												
Low Alloy & Carbon Steel												
<b>CVCS, 115-290F, PWR Primary Water</b>												
Low Alloy Steel Bolts (assume leakage)												
Wrought Stainless Steel, 304/316												
Stainless Steel Welds 308/309												
Cast Stainless Steel CF8/CF8M												
<b>Emergency Core Cooling System, 100-150 F, Borated Demin Water</b>												
Wrought Stainless Steel, 304/316												
Stainless Steel Welds 308/309												
Cast Stainless Steel CF8/CF8M												
<b>Component Cooling Water, 105-130F, Treated Water</b>												
Low Alloy & Carbon-Steel Piping / Fittings												
<b>Service Water System, 100F, Pond Water</b>												
Low Alloy & Carbon-Steel Piping / Fittings												
Wrought Stainless Steel, 304/316 HX tubing												
Stainless Steel Welds 308/309												
Copper base alloys HX tubing												

### A.3 Corrosion Basics

Corrosion of metals in aqueous environments involves various electrochemical and chemical reactions at, or close to, the material/environment interface. For instance simplified reaction equations may be formulated for the electrochemical oxidation of a metal atom to form either (a) a solvated metal cation (Equation A.1) or (b) in alkaline solutions, a metal anion (Equation A.2); or (c) an oxide may be formed directly on the surface (Equation A.3) by electron transfer. Alternatively, the oxide may also form adjacent to, and then deposit onto, the surface via a precipitation reaction (Equation A.4).



Extensive research and development over many decades has focused on the kinetics and thermodynamics of such reactions since they are central to the development of corrosion mitigation actions used in numerous industries; such actions include, for instance, anodic and cathodic protection, development of various inhibitors and paint schemes, alloy development, water chemistry control, etc. Discussion of such developments and the science behind them is outside the scope of this present discussion, and the reader is directed towards appropriate textbooks, such as References 1-6, for such details.

Under equilibrium conditions the change in Gibbs free energy,  $\Delta G$ , associated with those surface reactions involving electron transfer (Equations A.1-A.3) will have a related electrode potential,  $E$ , at that surface (Equation A.5) with the value of that potential being a function of temperature, metal cation or anion activity (for Equations A.1 and A.2) and pH (for Equations A.2 and A.3).

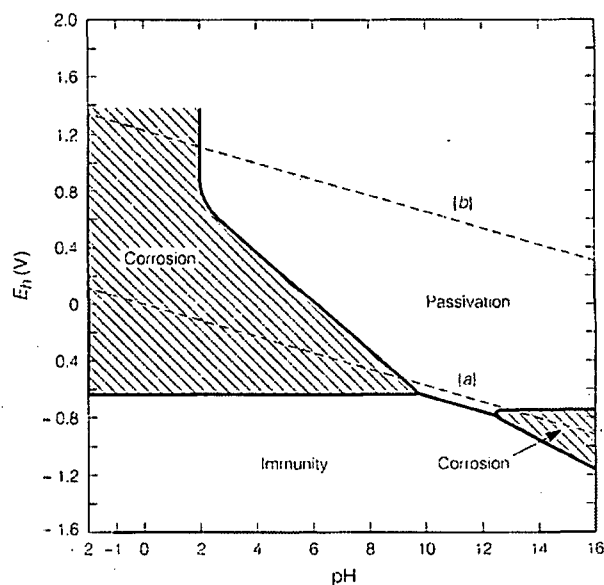
$$E = -\Delta G/zF \quad A.5$$

where  $F$  is Faradays constant (96,500 coulombs/equivalent), and  $z$  is the number of electrons (or equivalents) exchanged in the reaction.

Again the reader is referred to corrosion textbooks [1-6] for details of these electron transfer relationships, and the derivation (and measurement) of the electrode potential that exists at the metal/solution interface. The equilibrium stability of the precipitated oxide in Equation A.4 will be dependent on the interactions between temperature, pH and oxide solubility.

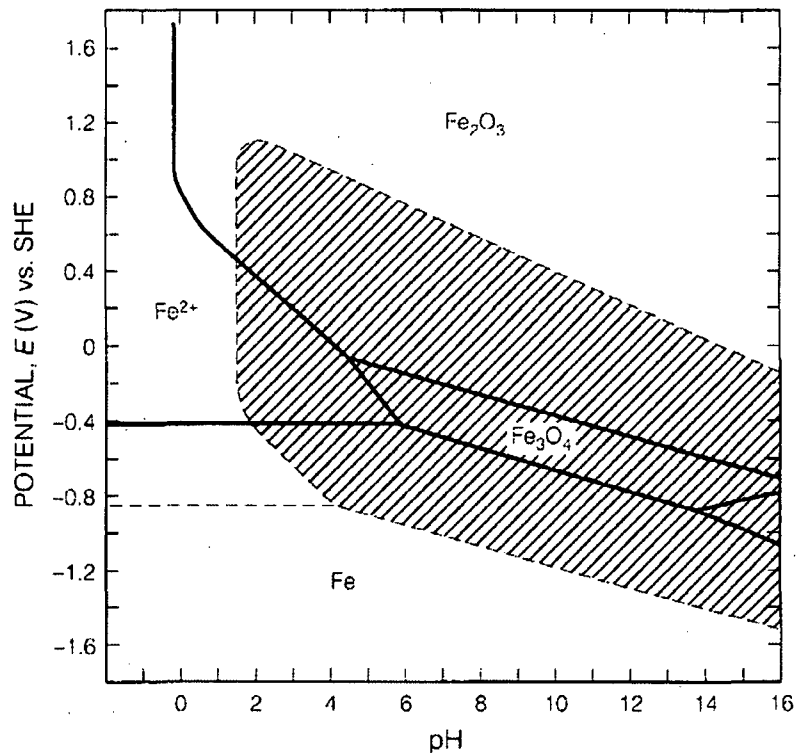
These fairly basic concepts lead to the construction of a Pourbaix diagram [7], which denotes the potential/pH combinations where various species ( $M$ ,  $MO$ ,  $M_{aq}^{z+}$ ,  $MO_n^{n-}$ ) are thermodynamically stable or metastable at a given temperature. Such diagrams are of extreme value in predicting corrosion events and in determining  $E/pH$  combinations where the metal is, (a) thermodynamically immune from corrosion or, (b) where it is possible that the surface may be protected by an oxide (or salt) which may, depending on its structure, confer "passivity" or, (c) where the metal may undergo active corrosion. With this knowledge, mitigation strategies associated with, for instance, water chemistry specifications or alloy choice can be formulated. The Pourbaix diagram for the iron-water system, at 25°C and activities of dissolved species of

$10^{-6}$  gm-equivalents/L, is shown in Figure A.1 as an illustration of these concepts. It is seen that, at lower potentials, there is a region in potential-pH space where the oxidation reactions (Equations A.1-A.3) are not possible thermodynamically, and iron is immune from corrosion. However, corrosion is possible at more positive potentials corresponding to the general oxidation Equations A.1 and A.2 where the dissolved species are  $\text{Fe}^{2+}$  or  $\text{Fe}^{3+}$  in acid solutions and  $\text{HFeO}_2^-$  in alkaline solutions.



**Fig. A.1 Pourbaix diagram for the iron-water system at 25°C, Activities of dissolved species of  $10^{-6}$  gm-equivalents/L [7] (© NACE International 1974)**

Oxides ( $\text{Fe}_3\text{O}_4$ ,  $\text{Fe}_2\text{O}_3$ ) are stable at intermediate pH values via oxidation reactions (Equation A.3) or dissolution/precipitation reactions (Equation A.4) and may, depending on the oxide structure confer corrosion protection. Alloying may significantly affect the oxide structure and the degree of protection or "passivation," which is conferred at various E/pH conditions. A simple example of this is shown in Figure A.2 where the stability region for  $\text{Cr}(\text{OH})_3$  is superimposed onto the Pourbaix diagram for the iron-water system. It is seen that the passivity region is considerably expanded, with the possibility of improved corrosion resistance in ferritic stainless steels (Fe-Cr alloys) and austenitic stainless steels (Fe-Cr-Ni) due to the formation of mixed spinel oxides on the metal surface. Again the reader is guided to the corrosion handbooks that refer to numerous papers that focus on the details of these phenomena.



**Fig. A.2 Superimposition of  $\text{Cr(OH)}_3$  stability region onto the Pourbaix diagram for the iron-water system at 25°C and activities of dissolved species of  $10^{-6}$  gm-equivalents/L. [4; adapted from 7]. Note that the alternate  $\text{Cr}_2\text{O}_3$  phase has a similar outline but with reduced stability regions in the acid and alkaline regions. (Reprinted by Permission of Pearson Education, Inc., Upper Saddle River, N.J.)**

Pourbaix diagrams may also be used for the prediction of corrosion degradation modes other than general corrosion, since many of these are dependent on the conjunction of reactions such as Equations A.1- A.4. Such a use is discussed in Appendix B relative to the E/pH combinations known to be relevant for various submodes of stress corrosion cracking of nickel-base alloys in PWR steam generators [see Appendix B.7].

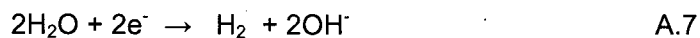
Finally, in discussing the thermodynamics of the various species at the metal – environment interface, it is important to point out that the Pourbaix diagram sets bounds on the kinetics of formation of those species. For example, metal dissolution (Equation A.1); cannot occur, even at extremely slow rates at potentials more negative than the reversible potential for that reaction. The rate of dissolution at potentials above the reversible potential will depend on various factors that are discussed below.

The extent of corrosion, or the mass of metal oxidized per unit area, is the faradaic equivalent of the oxidation charge density passed in Equations A.1-A.3. However, in order to conserve charge under open circuit conditions (i.e., the metal does not have an imposed current on it as would be the case with anodic or cathodic protection), the release of electrons in such oxidation reactions must be balanced by an equal consumption of electrons by reduction reactions. In LWRs such reactions commonly involve reduction of hydrogen cations (Equation A.6), water

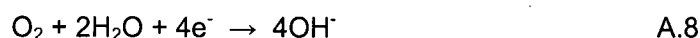
(Equation A.7), or dissolved oxygen (Equation A.8), or may be associated with other reactions associated with reduction of hydrogen peroxide, cupric cations, etc.



in acid solutions or, in neutral or alkaline solutions

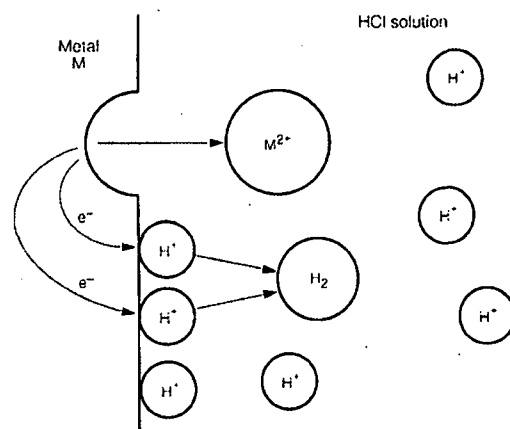


and



The fact that reduction reactions must also occur on the metal surface has an impact on the regimes on the Pourbaix diagram that are applicable for a given system. For instance, Equation A.6 is an appropriate reduction process in deaerated water, and the line "a" in Figure A.1 indicates the equilibrium potential/pH relationship for that process. Thus, in order to have reduction according to Equation A.6 in conjunction with oxidation of iron by Equations A.1-A.3, the relevant potential/pH area lies below line "a." By contrast in aerated water, where a relevant reduction reaction would be Equation A.8 (whose equilibrium potential / pH relationship is given by line "b" in Figure A.1), the relevant potential/pH area on the Pourbaix diagram where metal oxidation or corrosion can occur is considerably increased. Thus there is a thermodynamic reason why, in general, corrosion problems are potentially more significant in aerated vs. deaerated solutions.

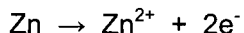
As shown schematically in Figure A.3 the oxidation and reduction reactions may take place on adjacent areas of the material surface, but this is not always the case, especially for localized corrosion modes when the "anodic" and "cathodic" sites (where the oxidation and reduction reactions respectively occur) may be separated for geometric or metallurgical inhomogeneity reasons.



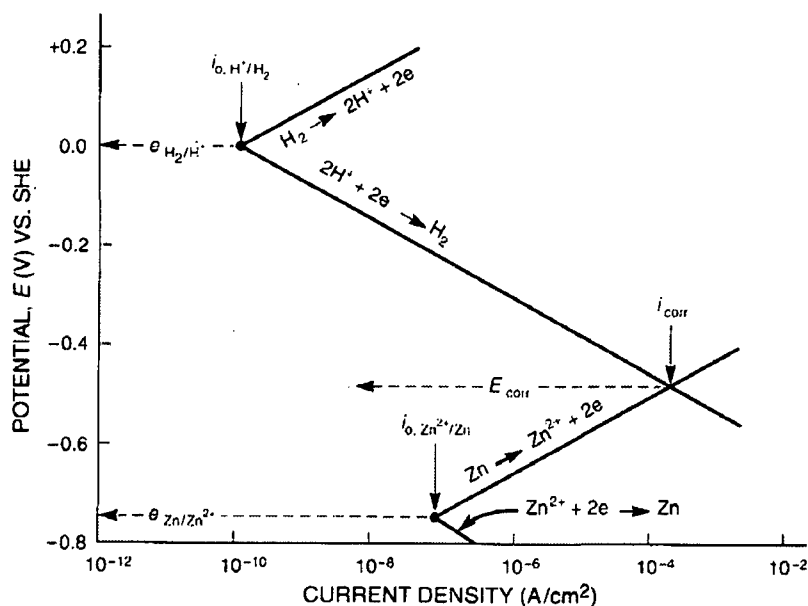
**Fig. A.3. Oxidation and reduction reactions occurring on adjacent areas of surface [4]**  
(Reprinted by Permission of Pearson Education, Inc., Upper Saddle River, NJ.)



The kinetics of the oxidation and reduction reactions for the simple case of zinc dissolving in an acid solution are shown in Figure A.4 in order to illustrate the concept of the equilibration of oxidation and reduction reaction rates. It is seen that the oxidation, or dissolution, rate for zinc, quantified by the current density for the reaction,



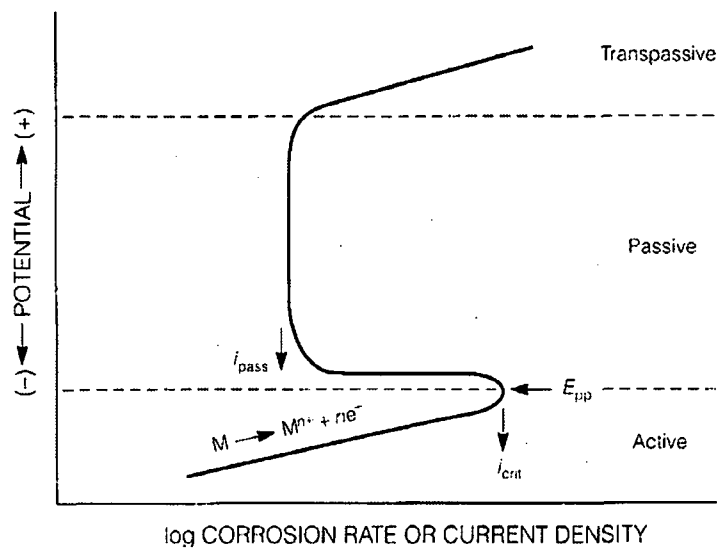
increases exponentially with the extent that the surface potential is increased from the potential associated with equilibrium for that oxidation reaction (i.e. approximately -0.75V vs. SHE); this difference between the equilibrium potential and the surface potential is known as the overpotential. Similarly the reduction rate of hydrogen cations (Equation A-6) occurring on the adjacent metal surface also increases exponentially with increasing overpotential from the equilibrium potential (i.e. 0V vs. SHE) for that reduction reaction. At a surface potential denoted as the corrosion potential,  $E_{\text{corr}}$  in Figure A.4 the rate of oxidation equals the rate of reduction, and the zinc corrosion rate is defined by the Faradaic equivalent of the corrosion current density,  $i_{\text{corr}}$ . Note that in terminology generally used in corrosion in nuclear systems,  $E_{\text{corr}}$  is usually termed the electrochemical corrosion potential, or ECP.



**Fig. A.4 Schematic “Evans” diagram indicating the equilibration of the oxidation and reduction rates for the dissolution of zinc in 1N HCl solution, and the associated “corrosion current, ( $i_{\text{corr}}$ )” and “corrosion potential, ( $E_{\text{corr}}$ )”.** [4] (Reprinted by Permission of Pearson Education, Inc., Upper Saddle River, NJ.)

This simple kinetic system may become more complicated when, as mentioned above, the “anodic” and “cathodic” sites are separated for geometric or metallurgical inhomogeneity reasons, or where the areas on the metal surface associated with oxidation and reduction reactions are markedly different. These are particularly important in localized corrosion events, and will be discussed later in the appropriate section.

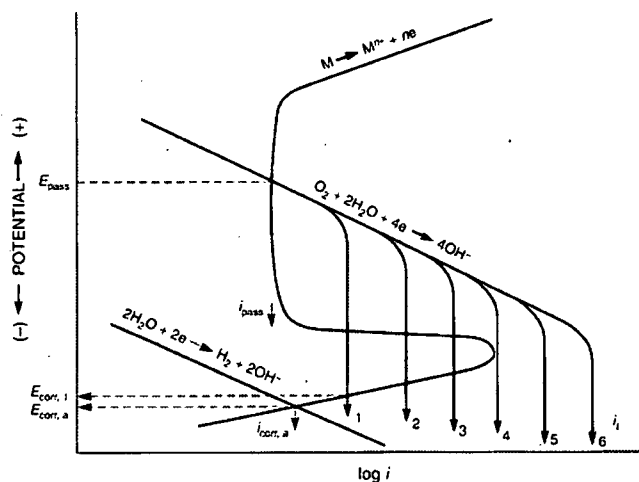
In order to control corrosion product (or "crud") release in the reactor coolant system, alloys are used that operate in the region of the Pourbaix diagram where surface protection is provided by the presence of a protective oxide film. The effect of the formation of such a film on the kinetics of oxidation is shown schematically in Figure A.5. As the overpotential for oxidation is increased so the corrosion rate may increase exponentially under "activation control" until a potential, predictable from the Pourbaix diagram, is reached when an oxide may form. This potential is denoted by  $E_{pp}$  in Figure A.5. Thereupon the oxidation rate decreases by a factor of  $10^4$  or more dependent on the structure, composition, and solubility of the surface oxide. The increased corrosion resistance may be maintained over a considerable potential range until, at more positive potentials, the oxide may lose its protective properties, either due to the onset of localized breakdown associated with the presence of aggressive impurity anions (such as chloride) leading to pitting [8, see Appendix B.9,] or, at more oxidizing conditions, to the dissolution of the passive film. This latter condition is known as "transpassivity" and an example would be dissolution of  $Cr_2O_3$ -rich surface oxides to  $HCrO_4^-$ .



**Fig. A.5 Schematic oxidation current density vs. electrode potential diagrams, indicating, for the oxidation reactions, transitions from activation control, to onset of passivation, to oxide break down due to transpassivity or pitting. [4] (Reprinted by Permission of Pearson Education, Inc., Upper Saddle River, NJ.)**

The prediction of the kinetics of corrosion reactions is further complicated by the fact that many of the oxidation and reduction reactions occurring on the metal surface may be ultimately controlled by the transport of either reaction products away from the surface, or by the transport of reactants to the metal surface. This is especially the case for material geometries, such as crevices and cracks; these situations will be discussed in the appropriate sections on localized corrosion later in this Appendix and in the topical reports in Appendix B. An example of such a complication due to mass transport under general corrosion conditions is shown schematically in Figure A.6 where the kinetics for the reduction of dissolved oxygen (Equation A.8) are superimposed on the metal oxidation kinetics from Figure A.5. In this situation it is seen that the "activation controlled" reduction kinetics increase exponentially with overpotential to a limiting value when the reduction rates become potential-independent. This limitation corresponds physically to the point when dissolved oxygen cannot arrive fast enough to the reacting surface to satisfy

any further increase in activation controlled processes. As would be expected, however, this condition is delayed if the bulk-dissolved oxygen content is increased or if the solution flow rate is increased; both of these actions effectively increase the concentration of oxygen and reduction kinetics at the reacting metal surface. This is illustrated in Figure A.6 by the vertical lines marked  $i_1, 2, 3, 4, 5,$  and  $6$ . It is apparent that the corrosion current density and corrosion potential can change in a non-monotonic manner with different changing system conditions (e.g., flow rate, oxidant concentration, turbulence), but these can be predicted via knowledge of the oxidation rates and the reduction rates associated, in this example, with dissolved oxygen content, solution flow rate, etc.



**Fig. A.6 Superposition of the reduction kinetics for dissolved oxygen on the metal oxidation rates from Figure A.5. In this case the reduction kinetics may be limited by the supply of oxygen to the reacting surface. [4] (Reprinted by Permission of Pearson Education, Inc., Upper Saddle River, NJ.)**

#### A.4 Description of Degradation Modes and their Predictability in LWRs

##### A.4.1 "Uniform" Corrosion

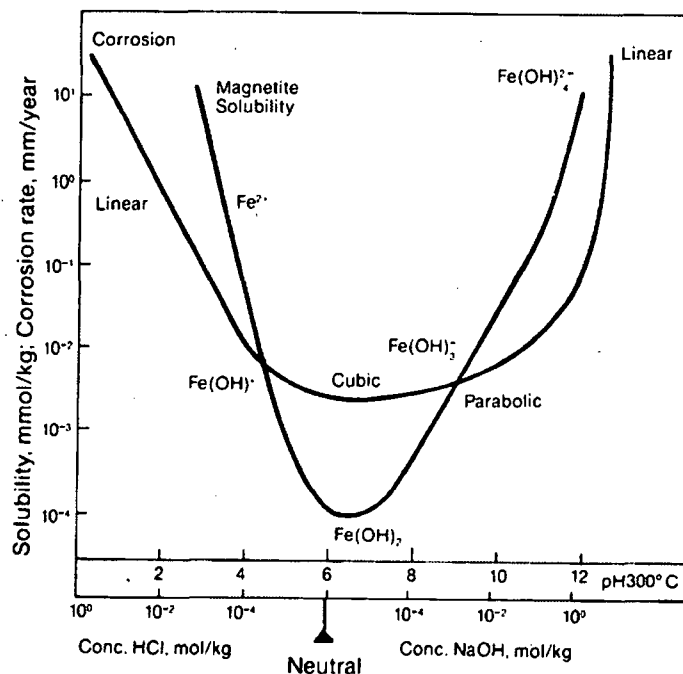
This section addresses degradation mechanisms, which result in loss of material over a reasonably large area (as opposed to localized corrosion that may occur over areas governed by metallurgical inhomogeneity defined broadly as less than 1-2 cm<sup>2</sup>). Such "uniform" degradation modes include general corrosion, boric acid corrosion and flow accelerated corrosion.

##### General Corrosion

General corrosion is characterized by uniform surface loss through material oxidation (i.e., general Equations A.1-A.3), and is deleterious to plant operation due to (a) loss of functionality of a pressure boundary due to loss of section thickness, (b) the presence of corrosion products ("crud") which may decrease the heat transfer efficiency when these deposit on e.g., steam generator tubes or fuel cladding, and (c) the presence of crud which is deposited and activated on the fuel cladding surface and, upon release, will increase the radioactivity levels in the RCS or, in the case of direct cycle BWRs, the balance of plant.

General corrosion issues are part of the design basis of the LWRs and are founded on a large body of research over many decades. Thus there is good reason for the judgments in Table A.5 that general corrosion is usually not an issue in LWRs. The following discussion is included, however, since the electrochemical details of general corrosion in LWRs forms a basis for understanding other corrosion-based degradation modes for which there may be less confidence in our ability to adequately address the situation.

As explained in Section A.3 the corrosion rates may be managed by consideration of the thermodynamically stable (or metastable) species (dissolved metal cations, oxides, salts, etc.) at the metal/water interface and the control of the relevant oxidation and reduction kinetics. In the case of the main materials of construction in LWRs importance is attached to the surface oxide solubility, which, as indicated in Figure A.7, for magnetite in the iron/water system at 300°C, exhibits a minimum at neutral or slightly alkaline conditions [9]. Very similar solubility /pH relationships are noted for chromium and nickel. Also shown in Figure A.7 is the dependency of the corrosion rate for mild steel on pH, which mirrors the oxide solubility dependency.



**Fig. A.7 Corrosion of mild steel and solubility of magnetite at 300°C showing corrosion rate laws [9]**

As explained in Section A.3 the corrosion rates of stainless steels and nickel-base alloys in high temperature water are significantly lower than those of carbon steels due to spinel type oxides composed of a mixture of  $\text{NiFe}_2\text{O}_4$ ,  $\text{Fe}_3\text{O}_4$  and  $\text{FeCr}_2\text{O}_4$ . Consequently in the high temperature RCS, the internal surfaces of the low alloy steel pressure vessel, pressurizer and steam generator are clad with type 308/309 stainless steels. However there are carbon steel components exposed to high temperature water/wet steam such as feedwater piping, main steam lines and some parts of the pressure vessel left exposed following repair procedures at, for instance, vessel penetrations such as CRDM or instrumentation tubes. For these reasons, amongst others

associated with control of localized corrosion, both PWR and BWR operations are subject to strict water chemistry control, as discussed below.

Because of the dependencies of corrosion rate and oxide solubility on pH, the water chemistry specifications for PWRs impose a tight control on the pH values, which may vary slightly from one plant to another, and between primary [see Appendix B.11] and secondary [see Appendix B.12] systems. This control is achieved via injection from the Chemical Volume and Control System (CVCS) to the primary system of LiOH, and boric acid (for chemical shim control of core reactivity). Early water chemistry specifications imposed a  $\text{pH}_{300\text{C}}$  specification of  $6.9 \pm 0.2$ , corresponding to the minimum in magnetite solubility (Figure A.7), but more recent specifications have increased this  $\text{pH}_{300\text{C}}$  specification range to 7.1-7.3, in order to take advantage of both the corrosion resistance due to nickel ferrite and the improved control of crud build up and shutdown dose rates. There is a limit to which this alkalinity increase can be allowed which is associated with an increase both in corrosion rate of zirconium alloy fuel cladding, and in susceptibility to stress corrosion cracking of Alloy 600 steam generator tubing.

In addition to pH control for PWRs associated with the thermodynamic stability of a protective oxide on the surface, the kinetics of corrosion are also, as discussed in section A.3, a function of the presence of oxidizing species. Consequently, the RCS primary system has an overpressure (approx. 15 KPa) of hydrogen to minimize the reduction kinetics of Equation A.7. A maximum limit in the amount of hydrogen overpressure is determined by avoidance of hydriding of the zirconium alloy cladding. Additional overpressure via operation of the pressurizer also ensures that, under normal operating conditions, boiling in the reactor core is largely suppressed, thereby minimizing the possibility of concentration of, e.g., impurities at heat transfer surfaces in the primary side and the consequent increase in corrosion rate at these boiling sites.

In the PWR secondary system the dissolved oxygen concentration (which affects both the activation and diffusion controlled reduction kinetics and, thereby, the metal corrosion rate), is controlled by the presence of hydrazine [see Appendix B.12]. However since boiling occurs on the secondary side of the steam generator tubes, it is possible to have accelerated corrosion in occluded regions such as tube/tube support regions; this will be discussed later in the section on crevice corrosion.

Control of general corrosion in the lower temperature systems such as the service water system, where the piping is predominately carbon steel, can present a potential problem since the water supplies for such systems are "uncontrolled" sources such as the ultimate heat sink, lake water, or sea water. Moreover, under such lower temperature conditions the surface oxide is not as protective as that at higher temperatures in the pH range specified for, e.g., the RCS. However, generally accepted corrosion prevention methods widely used in other industries (transportation, petrochemical, marine, etc.) are applied, including the use of cathodic protection, (for submerged pumps and underground piping), inhibitors (such as phosphates) or biocides to control microbiologically induced corrosion.

Chemistry control for general corrosion in direct cycle BWRs is largely driven by the fact that, under "normal water chemistry" (NWC) conditions, there is an excess of dissolved oxygen in the coolant, since the other product of the radiolytic breakdown of water, hydrogen, is preferentially partitioned to the steam phase. This dissolved oxygen has a deleterious effect on stress corrosion cracking of most of the BWR materials of construction, as will be discussed later. Consequently the main driving force in chemistry control for BWRs [see Appendix B.10] has been to lower the dissolved oxygen concentration (or more accurately, the corrosion potential) by both injection of hydrogen (**Hydrogen Water Chemistry**) and control of the dissolved impurity level.

As a result of these industry actions, the level of impurity contents in the reactor coolant has dropped markedly over the last few decades, with current coolant conductivities approaching that of theoretically pure water; moreover, virtually all of the U.S. BWRs now operate under HWC with modifications due to the addition of noble metals (Noblechem™) to the coolant that improve the efficiency of the oxygen/hydrogen recombination [10, 11, see Appendix B.10].

Although these actions have been extremely effective in controlling stress corrosion, the addition of hydrogen can have a deleterious impact on radioactivity release due to both  $^{16}\text{N}$  during power operation and the creation and release of activated corrosion byproducts, mainly  $^{60}\text{Co}$ , during plant shutdown and/or changes between NWC and HWC.

In the former case the release of  $^{16}\text{N}$  to the steam and off-gas systems is aggravated by the addition of hydrogen to the coolant and the effect that this has on the formation of volatile nitrogen bearing species originating from  $^{16}\text{O}(n,p)^{16}\text{N}$  reactions in the core region. This increase in the  $^{16}\text{N}$  content effectively limits the hydrogen addition to the feedwater to 200-300 ppb. In more recent times the widespread adoption of noble metal technology, and especially Noblechem™, has minimized the HWC/ $^{16}\text{N}$  problem and has allowed the efficient reduction of the corrosion potential without the deleterious radioactivity offgas release [11].

The creation and release of  $^{60}\text{Co}$  is directly relatable to the presence of  $^{59}\text{Co}$  in corrosion products from cobalt-rich, wear resistant Stellite valve seatings, roller bearings, etc, or to cobalt impurities in the nickel base components and stainless steel piping and, especially, control rod blade sheaving. Once this crud is deposited and the  $^{59}\text{Co}$  is activated on the fuel cladding, the resultant  $^{60}\text{Co}$  is transported to the stainless steel piping where it is incorporated into the oxide spinel structure. The mitigation for this deleterious general corrosion related phenomenon [see Appendix B.10] is to (a) reduce the cobalt inventory in the reactor circuit by using alternatives to cobalt-rich Stellites, (b) minimizing the crud formation (which acts as a transport vehicle for the activated  $^{60}\text{Co}$  from the core to the piping) by control of the anionic impurity and the dissolved iron concentrations and, (c) add 10-100ppb zinc to the coolant. In this latter case the zinc inhibits the corrosion of stainless steel, resulting in thinner spinel films, and also takes up competing sites where  $^{60}\text{Co}$  could reside in the oxide spinel structure.

Although the reduction in dissolved oxygen content and corrosion content via HWC/ Noblechem™ has been successful in reducing the extent of stress corrosion cracking in BWRs, it has introduced a problem of increased corrosion of carbon steel feedwater lines [12,13] due to the formation of non-protective magnetite films at the low corrosion potentials associated with oxygen contents <5-10 ppb. Consequently BWR water chemistry guidelines [see Appendix B.10] specify a minimum dissolved oxygen content of 30 ppb in the feedwater lines to ensure the creation of a more adherent and protective magnetite film which is stable at the more elevated corrosion potentials.

From a life-management standpoint, it is apparent that the knowledge base exists to predict and control the general corrosion behavior in most of the materials of construction in LWRs via appropriate water chemistry control. Indeed there is some considerable margin in the design basis to account for general corrosion since actual corrosion rates are significantly below the design-basis allowable values. For instance, the design specification provides a general corrosion allowance of 120 mils for the carbon steel main steam system. The actual general corrosion rate for carbon steel piping in a steam environment is less than 0.16 mils per year. Similarly, the corrosion allowance for stainless steel piping operating in the 260-316°C (500-600°F) range is 2.4

mils. The actual general corrosion rate for stainless steel in this temperature range is 0.01 mils/year of service life.

### **Boric Acid Corrosion**

Although, as discussed in the section above, the general corrosion rates of the LWR materials of construction are well below the design values required to maintain structural integrity, and the radioactivity issues associated with activation of the corrosion products can be managed, there are situations where very high corrosion rates can occur over significant areas.

One such situation is the corrosion of carbon and low alloy steels due to boric acid in PWR primary environments [14, 15, see Appendix B.18,]. Under normal operating conditions the corrosion rate of carbon and low alloy steels in borated, hydrogenated, primary water is <0.025 mm/year, but problems have occurred in operating plants when borated water leaks from the PWR RCS onto an external carbon or low alloy steel surface. Under these leakage situations the boric acid concentration on the external component will increase due, for instance, to steam flashing and alternate wetting and drying cycles that produce, ultimately, a low pH boric acid slurry which, in combination with an oxygenated air atmosphere, can cause very high corrosion rates of approximately 25 mm/year, (Figure A.8). Such an increase in corrosion susceptibility is predictable via reference to the Pourbaix diagram for the iron/water system (Figure A.1), which indicates that, under acidic, and especially under higher surface potential, oxygenated conditions, corrosion is likely, and that it is unlikely that any protection due to a surface oxide would be forthcoming given the high oxide solubility under these acidic conditions (Figure A.7).

Problems of boric acid wastage of closure studs in the pressurizer, reactor coolant pump, steam generator manways, etc. have been associated with leaks due to gasket failures or through wall cracks in the component. The most notable recent observation of such a degradation mode was the through-wall corrosion of the pressure vessel head at Davis Besse in 2002 associated with stress corrosion cracking of nickel-base alloys in the vessel head penetration assembly and subsequent leakage of primary coolant into a restricted geometry between the outside of the pipe and the reactor pressure vessel head. The result was that boric acid concentrated due to boiling and evaporation to levels that led to excessive corrosion of the low alloy steel pressure vessel. All of these incidents are in the higher temperature RCS where such concentration mechanisms are possible. By contrast, boric acid wastage problems would not be expected to be associated with leaks in lower temperature systems (<100°C) such as the ECCS and CVCS since, although these systems are borated, there would be no mechanism to concentrate the boric acid sufficiently to achieve the low pH values needed for high low alloy steel corrosion rates.

As indicated in Figure A.8 the corrosion rate of carbon and low alloy steels increases with increasing acidity and is, depending on the pH value greatest at temperatures between 80 and 150°C. Such a surface temperature range is achievable due to evaporative cooling of the escaping high pressure coolant impacting on the external component.

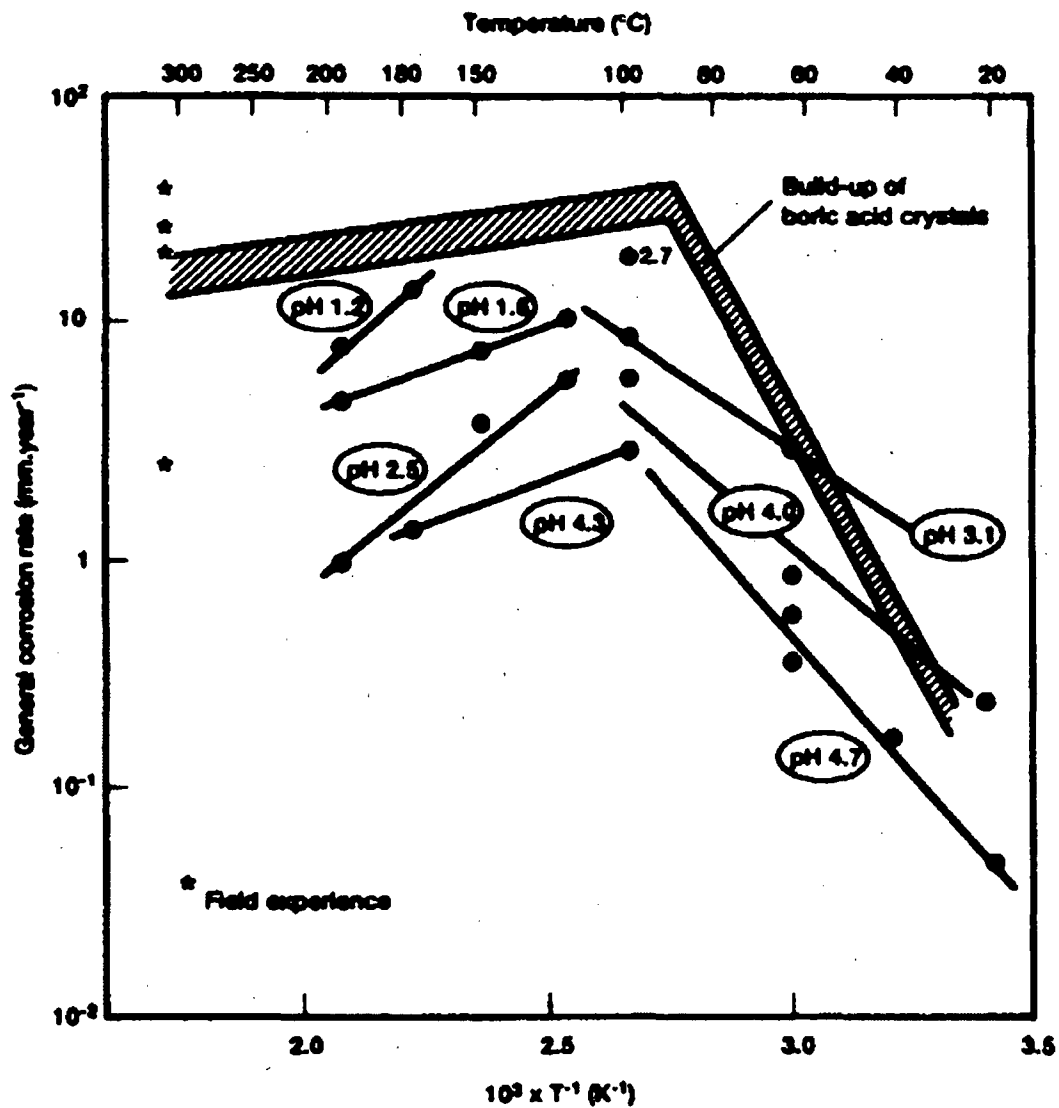


Fig. A.8. Relationship between the corrosion rate of carbon and low alloy steels in various acidified boric acid solutions as a function of temperature. [15]

As discussed in Appendix B.18, the Davis Besse incident does present some challenges to the assertion that all boric acid wastage is predictable since, in this particular geometry, it was unclear that very low pH values could be achieved. As a result there are ongoing research efforts both in the industry and the NRC to determine, for instance, the interactions between the corrosion rate and various factors such as the leakage rate (and the role of erosion-corrosion or impingement), the chemistry of the escaping coolant, the extent of evaporative cooling of the low alloy steel surface, and the role of the geometry of the assembly (for instance, the dimensions of the annulus between the CRDM pipe and the pressure vessel in the case of Davis Besse), which will affect the mass transport of oxygen and liquid within the crevice.

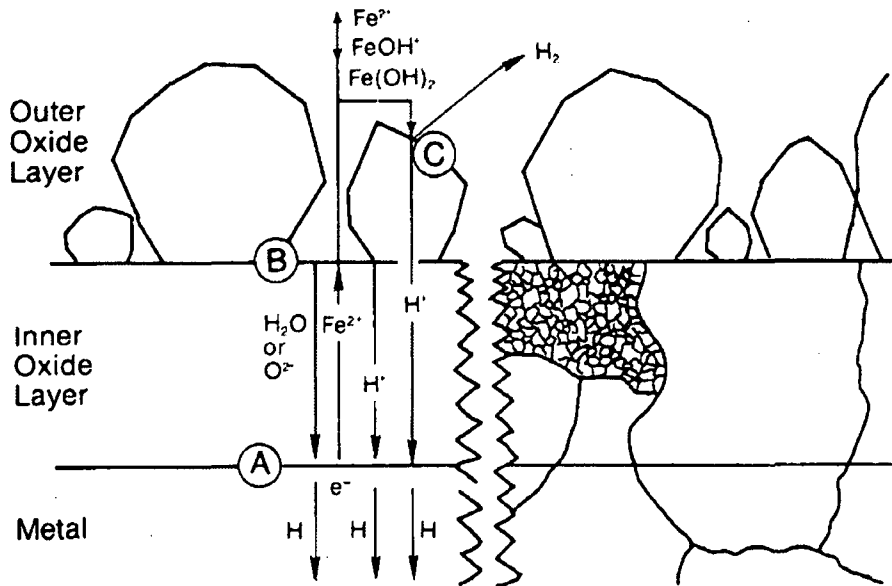


## Flow-Accelerated Corrosion and Erosion-Corrosion

Flow-accelerated corrosion is frequently localized at areas of high turbulence, often associated with geometrical discontinuities or abrupt changes in flow direction, and this manifests itself as a localized wall loss. There are well-defined electrochemical and mechanical reasons for such degradation since the water or steam flow past the metal component may increase the kinetics of corrosion in various ways, as discussed below.

At the simplest level the corrosion kinetics may be increased under both laminar and turbulent flow regimes due to an increase in diffusion rates of, for instance, dissolved oxygen, to the metal surface, or the increase in removal rate of oxidized species from the metal surface. These concepts were discussed in relation to Figure A.6. If the oxide film has a two layer structure, as seen and discussed above for the general corrosion of carbon and low alloy steels in high temperature water, (Figure A.9), then increasing flow rate may also remove the outer oxide layer under turbulent flow conditions. Under these conditions the flow-accelerated corrosion rates will be controlled ultimately by the reductive dissolution of the inner oxide layer and the diffusion kinetics of Fe(II) species away from the surface. Under such conditions the corrosion rate may be considerably enhanced and be of the order of 10 mm/year.

It is apparent that these controlling conditions are primarily electrochemical in nature. It is also possible to accelerate the corrosion rate even further by imposing a mechanical factor to the removal of the outer oxide layer, including the effect of the impact of water droplets on the surface in two phase flow steam systems (e.g., wet steam in main steam lines or cross-around piping in turbines), cavitation effects (e.g., impeller blades in pumps) or, in extreme situations, entrained particles, such as sand, in service water systems. Such mechanically dominated effects are normally described as "erosion-corrosion" or "erosion" depending on the degree of the mechanical contribution.



**Fig. A.9. Schematic of two-layer oxide structure on carbon steel in high temperature water. [16] (© NACE International 1981)**

As mentioned above, the extent of flow-accelerated electrochemically-controlled corrosion in high temperature aqueous environments is very much a function of the material/environment combinations that affect the structure of the oxide layers and their chemical and mechanical stability. Following the catastrophic failure of a carbon steel suction line to the main feedwater pump at Surry-2 PWR [17], there was considerable study [18] of the factors controlling flow accelerated corrosion in LWRs, leading up to the development by EPRI of the CHECWORKS™ prediction code [19]. As discussed in more detail in Appendix B.17, the flow rate effect on the corrosion rate for carbon or low alloy steels is a function of the material composition, piping geometry, single vs. two-phase environment, temperature, pH, laminar vs. turbulent flow and the local corrosion potential. As indicated in Figure A.10 for flow accelerated corrosion of carbon steel in deoxygenated ammoniated water, the corrosion rate is a non-monotonic function of temperature, with a maximum occurring in the range of 130-150°C for single phase fluids; the peak corrosion rates occur at a higher temperature range for two-phase environments (e.g., wet steam in the main steam line and turbine cross-around piping).

Control of the local corrosion potential (or dissolved oxygen content) is a key factor in managing flow accelerated corrosion of carbon and low alloy steels in the main steam, feedwater, condensate and moisture separator piping in BWRs. As indicated in Figure A.11, the flow-accelerated corrosion rates in condensate and moisture separator reheater drain systems are a function of the local dissolved oxygen content; such an observed relationship is in agreement with the CHECWORKS™ predictions.

The ability to minimize the corrosion rate by maintaining the local dissolved oxygen content above 30 ppb will be a function of the amount of air in-leakage from the turbine condenser and, as mentioned earlier in the general corrosion section, the degree of oxygen dosing in the feedwater lines. The amount of oxygen control required to minimize flow-accelerated corrosion in the two-phase environment in the main steam line will be a function of the amount of radiolysis occurring in the reactor core, the degree of hydrogen water chemistry/ Noblechem™ and the extent of venting being applied in the moisture separators. The ultimate remedy is to make use of the more protective and adherent films associated with chromium alloying; hence the replacement of the susceptible lines with low alloy steels with higher chromium content, stainless steels or the use of a higher chromium content coating deposited by thermal spray or weld overlay.

The message here is that the extent of flow-accelerated corrosion that can occur in carbon and low alloy steels in PWRs and BWRs is predictable, and the mechanism is understood. The prediction algorithms (i.e., CHECWORKS™) are routinely used in individual plant Aging Management Programs to assign inspection priorities. It has generally been found that, where problems do occur, it is apparent that these analyses and inspection priority methodologies have not been followed.

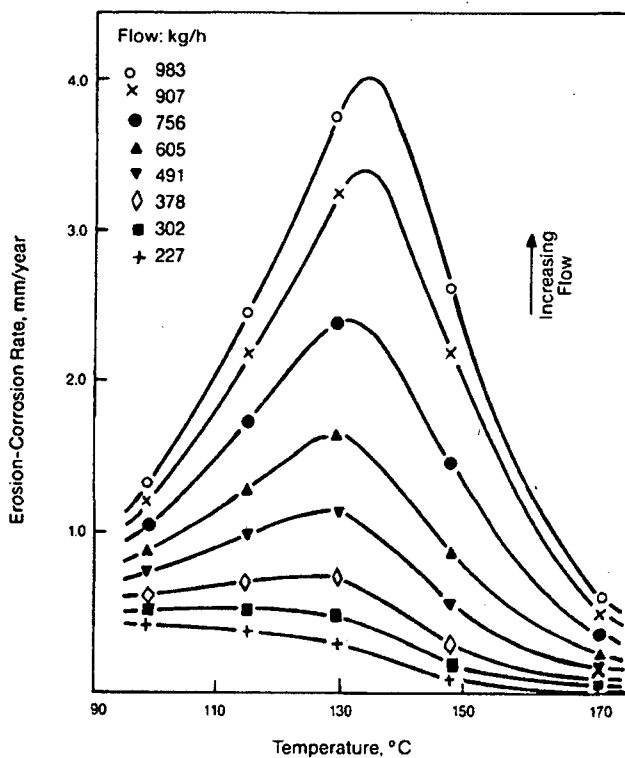


Fig. A.10. Effect of temperature on the flow accelerated corrosion rate of carbon steel in deoxygenated ammoniated water. [20] (DR 1982 EDF)

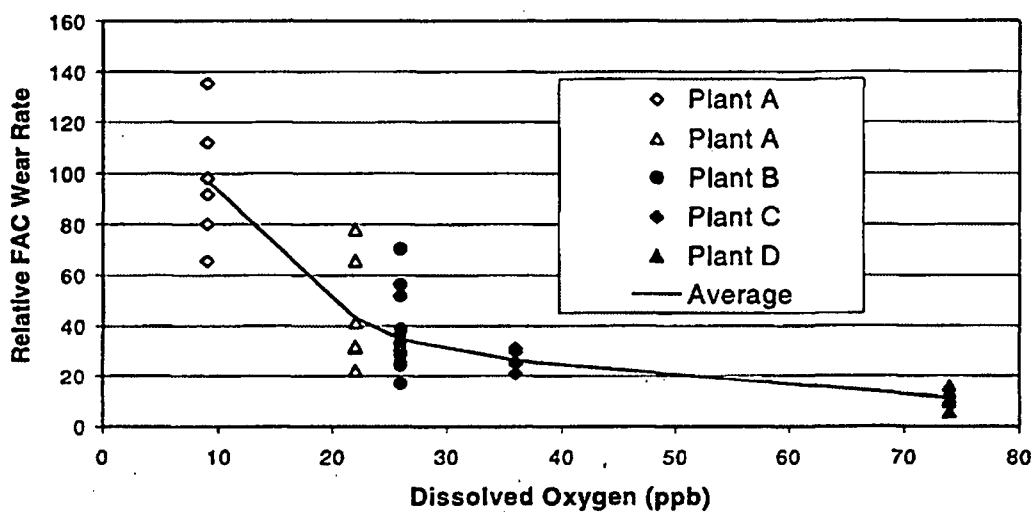


Fig. A.11. Flow-accelerated corrosion data for condensate and moisturizer separator re-heater drain systems in four BWR plants as a function of the local dissolved oxygen contents [Appendix B.10]

## **A.4.2 Localized Corrosion**

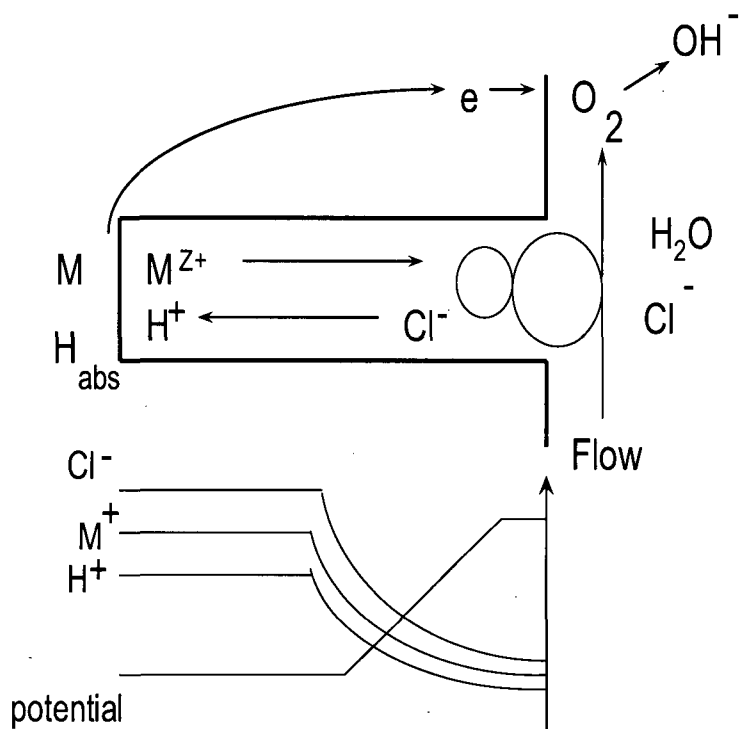
This section addresses materials degradation modes, where the corrosion damage occurs over relatively small areas but, potentially, may occur at high penetration rates. The result in such cases may be localized leakage or, in more extreme situations, lack of structural integrity and catastrophic failure. Such degradation modes include, crevice, pitting, galvanic and microbially induced corrosion and environmentally assisted cracking. This latter category includes stress corrosion cracking, strain-induced cracking, and corrosion fatigue (discussed in Section A.4.4 on Fatigue).

### **Crevice Corrosion**

As the title suggests, this phenomenon is associated with crevices inside which a relatively stagnant solution is present and where there is a mechanism to make that solution more aggressive (e.g., increased acidity and increased anionic impurity concentration), and thereby increase the local metal corrosion rate. The crevices may be inherent in the component design (such as at gaskets, lap joints, bolt heads and threads), or may occur under corrosion deposits and sludge piles. The critical factors in controlling this form of attack are (a) the geometry of the crevice, and the conditions that affect the thermal hydraulics within the crevice, and (b) the mechanisms that change the cationic and anionic concentrations within the crevice.

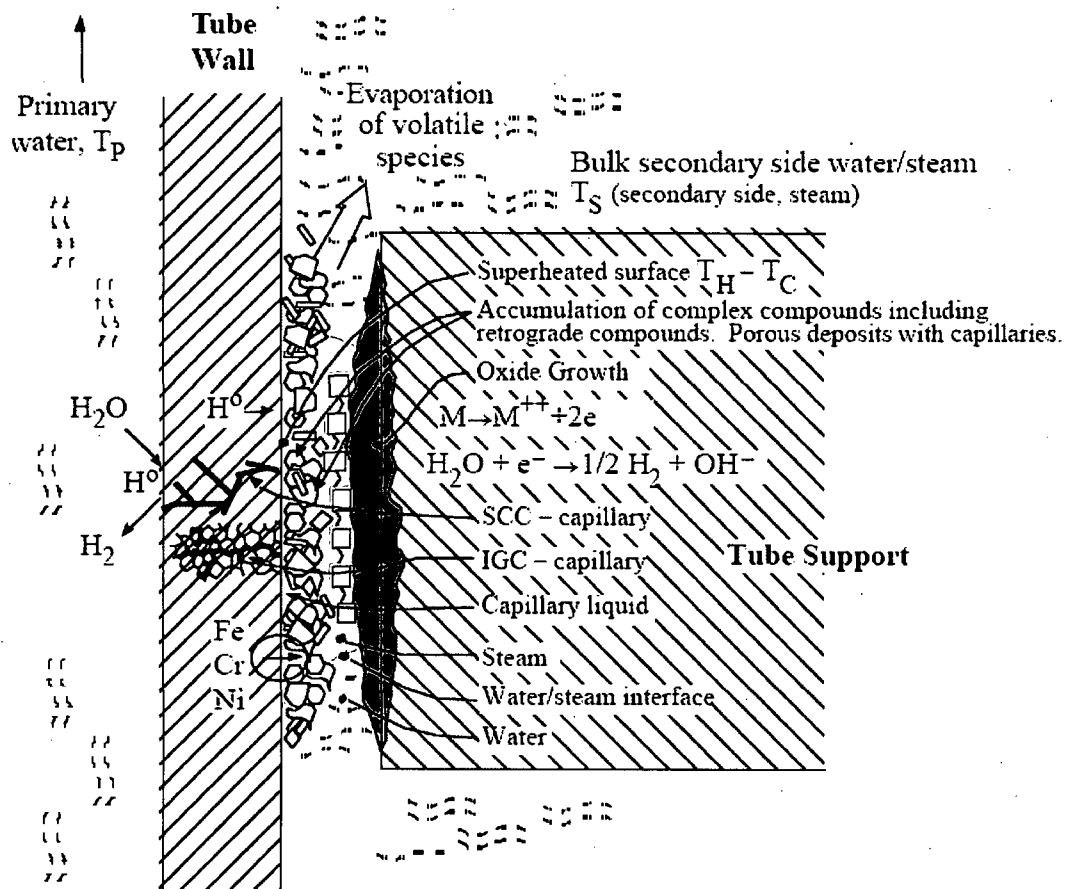
The thermal hydraulics and mechanisms of crevice corrosion have been extensively researched over the last 30 years and, as a result, control techniques are available (see, for instance, References 21 and 22). Examples of this understanding/control synergy are given below.

As indicated schematically in Figure A.12 there is the possibility that, in aerated solutions, the site for oxygen reduction is concentrated on the exposed surface at the mouth of the crevice. A reason for this is that the convection-controlled transport rate of dissolved oxygen into the crevice is insufficient to make up for the removal of dissolved oxygen due to general corrosion on the crevice sides. The resultant separation of the oxygen reduction site at the crevice mouth from the metal oxidation site at the tip of the crevice imposes a potential gradient down the crevice, thereby giving rise to potential-driven diffusion of anionic impurities (e.g., chloride) to the crevice tip. In order to maintain electroneutrality it is necessary that there be an increase in acidity within the crevice by, for instance, the hydrolysis of the dissolved metal cations (Equation A.4). Thus, the environmental conditions of low pH and high anionic impurity concentration are created within the crevice that could lead to an increase in metal corrosion rate.



**Fig. A.12. Schematic of crevice in aerated solution, indicating the separation of the metal oxidation and oxygen reduction sites, and the consequent changes in pH and anionic concentrations**

A further crevice corrosion mechanism is possible at heat transfer surfaces, where concentrations of species may occur due to their distribution between the aqueous and gaseous (e.g., steam) phases or the evaporation of volatile species. This concentration of acidity, alkalinity, or other aggressive non- $OH^{-}$  anions may be retained in an occluded region under specific geometrical conditions which inhibit solution redistribution. A classical example of this is the localized corrosion of carbon steel tube support plates in PWR steam generators, as illustrated in Figure A.13 [see Appendix B.7], which has led to denting of the Alloy 600 tube and subsequent stress corrosion cracking on the primary and secondary sides of the tube.



**Fig. A.13. Schematic of crevice formed at PWR steam generator tube/ carbon steel tube-support, together with the phenomena that give rise to the localized corrosion. [23]**

Such understanding of the mechanisms of crevice corrosion lead to logical methods of controlling the problem including, for instance, ensuring that there is adequate flow in the crevice, as illustrated by the redesign of BWR pressure vessel inlet safe ends and steam generator tube support structures, and by the control of the amount of oxidant in the environment at the mouth of the crevice. Examples of this latter control method are the adoption of hydrogen water chemistry/ NobleChem™ in BWRs, and the appropriate use of hydrazine in PWR secondary systems. The hydrogen overpressure in a PWR reactor coolant system provides adequate protection against crevice corrosion for the internal surfaces of RCS components. As indicated in Table A.5, residual concerns for control of crevice corrosion are mainly for carbon steels, which have an inherently weaker corrosion resistance (compared with austenitic alloys) in the aggressive environments in the crevices and, especially, in systems where it may be more difficult to control the creation of an aggressive water chemistry in the crevice, such as in aerated service water systems or at restricted heat transfer sites in the secondary side of steam generators. It should be pointed out, however, that other forms of localized degradation such as stress corrosion cracking or intergranular attack in stainless steels and nickel-base alloys can be accelerated in crevice environments.

## Pitting Corrosion

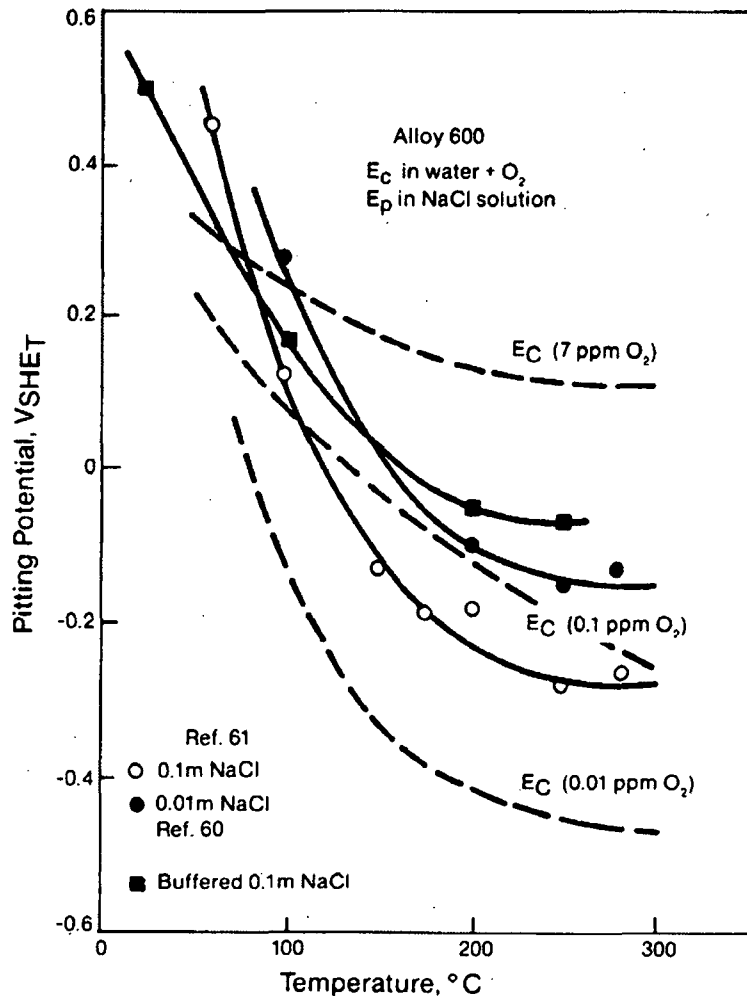
Pitting corrosion has very similar attributes to crevice corrosion in that it depends in part on the creation of a localized environment; however the important difference is that the geometric features that lead to degradation are inherent in the material microstructure and may be manifested by long incubation periods before the pits grow. Again this is a topic that has received much attention and research [8, 21, 22, 24, 25] over many decades and is covered in part in Appendix B.3. Thus the judgment indicated, for instance, in Table A5 is that there is adequate understanding to manage this phenomenon in LWRs, with the biggest uncertainty being associated with reactor systems where there might be lesser knowledge or control over the environmental conditions.

Quantitative models for predicting and controlling pitting corrosion in nuclear systems focus on taking into account the following sequence of events:

(a) Localized breakdown of the surface oxide, usually due to the presence of aggressive anions. The aggressive anions are normally associated with chlorides originating from, for example, condenser leaks, but damage can also be associated with other halides, or with sulfates, perchlorates, etc. The metallurgical sites for such oxide breakdown may be random, but are usually associated with inhomogeneities such as surface breaking precipitates or with grain boundaries over which the oxide is of a less protective nature. The breakdown of the oxide occurs at surface potentials above a critical value (known as the "pitting potential"), which is a function of the anion type and its concentration, the material composition, temperature, etc. Thus pitting is a possible concern if the corrosion potential is more positive than the pitting potential, and such a criterion puts a limitation on the system conditions under which pitting corrosion would be a problem. This is illustrated in Figure A.14 by the temperature dependence of the corrosion potential and pitting potential of Alloy 600 in water containing various concentrations of chloride. [26, 27] It is seen that under low dissolved oxygen conditions the corrosion potential is always lower than the pitting potential (for the indicated range of chloride concentrations) and, therefore, over a wide temperature range, pitting should not be a concern. At higher oxygen content conditions, however, pitting might be a concern, especially at lower temperatures and at higher chloride concentrations.

The pitting potential will also be a function of alloying content (and therefore the extent of passivity or corrosion resistance) and will increase with both chromium content and molybdenum content; thus nickel-base alloys and ferritic or austenitic stainless steels (and especially molybdenum-containing Type 316 stainless steel) will exhibit better pitting resistance than lower alloyed materials.

(b) Once the conditions for oxide breakdown have been met, then localized corrosion, or pit growth, may occur at a rate that is, amongst other parameters, a function of the degree that the corrosion potential exceeds the pitting potential, and the maintenance of the aggressive environment in the growing pit (i.e., the conditions discussed in the section on crevice chemistry).



**Fig. A.14. Pitting, shown by the solid lines, and corrosion potential, ( $E_c$ ), shown by the dashed lines, for Alloy 600 in water containing chloride anions as a function of temperature. [26, 27] (© NACE International 1985)**

Although the essential controlling parameters of importance in the initiation and growth of pits are known, it is also apparent that many of these parameters are dependent on random events [28, 29] and that, therefore, there will be a distribution associated with both the stochastic [28, 29] and deterministic model [30, 31] predictions. Such effects on the variability in predictions are discussed in separate background papers [see Appendices B.15 and B.19]. Regardless of these aleatory uncertainties, the basic knowledge of the conjoint conditions for pit initiation and growth exists, thereby allowing management of potential pitting damage in LWR systems. This knowledge includes the material choice and degree of environment (water purity, flow rate) control that is needed. Prediction uncertainties arise when there are unanalyzed changes in plant configuration; an example of this might be the removal of certain insulation materials from stainless and carbon steel piping, e.g., mitigation of sump screen blockage concerns, when the chemical makeup of that insulation material (for example, silica) might be conferring pitting (and stress corrosion cracking) resistance to the piping.



## Galvanic Corrosion

Galvanic corrosion is the loss of material, generally measured as a *local* rate of loss of surface material, caused when two materials with substantially different corrosion potentials are in electrical contact in the presence of a corrosive (and electrically conductive) environment. In such cases the corrosion rate of the more active material (i.e., that with the more negative corrosion potential) is increased, with the magnitude of that increase being a function of the relative areas of the two metals, and the difference in corrosion potentials. Thus the corrosion rate of mild steel condenser tube sheets exposed to seawater may be increased by a factor of 3-7 in the area adjacent to a copper based condenser tube that is rolled into it, with the precise acceleration factor being a function of the excess area of the copper tubes. Similarly, carbon and low alloy steels in service water environments have substantially lower corrosion potentials than stainless steels and titanium alloys, and would be preferentially attacked in a galvanic couple.

As with general corrosion, galvanic corrosion is a well-understood phenomenon, being the theoretical basis for sacrificial anode protection techniques used in many industries. Consequently, although the possibility of galvanic corrosion exists, it is relatively rare in reactor service since the corrosion potentials of the various materials in the higher temperature systems are reasonably similar, and in the lower temperature systems involving large surface areas in cooling water such as condensers [32] the phenomenon is generally accounted for at the reactor design and construction stage.

## Microbiologically Influenced Corrosion (MIC)

MIC is associated with the presence and biological activity of various bacteria and fungi which, upon interaction with nutrients in the environment, produce organic acids that may lower the local pH level to 2.5 thereby increasing the metal corrosion rate (Figure A.1). The "environment" in this case may be not only untreated service water, for example, but also greases applied to external structures for general corrosion protection [33]. Damaging species other than organic acids may be formed which are specific to the bacteria and fungi microorganism [see Appendix B.16]. For instance, anaerobic sulphate-reducing bacteria (SRB) produce reduced sulphur compounds that may increase the localized corrosion rate of carbon and low-alloy steels. On the other hand, aerobic bacteria, which require oxygen for survival, are sulphate oxidizing, producing sulphuric acid, and a local increase in acidity. In addition such bacteria form slimes, which cover the metal surface, thereby creating an oxygen-starved region that allows the development of anaerobic bacteria. In such cases, biological fouling can be so severe that it not only forms corrosive crevices, but can also block flow in service water piping.

These various bacteria each have very specific conditions of survival in terms of pH, temperature, dissolved oxygen content, and supply of appropriate nutrients. From a control viewpoint, however, MIC is not expected for any extended period at temperatures above 99°C or in borated- or hydrazine treated water. For instance, treated water systems, such as PWR borated emergency core cooling systems, have operated for many years with no evidence of MIC. However, damage might be expected in cooling water and service water systems that have a flow rate low enough to ensure an adequate nutrient supply rate without physically removing the bacteria. Another process that exacerbates MIC is the intermittent flushing of water lines that are otherwise stagnant, such as fire protection lines. The periodic flushing introduces new nutrients to the stagnant lines, increasing biological activity and increasing the risk of bacteriologically induced corrosion and fouling. Consequently, MIC damage has been observed in LWR structures such as carbon and stainless steel piping and tanks, copper-nickel, stainless steel,

brass and aluminum bronze cooling water pipes and tubes, especially during construction, hydrotest and outage periods [4]. Effective control in these potentially susceptible systems is achieved by the use of biocides and controlling the nutrient supply rate.

### **Environmentally Assisted Cracking**

Environmentally assisted cracking is closely related to the principles of other localized corrosion phenomena, such as pitting, crevice corrosion and intergranular attack, and these may well act as the precursor [see Appendix B.15] to sustained crack initiation and growth when that localized corrosion process has the added contribution of tensile stress.

Environmentally assisted cracking phenomena cover a wide spectrum of degradation modes, categorized in terms of stress corrosion cracking, hydrogen embrittlement, strain-induced cracking, and corrosion fatigue. Even within these categorizations there are submodes that may be defined in terms of the morphology of cracking (e.g., transgranular, intergranular, interdendritic, granulated), the effect of specific environments (e.g., irradiation, "external, contaminated," primary-water) or subsets of an existing cracking mechanism (e.g., low-temperature crack propagation as a subset of hydrogen embrittlement). To a large extent such a confusing categorization has arisen because of the historical nature of the first laboratory and reactor observations, plus the fact that, at that time, it was not recognized that many of the cracking modes were not new mechanisms, per se, but merely associated with changes in a rate controlling parameter. For instance, as shown in Figure A.15, the subcritical crack propagation rates in stainless steels strained at various rates in oxygenated water at 288°C have a monotonic relationship with strain rate; those observed at slow strain rates, associated with creep under constant load (e.g., stress corrosion cracking), are an extension of both those observed under applied, monotonically-increasing strains (e.g., strain induced cracking), and those at even higher applied strain rates under cyclic loading (e.g., corrosion fatigue). Thus, for this system, there is no difference in the environmentally enhanced crack propagation mechanism between stress corrosion cracking, strain induced cracking and corrosion fatigue, although the sensitivity of the cracking response to e.g., environmental or material conditions may change significantly at different strain rates. Similarly the effects of irradiation on the cracking susceptibility are now recognized as merely changing the rates of various rate-controlling parameters, rather than introducing an entirely new mechanism of crack propagation.

It has long been recognized that there are three requirements for environmentally assisted cracking to occur (Figure A.16); a "susceptible" material condition, an "aggressive" environment and a tensile stress. The extent of these conjoint criterion will change with the specifics of the system but, in general, if one of these attributes is completely absent then the cracking phenomenon will not occur; this very qualitative observation was the root of many of the early mitigation actions, e.g., stress corrosion cracking in BWRs.

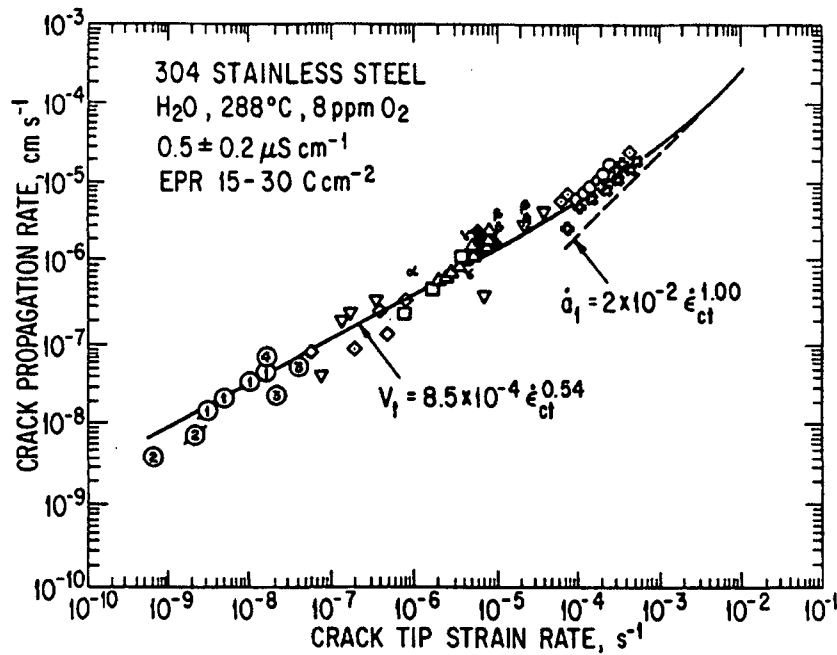


Fig. A.15. Observed and theoretical crack propagation rate vs. crack tip strain rate relationships for sensitized 304 stainless steel in oxygenated water at 288°C. (© NACE International 1990) Note that the numbered data at the lowest crack tip strain rates were obtained under constant load or displacement conditions, whereas the data marked by geometric symbols were obtained under cyclic loading. Intermediate data, identified by Greek symbols where obtained under monotonically rising “slow strain rate” conditions [34, 35]

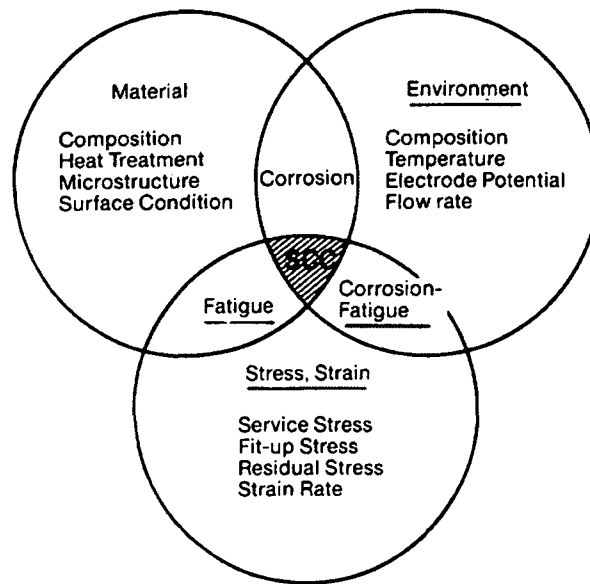


Fig. A.16. Conjoint material, stress and environment requirements for stress corrosion cracking [36] (Courtesy of Plenum Press)

The management of environmentally assisted cracking has moved in the last 25 years beyond reliance on a largely qualitative understanding of the various phenomena inherent in Figure A.16, to the development of a quantitative understanding of the multidimensional interactions between the parameters that control the cracking susceptibility, backed up by an understanding of the mechanisms of crack initiation and propagation. Such developments are central to the definition of appropriate inspection procedures. The fact that the system parameters are not always defined adequately, and the interactions between these parameters are not always well quantified or understood from a mechanistic viewpoint, are the basic reasons why stress corrosion cracking appears as a potential concern area for so many of the reactor systems in Table A.5.

The challenges in predicting the occurrence of environmentally assisted cracking were discussed in Sections 2.5 and 4.2, and several background papers in Appendix B listed below address specific issues associated with, for instance, irradiation, the overall environment, and the alloy composition:

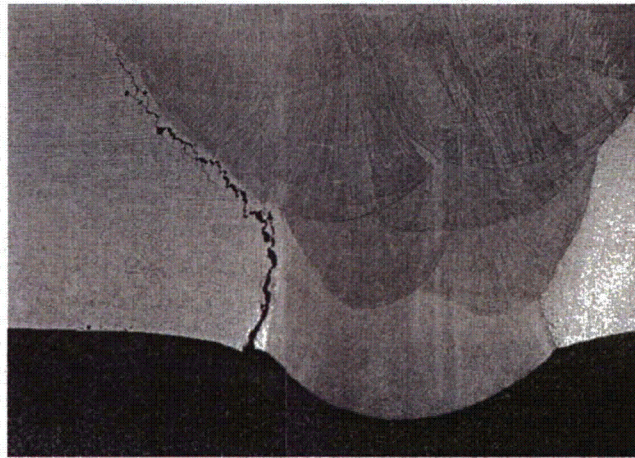
- SCC of Sensitized and Non-Sensitized Austenitic Stainless Steels and Weldments [see Appendix B.1]
- IASCC of Stainless Steels and Other Irradiation Phenomena [see Appendix B.2]
- SCC of Alloys 600, 690, 182, 152 and 52 in PWR Primary Water [see Appendix B.6]
- Corrosion of Steam Generator Tubes [see Appendix B.7]
- Stress Corrosion Cracking of Carbon and Low Alloy Steels [see Appendix B.8]
- Environmental Degradation of High Strength Materials [see Appendix B.9]
- Degradation of Fracture Resistance; Low Temperature Propagation (LTCP) in Nickel-Base Alloys [see Appendix B.13]

In many of these systems there is a considerable database to allow analysis of the effects of system variables on the cracking response. In some cases, however, there is cause for concern about the data quality (due to lack of experimental control during older data collection programs), which gives rise to excessive data variability and, therefore, uncertainty in the predictions of future behavior. In other cases the variability is to be expected due to the stochastic nature of some of the cracking phenomena [see Appendix B.7] and, in such cases, there are well-accepted data analysis techniques [see Appendix B.19] to address this. In other systems (such as stress corrosion cracking of carbon and low alloy steels [see Appendix B.8] and austenitic stainless steels under unirradiated [see Appendix B.1] and irradiated [see Appendix B.2] conditions), there is sufficient mechanistic understanding of the effects of the various system variables to give assurance that the potential cracking in the future could be mitigated. However, in other systems (such as stress corrosion cracking of some nickel base alloys in PWR primary coolant [see Appendix B.6] at operating temperatures, or under dynamic straining conditions at lower temperatures [see Appendix B.13], further development of mechanistic understanding of the cracking process will provide adequate support to data-based mitigation actions.

The following discussion presents a relatively high level treatment of some of these topics in order to provide a background to the details given in the topical reports in Appendix B. Focus is placed on certain aspects of environmentally assisted cracking which are highlighted in the PIRT panel judgments; namely changes in the morphology of cracking (transgranular vs. intergranular), the effect of environment (effects of irradiation and PWR primary water) and "new" modes of cracking (low temperature crack propagation).

### *Intergranular Stress Corrosion Cracking (IGSCC)*

IGSCC is associated particularly with the cracking of austenitic alloys used in, e.g., stainless steel piping (Figure A.17) and internals and in nickel base alloys in BWRs. The specifics of IGSCC of nickel-base alloys in PWR primary environments are discussed in a separate part of this section. Under BWR operating conditions the conjoint requirements for cracking given in Figure A.16 correspond to an environment that is oxidizing (due to an excess of radiolytically-produced oxygen or hydrogen peroxide), a microstructure that is "sensitized" (due to thermal sensitization during welding and/or stress relief heat treatment) to produce a chromium depleted region adjacent to the grain boundary, and a tensile stress associated primarily with weld residual stresses.



**Fig. A.17. IGSCC in a 400 mm (16 in.) diameter welded Type 304 pipe exposed to oxygenated water at 288°C. Note propagation adjacent to the weld heat affected zone, in a region associated with maximum grain boundary chromium depletion and weld residual tensile stress [37]**

IGSCC has been extensively researched [34,35,37,38] and is considered, at least for austenitic stainless steels and nickel-base alloys in BWRs, to proceed primarily by a slip oxidation (dissolution) mechanism [34,35], which relates the propagation rate to the continual rupture of the protective oxide at the crack tip and the associated increase in oxidation rate in this region. This process (Figure A.18) has been successfully quantified in terms of key parameters such as crack tip strain rate (i.e., a function of applied/residual stresses), corrosion potential and conductivity (i.e., functions of surface chemistry/bulk water composition) and material composition/microstructure (i.e., function of fabrication conditions).

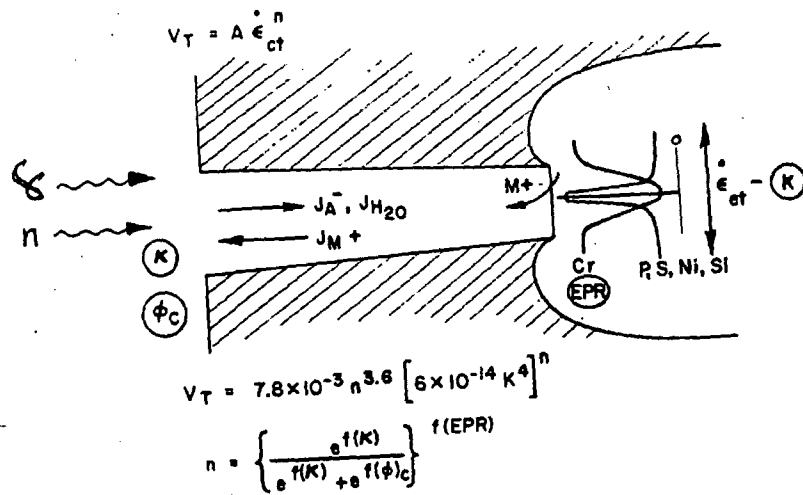


Fig. A.18. Schematic of the crack enclave and the relevant phenomena associated with the slip oxidation mechanism of crack advance. Quantification of these phenomena has led to a life prediction methodology for austenitic stainless steels and nickel-base alloys in BWRs. [34, 35]

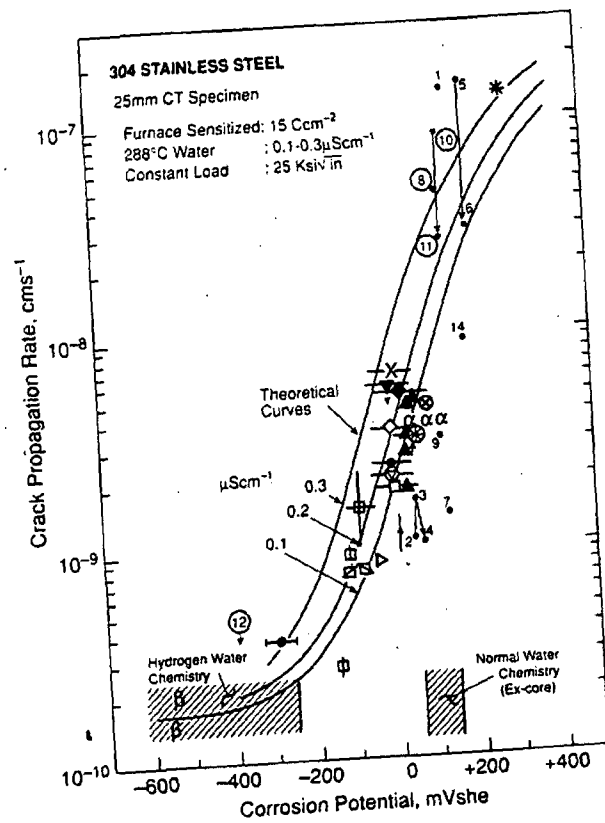


Fig. A.19. Observed and predicted dependency between crack propagation rate for sensitized stainless steel and corrosion potential. [34, 35]

Mitigation of IGSCC is focused primarily on improved coolant chemistry (e.g., hydrogen water chemistry (HWC) and dissolved impurity reduction in BWRs, [see Appendix B.10] sometimes together with surface modification of the component (e.g., Noble Metal Chemical Addition (NMCA) or zirconia coating). For instance the predicted and observed benefit of reducing the corrosion potential of sensitized stainless steel in 288°C water and consequently decreasing the stress corrosion crack propagation rate is apparent in Figure A.19. Such a mechanistic understanding and data base offers the quantitative rationale for adopting HWC and NMCA water chemistry control in BWRs. Such an understanding also explains the generally high stress corrosion resistance of stainless steels in the deaerated PWR secondary circuits where the corrosion potentials are low. Similar rationales are available to support the control of anionic impurities; especially chloride and sulphate (see Appendices B.1 and B.10).

Stress reduction has also been used extensively (e.g., weld overlays for piping and clamps for internals in BWRs, improved tube support plate structures in PWR SGs, etc.). The primary emphasis has been on significantly reducing crack growth since minor intergranular attack (IGA) of austenitic alloys, which is a common initiating precursor, is often present from fabrication, and/or cannot be prevented in operation. As indicated in Figure A.20, the quantitative understanding of the mechanism of crack propagation gives support to data-based estimates of the benefits of various mitigation actions, thereby offering assurance about successful future plant performance.

Key areas for further research include the effects of cold work (including local strain concentration in weld heat-affected zones) and the behavior of cast stainless steels and nickel-based weld metals, as well as the influence of specific, deleterious coolant impurities (e.g., lead, residues from ion exchanger resins). All of these topics are covered in greater detail in appendix B and in Section 3.3 "Generic Materials Degradation and Life Management Issues."

IGSCC of carbon and low alloy steels does not normally occur in LWR media [see Appendix B.8], but limited cracking of this type has been observed in CANDU reactors and it should also be considered a possible degradation mechanism in concentrated boric acid environments, such as might form on external surfaces following leakage of PWR primary coolant.

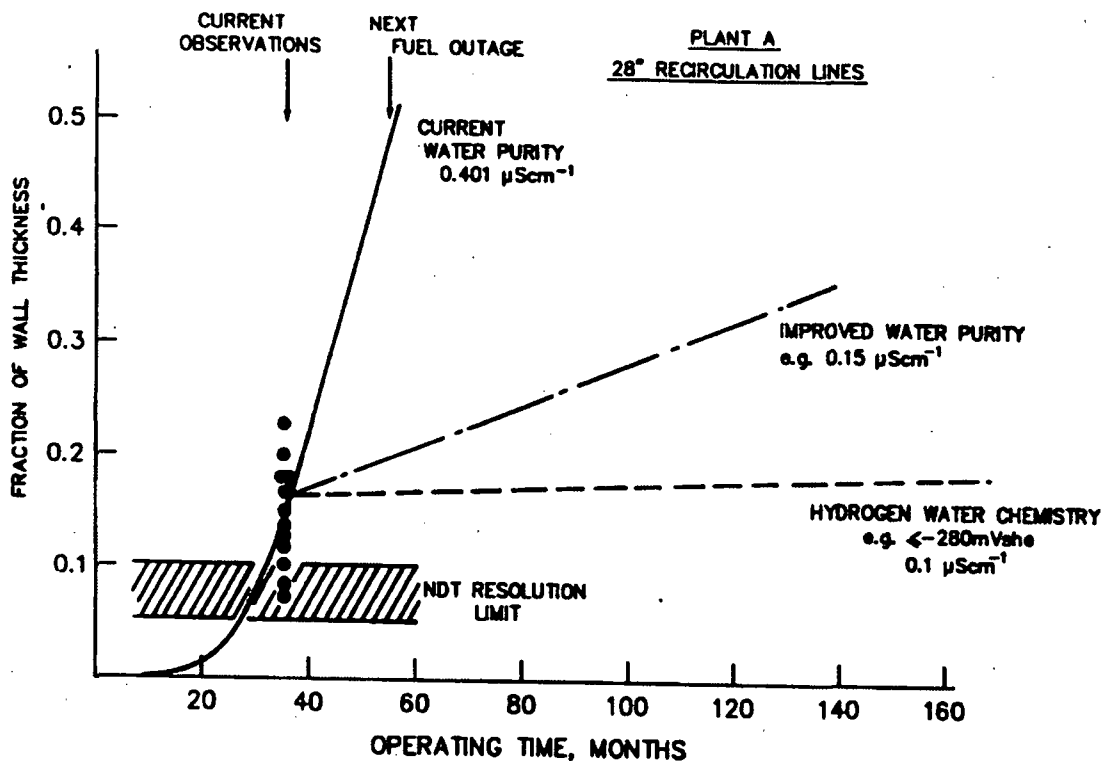
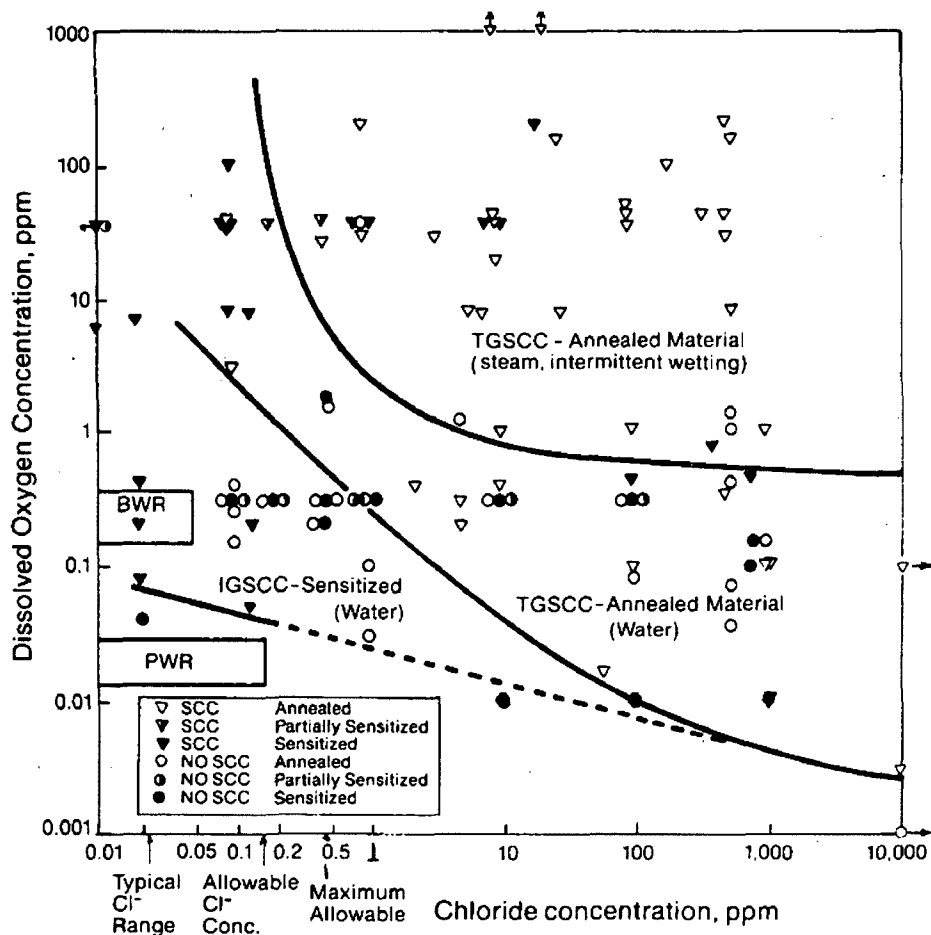


Fig. A.20. Predicted response of defected piping for defined changes in water chemistry in BWR plant. [35] (© NACE International 1990).

#### Transgranular Stress Corrosion Cracking (TGSCC)

TGSCC may be observed in solution-annealed stainless steels since there is no metallurgical feature in the grain boundary akin to grain boundary chromium depletion in the sensitized condition to concentrate the corrosion processes in that region. In such cases the extent of cracking is governed by slip features that maintain a high oxide rupture rate at the crack tip, and environmental conditions such as the corrosion potential (i.e., function of dissolved oxygen or other oxidants) and aggressive impurities (e.g., chlorides) that affect the chemistry at the crack tip (see earlier discussion on crevice chemistry). As would be expected from the discussion above on IGSCC it is possible to transition from IGSCC to TGSCC morphologies depending on the materials' degree of sensitization, slip characteristics (i.e., function of yield stress or degree of cold work) and dissolved oxygen/chloride content. An example of such transitions is shown in Figure A.21. It is apparent that TGSCC would not be expected to be a common phenomenon under normal BWR and PWR water chemistry regimes. However, as pointed out in the main report, such TGSCC incidences may become of importance for stainless steels, especially if the surface is highly cold worked, or on external component surfaces which may be contaminated with chloride deposits, or, in dead legs (e.g., for CRDMs and canopy seals in PWRs.) where impurities cannot be dispersed.





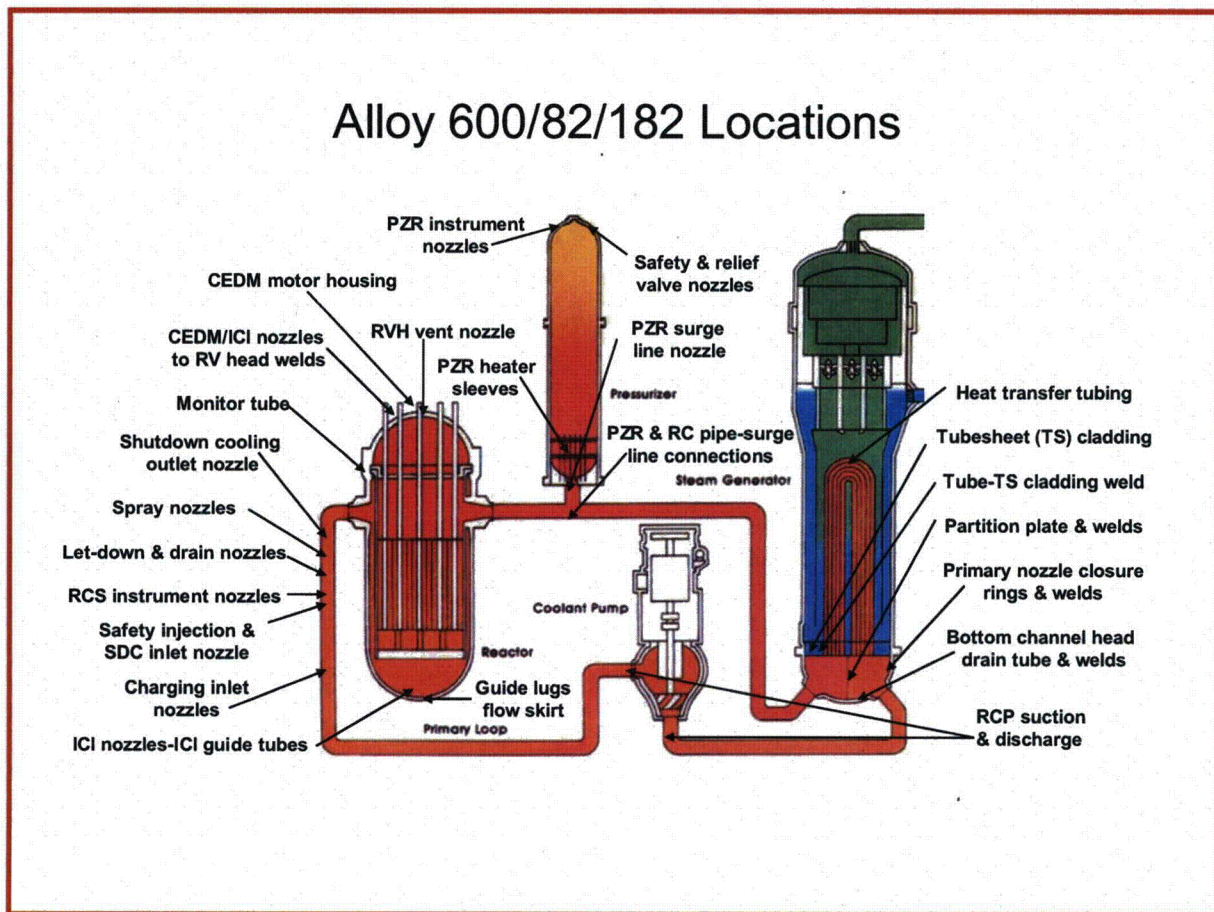
**Fig. A.21. Effect of oxygen and chloride concentration on the SCC of austenitic stainless steels in 250-350°C water, together with the oxygen/chloride ranges in BWR and PWR environments. [38] (© NACE International 1980)**

As discussed in Appendix B-8, although the ferritic carbon and low alloy steels are regarded as resistant to SCC under well controlled LWR operating conditions [see Appendix B.6], limited TGSCC has been observed, e.g., in SG shells exposed to faulted secondary water, and in BWR components subjected to high, local loads while operating with normal (oxygenated) water chemistry. Recent research suggests that occasional susceptibility may also be related to chloride chemical transients and changes in the deformation behavior of particular low alloy steels associated with the dynamic strain aging which can occur at intermediate operating temperatures.

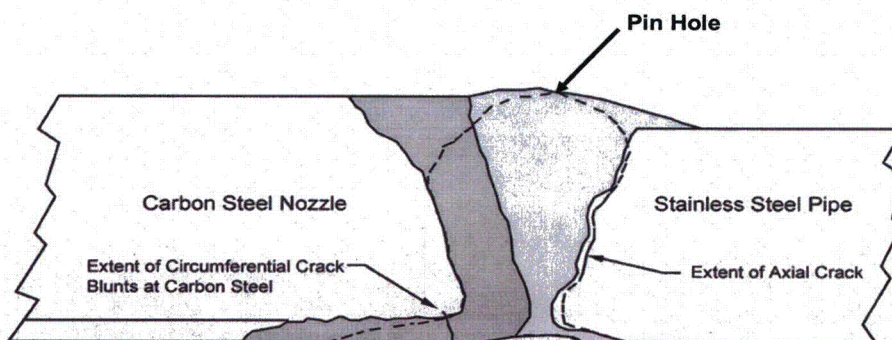
#### *Primary Water Stress Corrosion Cracking (PWSCC)*

PWSCC refers to intergranular cracking of any material, but particularly of Ni- base alloys such as Alloy 600 and its weld metals, Alloys 182 and 82, in PWR primary coolant (i.e., containing lithium, boric acid, and hydrogen). Figure A.22 illustrates the main locations where PWSCC has occurred [see Appendix B.6], whereas the schematic drawing in Figure A.23 illustrates the relationship between the shape of the axial crack in the Alloy 82/182 weld and Alloy 182 butter and the dissimilar metal low-alloy steel and stainless steel components.

## Alloy 600/82/182 Locations



**Fig. A.22. Regions in the PWR Primary Reactor Coolant System where PWSCC of nickel base alloys have been observed.**



**Fig. A.23. Schematic diagram illustrating the locus of an axial PWSCC crack front in the Alloy 82/182 weld between dissimilar alloy carbon and stainless steel components.**

Over the last thirty years, intergranular stress corrosion cracking in PWR primary water (PWSCC) has been observed in numerous components made of these nickel-base alloys sometimes after relatively long incubation times. In stark contrast to IGSCC of Ni-base alloys in other media (e.g., on the PWR secondary side) or austenitic alloys in BWRs discussed above, sensitization of the material through intergranular precipitation of chromium-containing carbides is beneficial to the PWSCC resistance of Alloy 600, which justifies its consideration in a separate category of cracking mechanism. However, large variations exist in the susceptibility of individual heats of material, even of nominally similar composition and thermomechanical processing history, so that prediction of service behavior is difficult. Cold work is highly detrimental, in agreement with observations in many other stress corrosion alloy/environment systems in LWRs.

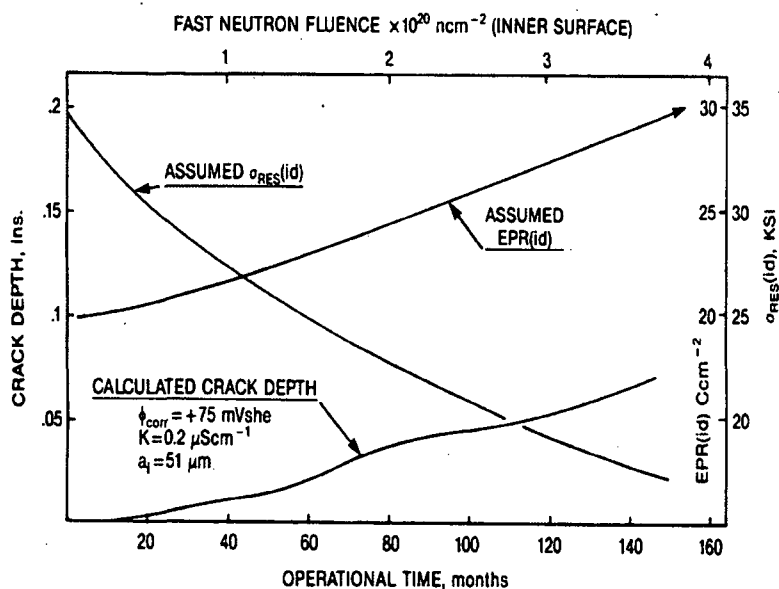
Cracking, which can also occur in pure hydrogenated water or steam, is highly temperature-dependent and is associated with environmental conditions under which the surface films are in the transition region of Ni/NiO stability. Despite intensive research, there is no general agreement on the mechanism of PWSCC. Candidate theories include hydrogen assisted cracking, slip oxidation, thermally activated dislocation creep and internal oxidation. The latter has a particular attraction, since it could explain the very long times (>100,000 hours) sometimes necessary for cracking to initiate, even under conditions where subsequent crack propagation is relatively rapid. PWSCC of weld metals (and its possible interaction with fabrication defects such as hot cracking) is currently a high-profile topic that has been insufficiently studied and is not well understood.

To date, mitigation of PWSCC has usually involved repair and replacement actions using more resistant materials (such as Alloy 690). In addition, increased attention is now being paid to possible mitigation measures involving surface treatment (e.g., water-jet peening), chemistry optimization (e.g., adjustment of hydrogen levels and/or addition of potentially inhibiting species such as zinc), and various mechanical options to achieve a reduction in tensile stress levels.

#### *Irradiation Assisted Stress Corrosion Cracking (IASCC)*

The SCC behavior of irradiated stainless steels is a natural extension of IGSCC of un-irradiated stainless steel [see Appendix B.2], but the critical fluence level above which irradiation effects begin to dominate material behavior is hard to define because of the interactions of several material, stress and environmental factors. A lower value of  $\sim 5 \times 10^{20}$  n/cm<sup>2</sup> is often quoted for BWR internals, with saturation of the irradiation effects beginning at around  $3 \times 10^{21}$  n/cm<sup>2</sup>, i.e., shortly before the expected end-of-life (EOL) fluence of  $\sim 8 \times 10^{21}$  n/cm<sup>2</sup>. In contrast, IASCC in the very different primary water chemistry in PWRs has only been observed (e.g., in baffle/former bolts) to start after reaching a fluence of  $\sim 2 \times 10^{21}$  n/cm<sup>2</sup> and little information is available about expected behavior near the much higher EOL fluence values typical of PWRs.

The mechanism of IASCC in PWR primary water is currently unclear, with no evidence that locally oxidizing conditions, grain boundary segregation, helium formation, or hydrogen embrittlement play a major role, although high strength from irradiation hardening does appear to be important (possibly analogous to the effects of cold work in SCC without irradiation). Mitigation measures are not yet available.



**Fig. A.24. Calculated change in crack depth in irradiated stainless steel as a function of fluence (e.g., time) due to specified changes in residual stress and degree of grain boundary sensitization. [see Appendix B.2]**

By contrast, the mechanistic understanding of the roles that irradiation has on stress corrosion cracking of stainless steel core components in BWRs, and its relationship to the cracking that occurs in thermally sensitized microstructures, is relatively advanced [see Appendix B.2] and this has an impact on the judgments of the future IGSCC/IASCC performance of such components. For instance, apart from its role in reducing fracture toughness, irradiation in BWRs is best viewed as an accelerant of many of the features shown schematically in Figure A.19. For instance, fast neutron irradiation increases the extent of grain boundary chromium depletion, it affects the crack tip strain rate through both irradiation induced hardening and relaxation of the residual stresses and, finally there is an elevation of corrosion potential. Such interacting irradiation effects affect the IASCC cracking kinetics in a sometimes non-monotonic fashion, as illustrated in Figure A.24.

Mitigation of IASCC in BWRs is focused primarily on reductions in corrosion potential through the use of HWC/NMCA, and the improvement in water purity, i.e., an extension of the approaches already taken for IGSCC.

#### *Low-temperature Crack Propagation (LTCP)*

LTCP refers both to high sub-critical crack growth rates (i.e., SCC, most likely from hydrogen assisted cracking) and to reduced fracture toughness [see Appendix B.13]. Such degradation has been observed in laboratory tests on nickel-base alloys under very specific conditions of temperature, strain rate and the extent of hydrogenation, and is of potential concern in PWR primary systems operating under very limited conditions. While the greatest concerns are for higher strength Ni alloys (e.g., Alloy X750 and Alloy 182/82 weld metals), there are possible concerns for base metals (such as Alloy 600 or 690), particularly (but not only) if the yield strength is elevated (e.g., from cold work or irradiation).

Initial studies in the 1980s [ 39, 40 ] showed very rapid crack propagation in the temperature range 70-140°C in moderate to high strength Ni base alloys once IG SCC cracks had formed in high temperature water. The highest rates were observed in Alloy X750, although large effects were also observed for Alloy 182 and 82 weld metals and other Ni base alloys (e.g., aged Alloy 625, Alloy 718, and Alloy 690). The observations occurred in constant displacement (wedge/bolt loaded) specimens, in actively loaded specimens, and also in specimens exposed only to gaseous hydrogen in this temperature regime (leading to the reasonable conclusion that it's a hydrogen related phenomenon). . More recently, it has been observed that significant reduction in fracture toughness (e.g., in J-R tests) can occur in the same temperature regime, under very specific loading rates.

The fact that these degradation effects are only observed when the specimens have been exposed to hydrogen (e.g., hydrogenated water) above a specific level strongly implies that the mechanism of both embrittlement and increased subcritical crack propagation is related to hydrogen embrittlement. However, the exact mechanism is unknown, and the conjunction between the PWR plant operations and the observed requirements of temperature, alloy content and microstructure, and strain rate for these degradation phenomena to become significant, is the object of high priority studies.

#### **A.4.3 Under-clad Cracking and Clad Disbonding**

Three types of cracking have been recognized as potentially affecting the heat affected zones of bimetallic joints such as those made between low alloy reactor pressure vessel steels and overlay cladding of austenitic stainless steel: hot cracking (sometimes called liquation cracking), reheat cracking and cold cracking.

Hot cracking usually arises from a combination of the formation of a liquid metal phase at grain or dendrite boundaries at very high temperatures during welding and the contraction forces that develop during cooling of the weld pool. Due to the high temperature necessary for such cracking, it is only encountered in the deposited weld metal or very close to the fusion line. Under-clad cracks of this type are therefore <1 mm in depth below the cladding. They are rarely found when cladding low alloy steel and do not lead to clad disbonding.

Reheat cracking [41] occurs as a result of a creep mechanism during stress relief heat treatments at temperatures in excess of 550°C. In practice, the low alloy pressure vessel steels used in the nuclear industry are relatively insensitive to this form of cracking except in zones of elemental segregation (C, Mn, Mo, S, and P). When observed, the cracks are perpendicular to the fusion line, less than 4 mm in height, and are situated exclusively in zones of large grains that may be formed in the heat affected zone where two successive weld beads overlap. The large grain zones have reduced ductility that allows intergranular cracking to develop under the influence of the stresses arising from the difference in coefficients of thermal expansion of austenitic and ferritic steels. Creep cavities are easily seen on the intergranular facets generated by reheat cracking. This cracking phenomenon is avoided by adjusting the welding procedures to avoid the development of large grain heat affected zones.

Cold cracking [42-44] is caused by the combined action of residual welding stress and hydrogen introduced into the substrate low alloy steel during welding. Three factors are associated with the appearance of this cracking: a mixed martensitic-bainitic microstructure in the heat affected zone of the low alloy steel; residual welding stress (that typically reaches a maximum 5 to 10 mm from the fusion line); high concentrations of hydrogen in the low alloy steel heat affected zone after welding (with up to 15 ppm in the austenitic weld deposit) compared to <0.2 ppm in

the base material before welding. The hydrogen originates from moisture absorbed by the coating of weld electrodes or by the flux used for strip cladding. Hydrogen diffuses into the substrate low alloy steel heat affected zone where it may reach temporarily 10 ppm while the temperature is high enough for the metal to be austenitic. The susceptibility of the heat affected zone is enhanced by the presence of zones of elemental segregation (C, Mn, Mo, S, P), particularly in large forgings. The cracks have a mixed intergranular and transgranular quasi-cleavage morphology. Usually, due to constraint, the cracks are orientated perpendicular to the fusion line with defect heights typically up to 7 mm, exceptionally up to 12 mm. In some special cases, (e.g., welding on a re-entrant angle, which leads to stresses perpendicular to the interface, and in the presence of a hard zone with precipitates at the fusion boundary), cracking may take place parallel to the fusion line and lead to clad disbonding. The main remedies are to ensure adequate preheat, interpass and post weld soak temperatures that allow the hydrogen to diffuse away prior to stress relief, to keep welding consumables as dry as possible, and to avoid as much as possible weld cladding the most segregated zones of low alloy steel forgings.

#### **A.4.4 Fatigue**

This section addresses materials degradation due to fatigue, an aging degradation mechanism that can affect a number of major components throughout the primary pressure boundary of both PWRs and BWRs. [see Appendix B.14]. Components that may be affected range from the low alloy steel reactor pressure vessel, pressurizer, and steam generator shell to stainless steel pumps, piping etc. to nickel base alloy welds, tubing, etc. This degradation mode is an extremely well researched topic, fatigue being, unlike many of the other degradation modes, considered in the original reactor design basis.

From a categorization viewpoint, fatigue may be regarded in terms of "High Cycle Fatigue," "Low Cycle Fatigue," "Thermal Fatigue" and "Environmental (or Corrosion) Fatigue." Superimposed upon these categorizations is the (sometimes semantic) division of degradation periods between "initiation" and "propagation." Some of these categorizations and environmental impacts may be understood in relationship to Figures A.25 (a) and (b). At the reactor design stage the fatigue life, which forms part of the design basis, is calculated from a stress-amplitude vs. fatigue cycle database that relates to the curves in Figures A.25a and A.25b marked "air." These curves (in this example for carbon steel) are based on data obtained in air at 25°C for smooth cylindrical specimens, fully reversed cyclically loaded under strain control; "initiation" in this case is defined as a drop in maximum load by 25%, which physically corresponds to a crack of 2-3 mm depth.

The categorization of "high-cycle fatigue" refers to a high number of cycles at a relatively low stress amplitude (typically below the material's yield strength but above the fatigue endurance limit of the material), with the driving force for the cyclic loading coming from, for instance, flow induced vibrations and/or instabilities in thermal mixing of the coolant. On the other hand "low-cycle fatigue" refers to the higher stress/strain amplitude regime, where the local yield stress may be exceeded leading to correspondingly shorter fatigue lives; such a regime is associated with, for instance, lower frequency operational transients (such as plant start-up/shut-down or hot stand-by). "Thermal fatigue" is due to cyclic stresses/strains that result due to changing temperature conditions in a component or in the piping attached to the component. Thermal fatigue may involve a relatively low number of cycles at a higher stress (e.g., plant operational cycles or injection of cold water into a hot nozzle) or due to a high number of cycles at low stress amplitude (e.g., local leakage effects or cyclic thermal stratification).

Design against fatigue damage is based primarily on the fatigue curves in Section III, Appendix I of the ASME Code. In this design process, the fatigue cycles are decreased from those denoted by the "air" data lines in Figure A.25, in order to take into account the unknown (at that time) effects of a) materials variability and data scatter, b) component size, and c) surface roughness. The extent of this decrease was based on engineering judgment and, as indicated in Figure A.25b, the "design curve" is displaced from the data curve by a factor of two (on stress/strain amplitude) or 20 (on fatigue cycles), whichever was the more conservative. It is this design curve that the fatigue "Cumulative Usage Factors" (CUF) are calculated during the design process aimed at maintaining CUF below 1 through the design life of the component. As discussed in Appendix B.14, there is much discussion internationally about the appropriateness of this "2 and 20" design line, especially when environmental effects need to be accounted for [45-50].

This concern for the effect of the environment on crack initiation is discussed in Appendix B.14, but the essence is illustrated in Figure A.25 for the specific case of carbon steel in LWR environments. It has been demonstrated in several studies that the decrease in the fatigue life below that observed in dry air is a function of the strain rate applied during the loading period, corrosion potential, temperature, and water purity. To a large extent these dependencies are predictable via the knowledge of the environmentally assisted cracking mechanisms discussed earlier [45]. Moreover similar dependencies are observed for most of the ferritic and austenitic alloys in LWRs and as indicated in Figure A.25 (b) for carbon steel piping there are combinations of these system parameters that lead to fatigue lives that are less than the currently accepted design values.

As also discussed in Appendix B.14, there are similar concerns about the effect of the environment on the fatigue crack propagation rates that are used for crack disposition decisions according to ASME XI procedures. In this case significant progress has been made, for the specific case of LAS in PWR reactor water through the introduction of Code Case N-643 [51], which is currently undergoing further refinement.

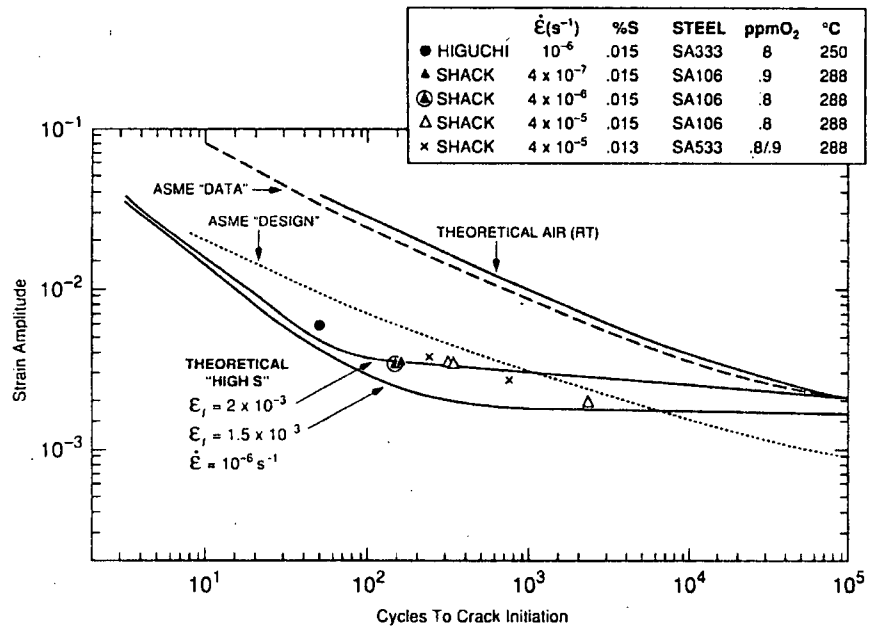
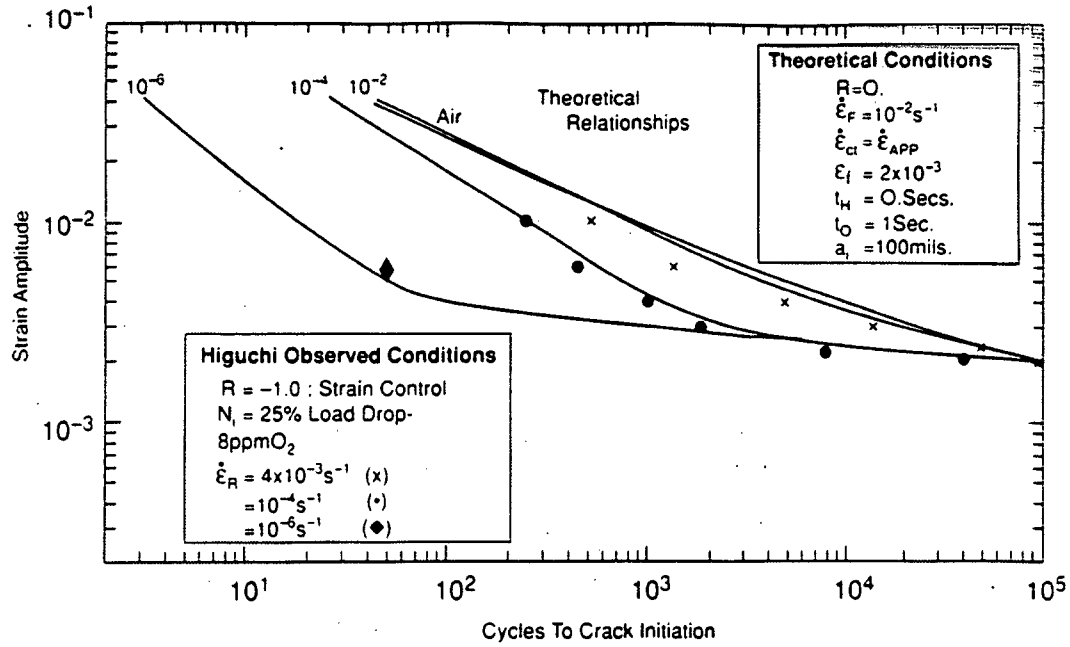


Fig. A.25. (a) Predicted [45] and observed [46] strain amplitude versus cycles to crack initiation relationships for unnotched carbon steel in 288°C, 8 ppm oxygenated water with strain applied at different rates. (b) Predicted [45] and observed [46,47] strain amplitude versus cycles to crack initiation relationships for unnotched carbon and low alloy steels in 288°C water, under the worst combination of material and environmental conditions. (Reprinted with Permission from TMS) Note the non-conservatism of the ASME III design curve under these conditions at certain strain amplitudes



#### **A.4.5 Loss of Fracture Resistance**

This section addresses material degradation mechanisms that lead to a reduction in the fracture toughness of the material with increasing time. Because a high level of fracture toughness is a design assumption for the LWR pressure boundary and internal components, degradation mechanisms that lead to reductions of toughness are of high significance.

Two distinct degradation mechanisms, which are relevant to many of the materials of LWR construction, are addressed in this section, radiation embrittlement and thermal aging. In some cases, arguments have been made for synergistic effects between the two degradation modes. An example of this, identified by the NRC in Safety Evaluation Reports, would be cast austenitic alloys in PWRs. To date, however, no data have been presented to prove or disprove the existence of such synergistic effects.

A third loss of fracture resistance issue, associated with some nickel-base alloys after having been exposed to hydrogenated water, and tested at specific loading rates in a specific temperature range was discussed previously in this Appendix, and this is discussed in more detail in Appendix B.13.

#### **Irradiation Effects**

- Neutron Embrittlement

Radiation embrittlement results in an increase in the material's yield and ultimate strengths, with a corresponding decrease in material ductility and resistance to flaw propagation (fracture toughness). Radiation embrittlement in ferritic steels is measured by an increase in the ductile-to-brittle transition temperature ( $RT_{NDT}$ ) and a drop in the Charpy upper shelf energy. Embrittlement in ferritic steels is primarily caused by the formation of copper-rich precipitates that harden the matrix and reduce toughness. Neutron irradiation enhances the formation of these precipitates.

Extensive databases exist for evaluating and predicting embrittlement in reactor vessel steels. These data are obtained from vessel material surveillance capsules in both PWR and BWR vessels, and from test reactors. Embrittlement trend curve models given in various literature citations such as Regulatory Guide 1.99, Rev. 2 are used to predict the shift in  $RT_{NDT}$  and drop in upper shelf energy as a function of copper, nickel, and fluence.

Significant variations in radiation embrittlement have also been observed between different types of steel (carbon and low alloy steels, etc.) and even between different heats of the same steel. These differences are caused by variations in metallurgical structure and composition. Improved empirical trend models have recently been developed to describe the combined effects of copper, nickel, phosphorus, irradiation temperature, and neutron flux and fluence on the embrittlement of pressure vessel steels. Steels with a very low copper content show little embrittlement in spite of high radiation doses. The effect of irradiation exposure at low temperatures (below 525°F) increases the rate of embrittlement damage. Weld metal is generally more sensitive to radiation embrittlement than base metal. Impurity chemistry, chemistry variability, and different micro-structure are responsible for the greater sensitivity of the weld metal. In 2002, this improved trend curve model was approved in a revision to ASTM Standard Guide E900.

Stainless steels are also affected by irradiation exposure [see Appendix B.2], but do not exhibit

a ductile-to-brittle transition. In stainless steels, reduction in the ductile fracture toughness properties is associated with microstructural changes resulting from the effects of neutron/atom interactions. Neutrons interact with atoms in the crystal lattice, both directly and indirectly, to displace atoms in the lattice and alter material properties through formation of dislocations, interstitials, and vacancies. Segregation of material impurities also occurs.

Data are available from austenitic stainless steel components exposed to neutron irradiation in experimental and thermal reactors. They show that significant reductions in material J-integral values and tearing modulus values appear at approximately one displacement per atom (dpa). Reductions in these fracture toughness properties appear to saturate at fast neutron exposures greater than 10 dpa.

Currently, there is a lack of substantive fracture toughness data for austenitic stainless steels exposed to a neutron fluence exceeding  $\sim 10^{21}$  n/cm<sup>2</sup> in an LWR environment. The bulk of existing data are developed from materials irradiated in experimental reactors. Differences in neutron spectra of experimental reactors and light water reactors could result in actual material property changes. Specific data regarding irradiation exposure of cast stainless steels in an LWR environment are particularly limited.

- Void Swelling Effects

Void formation is a mechanism in which radiation-induced vacancies accumulate in metal to form microscopic voids. If a large number of voids form, termed void swelling, dimensional changes can occur and loads at connection points (for example, at bolted or welded joints of structural members) may also be altered. Thus void swelling could potentially affect the intended functionality of certain component(s). Based on available fast-reactor data, significant fracture toughness reduction of stainless steels can also occur if void swelling is large (i.e., greater than several percent).

### **Thermal Aging**

Thermal aging [see Appendix B-4] of the duplex austenite/ferrite structures of cast austenitic stainless steels (CASS) has been shown to cause precipitation of additional phases in the ferrite such as formation of a  $\alpha$  phase by spinoidal decomposition, nucleation and growth of a  $\alpha$  phase, or nucleation and growth of carbides at the ferrite/austenite phase boundaries. Development of these additional phases results in an increase in hardness and yield strength of the casting, with a corresponding reduction in fracture toughness properties. As a result, the component becomes more susceptible to brittle fracture when sufficient tensile loadings are present to drive crack growth. A brittle fracture occurs when the ferrite phase becomes continuous or the ferrite/austenite phase boundary provides an easy path for crack propagation in the presence of an existing flaw and sufficient stresses. This type of failure is due to cleavage of the ferrite or separation of the ferrite/austenite boundary and is termed "channel fracture."

The effects of thermal aging on casting fracture toughness have been shown to saturate once conditions leading to predominantly brittle fracture occur. This saturation effect is associated with development of channel fracture conditions. While the extent of reductions in casting fracture toughness due to thermal aging is related to operating temperature, time at temperature, casting method (static vs. centrifugal), and material composition (molybdenum and ferrite content), available research results indicate that the saturation fracture toughness ( $C_{vsat}$ ) can be correlated to casting chemical composition, material properties and the casting method. The actual casting toughness decreases logarithmically with increased operating time toward this "infinite-time" saturation value; thus the use of  $C_{vsat}$  as a measure of casting fracture toughness is conservative.

Thermal aging embrittlement of materials other than CASS used in reactor components includes (1) temper embrittlement and (2) strain aging embrittlement. Ferritic and low alloy steels are subject to both of these degradation mechanisms but wrought stainless steels are not affected by either mechanism.

Temper embrittlement of low alloy steels is caused by the diffusion and segregation of impurity elements, such as phosphorous, tin, antimony and arsenic, into the grain boundaries after prolonged exposure to temperatures in the range 350°C (662°F) to 575°C (1067°F). At temperatures above this range, the impurities tend toward solution in the ferrite matrix. For example, little or no grain boundary segregation is observed at temperatures above 625°C (1157°F). At temperatures below this range, very long exposure times are necessary for the impurities to diffuse to, and segregate in, the grain boundaries. The presence of carbon tends to accelerate the embrittlement process, due to preferential segregation of the impurities at the interface between grain boundary carbides and ferrite grains. The role of other alloying elements, such as chromium, nickel, magnesium, and molybdenum, in the acceleration or retardation of the temper embrittlement process has been studied extensively. The principal manifestation of temper embrittlement in low alloy steels is an increase in ductile-to-brittle transition temperature, due to the change from predominantly cleavage fracture (before temper embrittlement) to predominantly intergranular fracture along impurity segregation paths (after temper embrittlement).

Strain aging embrittlement occurs in cold worked ferritic steels when they are subjected to temperatures in the range of 260-371°C (500-700°F), and is caused by the pinning of dislocations by interstitial impurities (nitrogen, carbon, etc.). Post-weld heat treatment of reactor vessel components following cold working during fabrication mitigates, but does not eliminate, the effects of strain aging embrittlement. However, following post-weld heat treatment, residual strain aging embrittlement has only a slight effect on the ductility and fracture toughness of LWR vessel component materials under the environmental and loading conditions of interest.

## A.5 References

- [1] "Corrosion," Vol. 13, Metals Handbook, ASM International, 1987.
- [2] "Uhlig's Corrosion Handbook," Ed R.W. Revie, J. Wiley and Sons, Inc, 2<sup>nd</sup> Edition, 2000.
- [3] "Corrosion," Ed. L.L. Shrier, R.A. Jarman & G.T. Burstein, Butterworth-Heinemann Ltd, 3<sup>rd</sup> Edition, 1994.
- [4] D.A. Jones, "Principles and Prevention of Corrosion," Prentice Hall, 2<sup>nd</sup> Edition, 1996.
- [5] D.D. Macdonald, G.A. Cragnolino, "Corrosion of Steam Cycle Materials," Chapter 9 in "The ASME Handbook on Water Technology for Thermal Power Systems," Ed. Paul Cohen, Pub. ASME, 1989.
- [6] M.G. Fontana, "Corrosion Engineering," Pub McGraw Hill, New York, 3<sup>rd</sup> Edition, 1986.
- [7] M. Pourbaix, "Atlas of Electrochemical Equilibria in Aqueous Solutions," Ed. NACE, 1974.
- [8] Z. Szklarska-Smialowska, "Pitting Corrosion of Metals," Pub NACE, 1986.
- [9] G.M.W. Mann, "History and Causes of on-Load Waterside Corrosion," Br. Corrosion Journal, 1, pp. 6-14, 1977.
- [10] B.M. Gordon, et al., "Mitigation of Stress Corrosion Cracking through Suppression of Radiolytic Oxygen," Proceedings of First International Symposium on Environmental Degradation in Nuclear Power Systems – Water Reactors. Myrtle Beach August 22-25, 1983.
- [11] S. Hettiarachchi, "NobleChem from Concept to Operating Commercial Power Plant Application." Proceedings of Tenth International Conference on Environmental Degradation in Nuclear Power Systems – Water Reactors, Eds. F.P. Ford, G. Was, National Association of Corrosion Engineers, Lake Tahoe, August 5-9, 2001.
- [12] E.G. Brush, W.L. Pearl, "Corrosion and Corrosion Product Release in Neutral Feedwater," *Corrosion*, Vol. 28, No. 4, pp. 129-136, 1972.
- [13] R.K. Freier, "Operating Experiences with Protective Layers of Metal Oxides, Using Addition of Oxygen," *Vom Wasser*, 38, Ed. Verlag Chemie GmbH, Weinheim, Bergstr., 1971.
- [14] "Boric Acid Corrosion of Carbon Steel Reactor Pressure Boundary Components in PWR Plants," NRC Generic letter 88-05, March 17, 1988.
- [15] "Boric Acid Corrosion Guidebook." EPRI Report 1000975, Electric Power Research Institute, 2001.
- [16] L. Tomlinson, "Mechanism of Corrosion of Carbon and Low Alloy Steels by High Temperature Water," *Corrosion*, 37, pp. 591-596, 1981.
- [17] C. Czajkowski, "Metallurgical Evaluation of an 18 inch Feedwater Line Failure at the Surry Unit 2 Power Station," NUREG/CR-4868, Brookhaven Nat. Lab., March 1987.
- [18] B. Chexal, et al., "Flow Accelerated Corrosion in Power Plants," EPRI Report TR-106611, Electric Power Research Institute, June 1996.
- [19] "CHECWORKS™ Computer Program Users Guide." EPRI Report TR103198-P, June 1998.
- [20] G.J. Bignold, K. Garbett, I.S Woolsey, "Mechanistic Aspects of the Temperature Dependence of Erosion – Corrosion," Proceedings of Conference "Corrosion Erosion of Steels in High Temperature Water and Wet Steam," Eds. Ph Berge, F. Kahn, Electricite de France, May 1982.
- [21] Conference on "Localized Corrosion," Dec 6-10, 1971, Williamsburg, Ed. B.F. Brown, J. Kruger, R.W. Staehle, NACE, 1974.
- [22] "Localized Corrosion-Cause of Metal Failure," ASTM STP 516, 1972.
- [23] R.W. Staehle, "Bases for Predicting the Earliest Penetrations due to Stress Corrosion Cracking for Alloy 600 on the Secondary Side of PWR Steam Generators," NUREG/CR-6737, U.S. Nuclear Regulatory Commission, 2001.
- [24] Kolotyrkin, Ya. M., "Pitting Corrosion of Metals," *Corrosion*, 19, 8, pp. 261t-268t, 1963.

- [25] Z. Szklarska-Smialowska, "Review of Literature on Pitting Corrosion Published since 1960," *Corrosion*, 27, pp.223-233, 1971.
- [26] M. Karaminezhaad-Ranjbar, J. Mankowski, D.D Macdonald, "Pitting Corrosion of Inconel 600 in High Temperature Chloride Solution under Controlled Hydrodynamic Conditions," *Corrosion*, 41, 4, pp.197-204, 1985.
- [27] J.R. Park, Z. Szklarska-Smialowska, "Pitting Corrosion of Inconel 600 in High Temperature Water Containing  $\text{CuCl}_2$ ," *Corrosion*, 41, 11, pp.665-675, 1985.
- [28] T. Shibata, H. Takamiya, "Effect of pH and  $\text{Cl}^-$  on the Stochastic Process of Pitting Corrosion of Mo Containing Stainless Steels," in Proceedings of "Critical Issues in Reducing the Corrosion of Steels," Ed. H. Leidheiser and S. Haruyama. USA-Japan Seminar Nillo Japan, 1985.
- [29] T. Shibata, T. Takeyama, "Stochastic Theory of Pitting Corrosion," *Corrosion*, 33, 243, 1977.
- [30] D.D. Macdonald, M. Urquidi-Macdonald, "Distribution Functions for the Initiation of Pitting Attack on Passive Alloys," *Ind. J. Technology*, 24, 485, 1986.
- [31] D.D. Macdonald, M. Urquidi-Macdonald, "Distribution Functions for the Breakdown of Passive Films," *Electrochimica Acta*, 31, 1079, 1987.
- [32] J.A. Beavers, et. al., "Corrosion Related Failures in Power Plant Generators," EPRI Report NP-1468, Electric Power Research Institute, 1980.
- [33] R.W. Staehle, B.J. Little, "Corrosion and Stress Corrosion Cracking of Post Tension Cables Associated with Funfal Action," *Corrosion*, 2002, April 7-11, 2002.
- [34] F.P. Ford, et al., "Corrosion-Assisted Cracking of Stainless Steel & Low-Alloy Steels in LWR Environments," Report NP5064S, Electric Power Research Institute, February 1987.
- [35] F.P. Ford, "The Crack Tip System & it's Relevance to the Prediction of Cracking in Aqueous Environments" Proceedings of First International Conference on Environmentally Assisted Cracking of Metals, pp.139-165. Eds. R. Gangloff & B. Ives, NACE, October 2-7, 1988.
- [36] M.O. Speidel, "Stress Corrosion Cracking and Corrosion Fatigue-Fracture Mechanics," in "Corrosion in Power Generating Equipment," Eds, M.O. Speidel, A. Atrens, Pub. Plenum Press, NY, 1984.
- [37] B.M. Gordon, G.M. Gordon, "Corrosion in Boiling Water Reactors." ASM Handbook Corrosion Vol 13, pp 929, 937, 1987.
- [38] B.M. Gordon, "The Effect of Chloride and Oxygen on the Stress Corrosion Cracking of Stainless Steels; Review of Literature," *Materials Performance*, 19, pp.29-38, 1980.
- [39] C.A. Grove, L.D. Petzold, "Mechanism of SCC of Alloy X750 in High Purity Water," *J. of Materials for Energy Systems*, 7, No. 2, p.147-162, Sept. 1985.
- [40] L.D. Petzold, C.A. Grove, "Mechanism of SCC of Alloy X750 in High Purity Water," Proc. of Corrosion of Nickel Alloys, Ed. R.C. Scarberry, ASM, 1985.
- [41] A. Dhooge, et al., "A Review Of Work Related To Reheat Cracking In Nuclear Reactor Pressure Vessel Steels," *Int. J. Pre. Ves. & Piping*, 6, pp 329-409, 1978.
- [42] F. Faure, et al., "Modified Implant Test For Studying Cold Cracking Sensitivity Of Interfaces Between Stainless Steel And Ferritic Steels," 4th Int. Conf. on Welding in the Nuclear Industry, Aix La Chapelle, November 1982.
- [43] M. Fondeviolle, A. Vignes, "Technology Of Joining The Dissimilar Metals Austenitic Stainless Steel Or Nicrfe Alloy To 20M5M Or 16MND5 Steels," 4th Int. Conf. on Welding in the Nuclear Industry, Aix La Chapelle, November 1982.
- [44] C.G. Interrante, G. M. Pressouyre in 'Disbonding Session', Proceedings of 1st Int. Conf. on Current Problems in Steel, ASM, November 1982
- [45] F.P.Ford, "Prediction of Corrosion Fatigue Initiation in Low Alloy Steel and Carbon Steel/Water Systems at 288°C," Proceedings of Sixth International Symposium on Envi-

ronmental Degradation in Nuclear Power Systems – Water Reactors, San Diego, Eds. E. Simonen, R. Gold, Published by National Association of Corrosion Engineers pp.9-16, August 1-5, 1993.

- [46] M. Higuchi, K. Iida, *Nuclear Engineering and Design* 129, pp. 293-306, 1991.
- [47] W. Shack, et al, "Environmentally Assisted Cracking in LWRs" NUREG/CR 4667, vol14, Argonne National Laboratory, 1992
- [48] "Effects of LWR Coolant Environments on Fatigue Design Curves of Carbon and Low-Alloy Steels," NUREG/CR-6583, Argonne National Laboratory, March 1998.
- [49] "Effects of LWR Coolant Environments on Fatigue Design Curves of Austenitic Stainless Steels," NUREG/CR-5704, Argonne National Laboratory, April 1999.
- [50] "Fatigue Analysis of Components for 60-Year Plant Life," NUREG/CR-6674, Pacific Northwest National Laboratory, June 2000
- [51] ASME Code Case-643, "Fatigue Crack Growth Rate Curves for Ferritic Steels in PWR Water Environment," May 2000.

## **Appendix B**

### **Background Papers**

#### **Foreword**

The intention in presenting the background papers in this appendix is to describe the broad basis for the scoring by the experts. The audience for these topical reports includes technical peers, corporate level engineers and regulators. The depth of knowledge (including plant experience and laboratory data) differs immensely among the topics, and the nature of the papers reflects this. The papers are not consensus documents, but have each been written by individual panel members and reviewed by one or more of the panel members. Differing opinions and additional factors that enter into each expert's scoring/judgments are addressed in the individual comments put in the spreadsheet used for scoring each sub-group of components. The background papers also rely on Appendix A, which provides an overview of all environmental degradation phenomena.

## Contents – Appendix B

	Page No.
Foreword.....	i
B.1 SCC of Sensitized and Non-Sensitized Austenitic Stainless Steels and Weldments .....	B-1
B.2 IASCC of Stainless Steels and Other Irradiation Induced Phenomena.....	B-21
B.3 Stress Corrosion Cracking and Pitting: Contaminating External Environments .....	B-45
B.4 Thermal Aging and Embrittlement of Cast Stainless Steels.....	B-50
B.5 SCC of Ni Alloy 600 and Alloy 182 and 82 Weld Metals in BWR Water .....	B-57
B.6 SCC of Alloys 600, 690, 182, 82, 152 and 52 in PWR Primary Water .....	B-79
B.7 Corrosion of Steam Generator Tubes .....	B-91
B.8 Stress Corrosion Cracking of Carbon and Low Alloy Steels .....	B-135
B.9 Environmental Degradation of High Strength Materials .....	B-158
B.10 BWR Water Chemistry: Effects on Materials Degradation and Industry Guidelines ..	B-165
B.11 PWR Primary Water Chemistry Guidelines.....	B-186
B.12 PWR Secondary Water Chemistry Guidelines .....	B-191
B.13 Degradation of Fracture Resistance: Low Temperature Crack Propagation (LTCP) in Nickel-Base Alloys .....	B-195
B.14 Fatigue .....	B-202
B.15 Predicting Failures Which Have Not Yet Been Observed – Microprocess Sequence Approach (MPSA).....	B-211
B.16 Microbiologically Influenced Corrosion (MIC).....	B-268
B.17 Flow-Accelerated Corrosion.....	B-273
B.18 Boric Acid Corrosion (BAC).....	B-278
B.19 Variability in the Corrosion of Materials in LWR Environments.....	B-296



## B.1 “SCC of Sensitized and Non-sensitized Austenitic Stainless Steels and Weldments,” by Peter L. Andresen

This background overview paper provides a foundation for understanding the proactive materials degradation concerns for stress corrosion cracking (SCC) of **wrought, unirradiated austenitic stainless steels in both boiling water reactor (BWR) and pressurized water reactor (PWR) environments, including weldments**. There are separate papers for irradiated assisted SCC of stainless steels, for SCC of cast stainless steels, and for lower temperature, mostly-chloride-related pitting and SCC of stainless steels. There are also papers related to BWR and PWR water chemistry, evolving operational practice, start-up and shutdown, and other considerations that influence SCC.

There is a long history of SCC in stainless steels exposed to high temperature water [1-4], and extensive research work designed to understand the dependencies and underlying causes [1-8]. While the mechanical behavior of stainless steels is not dramatically different at 300 °C than at room temperature, many aspects of corrosion and SCC are quite different. All structural materials (e.g., iron and nickel base alloys) are suitable for service in water environments because they form a protective passive film on the surface. When the film is broken (e.g., by scratching or plastic straining), the “bare surface” corrosion rates are *very high*, decaying in a logarithmic fashion over time as the protective oxide film reforms. Even after long time, the corrosion rate does not decrease to zero, but is sustained at a low, “passive” current density.

The nature of the oxide film on stainless steel is quite different in high temperature water (in this context, defined to be above about 150 °C). Near room temperature, the films on stainless steel are very thin (nanometers) and very protective (in terms of passive corrosion current). However, the films on standard “18Cr-8Ni” stainless steels are not that protective in terms of their resistance to aggressive species like chlorides, and even this limited resistance decreases as temperature increases [9,10]. The breakdown of the film can lead to pitting corrosion, crevice corrosion, stress corrosion cracking, etc., with the primary aggravants being increased chloride (halide),  $H^+$  (lower pH), temperature, and oxidant concentration.

Above  $\approx 150$  °C, the oxides become much thicker (hundreds or even thousands of nanometers) and somewhat less protective (both in terms of passive current density and tolerance for breakdown from, e.g., chloride) [11]. The composition of the films is not uniform, either through thickness or from environment to environment [11]. For example, in oxidizing (e.g., traditional BWR) environments, Cr is oxidized from  $Cr^{3+}$  (e.g.,  $Cr_2O_3$ ) to  $Cr^{6+}$  (e.g.,  $CrO_4^{2-}$ ), which is soluble in water (Figure B.1.1). Thus, these films have an inner layer, which is Cr-rich and an outer layer low in Cr. In deaerated water, the addition of  $H_2$  reduces the corrosion potential (lowering line (a) in Figure B.1.1, which is the  $H_2/H_2O$  reaction), which results in an increase in the solubility of  $Fe^{2+}$  (more in pure water than in PWR primary water, whose  $pH_T$  is  $\approx 1.5$  units higher). Note that oxidants like  $O_2$  are consumed in cracks and crevices, so those films are somewhat different than exterior films (in oxidizing environments). Both films form oxide crystallites on the surface by re-precipitation, which are typically 0.1 – 10 micrometers in size. The films that form in the presence of oxidants are somewhat more protective (i.e., lower passive current density) [11,12].

While there is not complete concurrence on the mechanism(s) of SCC of stainless steels in hot water, the consensus opinion is that SCC growth occurs by a process involving localized deformation (e.g., at the crack tip), which is a shear process that “breaks” or damages the inner protective oxide and produces an accelerated oxidation process as the film repairs. This was

originally conceived as “slip – film rupture – dissolution,” but there is in fact no requirement for an aqueous electrolyte since steam, air or other gaseous environments produce oxidation, which meets the requirement for the underlying mechanism. Thus, many people refer to the mechanism as “slip – oxidation.” An important element of this mechanism is that it is not fundamentally related to (local) stress per se, but to (local) dynamic strain that damages the protective film. Dynamic strain at constant load (e.g., when cracks grow primarily from weld residual stresses) is sustained because the stress / strain field at the crack tip is redistributed as the crack advances, and this requires local strain. Thus, there is an inherent inter-dependency between dynamic strain that produces crack advance, which in turn sustains the dynamic strain. The slow repassivation process in hot water, long term thermal creep, the interaction among crack advance in adjacent grains, irradiation creep, operating fluctuations (e.g., in temperature or pressure), start-up and shut-down, etc. also help sustain crack advance.

Factors such as simplistic or flawed experiments and extrapolation of room temperature data led to the early presumption that SCC would not occur in non-sensitized, unirradiated stainless steel; or in high purity water; or without oxidants in the water, etc. However, it is now recognized that SCC can occur in essentially any environment-material combination in high temperature water, although the ease of initiation and rate of SCC growth can vary markedly. Thus, the concepts of *thresholds* (e.g., in sensitization, water purity, oxidant level, radiation dose/fluence, etc.) that produce immunity to SCC have given way to an understanding of an inherent susceptibility to SCC that varies markedly with material, environment and stress. However, pragmatically, in many cases there are conditions of use that lead to very long lives.

The traditional view of SCC is reflected in Figure B.1.2, which expresses the need for a confluence of stress, environment and metallurgical parameters to exist for SCC to occur. (Drawn today, the central over-lapping region of SCC susceptibility would be much larger). The various parameters that control the initiation or growth rate do not operate independently but rather inter-dependently; thus, some factors (e.g., 10 – 30 ppb sulfate) can have a huge influence under some conditions (e.g., in oxidizing water), but not under other conditions (e.g., deaerated / hydrogenated water). Many such inter-dependencies exist in SCC; indeed, to some extent the effect of essentially all factors are influenced by all other factors. Thus, focusing on the engineering factors that influence SCC can produce a confusing variety of observations, and successful understanding and prediction of SCC must be built on an accurate image of the “crack tip system.”

The primary factors that control SCC of stainless steels in hot water are:

- Degree of sensitization. Sensitization results from Cr carbides that form during thermal exposure (from heat treatment or welding) in the range of 550 – 750 °C, although Cr carbide nucleation can occur below 400 °C in cold worked stainless steels, and growth of existing Cr carbides can occur below 300 °C. The fundamental phenomenon relates to the formation of Cr carbides (usually Cr<sub>23</sub>C<sub>6</sub> in stainless steels), which nucleate preferentially in the grain boundaries. Because C diffuses much faster than Cr, a Cr depletion profile is created adjacent to the grain boundary (the diffusivity of Cr within the grain boundary is much higher than within the grain, so the Cr concentration is reasonably constant along the grain boundary). At higher temperature, the Cr profile is deeper and wider. When the carbon is consumed, the carbide stops growing, and the Cr depletion profile eventually vanishes. This is difficult to accomplish in stainless steels, but such “healed” microstructures can be fairly readily produced in nickel-base alloys.

The effect of Cr depletion is most evident in oxidizing and/or pH-shifted water chemistries (oxidizing environments create a pH shift in cracks and crevices). In oxidizing (e.g., traditional BWR) environments with impurities (e.g., 50 – 100 ppb sulfate), the presence of sensitization can produce a > 20X increase in crack growth rates, and a similar acceleration in crack initiation. However, in deaerated, near-neutral pH water, Cr depletion plays a much lesser role; indeed, the presence of carbides in the grain boundary reduces SCC susceptibility, apparently by making deformation in the grain boundaries more difficult.

Nucleation of Cr carbides is greatly delayed in time, e.g., by reducing the C content (L-grade stainless steels) and adding Mo (type 316 stainless steels). Thus, modern stainless steel components are either not welded or are fabricated from L-grade stainless steels.

Cr depletion also develops during irradiation due to *radiation-induced segregation*. The Cr profiles are much narrower, and the minimum Cr level is generally higher – usually in the range of 12 – 14% Cr for stainless steels containing  $\approx$  18% Cr. The report on irradiation assisted SCC goes into this phenomenon in more detail.

- Oxidants and Corrosion Potential. The presence of oxidants like dissolved  $O_2$ ,  $H_2O_2$ , and Cu ion can increase SCC and corrosion fatigue (CF) growth rates markedly. Oxidants react on metal surfaces and elevate the corrosion potential. As oxidants diffuse into cracks and crevices, they are consumed (electrochemically balanced by reaction with  $H_2$  or metal corrosion). Thus, the interior of cracks and crevices are at low corrosion potential, and the difference in corrosion potential drives migration of anions (like chloride) into the cracks, and cations (like  $H^+$  and  $Na^+$ ) out of the cracks. The effect on SCC and CF of a complex mix of oxidants (and reductants) is fully captured by their effect on corrosion potential. The corrosion potential is not linear with oxidant concentration, and small (ppb) levels of oxidants can produce large (> 300 mV) change in corrosion potential.

Figure B.1.3 shows an example of the effect corrosion potential of SCC. While its effect is very strong on sensitized stainless steels, it also affects non-sensitized stainless steel (and nickel-base alloys, and carbon and low alloy steels). However, SCC growth occurs at moderate rates in deaerated water (and without any prior exposure to water containing oxidants) and so is also a potential concern in PWRs if cracks can initiate.

- Water Purity and pH. Water purity has a profound effect on SCC and CF, and in oxidizing water there is sensitivity to  $\approx$  10 ppb levels of impurities. The most damaging impurities are chloride and sulfate, but most impurities are damaging. In oxidizing environments, even buffering chemistries (e.g., the B/Li chemistries used in PWRs) produce accelerated growth rates (compared to pure water) in oxidizing environments. Because the oxidizing conditions produce a pH-shifted chemistry in cracks and crevices, there is somewhat less sensitivity to bulk pH (for crack growth – crack initiation is more directly dependent on the bulk chemistry).

In deaerated water (where essentially no difference in corrosion potential occurs in cracks), the sensitivity to impurities is low, although levels > 1 ppm can accelerate SCC. The relatively minor shifts in pH associated with pure (deaerated) water ( $pH_{300C} \approx 5.63$ )

and various standard levels of B (as  $\text{H}_3\text{BO}_3$ ) and Li (as  $\text{LiOH}$ ) ( $\text{pH}_{300\text{C}} \approx 6.8 - 7.4$ ) have a relatively minor effect on SCC growth rates.

The addition of  $\text{H}_2$  to deaerated water produces a small decrease in corrosion potential (59.3 mV per 10X change in  $\text{H}_2$  at 325 °C). This is very important for nickel-base alloys, because it can produce a transition across the Ni/NiO phase stability. However, there is pragmatically no way to cross the Fe/ $\text{Fe}_3\text{O}_4$  phase boundary by adding  $\text{H}_2$ . There is evidence that increasing  $\text{H}_2$  produces somewhat enhanced SCC susceptibility, but this has been observed in slow strain rate tests on smooth specimens, and may be associated with accelerated initiation under these conditions – a broadly parallel observation to enhanced corrosion fatigue initiation in stainless steels at low potential vs. high potential.

- Yield Strength / Cold Work / Weld Shrinkage Strain. There are multiple factors that can increase the yield strength in materials, including cold work, irradiation, precipitation hardening, etc. It appears that all have a similar effect on SCC growth rate. For stainless steels, the primary factors are cold work and irradiation, and irradiation is covered in a separate report on irradiation assisted SCC. Cold work occurs as bulk cold work; surface cold work from machining, rolling, grinding, etc.; and weld shrinkage strain in the heat-affected zone adjacent to welds. The latter factor has only recently been recognized and quantified, and equivalent room temperature strains of >20% are often observed near the fusion line. This explains the shift in location of most cracks from  $\approx 6 - 8$  mm (depending on wall thickness) from the fusion line in sensitized piping compared to  $\approx 1 - 3$  mm for unsensitized piping observed in BWRs.

As materials are cold (or warm) worked, the effect of yield strength increases, and its effect on SCC growth rates appear to be captured by yield strength. The presence or absence of martensite in the deformed structure is small, at least for crack growth in high temperature water; martensite might affect crack initiation and lower temperature SCC response (e.g., < 150 °C). Figure B.1.3c shows the effect of cold work. Figure B.1.4 shows that the increase in growth rate is not linear with yield strength, and that yield strength affects SCC in a similar fashion at low and high corrosion potential.

- Temperature. In the range of 250 – 350 °C, increasing temperature increases SCC growth rates. Equally importantly, it appears to help sustain SCC growth. At lower temperature – all things being equal – the growth rates may continue to decrease; but “all things” are never equal. In particular, the corrosion potential changes with temperature; this is especially pronounced and important in the presence of oxidants (Figure B.1.5). Pragmatically, as components cool down, many are exposed to unusual loading and/or water chemistry. BWR components vary only between 274 and 288 °C, where the difference in growth rates is limited. In PWRs, the temperature ranges from 286 °C (core inlet) to 323 °C (core outlet) to 343 °C (pressurizer), and the crack growth rate varies more significantly.
- Stress and Stress Intensity Factor. Stress and stress intensity factor obviously play a large role in SCC initiation and growth. In general, few components are designed for use above a nominal stress  $\approx 80\%$  of the yield strength. The effect of stress intensity factor on crack growth rate appears to vary with water chemistry, and tends to be in the range of  $K^2$  to  $K^3$  (Figure B.1.6). Many cracks grow adjacent to welds, where the weld residual stress profile must be accounted for along with operating stresses. The weld

residual stress profile combined with the inherent effect of crack length,  $a$ , on stress intensity factor ( $K \propto \sqrt{a}$ ), causes a large variation in  $K$  vs. crack length – sometimes resulting in an increase in  $K$ , and sometimes in a  $K$  that rises, then drops to zero.

- Low frequency vibratory loading, high frequency “ripple” loading, and even occasional load perturbations can significantly accelerate SCC growth rates. The distinction between SCC and corrosion fatigue (CF) is poorly demarcated, and with good reason: in most if not all cases, SCC and CF represent a continuum in the *environmentally assisted cracking* spectrum, with increasing strain rate causing higher propagation rates but a lower factor of improvement for SCC mitigation approaches such as water chemistry or material modifications (Figure B.1.7).

$K_{ISCC}$  was once considered to be an invariant material property. However, there is extensive evidence that “ $K_{ISCC}$ ” depends on many parameters – indeed, the evidence of “ $K_{ISCC}$ ” has been based on non-optimal experiments (e.g., use of transgranular fatigue pre-cracked specimens as a basis for growth or non-growth of intergranular stress corrosion cracks). Other tests were performed under decreasing stress intensity factor conditions where the change in  $K$  was large and/or the increment of growth small (e.g., compared to the size of the plastic zone). More recent data has shown well-behaved crack growth rates as low as  $5.5 \text{ MPa}\sqrt{\text{m}}$ . It is impossible to prove that a  $K_{ISCC}$  *doesn't exist*, because one can always choose an incrementally smaller  $K$ , and the growth rates become too small to study in a realistic time frame, e.g., below  $3 \text{ MPa}\sqrt{\text{m}}$ .

### **Predictability of SCC of Stainless Steels**

A strong qualitative understanding and good quantitative predictive capability exists for SCC of stainless steels, esp. for BWR water chemistries and temperatures where extensive SCC has occurred, initially in sensitized pipe weld heat affected zones, and later in unsensitized vessel internal components (while there is a well-behaved continuum between unirradiated and irradiated stainless steels, SCC has occurred in stainless steel components that receive essentially no radiation damage (e.g.,  $<0.01 \text{ dpa}$ , such as the core spray lines).

The distinction between BWR and PWR primary operating conditions is not nearly as great as once thought, esp. as BWRs shift toward low corrosion potential operating by adding  $\text{H}_2$  and, far more effectively, introducing NobleChem™ (which creates a sub-monolayer of Pt or Pt/Rh on all wetted surfaces [13-15]. Under such conditions, the primary differences between BWR and PWR primary water chemistry are coolant additives (typically  $\text{H}_3\text{BO}_3$  and  $\text{LiOH}$ ) that shift the pH at temperature from 5.6 to  $\approx 7.2$ ;  $\text{H}_2$  fugacity ( $\approx 50$  vs.  $3000 \text{ ppb H}_2$ ); and temperature ( $274 - 288 \text{ }^\circ\text{C}$  vs.  $286 - 343 \text{ }^\circ\text{C}$ ). Of these, temperature may be the most important factor for stainless steels; for nickel alloys (where the Ni/NiO transition can be traversed) both temperature and  $\text{H}_2$  fugacity are important [4-8].

Examples of crack growth predictive capability are shown in Figures B.1.3, 4, 6 and 7 for sensitized and cold worked stainless steel [6,16-19]. Cold work is a particular concern – not only are some components used in a cold worked state (such as PWR baffle bolts), but most fabricated components have a surface layer of deformed, hardened material. Shrinkage strain during welding also produces a residual strain profile in the heat-affected zone (and the weld metal) in addition to the more-thoroughly studied residual stress profile [6,16-19]. These strains usually peak at the weld fusion line, generally at an equivalent room temperature cold work level of 15 – 20% (but sometimes higher) (Figure B.1.8).

Quantifying and understanding SCC in most systems relies predominantly on high quality, reproducible, consistent SCC data [20,21]. This has proven difficult enough in crack growth rate measurements, but is generally more difficult in crack initiation experiments as well as evaluation of plant data.

It is important to understand that the effect of individual changes (such as corrosion potential, water purity, temperature, cold work, stress intensity factor, irradiation, etc.) on SCC cannot be viewed in isolation in most experiments, and rarely if ever in plant components. For example, the effect of BWR water purity is dramatically different at moderate to high corrosion potential than at low corrosion potential (as indicated by the predicted curves in Figure B.1.3). Similarly, the factor of improvement observed for various mitigation techniques varies with loading and water chemistry conditions (Figure B.1.7).

It must also be recognized that there is a time-based evolution (e.g., related to plant operating conditions, or to radiation damage – as addressed in the IASCC topical report) and a crack-depth based evolution (e.g., in residual stress, stress intensity, cold work, sensitization, microstructure...), and these produce complex changes in predicted and observed response. Figure B.1.9 shows an example of this interaction in terms of the predicted difference in crack growth trajectory vs. time in different welds. Figure B.1.10 shows an example of crack length vs. time observations and predictions for sensitized type 304 stainless steel pipes.

### ***SCC Mitigation***

There are many approaches that have been pursued and adopted to mitigation SCC in stainless steels. In BWRs, eliminating sensitization (grain boundary Cr depletion) was a primary focus in the 1970s, and most BWRs replaced all recirculation piping with grades of stainless steel that resisted weld sensitization (by lowering C, adding Mo, using lower heat input, etc.). Efforts were also made to reduce weld residual stress by last-pass heat sink welding, induction heating, and mechanical stress improvements. Some BWRs operated with high aqueous impurity levels (esp. chloride and sulfate), and major efforts were undertaken to improve water purity.

The most effective mitigation strategy for existing plant components is to reduce the corrosion potential (Figure B.1.3), and the most effective way to accomplish this is using electrocatalysis. The techniques to make surfaces electrocatalytic are numerous, but the most effective and economical approach is NobleChem™ [13-15], which involves the injection of ionic forms of Pt (or Pt and Rh), which electrolessly reduce and deposit on the surfaces of all wetted parts in BWRs. Applications have been performed on about 30 BWRs, and a new on-line application technique will be performed at a lead plant in 2005.

There is a possibility of attaining further SCC mitigation by adding Zn [22,23]. This is applicable to both BWRs and PWRs, and because Zn is a cation, it is most effective if the corrosion potential is low (i.e., BWRs operating with NobleChem™). Accurate quantification of the benefit of various Zn levels must still be performed and validated. Other approaches are more achievable only in new plants or if components are replaced. For example, the presence of grain boundary carbides or other particles impedes crack advance provided that they are not accompanied by Cr depletion [16,17].

### ***SCC of Stainless Steels – Concerns and Emerging Issues***

A number of ambiguities and emerging concerns exist in the area of SCC of stainless steels. Despite some improvements, the quality of experimental crack growth rate data is still a large factor in the observed scatter and disagreements over the quantitative effect of specific parameters. Even more problematical is the lack of statistical confidence and even qualitative insight into the controlling factors for crack initiation, although in general the same factors that enhance the crack growth rate also accelerate crack initiation.

Among the emerging concerns is that role of increasing stress intensity factor (K) as the crack grows ( $dK/da$ ) [24]. There is usually a large positive  $dK/da$  early in the crack growth process because  $K \propto \sigma\sqrt{a}$  (stress times the square root of crack depth), and the integrated effect of the weld residual stress profile produces an increasing stress at the crack as the crack grows. There continues to be a change in K as the crack grows longer, but the magnitude of the  $+dK/da$  or  $-dK/da$  is smaller (Figure B.1.11). Unfortunately, the few studies that have evaluated dynamic changes in K have been performed using a fixed change in load ( $dP/dt$ ) or displacement vs. time (similar to  $dK/dt$ ). However, this is expected and observed to yield non-conservative response because it does not produce the accelerating effect of *positive feedback* as the crack begins to grow faster, causing K to increase faster, causing the crack to grow faster... (Figure B.1.11) Conversely, with decreasing  $dK/da$ , as the crack slows, the rate of change of K slows, causing further slowing in the crack growth rate... At plant-relevant values of  $-dK/da$ , stable, well-behaved SCC can be sustained from 30  $\text{MPa}\sqrt{\text{m}}$  to below 12  $\text{MPa}\sqrt{\text{m}}$  [16,17,25]. Using  $-dK/dt$  (or  $-dP/dt$ ) fails to provide the important feedback between the rate of change of K and the rate of crack growth, and tends to produce crack arrest.

Another concern is the role of Si, which has been shown to cause elevated crack growth rates and a limited effect of stress intensity factor or corrosion potential (Figure B.1.12) [16,17,25]. While this may be a particular concern for irradiated materials, many stainless steels have a nominal Si content of 0.7 – 1.0%, which may be sufficient to cause elevated growth rates. Si readily oxidizes and is quite soluble in high temperature water – indeed, it is typically present in BWR (and probably PWR) water at levels about 100X higher than other impurities (typically 100 – 1000 ppb). It does not affect conductivity because it dissolves primarily in non-ionic form. A more speculative concern is the role of Mo, esp. in type 316 stainless steels, which have 2 – 3% Mo. Mo does not impart large improvements in corrosion or stress corrosion resistant in high temperature water (as it does below  $\approx 100$  °C), and it does readily oxidize and become soluble. Importantly, many Type 316 stainless steels show very high Mo segregation at the grain boundary (10 – 20% Mo), the extent of which peaks at certain cooling rates following annealing [26]. This could have a significant effect on SCC response, although no studies have yet been performed to confirm it.

A final concern relates to the role of environment in fracture toughness data. Essentially all of the fracture toughness data obtained above 200 °C were obtained in air. It is well established that high crack propagation rates under constant load – and reduced toughness in J-R tests – are observed in the range of about 75 – 140 °C for precipitation hardened Ni alloys [27-29], and it is reasonable to suspect that this might occur in stainless steels and Ni alloys like alloys 600 and 690 (esp. if their yield strength is elevated from cold worked, weld shrinkage strain or irradiation). Very preliminary data at 288 °C on cold worked stainless steel showed that the specimen unexpectedly failed as the K was allowed to increase to about 88  $\text{MPa}\sqrt{\text{m}}$  at the end of a test. The load was accurately known, as was the crack depth from post-test fractography at the point sudden failure occurred [17].

## References for B.1

- [1] R.L. Cowan, G.M Gordon, "Intergranular Stress Corrosion Cracking and Grain Boundary Composition of Fe-Ni-Cr Alloys," Stress Corrosion Cracking and Hydrogen Embrittlement of Iron-Base Alloys, Eds. R.W. Staehle, J. Hochmann, R.D. McCright and J.E. Slatern, NACE, Houston, 1977, p.1063-1065.
- [2] Proc., Fundamental Aspects of Stress Corrosion Cracking, Eds. RW Staehle, AJ Forty and D van Rooyen, NACE, 1969.
- [3] Proc. 1<sup>st</sup> – 11<sup>th</sup> Int. Symp. on Environmental Degradation of Materials in Nuclear Power Systems – Water Reactors, NACE / ANS / TMS, 1983 – 2003.
- [4] F.P. Ford, P.L. Andresen, "Corrosion in Nuclear Systems: Environmentally Assisted Cracking in Light Water Reactors," in "Corrosion Mechanisms," Ed. P. Marcus and J. Ouder, Marcel Dekker, p.501-546, 1994.
- [5] P.L. Andresen, F.P. Ford, "Life Prediction by Mechanistic Modelling and System Monitoring of Environmental Cracking of Fe and Ni Alloys in Aqueous Systems," Materials Science and Engineering, A103, p.167-183, 1988.
- [6] P.L. Andresen, "Perspective and Direction of Stress Corrosion Cracking in Hot Water," Proc. Tenth Int. Symp. on Env. Degradation of Materials in Nuclear Power Systems – Water Reactors, NACE, Houston, 2001.
- [7] P.L. Andresen, T.M. Angeliu, L.M. Young, "Immunity, Thresholds, and Other SCC Fiction," Proc. Staehle Symp. on Chemistry and Electrochemistry of Corrosion and SCC, TMS, Feb. 2001.
- [8] P.L. Andresen, "Conceptual Similarities and Common Predictive Approaches for SCC in High Temperature Water Systems," Paper 96258, Corrosion/96, NACE, 1996.
- [9] P.L. Andresen, D.J. Duquette, "The Effect of Chloride Ion Concentration and Applied Potential on the SCC Behavior of Type 304 Stainless Steel in Deaerated, High Temperature Water," Corrosion, Vol. 36, No. 2, p. 85 (1980).
- [10] P.M. Manning, D.J. Duquette, Corrosion Science 20, p.597-610, 1980. See also P. E. Manning, "The Effect of Environmental Variables on the Pitting Corrosion Behavior of Single and Duplex Phase 304L Stainless Steel," Ph.D. Thesis, Rensselaer Polytechnic Institute, December 1978.
- [11] Y.J. Kim, "Analysis of the Oxide Film Formed on 304 SS in 288C Water Containing O<sub>2</sub>, H<sub>2</sub> and H<sub>2</sub>O<sub>2</sub>," Corrosion 55, p.81, 1999.
- [12] Y.J. Kim, P.L. Andresen, "Data Quality, Issues and Guidelines for ECP Measurements in High Temperature Water," Corrosion 59, 7, p.584-596, 2003.
- [13] P.L. Andresen, "Application of Noble Metal Technology for Mitigation of Stress Corrosion Cracking in BWRs," Proc. Seventh International Symposium on Environmental Degradation of Materials in Nuclear Power Systems – Water Reactors, NACE, p.563-578, 1995.
- [14] S. Hettiarachchi, et al., "The Concept of Noble Metal Addition Technology for IGSCC Mitigation of Nuclear Materials," Proc. Seventh Int. Symp. on Environmental Degradation of Materials in Nuclear Power Systems – Water Reactors, NACE, p.735-746, 1995.
- [15] P.L. Andresen, T.P. Diaz, S. Hettiarachchi, "Effect on Stress Corrosion Cracking of Electrocatalysis and Its Distribution Within Cracks," Proc. of 11th Int. Symp. on Environmental Degradation of Materials in Nuclear Power Systems – Water Reactors, ANS, 2003.
- [16] P.L. Andresen, et al., "Effects of Yield Strength, Corrosion Potential, Stress Intensity Factor, Silicon and Grain Boundary Character on the SCC of Stainless Steels," Proc. of



- 11th Int. Symp. on Environmental Degradation of Materials in Nuclear Power Systems – Water Reactors, ANS, 2003.
- [17] P.L. Andresen, P.E. Emigh, L.M. Young, "Mechanistic and Kinetic Role of Yield Strength / Cold Work / Martensite, H<sub>2</sub>, Temperature, and Composition on SCC of Stainless Steels," Proc. Int. Symp. on Mechanisms of Material Degradation in Non-Destructive Evaluation in Light Water Reactors, Osaka, Japan, May 2002, published by Inst. of Nuclear Safety System, Japan, 2002.
- [18] T.M. Angeliu, et al., "Intergranular Stress Corrosion Cracking of Unsensitized Stainless Steels in BWR Environments," Proc. Ninth Int. Symp. on Environmental Degradation of Materials in Nuclear Power Systems – Water Reactors, AIME, 1999.
- [19] P.L. Andresen, et al., "Stress Corrosion Crack Growth Rate Behavior of Various Grades of Cold Worked Stainless Steel in High Temperature Water," Corrosion/02, Paper 02511, NACE, 2002.
- [20] P.L. Andresen, "SCC Testing and Data Quality Consideration," Proc. Ninth Int. Symp. on Environmental Degradation of Materials in Nuclear Power Systems – Water Reactors, AIME, 1999.
- [21] P.L. Andresen, K. Gott, J.L. Nelson, "Stress Corrosion Cracking of Sensitized Type 304 Stainless Steel in 288C Water: A Five Laboratory Round Robin," Proc. Ninth Int. Symp. on Environmental Degradation of Materials in Nuclear Power Systems – Water Reactors, AIME, 1999.
- [22] P.L. Andresen, T.P. Diaz, "Effects of Zinc Additions on the Crack Growth Rate of Sensitized Stainless Steel and Alloys 600 and 182 in 288C Water," Bournemouth Conference, BNES, England, October 1993.
- [23] P.L. Andresen, T.M. Angeliu, "Effects of Zinc Additions on the Stress Corrosion Crack Growth Rate of Sensitized Stainless Steel, Alloy 600, and Alloy 182 Weld Metal in 288C Water," Corrosion/95, Paper #95409, T-2A Symposium, NACE, 1995.
- [24] P.L. Andresen, M.M. Morra, "Effect of Rising and Falling K Profiles on SCC Growth Rates in High Temperature Water," Paper 71643, ASME PVP 2005, Denver, 2005.
- [25] P.L. Andresen, M.M. Morra, "Effects of Si on SCC of Irradiated and Unirradiated Stainless Steel and Ni Alloys," Paper 05591, Corrosion/05, NACE, Houston, 2005.
- [26] J. T. Busby, et al., "Influence of the Initial Grain Boundary Composition on the Evolution of Radiation-Induced Segregation Profiles," Proc. Mater. Res. Soc., MRS, vol. 540, 1999, pp. 451-456. See also E. P. Simonen and S. M. Bruemmer, "Thermally Induced Grain Boundary Composition and Effects on Radiation-Induced Segregation," Proc. 8th International Symposium on Environmental Degradation of Materials in Nuclear Power Systems–Water Reactors, ANS, 1997, p. 751.
- [27] C.A. Grove, L.D. Petzold, "Mechanism of SCC of Alloy X750 in High Purity Water," J. of Materials for Energy Systems, Vol. 7, No. 2, p.147-162, Sept 1985. See also, L.D. Petzold and C.A. Grove, "Mechanism of SCC of Alloy X750 in High Purity Water," Proc. Corrosion of Nickel Alloys, Ed. R.C. Scarberry, ASM, 1985, p.165.
- [28] G.A. Young, et al., "Microstructural and Microchemical Characterization of Dual Step Aged alloy X-750 and its Relationship to Environmentally Assisted Cracking," Proc., Tenth International Conference on Environmental Degradation of Materials in Nuclear Power Systems – Water Reactors, NACE, 2002.
- [29] Mills, W.J., Brown, C.M., Burke, M.G., "Effect of Microstructure on Low Temperature Cracking Behavior of EN82H Welds," Tenth International Conference on Environmental Degradation in Nuclear Power Systems – Water Reactors, NACE, 2002(a). See also C. M. Brown and W. J. Mills, "Effect of Water on Mechanical Properties and Stress Corrosion

Behavior of Alloy 600, Alloy 690, EN82H Welds, and EN52 Welds," Corrosion, Vol. 55, 1999, p. 173.

- [30] C.M. Chen, K. Aral, G.J. Theus, "Computer Calculated Potential pH Diagrams to 300 °C," EPRI NP-3137 Vol.2 (1167-2), June 1983.
- [31] M.E. Indig, A.R. McIlree, "High Temperature Electrochemical Studies of the Stress Corrosion of Type 304 Stainless Steel," Corrosion 35, p.288, 1979.

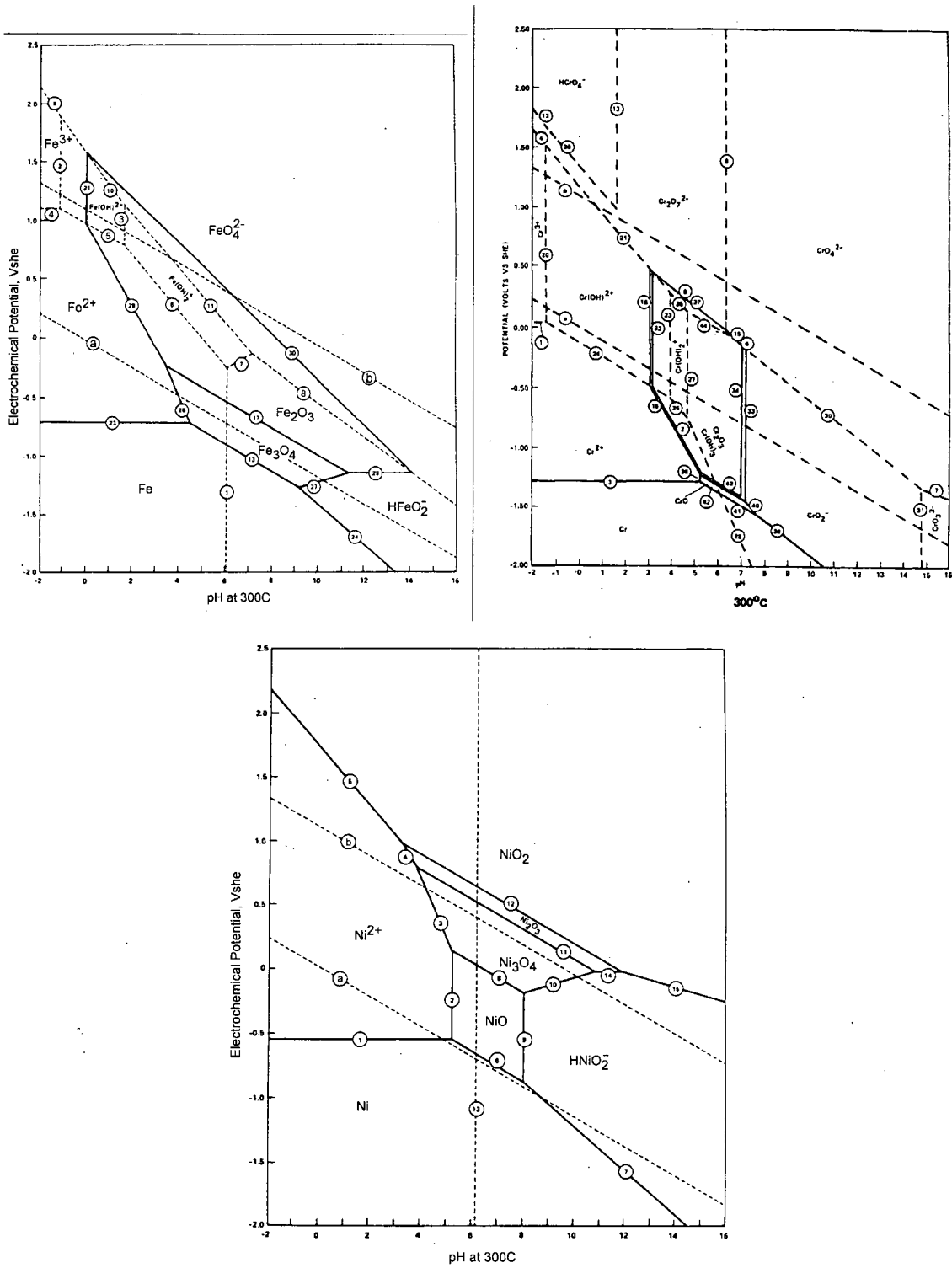


Figure B.1.1 Pourbaix diagrams for Cr, Fe and Ni in 300 °C water [30]. Used by Permission of EPRI.

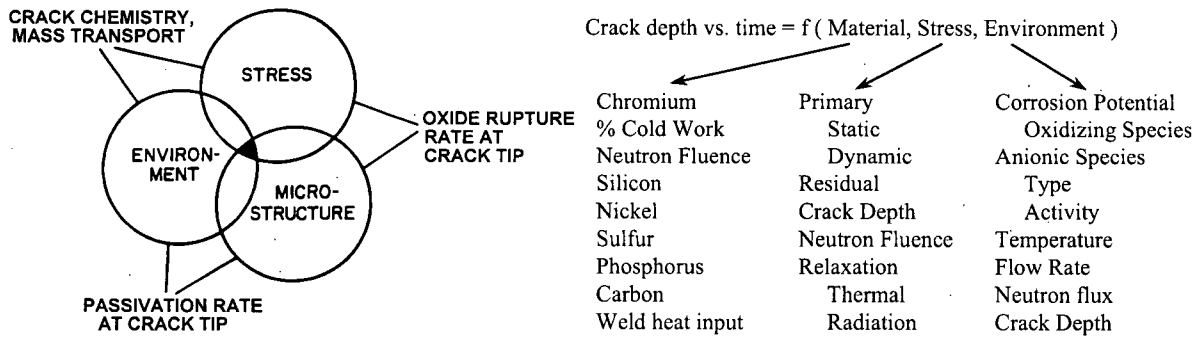
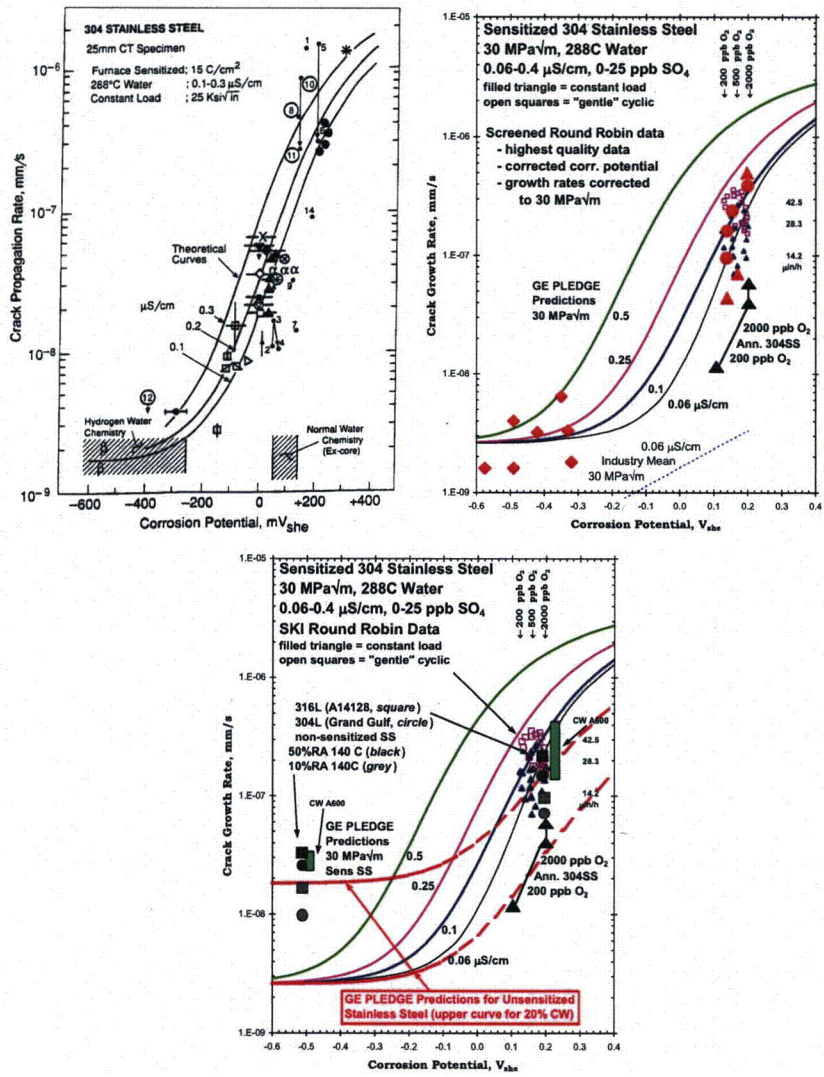
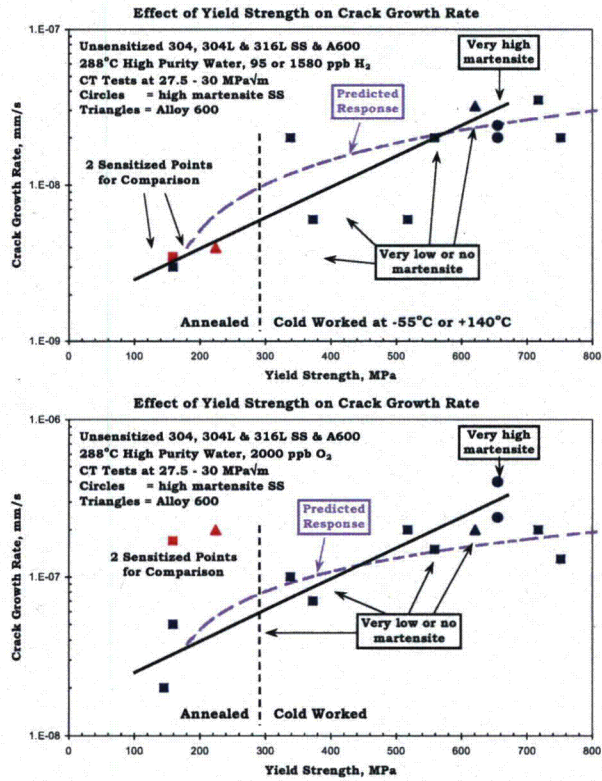


Figure B.1.2 The complexity of SCC is reflected in the large number of influential variables and the associated requirement that all 20 to 40 in a given system be adequately controlled [4,5].  
 © NACE International 2002.



(a) (b) (c)  
 Figure B.1.3 SCC growth rate vs. corrosion potential for stainless steels tested in 288 °C high purity water containing 2000 ppb O<sub>2</sub> and 95 – 3000 ppb H<sub>2</sub> [4,5,16,17]. © 2003 by The American Nuclear Society, La Grange Park, Illinois



(a)

(b)

Figure B.1.4 Effect of yield strength and martensite on the stress corrosion crack growth rate on stainless steel and alloy 600 in 288 °C, high purity water (<0.10 μS/cm outlet) at (a) low and (b) high potential [16,17] © 2003 by The American Nuclear Society, La Grange Park, Illinois

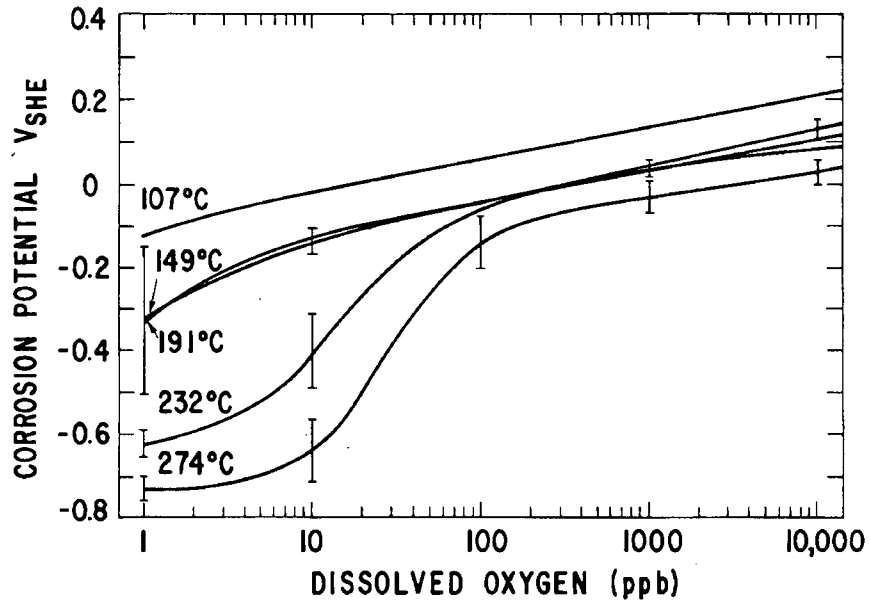


Figure B.1.5 Corrosion potential vs. dissolved O<sub>2</sub> and temperatures for stainless steels in pure water [31].

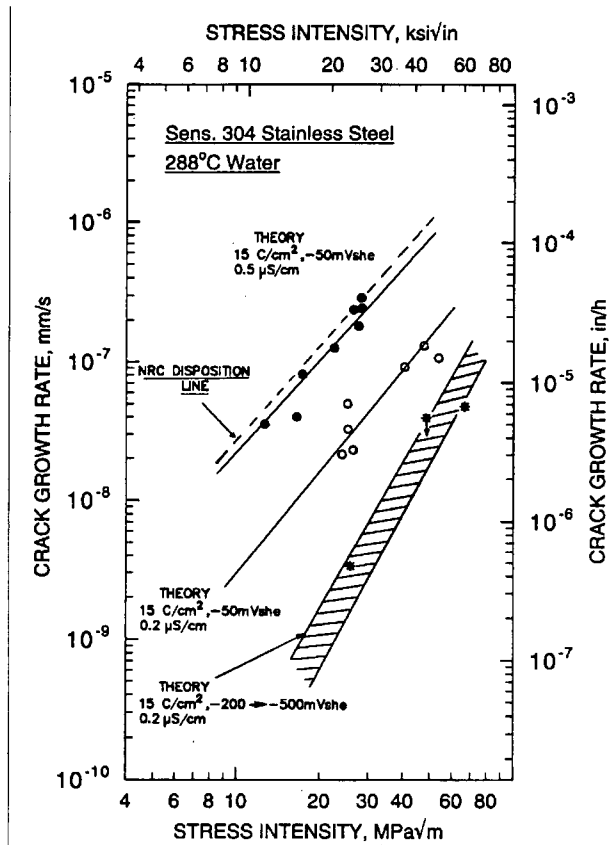


Figure B.1.6 Effect of stress intensity factor on the SCC growth rate of sensitized type 304 stainless steel in high temperature water [4,5]. (Reprinted with Permission from Elsevier)

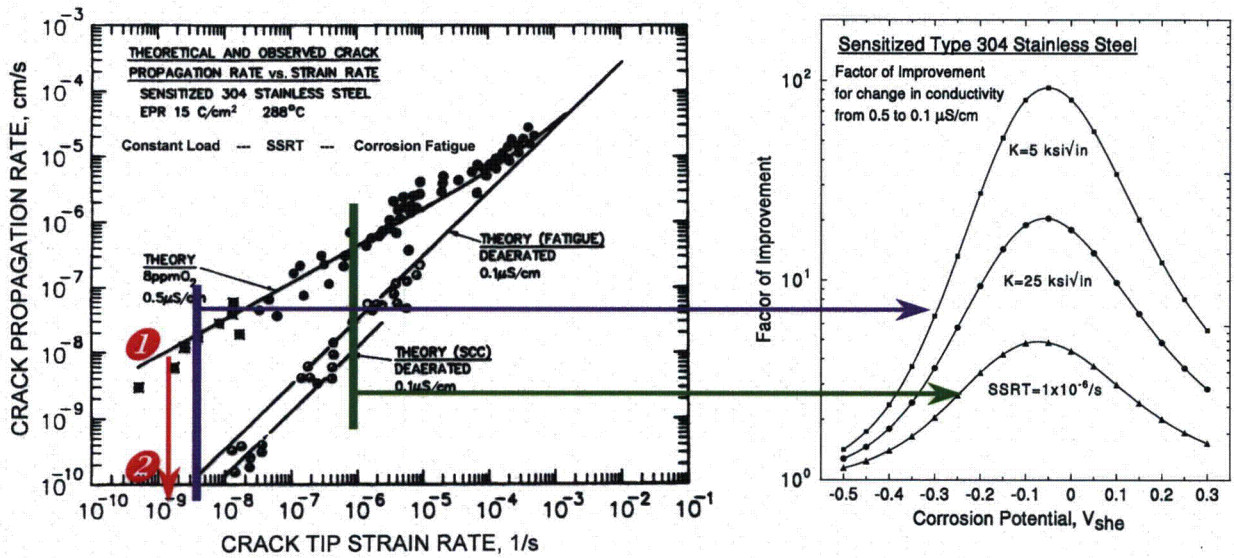


Figure B.1.7 Crack growth rate vs. crack tip strain rate showing the ability to predict environmental cracking across a range of constant load/K, slow strain rate and corrosion fatigue response. When water chemistry or the material is changed, the resultant curves are not parallel, but diverge at lower crack tip strain rate. Thus, the benefit observed in a laboratory test or component will depend on the testing condition, both loading and water chemistry [4-6]. (Courtesy of Taylor and Francis Group)

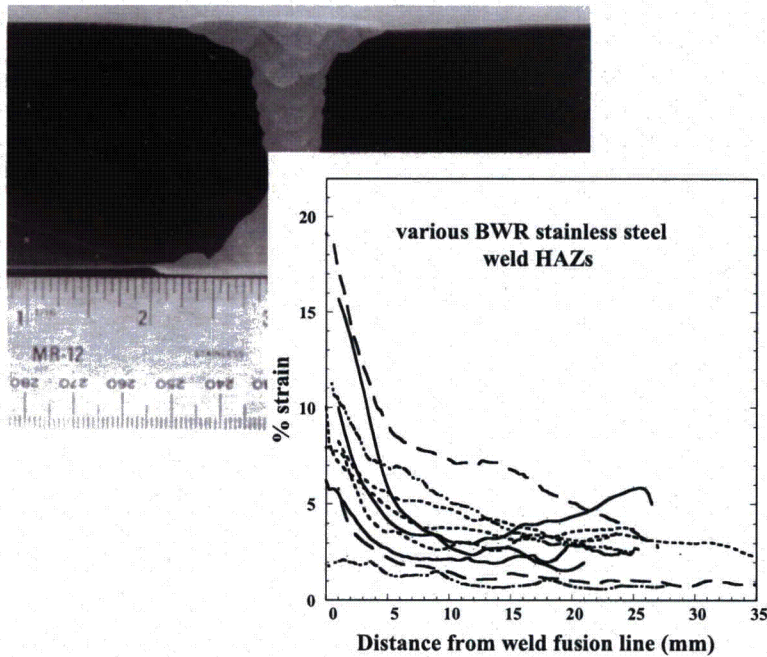


Figure B.1.8 Weld residual strain vs. distance from the weld fusion line for stainless steel welds. If the number of welding passes is limited, the peak residual strain can be below 10% equivalent room temperature tensile strain. However, most pipe welds that have been analyzed show residual strains in the range of 15 – 20%, with some slightly above 25%. The residual strain is also highest near the root of the weld [18]. (Reprinted with Permission from TMS)



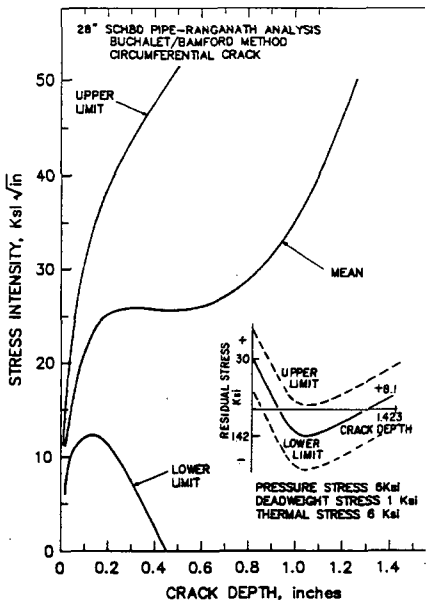
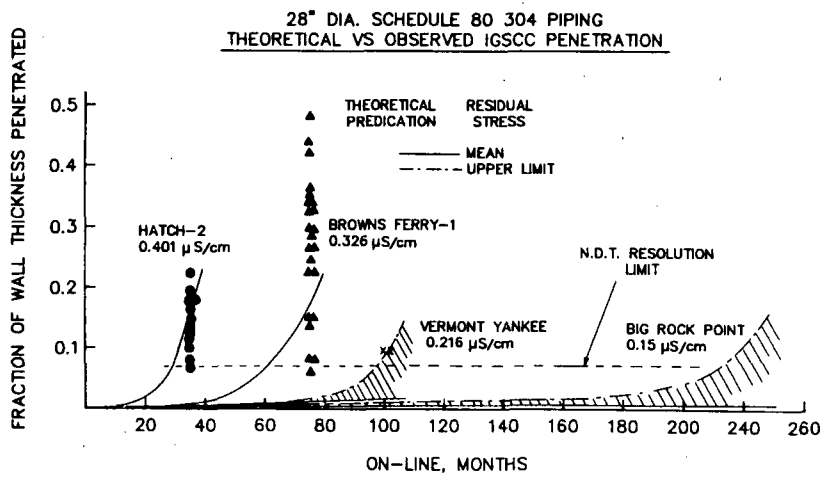


Figure B.1.9 (a) Crack length vs. time for pipe welds in various BWRs whose water purity varied markedly during their first years of operation. (b) Stress intensity factor vs. crack depth for pipe welds. The complex changes in residual stress, stress intensity factor and crack length vs. time that results in plant components. Irradiation makes the situation much more complex (see IASCC topical paper).

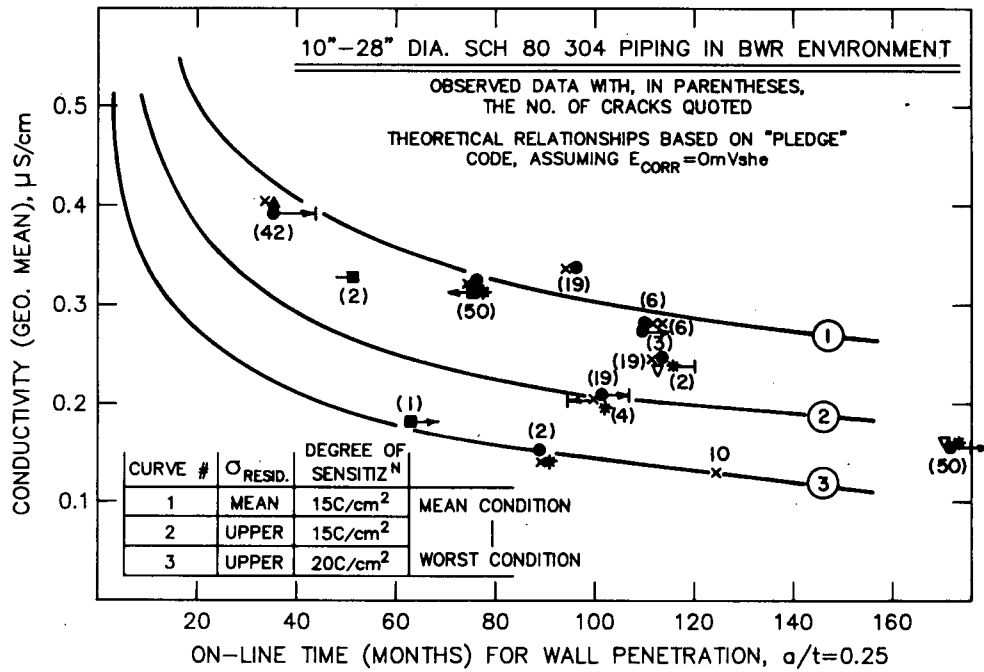


Figure B.1.10 The effect of conductivity on on-line months to achieve a crack depth of 25% of through-wall [4,5]. (Reprinted with Permission from Elsevier)

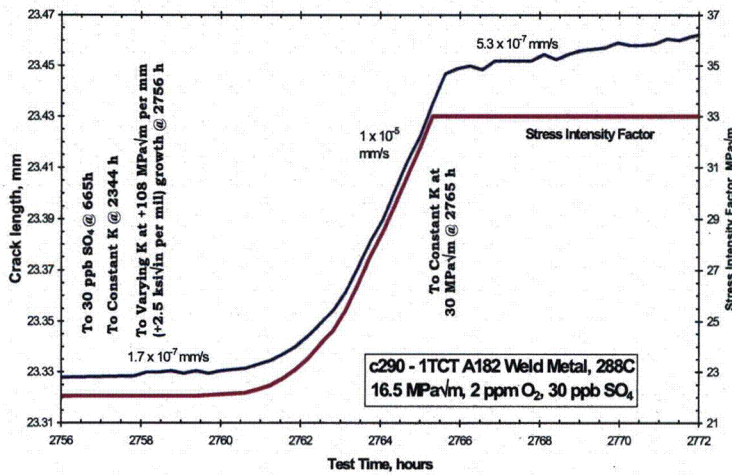
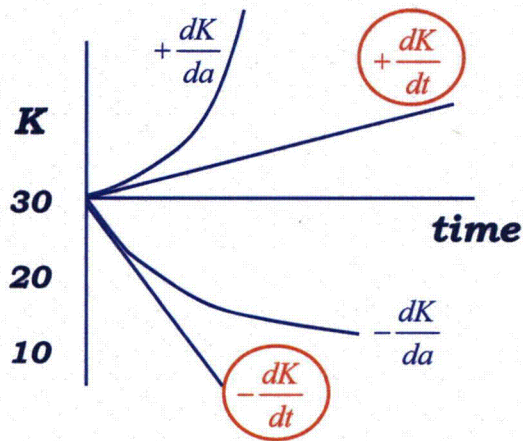


Figure B.1.11 Schematic and example crack length vs. time data showing the important role of  $+dK/da$  on crack growth rate, and the important difference between  $dK/da$  and  $dK/dt$  testing. In general,  $dK/dt$  always leads to non-conservative growth rates.  $+dK/da$  provide a positive feedback that often leads to dramatic increases in crack growth rate, while  $-dK/da$  represents negative feedback that slows the change in  $K$  as the crack slows down [24]. (Reprinted with Permission from ASME)

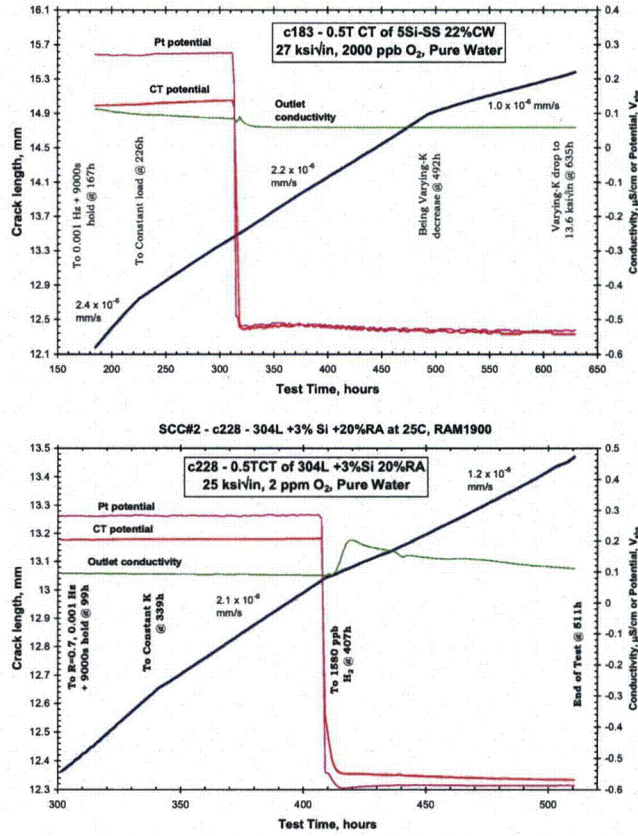


Figure B.1.12 Effect of Si on the crack growth rate of “stainless steels” whose bulk composition was designed to simulate an irradiated grain boundary. Reasonable questions can be raised about how realistic it is to create bulk alloys that represent the composition of a few nm region, but the qualitative observations remain important – i.e., that there is little effect of corrosion potential or stress intensity factor on crack growth rate [16,17,25]. (© 2003 by The American Nuclear Society, La Grange Park, Illinois)

## B.2 “IASCC of Stainless Steels and Other Irradiation Induced Phenomena,” by Peter L. Andresen and Peter M. Scott

This background paper provides a foundation for understanding the proactive materials degradation concerns originating from irradiation effects. The emphasis is on irradiation assisted stress corrosion cracking (IASCC) of *wrought, austenitic stainless steels* in BWR and PWR environments. Other radiation induced phenomena that are discussed include radiation creep relaxation, swelling and microstructural evolution. There are separate papers for SCC in unirradiated stainless steels, in cast stainless steels, and for lower temperature, mostly chloride related pitting and SCC of stainless steels. There are also separate papers related to BWR and PWR water chemistry, evolving operational practice, startup and shutdown, and other factors that influence SCC.

The paper on SCC of unirradiated stainless steels provides an introduction to the mechanisms, processes and dependencies in high temperature water. The primary factors that control SCC of stainless steels in hot water [1-8]—many of which are affected by radiation – include:

- Degree of sensitization, i.e., Cr depletion along the grain boundaries.
- Oxidants and corrosion potential, which affect the crack chemistry as well as the nature of the oxide films on the free surfaces.
- Water purity and pH, which primarily affects the crack chemistry.
- Yield strength, which produces an increase in crack growth rate. There are many ways by which yield strength is increased, including bulk or surface cold work, weld residual strain, precipitation hardening, etc., but not usually to the same degree as is caused by irradiation.
- Temperature.
- Stress and Stress Intensity Factor.

It is widely accepted that irradiation assisted SCC (IASCC) is literally that: an *irradiation assisted* process [2,9-19]. When viewed in a given time frame in plant components (Figure B.2.1a) or in accelerated laboratory tests, there can appear to be a threshold fluence for IASCC, but in fact SCC is observed in unirradiated stainless steels [2-5,9,15,16,20-22]. Irradiation is known to affect primarily the grain boundary chemistry (i.e., degree of sensitization), the oxidants and corrosion potential, the yield strength and the stress (via irradiation creep relaxation) components in this list of factors. In sufficiently careful and sensitive laboratory tests (e.g., crack growth rate tests), all grades of austenitic stainless steel have been shown to have inherent susceptibility to SCC. However, the numerous factors that promote SCC give rise to orders of magnitude difference in susceptibility, i.e., the incidence of cracking. Importantly, the effects of most parameters, such as corrosion potential, water impurities, stress, stress intensity factor, temperature, etc. are known to have a similar effect on both irradiated and unirradiated stainless steels.

The effect of corrosion potential (Figure B.2.1b) and water purity (Figure B.2.2) is similar for unirradiated and irradiated stainless steels exposed in BWR environments, which supports the concept that the underlying mechanisms and dependencies are similar. While the term “threshold fluence” appears in the literature, it should be recognized that unirradiated (and unsensitized, un-cold-worked) materials have some small susceptibility to SCC, and an apparent “threshold fluence” depends strongly on the details of other controlling parameters, such as the environment, loading, cold work, temperature, etc. Thus, a “threshold fluence” has relevance primarily from an engineering perspective within a specific context of environment, loading, etc. [5,9,11]

Figure B.2.1 shows the increasing SCC incidence with increasing fast neutron fluence in BWR crevice control blade sheath and in laboratory slow strain rate tests. While small amounts of intergranular cracking have been observed in tests in inert environments on irradiated stainless steels, there is an incontestable and dominant aqueous environmental effect. Thus, the concerns for cracking in irradiated components are appropriately characterized as IASCC, not as a simple effect on mechanical properties [2,9-19].

The radiation dose achieved in various components and the onset of various radiation effects is shown in Figure B.2.3 [11]. Most aspects of IASCC are well understood qualitatively, and a good quantitative description seems to exist in BWR water chemistry and temperature regime, but it is not completely clear that all of the aggravating effects of radiation on SCC are identified or qualified for all light water reactor conditions, esp. at the higher temperatures and fluences in PWRs. For all systems, the following factors are known to be important (Figure B.2 .4):

- I. **Radiation hardening (RH)**, in which the radiation generated defects produce an increase in yield strength (and a localization of deformation to “channels” in the material). Figure B.2.5 shows the increase in yield strength of a variety of austenitic stainless steels vs. irradiation dose. An increase in the yield strength from 150 – 200 MPa up to  $\approx$  700 – 1000 MPa is commonly observed, with a saturation after several dpa. Cold worked materials have a higher initial yield strength, but follow a broadly similar trajectory vs. dose. Much of the microstructural evidence of the initial cold worked microstructure has vanished after about 5 dpa.

The increase in yield strength results primarily from the formation of vacancy and interstitial loops (Figure B.2.6). Source hardening and dispersed barrier hardening models provide reasonable correlations between hardening and the dislocation loop microstructure, with the increase in yield strength (or hardness) proportional to  $(N_{loop} \times d_{loop})^{0.5}$ , where  $N_{loop}$  is the loop number density and  $d_{loop}$  is the loop diameter.

The effect of yield strength on SCC growth rates is discussed in the topical paper on unirradiated austenitic stainless steels, and appears to be a common effect among many materials and many mechanisms of yield strength enhancement (cold work, martensite formation, irradiation, precipitation hardening, etc.). Growth rates are increased in both BWR and PWR chemistries.

The homogeneous nature of deformation at low dose is replaced by heterogeneous deformation at higher doses as the defect microstructure impedes the motion of dislocations. Initial dislocations clear defects along narrow channels, and plasticity becomes highly localized. The channels are very narrow ( $< 10$  nm) and closely spaced ( $< 1$  mm) and typically run the full length of a grain, terminating at the grain boundaries. Dislocation channeling results in intense shear bands that can cause localized necking and a sharp reduction in uniform elongation, but the reduction in area generally remains very high. Dislocation channeling may also be an important in IASCC [11,19].

- II. **Radiation induced segregation (RIS)**, in which the migration of radiation generated defects (vacancies and interstitials) to sinks (esp. grain boundaries), alters the local chemistry within the material. Figure B.2.7 shows two examples of the grain boundary composition of high purity and commercial purity heats of stainless steel. The enrichment or depletion of major alloying elements and impurity elements can be significant [2,9-19], with depletion of  $>5\%$  Cr and enrichment of Si by  $>5-10X$  often observed [2,9-22].

RIS is driven by the flux of radiation-produced defects to sinks, and is therefore fundamentally different from thermal segregation or elemental depletion from grain boundary precipitation processes (e.g., sensitization from Cr carbide or boride formation and growth). In simple terms, radiation displaces an atom from its lattice site, and it comes to rest in a relatively distant location in an interstitial site. In fact, this primary displaced atom itself interacts with other atoms along its path, producing a cascade of damage as it loses energy and comes to rest. The resultant vacancies and interstitials can reach concentrations that are orders of magnitude greater than the thermal equilibrium concentrations. They migrate and are absorbed at sinks, creating profiles in concentrations of the constituent elements near grain boundaries. The species that diffuse more slowly by the vacancy diffusion mechanism are enriched at the grain boundary and the faster diffusers become depleted. Enrichment and depletion can also occur by association of the solute with the interstitial flux. In this case, the undersized species will enrich and the oversized species will deplete.

Even though the depletion and enrichment profiles are very narrow compared to those that form from, e.g., Cr carbide formation during welding or heat treatment, the effect on SCC remains very pronounced. For example, very narrow Cr depletion profiles can be generated during complex, multi-step heat treatments, and for a given level of Cr depletion, they have as strong an effect on SCC in high temperature water as much wider Cr depletion profiles.

Si enrichment is potentially of great concern because many stainless steels containing 0.5 – 1% Si can enrich to >5% at the grain boundary. Indeed, since the measurements are generally made by analytical electron microscopy, which has a 1 – 2 nm beam size, the actual Si concentration at the grain boundary can approach 50 atomic percent. Crack growth rate measurements on stainless steels with elevated Si levels (e.g., 1.5 – 5% Si) show high growth rates and limited or no effect of stress intensity factor and corrosion potential (Figure B.2.8) [20-22]. This may help explain the loss of the benefit of lowering the corrosion potential at high fluence in some stainless steels, esp. since Si enrichment appears to continue after Cr depletion saturates.

- III. **Radiation creep relaxation**, in which the migration of radiation generated defects under stress produces an accelerated creep rate (e.g., at constant load) and/or stress relaxation (e.g., at constant displacement, as for weld residual stresses, bolts and springs). Figures B.2.9 and 10 show two examples of radiation creep relaxation, which produces a large reduction in stress after a dose of several dpa. The radiation creep rate is proportional to the dose rate (flux) and stress.

Radiation creep relaxation is a mixed benefit. For welds, the weld residual stress is significantly relaxed in the same range of fluence where radiation hardening and segregation occur, and the net effect is generally beneficial. However, in many bolting application, the loss of stress over time can cause other problems related, e.g., to inadequate clamping forces that allow leakage that can produce erosion or fatigue. Because radiation creep inherently represents deformation, it can also promote SCC nucleation and help sustain crack growth. The radiation creep rates are very small compared to other sources (e.g., cyclic loading, slow strain rate testing, and strain redistribution at the tips of SCC cracks), so there is no evidence or expectation that growth rates will be elevated. However, the low rates of continuous deformation resulting from radiation creep may promote crack nucleation and help sustain crack advance.

Radiation creep provides a good example of a complicating factor in understanding the effects of radiation. Because radiation affects grain boundary chemistry and increases yield strength while it simultaneously reduces the stress near welds and in bolts, understanding and deconvoluting the effects of radiation on SCC is very difficult to do from field data. Add to this the effects of plant operating conditions (such as having high impurity levels early in BWR life), and it becomes very difficult to use plant data as a basis for understanding the real affects of various parameters on SCC, or to anticipate the response of one component (e.g., with constant displacement stresses) with others (e.g., with active pressurization stress). This is an example of the importance of developing a fundamental framework from which hypotheses can be formulated and tested. Such an approach has been undertaken, and even twenty years after the original hypotheses, this framework still represents the basis for current understanding of irradiation effects on SCC. While some improvements in quantifying some aspects of irradiation effects on yield strength, corrosion potential, radiation induced segregation and radiation creep relaxation could undoubtedly be made, there is a strong basis for both understanding and predicting radiation effects on SCC.

- IV. **Radiolysis**, in which  $H_2O$  is broken into various constituent elements, including  $H_2O_2$  and  $H_2$  (the longer lived species) as well as radicals (e.g.,  $e_{aq}^-$ ,  $H$ ,  $OH$ ,  $HO_2$ ): While stoichiometric quantities of oxidizing and reducing species are formed, the corrosion potential inevitably increases, sometimes dramatically. Radiolysis is suppressed at coolant  $H_2$  levels above about 500 ppb (5.6 cc/kg), so there is little concern for radiolysis in PWRs (whose coolant  $H_2$  level is typically 25 – 35 cc/kg).

In BWRs, the primary radiolytic species of interest are  $H_2$  and  $H_2O_2$ .  $H_2$  preferentially partitions to the steam phase, while  $H_2O_2$  remains in the recirculating water, creating a net oxidizing environment. The effect of these (and other) species on SCC is accurately characterized by their effect on corrosion potential. The corrosion potential on most structural materials is similar in deaerated water, and drops by about 57 mV per 10X increase in  $H_2$  and 114 mV per unit increase in pH at 300 °C. As soon as even very small amounts of oxidants are present (e.g., ppb levels), the corrosion potential can rise dramatically, generally increasing by 500 mV or more at >10 ppb of oxidant. Most importantly, when oxidants change the corrosion potential, a differential aeration cell forms, which produces an altered crack chemistry – this does not occur if only  $H_2$  is present because it is not consumed in cracks (as is  $H_2O_2$  and  $O_2$ ).

Concerns have been expressed that radiolysis could produce oxidizing conditions within cracks, and thereby alter the corrosion potential, mass transport processes, and SCC. However, an evaluation of the corrosion potential in a tight crevice under highly irradiated conditions showed no consequential elevation in corrosion potential (e.g., < 25 mV).

- V. **Radiation induced swelling**, in which voids form within the material that produce a change in material density and dimensions. This can produce distortion and warping, which can in turn produce elevation in stresses, e.g., in bolted structures. The occurrence of swelling in austenitic stainless steels is very rare and/or limited below 310 °C, even at high fluence (>30 dpa). Gamma heating of thick components can produce perhaps a 40 – 50 °C elevation in internal temperature, and at such temperatures swelling is more likely at moderate to high fluence.



One possible area of significance for void swelling is in PWR baffle plates and bolts. Because the bolts are fabricated from cold worked stainless steel, swelling is delayed compared to the adjacent annealed plates. Radiation creep relaxation will reduce the stress applied by the bolts, but differential swelling of the plates relative to the bolts will cause reloading of the bolts, which achieves some dynamic equilibrium (between reloading from differential swelling and ongoing radiation creep relaxation). This is difficult to quantify precisely at this time.

- VI. **Gamma heating** has already been mentioned in relation to swelling. Another possible consequence of gamma heating is superheating of crevices in PWRs above the temperature of the pressurizer (for example crevices between the shanks of baffle bolts and baffle plates). Thus local boiling with consequent changes in environmental chemistry can occur. Although there is no hard evidence that this has caused any environmentally induced cracking, the phenomenon cannot be ignored when searching for contributing factors in service failures.
- VII. **Fracture toughness** is reduced substantially in irradiated stainless steels. There is substantial scatter in the available data, but many stainless steels drop by a factor of five or more from 250 – 300 MPa√m to 50 MPa√m or even slightly lower (Figure B.2.11). These are also data obtained in air, and there may be further environmental degradation in fracture toughness in the environment, both at 288 – 323 °C and in the 75 – 140 °C regime [23].

### **Predictability of IASCC**

A solid qualitative understanding and at least semi-quantitative predictive capability exists for IASCC, esp. for BWR water chemistries and temperatures (there may be additional aggravating effects of radiation that become important at the higher temperatures and fluences in PWRs). The crack growth predictive capability is built on the basis of irradiation *assisted* SCC – that is, the understanding and predictive framework used for unirradiated stainless steels can be extended to radiation effects by defining key characteristics of SCC and quantifying those effects. This has been done for the four primary radiation induced phenomena: segregation, hardening, radiolysis and relaxation (Figure B.2.4) [2,9,15,17,18]. Figure B.2.12 shows the crack growth response at high and high corrosion potential of irradiated stainless steel and of sensitized stainless steel exposed to high and flow neutron fluxes. These (and other) data are replotted in Figure B.2.13 to show crack velocity vs. corrosion potential. Other examples of predictive capability are shown in Figure B.2.14, which shows the response of neutron irradiated stainless steel in slow strain rate and constant load tests in 288 °C water. As in many SCC systems, obtaining high quality, reproducible, consistent SCC data experimentally is often a limiting factor in quantifying and validating predictive models.

The effect of individual changes (such as flux, fluence, temperature, radiolysis, segregation, hardening, relaxation, etc.) cannot be viewed in isolation in most experiments, and rarely if ever in plant components. For example, the temperature of irradiation, the presence of stress, the radiation dose rate (flux), etc. can all affect the result at a given dose / fluence. It must also be recognized that there is a time-based evolution in radiation damage (Figure B.2.15), and these produce complex changes in predicted and observed response. In most components that undergo IASCC, there are damaging elements of radiation exposure (e.g., hardening and segregation) and beneficial elements (radiation creep relaxation of constant displacement stresses). There are then further complications when considering plant operation and the evolution of cracks. For example, if the water chemistry in BWRs is good, so that cracks don't

nucleate (or remain vanishingly small) by a dose of  $1 - 3 \times 10^{21}$  n/cm<sup>2</sup>, then the weld residual stresses will have markedly decreased and the likelihood that SCC will occur also decreases markedly. Figure B.2.15 shows an example of this interaction in terms of the predicted difference in crack growth trajectory vs. time for different water purities in a BWR core shroud. Figure B.2.16 shows an example of crack length vs. time predictions for a type 304 stainless steel BWR core shroud with multiple inspections and multiple cracks, and a comparison of observed and predicted crack depth for a number of BWR core shrouds.

IASCC in baffle bolts has also been evaluated and some controlling factors identified [24], although the state of knowledge does not yet permit prediction.

### ***IASCC Mitigation***

There are a variety of approaches for mitigating SCC in light water reactors, and they fall into categories of water chemistry, operating guidelines, new alloys, stress mitigation and design issues. Since most components in light water reactors are not intended to be replaceable (and are therefore very expensive to replace), water chemistry is the most attractive mitigation strategy, with operating guidelines and perhaps stress mitigation providing more limited opportunities. While the focus of this paper is on IASCC, most mitigation approaches (esp. water chemistry) are applicable to both irradiated and unirradiated components.

Water chemistry mitigation approaches are the easiest to implement and can often provide mitigation to many areas and components in the plant. In BWRs, the focus is primarily on lowering the corrosion potential, which can be done with H<sub>2</sub> injection, but is more effectively achieved using NobleChem™ [25-27]. In both BWRs and PWRs, the addition of Zn appears to provide some crack growth rate benefit for stainless steels, although more work is needed. Similarly, improvements in surface finish, stresses, etc. are effective in both reactor types.

Alloying with oversized elements reduces the extent of radiation-induced segregation (esp. Cr depletion) [19], but it's not clear that it will reduce Si enrichment. Cr depletion is less important in BWRs at low potential and in PWR primary water, but low potentials cannot be achieved in all locations in a BWR (it requires stoichiometric excess H<sub>2</sub> in the water, which doesn't exist in areas where boiling occurs). Radiation hardening differs somewhat among stainless steel types and heats, but it's not clear that it can be changed sufficiently to make an adequate difference in SCC response. Slip localization may aggravate SCC, and there are alloying approaches for altering stacking fault energy which influences slip localization [19]. Operationally, it is always wise to avoid higher stresses, vibration, start up and shutdown, fatigue (e.g., from mixing of cold and hot water, which has increased in low leakage core configurations in PWRs), etc. The timing of H<sub>2</sub>O<sub>2</sub> injection during PWR cooling and deaeration and H<sub>2</sub> injection during PWR heat up may be important. In BWRs, the early injection of H<sub>2</sub> during start up, and maintaining H<sub>2</sub> injection close to 100% of the time during operation should reduce SCC.

### ***IASCC – Concerns and Emerging Issues***

There remains a number of uncertainties and emerging concerns in the area of IASCC. The uncertainties arise in part from the huge scatter in data that has been obtained on irradiated stainless steel, much of which is caused by weaknesses in the experimental techniques. While factors such as good control and monitoring of water chemistry, transitioning from transgranular fatigue to intergranular SCC morphology, and similar concerns exist, perhaps the biggest issue is associated with K-size validity for crack growth specimens of irradiated materials [16,28]. There remain some concerns for the prospect of additional radiation related degradation (such

as precipitation of new phases, high He and void swelling) at higher temperatures and fluences associated with PWR components. As in all materials / systems, the understanding and prediction of crack nucleation is much weaker than for crack growth.

Among the emerging concerns is the role of Si, which appears to continue to segregate under irradiation at fluences where Cr depletion has effectively saturated. This may occur because Si undergoes radiation-induced segregation by a different (or an additional) mechanism than does Cr. Evidence of highly elevated (> 3%) Si levels in irradiated stainless steels and very pronounced effects of Si on crack growth rate are a significant concern, esp. since many stainless steels have a nominal Si level of 0.6 – 1%. Crack growth rate studies show elevated growth rates and a limited effect of stress intensity factor or corrosion potential (Figure B.2.8) [20-22]. Si readily oxidizes and is quite soluble in high temperature water – indeed, it is typically present in BWR (and probably PWR) water at levels about 100X higher than other impurities (typically 100 – 1000 ppb). It does not affect conductivity because it dissolves primarily in non-ionic form.

Another concern is that role of increasing stress intensity factor (K) as the crack grows (dK/da) [29]. Because  $K \propto \sigma\sqrt{a}$  (stress times the square root of crack depth), and because the weld residual stress profile changes vs. crack depth, there is usually a large positive dK/da early in the crack growth process. K also changes when the crack is longer, but the magnitude of the +dK/da or -dK/da is smaller. Unfortunately, most studies have been performed using a fixed change in load or displacement vs. time (similar to dK/dt), but this yields non-conservative response since it does not produce the accelerating effect of *positive feedback* as the crack begins to grow faster, causing K to increase faster, causing the crack to grow faster... Conversely, with decreasing dK/da, as the crack slows, the rate of change of K slows, causing further slowing in the crack growth rate... dK/dt fails to provide the important feedback between the rate of change of K and the rate of crack growth, and tends to produce crack arrest. Examples of this are shown in the topical paper on SCC unirradiated stainless steel and in reference [29].

Finally, fracture toughness data obtained in situ (after prolonged exposure to high temperature water) [21] might be substantially lower than the vast majority of available data, all obtained in air. The reduction in toughness from irradiation might be broadly representative of cold worked stainless steel (Figure B.2.11), and both may show significant effect of the environment, both in 288 C and ~100 °C tests, and in tearing resistance (e.g., J-R tests) and impact loading (e.g., Charpy or  $K_{IC}$ ).

## References for B.2

- [1] R.L. Cowan, G.M Gordon, "Intergranular Stress Corrosion Cracking and Grain Boundary Composition of Fe-Ni-Cr Alloys," Stress Corrosion Cracking and Hydrogen Embrittlement of Iron-Base Alloys, Eds. R.W. Staehle, J. Hochmann, R.D. McCright and J.E. Slatern, NACE, Houston, 1977, p.1063-1065.
- [2] F.P. Ford, P.L. Andresen, "Corrosion in Nuclear Systems: Environmentally Assisted Cracking in Light Water Reactors," in "Corrosion Mechanisms," Ed. P. Marcus and J. Ouder, Marcel Dekker, p.501-546, 1994.
- [3] P.L. Andresen, F.P. Ford, "Life Prediction by Mechanistic Modelling and System Monitoring of Environmental Cracking of Fe and Ni Alloys in Aqueous Systems," Materials Science and Engineering, A103, p.167-183, 1988.
- [4] P.L. Andresen, "Perspective and Direction of Stress Corrosion Cracking in Hot Water," Proc. Tenth Int. Symp. on Env. Degradation of Materials in Nuclear Power Systems – Water Reactors, NACE, Houston, 2001.
- [5] P.L. Andresen, T.M. Angeliu, L.M. Young, "Immunity, Thresholds, and Other SCC Fiction," Proc. Staehle Symp. on Chemistry and Electrochemistry of Corrosion and SCC, TMS, Feb. 2001.
- [6] P.L. Andresen, "Conceptual Similarities and Common Predictive Approaches for SCC in High Temperature Water Systems," Paper 96258, Corrosion/96, NACE, 1996.
- [7] Proc., Fundamental Aspects of Stress Corrosion Cracking, Eds. RW Staehle, AJ Forty and D van Rooyen, NACE, 1969.
- [8] Proc. 1st – 11th Int. Symp. on Environmental Degradation of Materials in Nuclear Power Systems – Water Reactors, NACE / ANS / TMS, 1983 – 2003.
- [9] P.L. Andresen, et al., Proc. Fourth International Symposium on Environmental Degradation of Materials in Nuclear Power Systems – Water Reactors, D. Cubicciotti and G.J. Theus, Eds., NACE, Houston, 1990, p. 1-83.
- [10] A.J. Jacobs, G.P. Wozadlo, "Irradiation Assisted Stress Corrosion Cracking as a Factor in Nuclear Power Plant Aging," Proc. Int. Conf. on Nuclear Power Plant Aging, Availability Factor and Reliability Analysis, San Diego, CA, ASM, p.173, 1985. See also, A.J. Jacobs, Letter Report and Literature Search, GE Nuclear Energy, San Jose, CA, May 1979.
- [11] S.M. Bruemmer, et al., Nucl. Mater., Vol 274, 1999, p 299-314.
- [12] G.S. Was, P.L. Andresen, J. Metals Vol. 44 (No. 4), 1992, p. 8.
- [13] P.M. Scott, J. Nucl. Mat., Vol 211, 1994, p. 101.
- [14] J.L. Nelson, P.L. Andresen, "Review of Current Research and Understanding of Irradiation-Assisted Stress Corrosion Cracking," Proc. Fifth International Symposium on Environmental Degradation of Materials in Nuclear Power Systems – Water Reactors, D. Cubicciotti, E.P. Simonen and R.E. Gold, Eds, American Nuclear Society, La Grange Park, IL, 1992, p 10.
- [15] P.L. Andresen, F.P. Ford, "Modeling and Prediction of Irradiation Assisted Stress Corrosion Cracking," Proc. Seventh International Symposium on Environmental Degradation of Materials in Nuclear Power Systems – Water Reactors, NACE, Houston, p.893-908, 1995.

- [16] P.L. Andresen, "Similarity of Cold Work and Radiation Hardening in Enhancing Yield Strength and SCC Growth of Stainless Steel in Hot Water," Corrosion/02, Paper 02509, NACE, 2002.
- [17] I. Suzuki, et al., "Perspective on PLEX Program at JAPEIC," Int. Conf. on Nuclear Plant Life Management and Extension, ANS, Nice, France, Nov 27-30, 1995.
- [18] P.L. Andresen, et al., "Life Prediction Of Boiling Water Reactor Internals," Proc., ICONE-4 Conference, ASME, 1996.
- [19] G.S. Was, P.L. Andresen, "SCC Behavior of Alloys in Aggressive Nuclear Reactor Core Environments," Topical Research Symposium on Corrosion in Aggressive Environments, Corrosion/05, NACE, Houston, 2005.
- [20] P.L. Andresen, et al., "Effects of Yield Strength, Corrosion Potential, Stress Intensity Factor, Silicon and Grain Boundary Character on the SCC of Stainless Steels," Proc. of 11th Int. Symp. on Environmental Degradation of Materials in Nuclear Power Systems – Water Reactors, ANS, 2003.
- [21] P.L. Andresen, P.E. Emigh, L.M. Young, "Mechanistic and Kinetic Role of Yield Strength / Cold Work / Martensite, H<sub>2</sub>, Temperature, and Composition on SCC of Stainless Steels," Proc. 10th Anniversary INSS Symp. on SCC in Nuclear Power Systems, Osaka, Japan, May 2002, published 2003.
- [22] P.L. Andresen, M.M. Morra, "Effects of Si on SCC of Irradiated and Unirradiated Stainless Steel and Ni Alloys," Paper 05591, Corrosion/05, NACE, Houston, 2005.
- [23] J.C. Van Duysen, P. Todeschini, G. Zacharie, "Effects of Neutron Irradiations at Temperatures below 550 °C on the Properties of Cold Worked 361 Stainless Steels: A Review," Effects of Radiation on Materials: 16th Int. Symposium, STP1175, ASTM, p.747-776, 1993.
- [24] P. M. Scott, et al., "An Analysis of Baffle/Former Bolt Cracking in French PWRs," Environmentally Assisted Cracking: Predictive Methods for Risk Assessment and Evaluation of Materials, Equipment and Structures, ASTM 1401, R. D. Kane, Ed., American Society for Testing and Materials, West Conshohocken, PA, 2000.
- [25] P.L. Andresen, "Application of Noble Metal Technology for Mitigation of Stress Corrosion Cracking in BWRs," Proc. Seventh International Symposium on Environmental Degradation of Materials in Nuclear Power Systems – Water Reactors, NACE, p.563-578, 1995.
- [26] S. Hettiarachchi, et al., "The Concept of Noble Metal Addition Technology for IGSCC Mitigation of Nuclear Materials," Proc. Seventh Int. Symp. on Environmental Degradation of Materials in Nuclear Power Systems – Water Reactors, NACE, p.735-746, 1995.
- [27] P.L. Andresen, T.P. Diaz, S. Hettiarachchi, "Effect on Stress Corrosion Cracking of Electrocatalysis and Its Distribution Within Cracks," Proc. of 11th Int. Symp. on Environmental Degradation of Materials in Nuclear Power Systems – Water Reactors, ANS, 2003.
- [28] P.L. Andresen, "K / Size Effects on SCC in Irradiated, Cold Worked and Unirradiated Stainless Steel," Proc. of 11th Int. Symp. on Environmental Degradation of Materials in Nuclear Power Systems – Water Reactors, ANS, 2003.
- [29] P.L. Andresen, M.M. Morra, "Effect of Rising and Falling K Profiles on SCC Growth Rates in High Temperature Water," Paper 71643, ASME PVP 2005, Denver, 2005. See also P.L. Andresen and M.M. Morra, "Effects of Increasing and Decreasing Stress Intensity Factor on SCC in Hot Water," Paper 05469, Corrosion/05, NACE, Houston, 2005.

- [30] G. Odette, P. Maziasz, J. Spitznagel, J. Nuclear Mat'ls, 85/86, p.1289, 1979.
- [31] P. Maziasz, "Effects of Helium on Microstructural Development in Type 316 Stainless Steel Under Neutron Irradiation," ORNL-6121, 1985.
- [32] A. Jenssen, L.G. Ljungberg, "Irradiation Assisted Stress Corrosion Cracking – Post Irradiation CERT Tests of Stainless Steels in a BWR Test Loop," Proc. 7th Int. Symp. on Env. Degr. Of Materials in Nuclear Power Systems – Water Reactors, NACE, 1995, p.1043-1054.
- [33] A.J. Jacobs, G.P. Wozadlo, "Stress Corrosion Testing of Irradiated Type 304 Stainless Steel Under Constant Load," Paper #41, Corrosion/91, NACE, 1991. See also Corrosion 49, p.145, 1993.

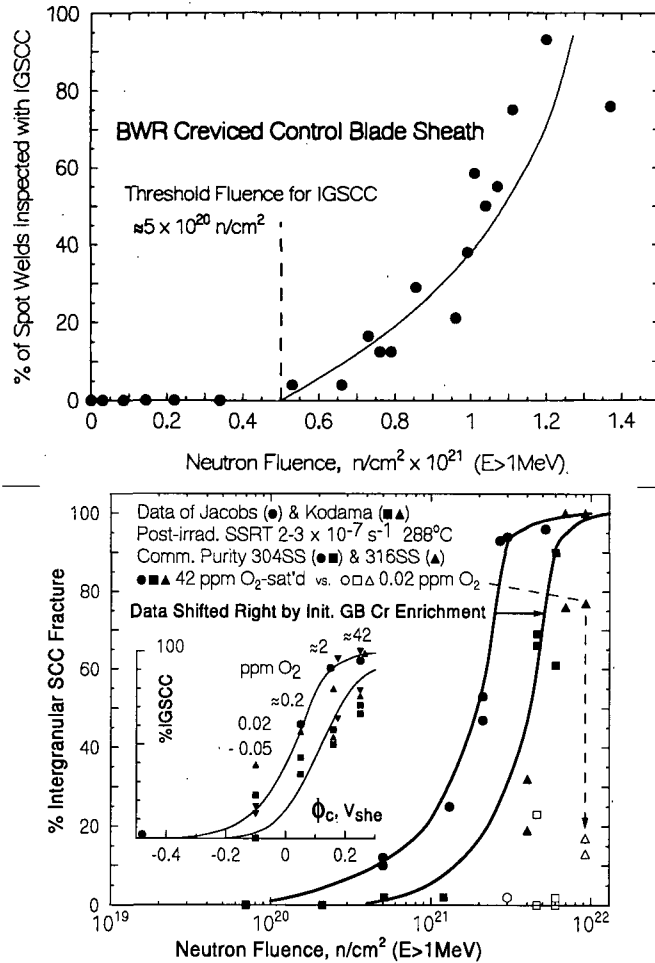


Figure B.2.1 Dependence of IGSCC on fast neutron fluence for (a) creviced control blade sheath in high conductivity BWRs and (b) as measured in slow strain tests at  $3.7 \times 10^{-7} s^{-1}$  on pre-irradiated type 304 stainless steel in 288°C water. The effect of corrosion potential via changes in dissolved oxygen is shown at a fluence of  $\approx 2 \times 10^{21} n/cm^2$ . The effect of corrosion potential on unirradiated and irradiated materials is similar under BWR conditions [2,9,15]. (© NACE International 1995)

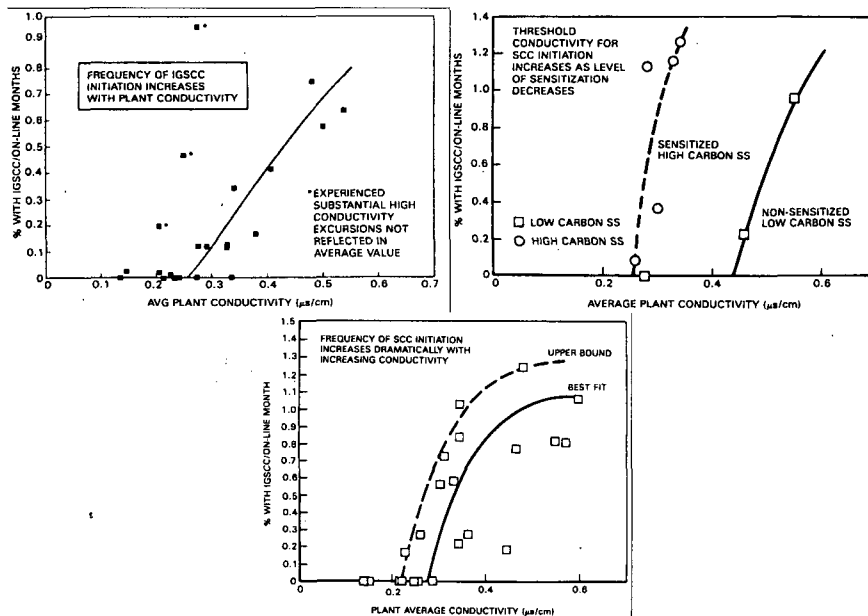


Figure B.2.2 The effects of average plant water purity are shown in field correlations of the core component cracking behavior for (a) stainless steel IRM/SRM instrumentation dry tubes, (b) creviced stainless steel safe ends, and (c) creviced Inconel 600 shroud head bolts, which also shows the predicted response vs. conductivity. The effect of conductivity on unirradiated and irradiated materials is similar under BWR conditions [2,9,15]. (© NACE International 1990)



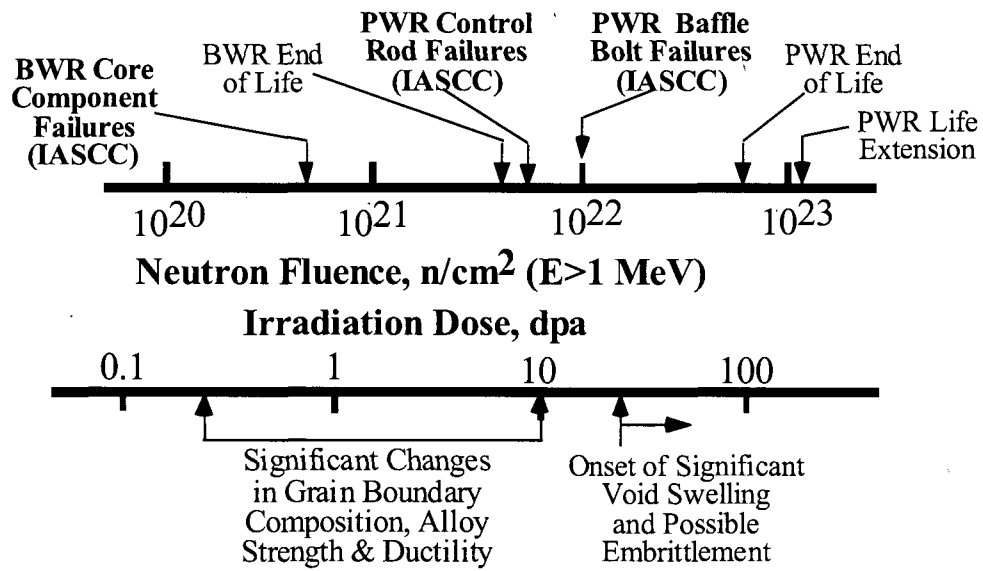


Figure B.2.3 Neutron fluence effects on irradiation-assisted stress corrosion cracking susceptibility of type 304SS in BWR environments [11]. (Reprinted with Permission from Elsevier)

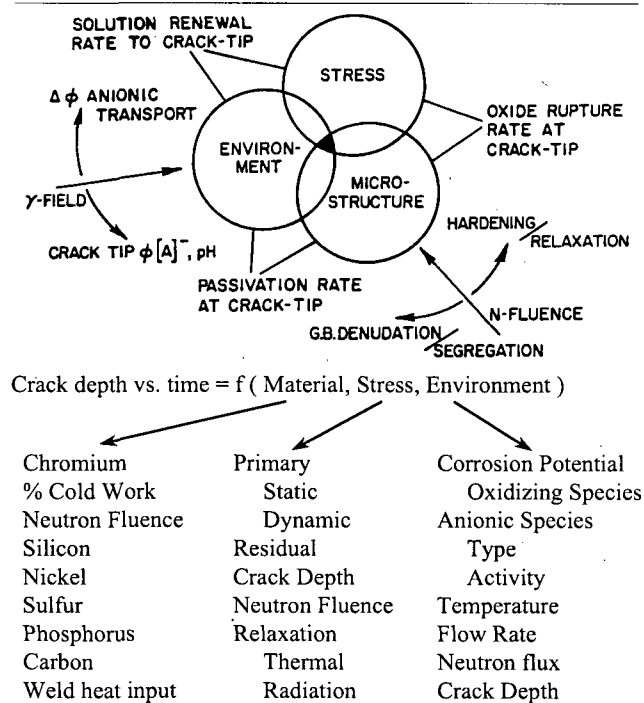


Figure B.2.4 Schematic diagram of the engineering parameters (stress, environment and microstructure), underlying scientific processes (mass transport, oxide rupture, and repassivation rates) and effects of radiation. The complexity of SCC is reflected in the large number of influential variables and the associated requirement that all 20 to 40 in a given system be adequately controlled, all of which are inter-dependently affect SCC [2,9,15]. (© NACE International 2002)

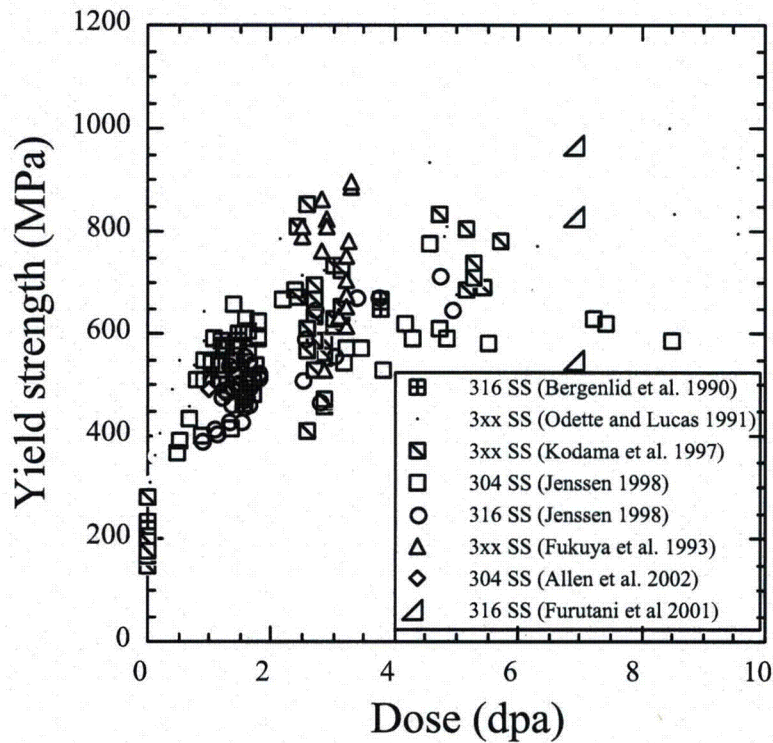


Figure B.2.5 Irradiation dose effects on measured tensile yield strength for several 300-series stainless steels, irradiated and tested at a temperature of about 300°C [11,19]. (Reprinted with Permission from Elsevier)

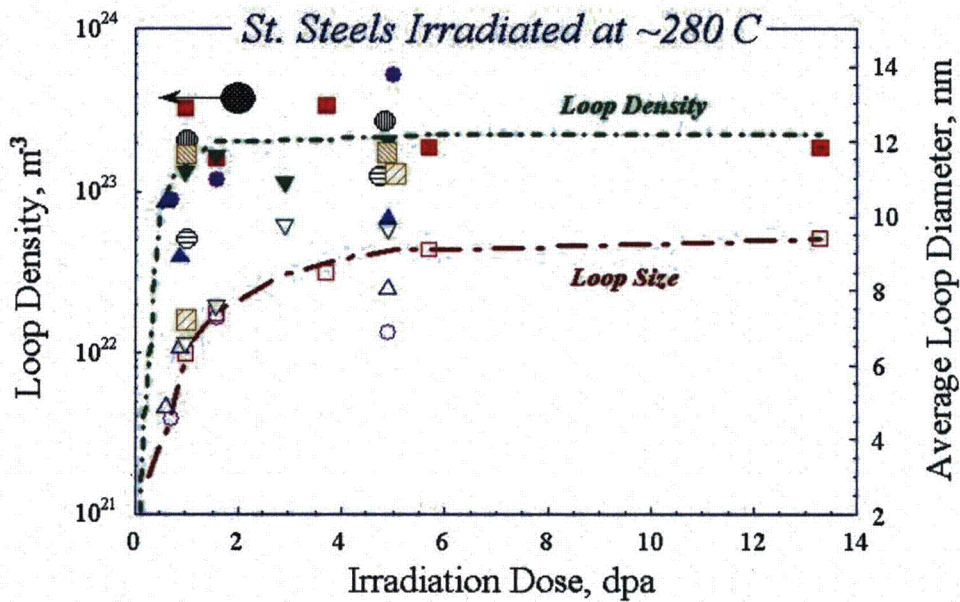


Figure B.2.6 Irradiation dose effects on the measured loop diameter and density for austenitic stainless steels at 280°C [11,19]. (Reprinted with Permission from Elsevier)

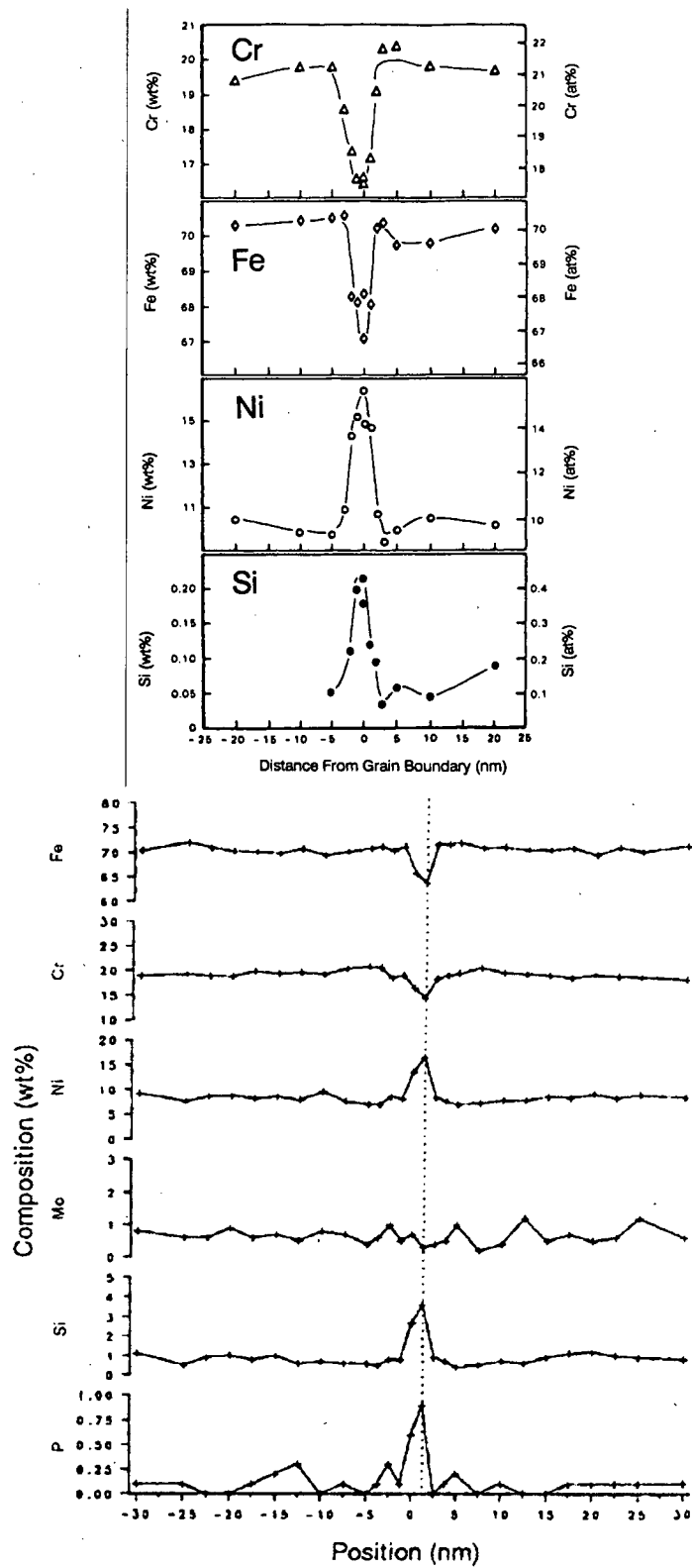


Figure B.2.7 Radiation induced segregation (RIS) of (a) high purity (including low Si) and (b) commercial purity stainless steel [9]. (© NACE International 1990)

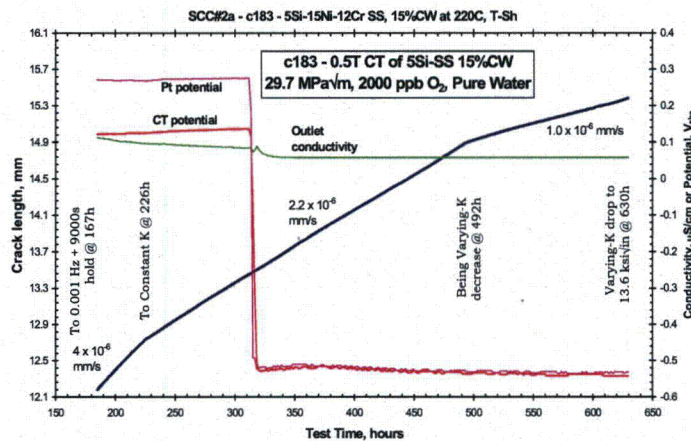
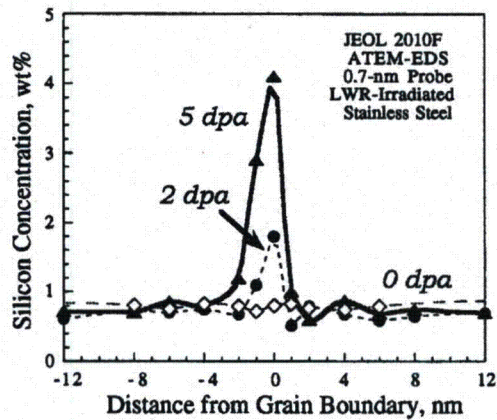


Figure B.2.8 (a) Grain boundary Si concentration in irradiated stainless steel. (b) Crack length vs. time for a 5% Si “stainless steel” whose composition simulates that in an irradiated grain boundary. No effect of corrosion potential and or stress intensity was observed. [20-22] (© 2003 by The American Nuclear Society, La Grange Park, Illinois)

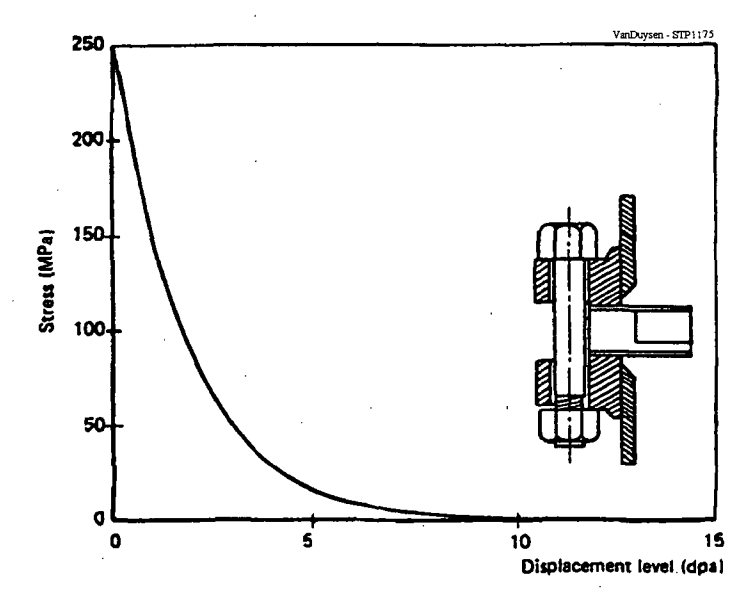


Figure B.2.9 The effects of radiation-induced creep on load relaxation of stainless steel in a constant displacement (bolt) condition [23]. (Reprinted with Permission from ASTM)

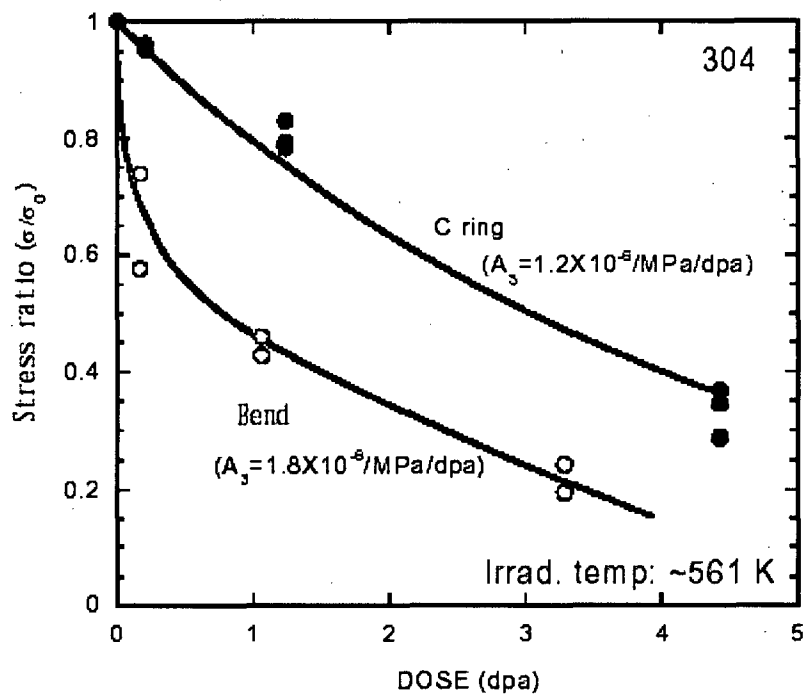


Figure B.2.10 Stress relaxation of bent beam and C-ring specimens of 304 SS in JMTR during irradiation at 288°C [23]. (Reprinted with Permission from ASTM)

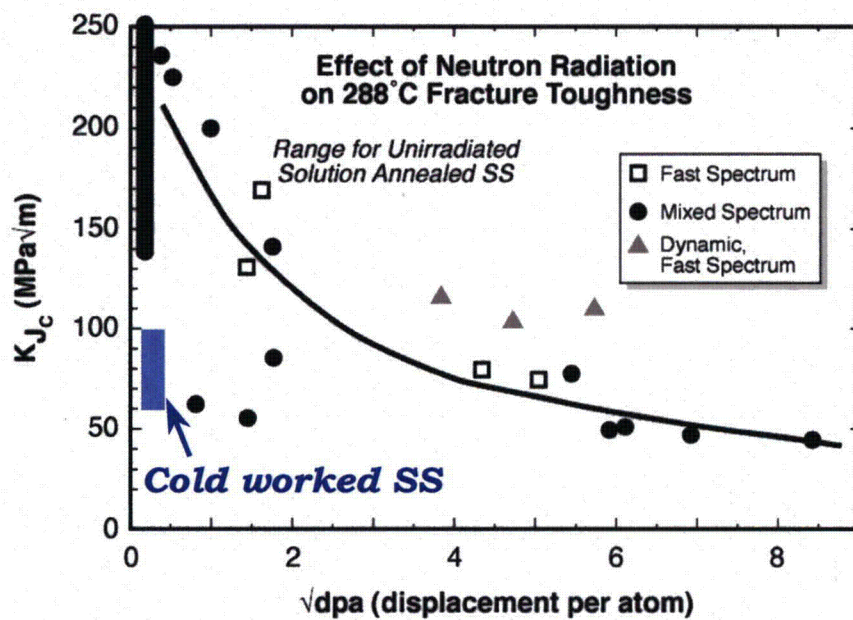


Figure B.2.11 The effect of fast neutron fluence under LWR conditions on fracture toughness of types 304 and 304L stainless steel at 288 °C [9,30,31]. A preliminary band based on the fracture toughness response of a few tests on unirradiated, cold worked stainless steel tested in-situ in 288 °C pure water is also shown [21]. (Reprinted with Permission from Elsevier)

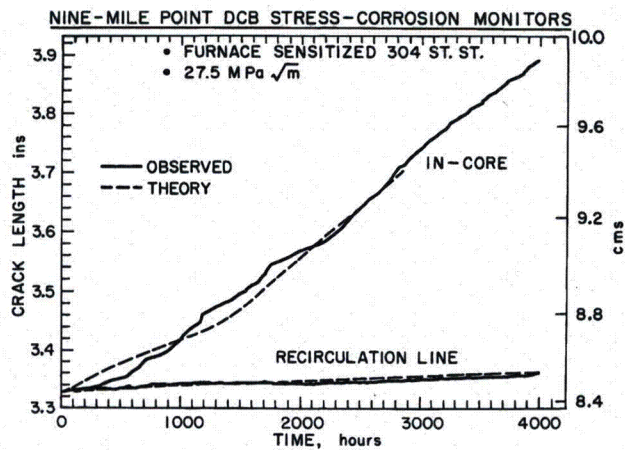
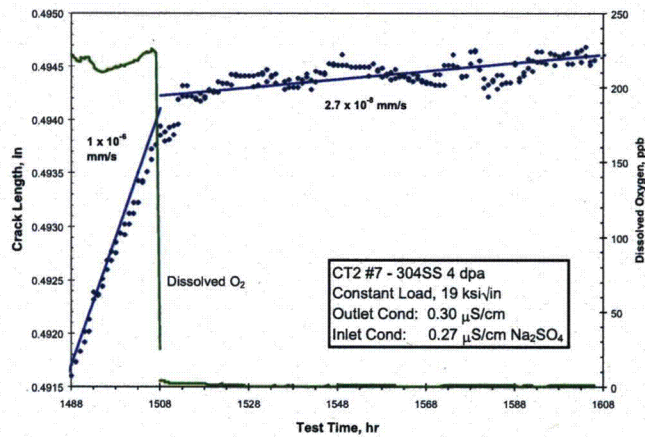


Figure B.2.12 Crack length vs. time for: (a) a CT specimen of irradiated type 304 stainless steel tested at constant load in 288 °C water at both high and low corrosion potential at 19 ksi/in. (b) DCB specimens of sensitized type 304 stainless steel exposed in core (high corrosion potential from radiolysis) and in the recirculation system [2,9,15-19]. (© 2003 NACE International 1995)



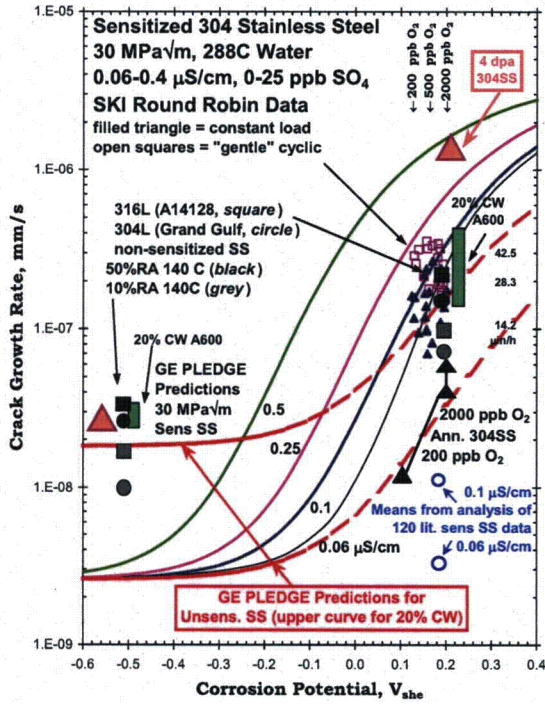
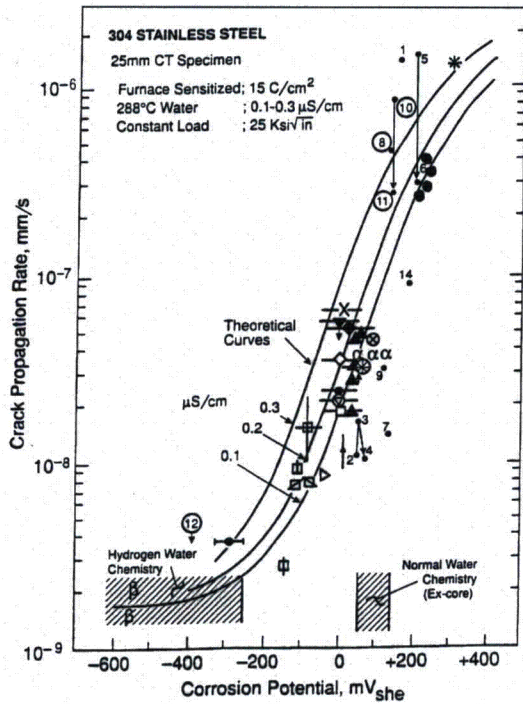
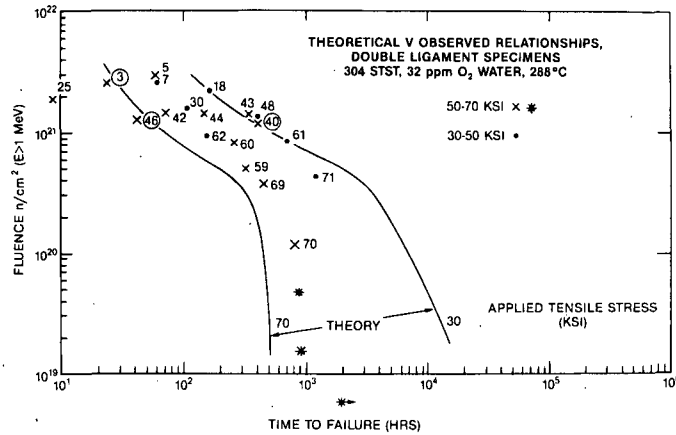
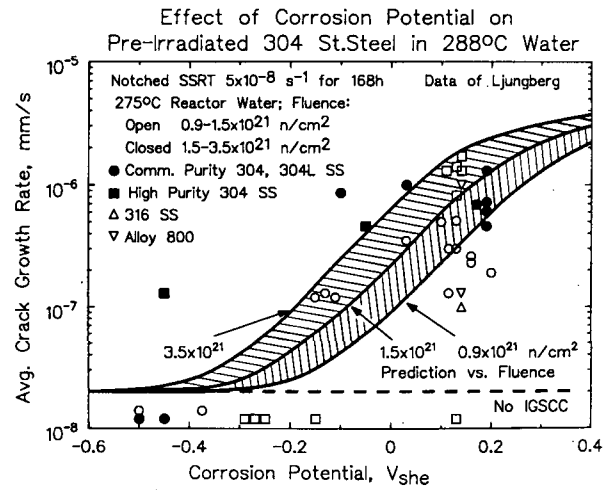
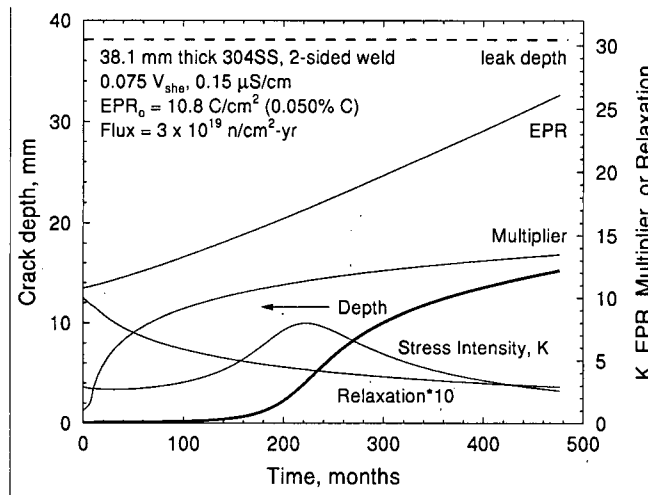


Figure B.2.13 SCC growth rate vs. corrosion potential for sensitized (left graph) and for annealed (black triangles), cold worked (large symbols), sensitized (small symbols) and irradiated (pink triangles) (right graph) SS in 288 °C water. Unirradiated and irradiated materials of similar yield strength show similar SCC response at low corrosion potential. At high potential, the combined effect of radiation hardening and radiation segregation produces a higher growth rate than either factor alone (i.e., in the unirradiated data that is either cold worked or sensitized). [2,9,15-19] (© 2003 by The American Nuclear Society, La Grange Park, Illinois)



**Figure B.2.14 Comparison of predicted and observed crack growth rates for stainless steels irradiated in a BWR at 288°C to various fluences [2,9,15-19]. (a) Notched tensile specimens were tested by Ljungberg [32] at a slow strain rate in 288°C pure water and interrupted after a given strain / time. (b) time-to-failure for the effect of fast neutron fluence on pre-irradiated type 304 stainless steel tested at constant load in the laboratory in oxygen saturated, 288 °C water [31]. (© NACE International 1995)**



H4 Shroud Beltline Weld #J4/5/6d

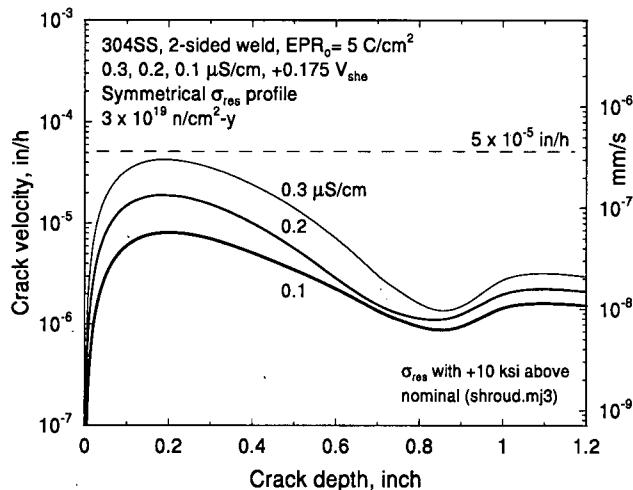
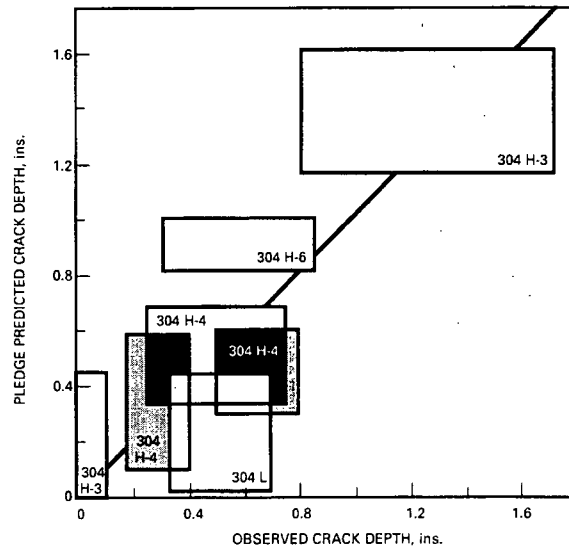
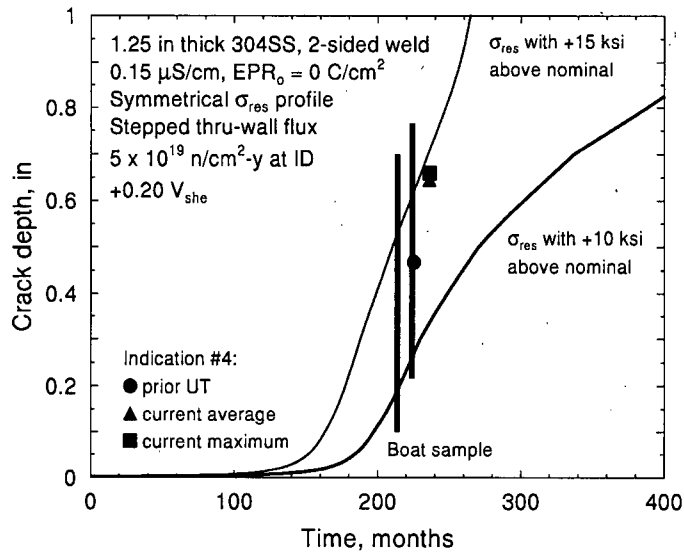


Figure B.2.15 Examples of IASCC predictions illustrating the interactions among radiation “damage” (segregation and hardening) and radiation creep relaxation (reduction in weld residual stress) for a BWR core shroud. (a) crack depth vs. time with individual curves for the increase in EPR (Cr depletion), stress relaxation, and “multiplier” (radiation hardening). The stress intensity factor is also shown, which goes through a peak due to the nature of the residual stress profile as well as radiation relaxation. (b) crack velocity vs. depth illustrating that at high coolant conductivity (0.3  $\mu\text{S}/\text{cm}$ ), cracks nucleate and grow earlier in life when the weld residual stresses are higher, resulting in higher growth rates and a shorter time to achieve a given crack depth [9,15].



**Figure B.2.16 (a) Crack length vs. time predictions and observations for a type 304 stainless steel BWR core shroud with multiple inspections and multiple cracks. (b) Comparison of observed and predicted crack depth for a number of BWR core shrouds. [9,15]. (© NACE International 1995)**

### **B. 3 “Stress Corrosion Cracking and Pitting: Contaminating External Environments,” by Robert L. Tapping**

#### **Background**

Since commercial nuclear power began, extensive research has been concerned with corrosion processes inside the piping and components. Most of this project is concerned with the results of this research including mitigations and improved procedures for operation. This chapter is concerned with corrosion in environments that are *outside* the piping and components. While the environments inside the boundaries of nuclear plants are reasonably well defined and monitored, there is a class of environments that occurs outside these pipes and components. Such environments are miscellaneous and result from impurities carried in the air, adventitious leaks, and animals including bacteria and fungi.

Many commonly used metallic materials are susceptible to localized and general corrosion when exposed to ambient, or external, conditions. Typically such corrosion occurs only when the external surface of the material or component is cool enough that ambient moisture, or in unusual circumstances, potentially corrosive non-aqueous vapors, can condense on the surface. For nuclear power plants the ambient external environment is assumed to be air, occasionally moist or wet and periodically contaminated with potentially corrosive species. The most important, and common, of these contaminants is the chloride ion, present either as salts from the local environment (sea air, for instance) or as a contaminant leached from the immediate environment, such as insulation. Sometimes contaminants arrive via animal wastes and at other infrequent times bacteria and fungi produce corrosive metabolic products.

In nuclear power plants, the most likely materials to be exposed to contaminated external environments are stainless steels (SS), usually austenitic stainless steels such as types 304 and 316, and carbon steels. The austenitic stainless steels are susceptible to stress corrosion cracking (SCC and pitting in chloride-contaminated aqueous solutions. Carbon steels may sustain [RT: a quirk of mine to avoid human emotions to describe physical processes; do as you wish] pitting in such environments. This Technical Supplement outlines the rationale behind judgments of susceptibility of nuclear power plant materials to contaminated external environments, predicted future behavior of these materials, and mitigation and life management strategies to avoid significant degradation or failures.

#### **Factors Influencing Material Susceptibility in External Environments**

This discussion emphasizes the corrosion behavior (susceptibility factors) for austenitic stainless steels and carbon steels in nuclear power plant systems where components fabricated from these materials present their outside surfaces to environments that may cause external damage. The knowledge bases underlying these susceptibility factors are discussed in the following sections. Note that for austenitic alloys and ferritic stainless steels also, containing more than about 20% Cr, the susceptibilities to such degradation is considerably less than that of the “18-8” Cr-Ni stainless steels, and commonly-used nickel-base alloys such as Incoloy 800 or 825. Thus a possible materials solution to under-deposit or marine corrosion could be selection of materials such as type 310 or 321 SS, or use of “superalloys such as AL-6X, or a Hastelloy.

However this is usually not a cost-effective solution for most nuclear applications, other than for steam condensers exposed to seawater or brackish water.

In the discussion that follows the modes of pitting and stress corrosion cracking are emphasized. These modes are the most likely to lead to damage especially as pitting might also initiate SCC or corrosion fatigue.

There are several different environments that can produce pitting and SCC. These include deposits that accumulate and crevices that form and contacts between metals or metals and non-metals. In addition bacteria and fungi can accumulate and through their metabolic processes can produce local corrosive conditions. The action of these microbes is favored by moisture and oxygen as well as nutrients. Finally, galvanic cells such as those as might occur with juxtaposed carbon and stainless steels. While the three sometimes lead to the terms "crevice corrosion, microbiological corrosion (MIC), and galvanic corrosion, these terms are really incorrect and are simply different environmental configurations where pitting and SCC both can occur.

With the configurations of crevices, MIC and galvanic juxtaposition, the chemistries that produce corrosion are acidic impurities in the atmosphere, salts such as chlorides from the ocean waters, the various chemistries of animal wastes, and acids from the metabolism of microbes. Also, corrosive chemicals are sometimes leached from insulation, polymers, paints, and floor dirt

#### Stress Corrosion Cracking:

SCC of austenitic SS occurs in low temperature environments only if the material is subject to high stress, the surface is abused by grinding or by poor machining practice, is exposed to a corrosive environment, and if the material is sensitized, for instance by heat treatment such as that which occurs on welding. Welding-induced residual stress is the most likely source of the high stresses necessary to initiate SCC, although fit-up stresses and other fabrication-related cold work (cold bending, for example) are other examples. Thus welds and bends are locations most likely to be susceptible to SCC. In the presence of chloride contamination (see below), the cracking usually takes the form of transgranular SCC (TGSCC).

The corrosive environment responsible for most external ambient temperature is oxygenated water contaminated with chloride ions. The usual temperature range of concern is from about 50°C (120°F) to about 100°C (212°F). The upper temperature depends on the dew point of the environment; typically the surface must be wet at least part of the time for SCC to occur. The source of the chloride is usually either ambient air or adjacent materials. Marine coastal environments are those most commonly chloride-contaminated, but nearby industrial sources may also occur if the power plant is situated near a large industrial complex that can emit chloride- or chlorine-contaminated air. Note that external pipe surfaces routinely exposed to rain, or frequently washed down, are at little risk of TGSCC or pitting, even in marine environments, since the rain and washing will remove the soluble chlorides.

Pipe insulation or polymeric materials such as tape are often contaminated with chloride, although the insulation sometimes contains a chemical inhibitor to reduce corrosion. For SCC to occur under insulation, or some other chloride-containing material, the material surface must be wet and in intimate contact with the insulation. Wet insulation is the

worst case, since the insulation provides a crevice environment as well as a chloride-contamination source, resulting in an increase in chloride concentration in the crevice with time. As noted above, a crevice environment can build up with time, so SCC conditions may not develop for several years.

SCC of carbon steels is unlikely to occur under these conditions but can possibly occur in the range of 100C if sufficient water and stress are available.

### Pitting

Pitting of stainless steels occurs under the same conditions as noted above for SCC, with the important exception that pitting does not require high stresses or sensitized material. Thus pitting can develop anywhere on a stainless steel component exposed to chloride contamination in a crevice environment. Austenitic SS with molybdenum additions (type 316SS, for example) are more resistant to pitting than non-Mo stainless steels such as type 304SS.

Pitting of carbon steels also can occur in external environments, although typically such pitting usually is associated with deposits or other crevices. Otherwise, carbon steels usually exhibit general or uniform corrosion in the presence of wet chloride-contaminated external environments.

### **Typical Occurrences of (TG) SCC and Pitting in Power Plants**

The most common occurrences of TGSCC or pitting of austenitic SS (primarily types 304 and 316) are under wet insulation or where piping is exposed to marine air and deposits can build up. Insulation can become wetted by water leakage from adjacent components, by washing or by soaking as a result of fire sprinkler action. Chlorides in the insulation leach out and deposit on the piping, eventually reaching concentrations sufficient to cause SCC (highly stressed areas, typically near joints/welds or at bends) or pitting. Examples of this are SCC of instrument lines and other small diameter lines.

### **Inspection and Remediation Strategies**

Inspection strategies require an assessment of which sections of piping are exposed to conditions which can promote SCC or pitting. These locations are those which can be wetted and which are in contact with chloride-contaminated insulation or coatings/adhesives/tapes, or where deposits can build up and chloride contamination is also present. Typical areas at risk are in the temperature range 60°C to about 100°C. Visual inspection for water drips, wet areas on the pipe, deposits and rust stains are a first step required to focus any further inspection. Where insulation or other coverings are present, these may need to be removed to allow an effective visual inspection. If any welds, bends or other stressed areas show any visual evidence for possible corrosive conditions, non-destructive examinations (NDE) should be carried out. Surface eddy current, ultrasonic inspection, magnetic particle, radiography or equivalent alternative and qualified procedures may be used for these inspections.

Mitigation strategies center around preventing wetting of the pipe surface or any surrounding materials that might contain chlorides. Most insulation contains corrosion inhibitors that are designed to prevent corrosion of adjacent contacted surfaces, but this needs to be verified for specific plants. Much of the insulation in power plants is covered

with metallic water-resistant jackets, and this is a good mitigation strategy, although it does interfere with any subsequent inspections. For piping exposed to outdoor environments, the mitigation strategy is to keep the piping clean and free of deposits. This is of most concern in marine environments, or areas where chloride-contaminated deposits may build up. Washing down such piping periodically is a good counter-measure. For piping that does not see high temperature internal fluids, coatings are a good corrosion prevention approach.

As noted earlier, a possible remediation strategy is to use highly corrosion-resistant materials for components exposed to potentially corrosive external environments, rather than 18-8 stainless steels or carbon steels, but this is not normally a cost-effective solution compared to good maintenance practices.

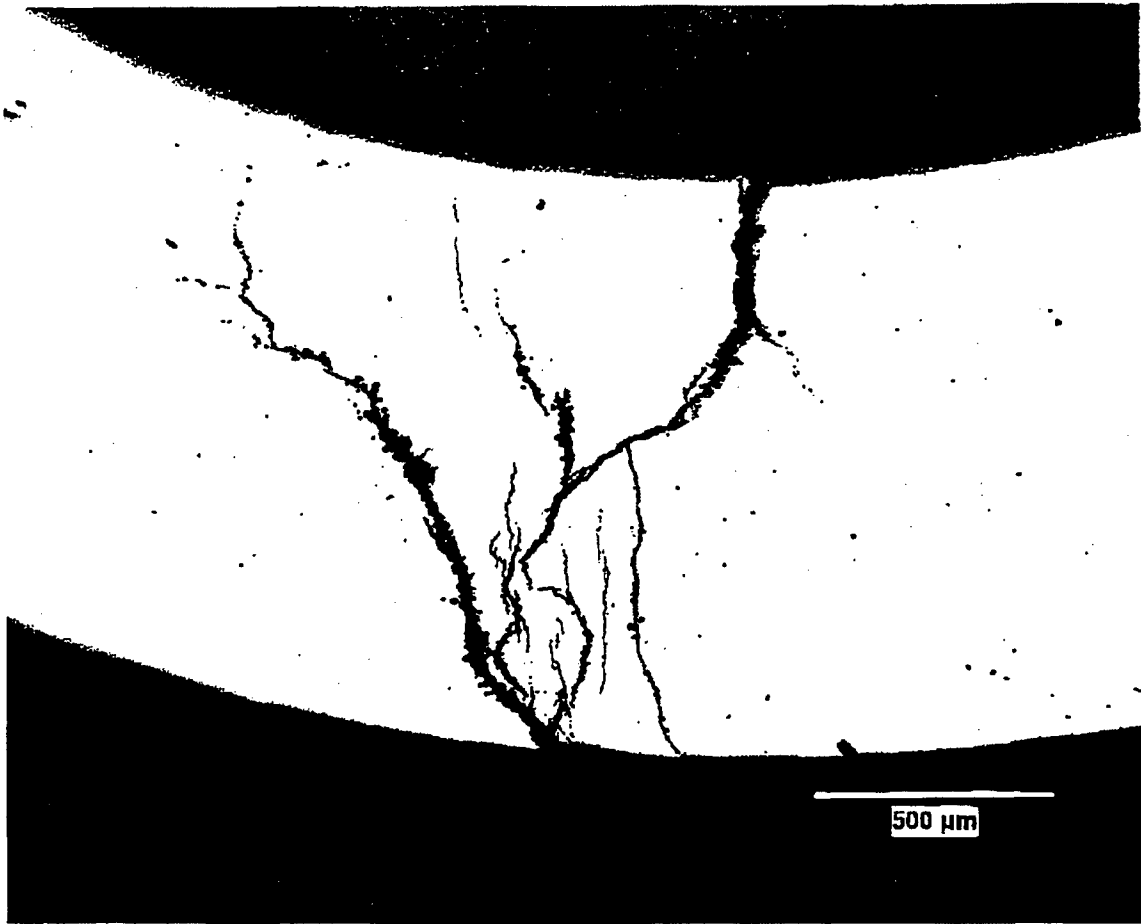
### **Life Management Issues**

Current industrial practice should include routine visual inspections for wetted, rust-stained, or fouled areas of low temperature piping. This would be an effective mitigation strategy for the longer term if accompanied by cleaning/washing and/or NDE as appropriate. It is not clear if visual inspections are a routine practice at nuclear power plants; many incidents of TGSCC of low temperature piping are managed by repair following detection of a leak. This is feasible because the low temperature piping sections or systems may be isolated and repaired on-line.

### **References for B.3**

- [1] *Uhlig's Corrosion Handbook*, Ed. R. Winston Revie, Second Edition, The Electrochemical Society, John Wiley & Sons, New York, 2000.
- [2] *Corrosion*, Volumes 1 and 2, Ed. L. L. Shreir, Second Edition, Newnes-Butterworths, Boston, 1976.
- [3] *Atmospheric Corrosion*, W. H. Ailor, The Electrochemical Society, John Wiley and Sons, 1982.
- [4] *Metals Handbook, Volume 13, Corrosion*, Ninth Edition (or latest), ASM International, Metals Park, Ohio, 1987
- [5] *Stress-Corrosion Cracking*, Ed. R. H. Jones, ASM International, Materials Park, Ohio, 1992.
- [6] *Pitting Corrosion of Metals*, Z. Szklarska-Smialowska, National Association of Corrosion Engineers, Houston, Texas, 1986.





**Figure B.3.1: Cross-Section of OD-initiated transgranular cracking in a cold-worked stainless steel line.**

## **B.4 "Thermal Aging and Embrittlement of Cast Stainless Steels,"** by Peter M. Scott

### **Introduction**

Cast stainless steels (CASS) are used for many components in Light Water Reactors including piping, elbows and T's, and particularly those components with complex shapes such as pump and valve bodies. They are not normally subject to high neutron fluxes although some CASS components on the edges of PWR cores may reach fast neutron fluences on the order of  $10^{20}$  n/cm<sup>2</sup> at end of life (for 40 years initial licensing period).

The most commonly used CASS materials are SA-351 grades CF-3, CF-3A, CF-8, CF-8A and CF-8M, the specifications of which are shown in Table B.4.1. They have a duplex ( $\gamma$ ) austenite /  $\delta$  ferrite microstructure and are susceptible to thermal aging embrittlement of the  $\delta$  ferrite phase at typical PWR and BWR operating temperatures. The volume fraction of ferrite is typically 10 to 20% but may attain 25%; only the lower limit is imposed by the ASME code. Stainless steel weld deposits, typically Type 308 and 309, have a similar duplex microstructure but with a lower volume fraction of ferrite typically in the range 5 to 10% and notably lower Cr contents.

Embrittlement of the  $\delta$  ferrite phase results in an increase in hardness and loss of ductility and of fracture toughness. The mechanisms of thermal aging have been extensively studied from the point of view of microstructural changes resulting in the formation of nanometer-scale embrittling phases. Predictive, albeit empirical, equations have been developed for the purpose of forecasting the deterioration in mechanical properties over typical reactor lifetimes.

The purpose of this appendix is to provide a summary of current understanding of the thermal aging mechanism of CASS and the application of that knowledge currently proposed in the United States for predicting changes in mechanical properties and loss of fracture toughness in PWR and BWR components [1,2,3]. There are no known published studies of the stress corrosion resistance of these materials in the aged and embrittled condition when exposed to PWR or BWR primary coolants although there are some instances of stress corrosion cracks propagating into stainless steel weld metals in BWRs, apparently along the  $\delta$  ferrite, after long periods of service. There are also no known published studies of the influence of these aqueous environments compared to air on fracture resistance.

### **Mechanism of thermal aging**

Thermal aging embrittlement of CASS at temperatures below about 400°C arises primarily as a consequence of a thermally activated separation of chromium by diffusion in the Fe-Cr solid solution of the  $\delta$  ferrite phase resulting in the formation of an iron rich  $\alpha$  phase and a chromium rich  $\alpha'$  phase. This process is called 'spinodal decomposition' and occurs mainly at the higher chromium contents greater than ~23% in the  $\delta$  ferrite (for temperatures <400°C). The  $\alpha'$  phase may also form by precipitate germination and growth, particularly at temperatures >400°C, but can also contribute at lower temperatures depending on the precise combination of chromium content and temperature e.g. <~26%Cr at 400°C and <~23%Cr at 300°C. The austenite phase of CASS is unaffected by thermal aging in the same temperature range:

The formation of  $\alpha'$  during thermal aging can affect all Fe-Cr solid solutions with Cr contents in solution >10%. An "oscillation" in the resulting Cr distribution is observed by high resolution microscopic techniques with "wavelength" (measured in nanometers) and amplitude increasing with aging time and temperature. The effect increases notably with the Cr and Mo content of

the ferrite phase and consequently CF-8M is less resistant to aging than CF-8 or CF-3 without Mo. The formation of embrittling  $\alpha'$  phase from  $\delta$  ferrite is enhanced by other alloying elements such as silicon which together with Cr and Mo can be represented by the chrome equivalent. The presence of the adjacent austenite phase in CASS appears to exert a detrimental influence relative to purely ferritic alloys of similar composition.

Other precipitation phenomena occur in the  $\delta$  ferrite phase and at the ferrite-austenite interfaces above about 350°C, particularly the formation of the fcc Ni,Si,Mo rich G phase which can reach up to 12% by volume in Mo containing CASS. Carbon also enhances G phase precipitation. Nevertheless, G phase does not appear to contribute significantly to hardening and loss of toughness. At higher temperatures between 400 and 500°C other intermetallic phases precipitate but to a much lesser extent than G phase. However, extensive carbide (and sometimes nitride) precipitation, particularly at austenite-ferrite interfaces, occurs in the Mo-free CASS.

Although the microstructural evolution of CASS during thermal aging is fundamentally driven by solid-state diffusion processes, the complexity and changing nature of the phenomena with temperature is such that extrapolation over large temperature ranges using Arrhenius type relations is very difficult. Accelerated thermal aging for PWR and BWR applications is generally only carried out up to 400°C where hardening of the  $\delta$  ferrite by  $\alpha'$  formation is the predominant aging process. Even with this restriction, the apparent activation energy observed for changes in mechanical properties such as hardness and toughness (see next section) can be very variable and sometimes significantly below the activation energies of 210 to 260 kJ/mole associated with diffusion of metallic species, particularly Cr, in ferrite.

### **Mechanical properties of thermally aged CASS**

The complexity of the microstructural changes associated with thermal aging of CASS gives rise to very strong material and heat dependencies for the extent and kinetics of evolution of mechanical properties. Consequently, very careful studies have been necessary to determine the range of temperature, composition etc for which mechanical properties data obtained from accelerated aging tests can be applied to service conditions.

The overall degree of embrittlement depends strongly on the amount, composition and distribution of the ferrite phase. The increase in hardness and decrease of ductility of the ferrite phase due to thermal aging promotes premature cleavage in this phase that can extend preferentially through it if there is a continuous ferrite network. Even if the fracture path intersects the austenite, deformation induced martensitic transformation can allow the brittle fracture to extend beyond the embrittled ferrite.

The main parameter used for characterizing the evolution of mechanical properties due to thermal aging has been the Charpy impact energy. Measurements of tensile properties, hardness, microhardness of the ferrite phase and J-R fracture resistance curves have also been made.

Thermal aging of CASS at BWR and PWR operating temperatures is characterized by an increase in hardness and tensile strength and a decrease in ductility, impact strength and toughness. In addition, the "brittle-ductile" transition temperature increases and the upper shelf decreases. Examples of Charpy impact energy measurements at room temperature on many heats of CASS are shown in Figure B.4.1. Although the dispersion in the results is large, all heats show a clear trend to a saturation of the aging effect (lower plateau value of Charpy

impact energy) that is independent of aging temperature, at least up to 400°C. The main trends in the data are with chemical composition, the plateau Charpy impact energy decreasing with increasing ferrite and chrome equivalent.

A procedure proposed in the United States for estimating the toughness of CASS components in service is based on empirical equations relating Charpy impact energy to the chemical composition, notably Cr, Mo, Si and C (i.e.  $Cr_{eq}$ ), and time and temperature, including accelerated aging data at temperatures up to 400°C. The kinetics of aging are based on Arrhenius type correlations in which the apparent activation energy also depends on the concentrations of the aforementioned elements. The toughness ( $J_{0.2}$ ) and J-R curve are then estimated from empirically established correlations with the Charpy impact energy from room temperature to normal operating temperatures. Lower bound estimates of end-of-life toughness are made based only on the chemical composition and lower bound correlations if no further details of the microstructure are available. The procedure can be refined if the initial Charpy impact energy and/or ferrite content are known, for example by classifying the material into three groups defined for <10%, 10 to 15%, and >15% ferrite.

A method proposed in the United States for screening CASS components for their potential susceptibility to thermal aging embrittlement is to divide all such components into six categories as shown in Table B.4.2. The indicated ferrite levels may be calculated or measured. All components identified as having a potentially significant reduction in fracture toughness due to thermal aging are then placed in an aging management program. The NRC staff position is described in a letter dated May 19, 2000 from C.I. Grimes (NRC) to D. J. Walters (NEI). A corollary of this classification is that no significant thermal aging is anticipated for stainless steel weld deposits because of the low ferrite contents relative to CASS. However, studies of the fracture properties of weld heat affected zones in aged CASS do not appear to have been published.

It is important to note that there is significant variability internationally in approaches used to estimate the degradation in CASS toughness that can lead to differing judgments of the significance and extent of thermal aging embrittlement. In particular, the US approach eliminates from consideration all heats known or believed to contain niobium on the grounds that these are out of specification in the USA. The counter argument is that niobium precipitates as niobium carbide very quickly and in any case has no significant effect on toughness in either the as-received or thermally aged condition. An even greater dispersion in possible toughness levels and a significantly reduced lower bound compared to that adopted in the US have been measured [1,4], i.e., significantly lower than the saturation room temperature impact energy of  $\sim 25 \text{ J/cm}^2$  seen in Figure B.4.1. It is acknowledged, however, that the very low toughness heats in the international population of CASS heats is strongly influenced by heats from a particular foundry that has not supplied the US market. Nevertheless, the range of ferrite contents and chrome equivalents are not considered to be unrepresentative of the range encountered in CASS used in US plants.

### **Other possible degradation phenomena**

As mentioned in the Introduction, some CASS components below or above the core can be irradiated possibly up to  $\sim 10^{20} \text{ n/cm}^2$  at the end of a 40 year licensing period. Since the fracture resistance of fully thermally aged CASS is essentially that of the network of austenite (because the fully thermally aged ferrite is so brittle and hardly contributes at all to remaining fracture toughness), the effect of irradiation damage will only be significant if the austenite is embrittled by neutron irradiation. At a neutron fluence of  $\sim 10^{20} \text{ n/cm}^2$  the mechanical properties of

austenitic stainless steels are scarcely affected. It follows, therefore, that no significant effect of irradiation damage on fracture resistance of CASS is anticipated in the fully thermally aged condition. Of course, at intermediate stages of thermal embrittlement of the ferrite phase, the effect of irradiation damage on fracture toughness could be more marked. The industry is currently investigating the mechanical and fracture of irradiated CASS to check the anticipated behavior described.

It is well known that fracture resistance can be affected by the environment in which the fracture events occur. For example, the fracture resistance of nickel base weld metals appears to be significantly reduced in a PWR primary water environment compared to air at temperatures below about 150°C, probably due to hydrogen embrittlement (See Paper B.13 N° 13). Given the nature of the embrittlement of the ferrite phase in CASS, it is reasonable to suppose that some effects of hydrogen embrittlement may also combine with thermal aging embrittlement in this case. However, there are no known published studies of the effects of aqueous environments on fracture resistance of CASS although certain electrochemical non-destructive tests proposed for the detection of thermal aging embrittlement of CASS depend on different dissolution response between aged and non-aged material[5,6]. In oxidizing environments such as BWR normal (oxygenated) water chemistry, this could result in preferential dissolution/oxidation at the  $\gamma$ -ferrite interface. Such differences would be less likely in hydrogenated BWR hydrogen water chemistry or PWR primary water chemistry. On the other hand, hydrogen entry into the aged duplex stainless steels, especially into the hardened ferrite phase, may raise some concerns.

An ancillary question to the one posed above concerns the stress corrosion/hydrogen embrittlement behavior of thermally aged CASS but again there are no known published studies other than the (unexpected) observations of stress corrosion cracks propagating into stainless steel weld metals mentioned in the Introduction.

Some effort has been devoted to examining fatigue and corrosion fatigue S-N and fatigue crack propagation behavior of CASS. The corrosion fatigue data for de-oxygenated PWR environments appear to present similar environmental effects as wrought stainless steels. Given the unresolved controversy regarding how to incorporate such environmental effects in fatigue evaluations no further discussion is given here. The extent to which these corrosion fatigue studies extend to thermally aged material is not known.

#### References for B.4

- [1] M. Guttman, "Intermediate temperature aging of duplex stainless steels. A review," pp 79- 92, Proceedings of "Duplex Stainless Steels '91," October 28-30, 1991, Beaune, France. Ed J. Charles & S. Bernhardsson.
- [2] O. K. Chopra, "Estimation of fracture toughness of cast stainless steels during thermal aging in LWR systems – Revision 1," NUREG Report CR-4513-Rev1, August 1994.
- [3] License Renewal Issue No. 98-0030, "Thermal aging embrittlement of cast austenitic stainless steel components," NRC, May 19, 2000.
- [4] A. Bache, M. Akamatsu, P. Ould, P. Thibaut, H. Churier-Bossenec, G. Bezdikian, "Contribution de l'expertise des coudes déposés lors de RGV à la validation des méthodes de caractérisation et la justification de la tenue en service des produits moulés" (Translated: "Contribution of experimental investigations on cast elbows removed from service during steam generator replacement and validation of the methods used for characterizing and justifying the in-service behavior of CASS"), pp

967-976, Proceedings of International Symposium Fontevraud V, 23-27 September 2002.

- [5] Y. S. Yi and T. Shoji, "Detection and Evaluation of Material Degradation of Thermally Aged Duplex Stainless Steel: Electrochemical Polarization Test and AFM Surface Analysis". *Journal of Nuclear Materials*, 231, (1996), 20-28.
- [6] Y. S. Yi and T. Shoji, "Quantitative Evaluation of Material Degradation of Thermally Aged Duplex Stainless Steels Using Chemical Immersion Test ". *Journal of Nuclear Materials*, 240, (1996), 62-69.

**Table B.4.1 ASME Specifications for CASS Grades Commonly Used in PWR and BWR**

	CF-3	CF-3A	CF-8	CF-8A	CF-8M
Carbon %max	0.03	0.03	0.08	0.08	0.08
Manganese %max	1.50	1.50	1.50	1.50	1.50
Silicon %max	2.00	2.00	2.00	2.00	1.50
Sulfur %max	0.040	0.040	0.040	0.040	0.040
Phosphorus %max	0.040	0.040	0.040	0.040	0.040
Chromium	17.0-21.0	17.0-21.0	18.0-21.0	18.0-21.0	18.0-21.0
Nickel	8.0-12.0	8.0-12.0	8.0-11.0	8.0-11.0	9.0-12.0
Molybdenum %max	0.50	0.50	0.50	0.50	2.0-3.0
Tensile strength Min Ksi (MPa)	70 (485)	77 (530)	70 (485)	77 (530)	70 (485)
Yield strength Min Ksi (MPa)	30 (205)	35 (240)	30 (205)	35 (240)	30 (205)
Elongation Min %	35.0	35.0	35.0	35.0	30.0

**Table B.4.2 Proposed Thermal Aging Screening Criteria in EPRI TR 106092**

Mo Content (Wt. %)	Casting Method	Ferrite Content	Significance of Thermal Aging
High (2.0 – 3.0)	Static	All	Potentially significant
	Centrifugal	>20%	Potentially significant
		<20%	Non-significant
Low (0.50 max.)	Static	> 20%	Potentially significant
		<20%	Non-significant
	Centrifugal	All	Non-significant

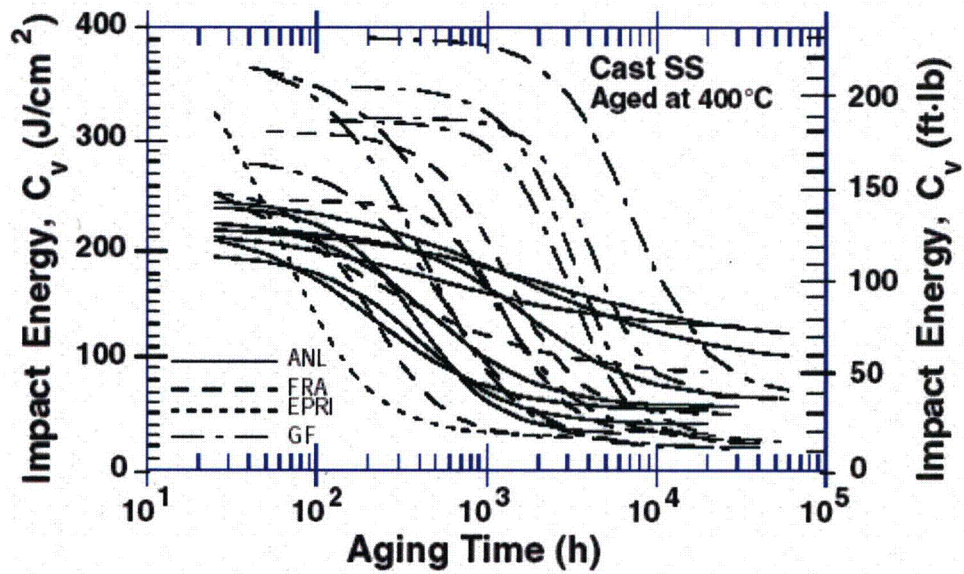


Figure B.4.1 Decrease in Charpy impact energy for various heats of cast stainless steels aged at 400°C (2).



## **B.5 “SCC of Ni Alloy 600 and Alloy 182 and 82 Weld Metals in BWR Water,”** by Peter L. Andresen

### **Introduction**

Nickel alloys were originally specified for BWR components for their resistance to corrosion and stress corrosion cracking (SCC) – as indicated by early laboratory data and field experience – and because their thermal expansion coefficient is similar to the low alloy steel used for the reactor pressure vessel. Typical compositions of the relevant nickel alloys are shown in Table B.5.1. Table B.5.2 provides a list of BWR components where Alloy 600 and Alloy 182 and 82 weld metals have been used.

Intergranular stress corrosion cracking (IGSCC, Figure B.5.1) susceptibility of Alloy 600 and high strength alloys (e.g., Alloy X750) in high temperature water was demonstrated in laboratory testing over 50 years ago [1]. Significant cracking of nickel alloys began to occur in BWR components in the 1970s, and SCC has become the primary materials issue with nickel alloys in light water reactors. For Ni alloy weld metals, so-called interdendritic cracking (actually intergranular, as grain boundaries form as groups of dendrites grow during solidification) is the morphology of SCC observed in plant components and relevant laboratory tests (Figure B.5.1).

While SCC of nickel alloys in PWR and BWR systems has been considered a distinct and different phenomena (e.g., as indicated by the term “Primary Water SCC,” or PWSCC in PWRs), there is a evidence showing that there are many common dependencies and a well-behaved “response surface” as a function of changing temperature, oxidant level, H<sub>2</sub> level, and water purity [2-7]. Appendix B.6 [8] provides a detailed description of SCC observed in various nickel alloys in PWR primary and secondary (steam generator) components. In PWR applications, when Alloy 600 components are replaced, it is usually by Alloy 690 and its compatible weld metals, Alloys 152 and 52. These have proven to be more resistant to PWSCC in severe laboratory tests and, to date, after 16 years in service. Alloy 800 steam generator tubes are also quite resistant to SCC, although their tolerance to poor secondary chemistry is probably lower. This Appendix focuses on the operating experience and known dependencies of nickel alloys in BWR environments.

### **Nickel Alloys Components in BWRs**

Nickel-base weld materials are used throughout the BWR [9], and are more prevalent than wrought nickel alloy components (Table B.5.2). Alloys 182 and 82 are used to join the low alloy steel pressure vessel and pressure vessel nozzles to wrought nickel alloys and austenitic stainless steel components. Alloy 182 is typically used as a coated stick electrode designed for manual welding, whereas Alloy 82 is typically used in wire form for automated TIG or MIG welding. Figure B.5.2 provides a schematic of the key components and their locations in GE BWRs, and Figures B.5.3 – B.5.8 show the configurations of various locations where Alloy 182 and 82 welds exist.

There are several different nozzle-to-safe-end welds where Alloy 182 weld metal has been used for the nozzle butter and/or the weld joint. These include the recirculation inlet and outlet nozzles, the core spray nozzles, the jet pump instrumentation nozzles, and the feedwater nozzles; the actual configuration depends on the specific vessel

fabricator. Figure B.5.3 shows the typical details of Alloy 182 and 82 weld build-up used in many BWRs. Alloy 182 was often used to butter the safe end, after which the vessel was heat treated (tempered) to restore its properties. Following this post-weld heat treatment (PWHT), the subsequent weld to the safe end was typically made with an Alloy 82 root pass, and then the weld was completed with Alloy 182. The dendritic structure shown in Figure B.5.1 develops during weld solidification of both Alloys 182 and 82 welds, with the dendrites growing toward the top of the weld. Even when the entire weld was nominally made of Alloy 82, weld repair records at some plants showed that Alloy 82 weld repair was performed by manual welding using Alloy 182 because of the repair geometry or limited access. Weld repairs in general are suspected of being the origin of preferred crack initiation and faster crack growth. Many weld repairs are poorly documented. The start and end point of welds (especially when performed by manual stick electrode) are also areas of concern.

Type 308/L stainless steel weld cladding is deposited over most of the exposed pressure vessel surface. Essentially all internal attachments to the pressure vessel are made using Alloy 182 pads that are welded directly onto the pressure vessel after the stainless steel cladding and before the post-weld heat treatment. Stainless steel weld metal has proved to be more resistant to SCC than Alloy 182 weld metal. The Alloy 182 attachments include the steam dryer hold down brackets, core spray brackets and shroud support structures. The latter was typically constructed of wrought Alloy 600, with Alloy 182 welds used for its construction and attachment to the vessel. This represents the largest circumference of nickel base weld. The structure in many cases is supported by legs that are welded to the bottom head of the RPV. Alloy 182/82 welds were used for many of the penetrations through the bottom of the pressure vessel – the most numerous being the control rod drive (CRD) housings. Finally, in most BWRs, water is pumped through the core using jet pumps, which require circular openings in the Alloy 600 support ledge, and are attached using Alloy 182/82 welds.

In the standard BWR environment (normal water chemistry, or NWC), the water chemistry is oxidizing and Alloy 182 is susceptible to SCC. Alloy 182 cracking was first discovered during replacement of weld sensitized stainless steel recirculation piping. Since then, there have been continuing instances of cracking in Alloy 182. This document discusses the field cracking characteristics of Alloy 182, SCC dependencies, mitigation techniques, and improved materials.

### **History of SCC in BWR Nickel Alloy Components**

All of the nickel alloy components and welds listed in Table B.5.2 and Table B.5.3 have experienced SCC at one time or another in BWRs. There has also been extensive cracking of creviced Alloy 600, primarily in the form of shroud head bolts, safe ends, and ledge and access hole covers. For nickel alloys and stainless steels, a high initial incidence of cracking occurred, primarily due to poor water chemistry during the early operation of most BWRs. While dramatic improvements were made in water purity, once cracks nucleated, growth was readily sustained even in good quality water. For example, Figure B.5.9 shows the correlation between BWR water purity and incidence of cracking in Alloy 600 shroud head bolts. In addition to the important effect of *average* water purity, both prediction and plant data show that very high conductivity early in life produced a different population of (more severe) cracking than is reflected by the plant *average* conductivity.

The overall experience with wrought nickel alloys in BWRs has been better than with welded austenitic stainless steels, where IGSCC has been widely observed in the heat affected zone of types 304 and 316 stainless steel (but rarely in type 308/L weld metal). This is especially true for weld sensitized stainless steel, but unsensitized stainless steel has also cracked extensively, primarily due to the combination of weld residual stresses and weld shrinkage strains. Residual strains peak at the weld fusion line and are generally equivalent to 15 – 20% room temperature tensile strain [10, 11].

There has been very good experience with Alloy 600 in the welded, uncreviced condition, particularly in the bottom-head region; extensive SCC of Alloy 600 has occurred in the creviced condition. Alloy 182 weld metal has not performed nearly as well. Initial concerns for the SCC performance of Alloy 182 were raised in laboratory test data from the US [12] and subsequently confirmed internationally, e.g. [13]. This led to the recommendation to inspect weld metal butters during replacement of recirculation piping that was necessitated by IGSCC of weld sensitized, large diameter Type 304 stainless steel pipes. The first inspection, performed at a BWR/3 in the 1984 timeframe, revealed cracking in several welds. Inspections were performed in the recirculation inlet and outlet safe ends during the piping replacement [14]. Cracking was detected using dye penetrant exams in 3 of 10 inlet nozzles and 1 of 2 outlet nozzles. The cracking was axial in all nozzle butters, with a maximum depth of about 70% of wall thickness. Boat samples were removed from one weld that attached the stainless steel safe end to the outlet nozzle. Metallography verified that the cracking was confined to the Alloy 182 weld and did not extend into the low alloy steel. It also established that cracking was "interdendritic" (actually along intergranular dendrite boundaries), and did not penetrate into the Alloy 82 root pass (corroborating the higher SCC resistance of Alloy 82 weld metal shown in laboratory data). Many axial segments initiated in the Alloy 182, with several circumferential segments that followed the fusion line.

Subsequently, cracking was detected in other BWRs. The number of nozzle-to-safe end welds affected varied from plant to plant, with one plant having six cracked nozzles. The frequency of cracking has now decreased but leakage has occurred in some smaller diameter pipes. Some cases were associated with weld repair locations and improper classification of inspection findings as weld geometry or internal weld defects. The cracked nozzles included recirculation inlet and outlet, core spray and feedwater nozzles. The cracking has remained primarily axial in nature, although there are some instances of circumferential cracking. Many of these cracked welds have been overlay repaired with a structural build-up of SCC resistant material to restore structural margin / integrity.

Knowledge of cracking in BWR core internal structures was very limited until the late 1990s, primarily because only a limited number of inspections were performed. The first components to be evaluated were the access hole covers, which were welded during plant construction after access was no longer needed to the lower plenum region. These welds were particularly susceptible because crevices existed where the cover recessed into the ledge. While cracking occurred in the creviced wrought Alloy 600 in many plants, it also initiated and/or propagated in the Alloy 182 weld metal. This heightened the concern for SCC of Alloy 182 in other locations.

The first instances of SCC in un-creviced attachment welds were found in hold-down brackets on the reactor vessel head that restrained the dryer assembly. These locations were readily inspected, and subsequent metallurgical evaluations confirmed the extent

and morphology of cracking. The extent of cracking could not be accurately detected visually; only PT examination or proper UT interrogation could accurately characterize the extent of the tight weld cracks. While the cracked areas could be removed or repaired, their proximity to the RPV material heightened the need for periodic inspection of Alloy 182 welds in the reactor. Improved inspection approaches were developed by the EPRI BWR Vessel and Internals Project (BWRVIP) between 1995 and 1998.

Subsequently, extensive SCC was discovered in Alloy 182 welds in the shroud support structure of a BWR-2 during a core shroud replacement in 1999. Visual inspections and liquid penetrant examinations were performed on the shroud support structure, revealing cracks in the attachment welds joining the conical support structure to the reactor vessel wall (Figure B.5.8). This cracking was found in the weld build-up pad on the vessel wall (designated the H9 weld), as well as in other Alloy 182 welds and adjacent Alloy 600 in the lower conical section. The cracking of greatest interest was that found on the inside weld (the lower bottom side) of the H9 weld, where nearly 300 individual cracks were found in 34 locations. These cracks were largely axial in nature (~90%); however, none of the cracks entered the RPV low alloy steel. Since cracking was associated solely with the underside of the actual core support structure, it was not detected during routine visual in-service inspection from the top surface. This led to inspections at other BWRs, and similar cracking was detected in another BWR/2 at the same H9 weld [15]. While the inspection technique was focused on circumferentially oriented cracking because the UT system was deployed from inside the vessel, the cracking appeared to be primarily axial.

### **Understanding Alloy 182 Behavior in BWRs**

Normal water chemistry (NWC) has existed over most of the life of the BWR fleet. NWC is oxidizing because radiolysis forms  $H_2O_2$  and  $O_2$ , and oxidizing conditions accelerate SCC initiation and propagation. The oxidizing conditions are properly characterized by their effect on the corrosion potential, which is a kinetic balance between reduction reactions (e.g.,  $O_2$  and  $H_2O_2$ ) and oxidation reactions (e.g.,  $H_2$  and metal oxidation). Given the large benefit of reduced corrosion potential, most BWRs have modified their operating environment by adding hydrogen, termed hydrogen water chemistry (HWC). In the last decade, most BWRs have also performed noble metal chemical addition (NobleChem™), which mitigates the oxidizing characteristics of the coolant environment by creating a catalytic surface, and reduces the amount of hydrogen addition required [16,17]. Provided there is sufficient  $H_2$  (i.e., twice the molar concentration of  $O_2$ ), all of the  $O_2$  that arrives at the surface is reacted to form water and the corrosion potential drops to very low values.

IGSCC in nickel alloys in BWR environments is best described by the slip dissolution / oxidation mechanism, which also applies to austenitic stainless steels. This mechanism accounts for the simultaneous requirement for stress, susceptible material and oxidizing environment [2-7], and quantifies their effects in terms of the *crack tip system* that exists as a crack advances. Over the last two decades the BWR community has performed extensive research to quantify the crack growth behavior of Alloy 182 and other nickel alloys as a function of corrosion potential, water purity, stress intensity factor, etc.

For example, Figure B.5.10 shows the strong dependence of growth rate on ECP in 288 °C water [7]. Figure B.5.11 shows the growth rate response vs. corrosion potential for a wider variety of Ni alloys, including Alloy X750, cold worked Alloy 600 and stainless

steel. It should be noted that weld shrinkage strains are typically equivalent to 15 – 20% room temperature strain in the heat affected zone. Figures B.5.12 and B.5.13 show the typical magnitude and timing of the change in crack growth rate as the water chemistry conditions are changed. An inter-relationship exists among most parameters that affect SCC; thus, for example, the effect of water purity varies with corrosion potential, and the effect of stress intensity factor (K) varies with water and material chemistry. Figure B.5.14 shows a low K dependence consistent with the mechanisms-based prediction for the aggressive water chemistry. In addition to extensive laboratory crack growth rate studies, there have been extensive crack initiation tests, component tests, in-reactor assessments of field cracking, and modelling of SCC growth rate response.

Based on these data, and data from many other investigators, e.g. [18], both NWC and HWC disposition rates for crack growth of Alloy 182 were developed [19]. The data clearly show a lower crack growth rate in HWC compared to NWC. However, measurable crack growth can occur at low corrosion potential, as shown by laboratory data on nickel alloys and stainless steels, and supported by fundamental insights into SCC. Figures B.5.10 – B.5.13 are examples of the crack growth response at low corrosion potential; with typical rates in Alloy 182 weld metal of  $\approx 5 \times 10^{-9}$  mm/s, with higher rates up to  $\sim 5 \times 10^{-8}$  mm/s for higher strength or cold worked alloys. Note however that these rates are still an order of magnitude lower than those expected when compared with comparable material conditions and “normal water chemistry.” The laboratory data and fundamental understanding accounts for the cracking found in BWR operating plants and supports the benefit of HWC in mitigating crack growth.

### **Comparison with PWR Environments**

Many of the factors used to distinguish SCC response in BWRs vs. PWRs have proven to be artificial [2,4,6,25]. The positive experience of thermally treated Alloy 600 in PWRs was considered to contradict the deleterious role of grain boundary carbides and Cr depletion in BWRs. However, grain boundary carbides are in fact beneficial in both environments, although when accompanied by Cr depletion, SCC susceptibility increased in oxidizing environments. This is clearly attributable to the slower repassivation rates at lower Cr concentrations in the pH-shifted chemistries that form when oxidants are present.

BWRs that employ NobleChem™ to catalytically achieve low corrosion potentials operate under conditions that are broadly similar to the PWRs primary environment. There are three primary differences: solution pH, H<sub>2</sub> fugacity, and temperature.

In deaerated (e.g., PWR water), variations in solution pH in the near-neutral regime have little effect on SCC [20], although it has some effect on the corrosion potential (112 mV / pH unit at 288 °C) because the corrosion potential under deaerated conditions is controlled by the H<sub>2</sub>O/H<sub>2</sub> reaction. Both pH and conductivity are higher in the PWRs as a result of H<sub>3</sub>BO<sub>3</sub> and LiOH additions, and there has been a trend upwards in pH operating point in most PWRs from about pH<sub>325C</sub> = 6.9 to 7.3 or 7.4. At 290 °C, the pH<sub>290C</sub> is now typically 6.8 to 7.2 in PWRs (pH<sub>290C</sub> represents 1100 ppm B and 2 ppm Li, which gives a pH<sub>325C</sub> = 7.25 and a pH<sub>340C</sub> = 7.58) vs. 5.65 in BWRs, and the conductivity is 166 μS/cm vs. 5 μS/cm. However, laboratory data show that the higher conductivity is not bad per se in deaerated water, nor is the shift in pH in this near-neutral range [20]. The shift in corrosion potential is unimportant because there is no difference in potential relative to metal – metal oxide phase transitions (esp. important is the Ni/NiO

equilibrium). Also, in the absence of oxidants, there is no potential gradient in the crack and therefore no aggressive crack chemistry develops.

Secondly, the difference in H<sub>2</sub> fugacity is about 60X, from 40 to 60 ppb H<sub>2</sub> in BWRs to about 3000 ppb in PWRs. This produces only a small change in corrosion potential of about 100 mV, which can nevertheless be important to SCC of Ni alloys. Its role is related to a shift in the stability of Ni vs. NiO, which is affected by both H<sub>2</sub> and temperature (Figure B.5.15). No potential gradient forms in the crack because H<sub>2</sub> is not consumed (unlike oxidants), so no aggressive crack chemistry forms whether the H<sub>2</sub> level is high or low.

The third difference is temperature. The temperature of most structural components is 274 °C in a BWR (the feedwater reduces the recirculating core outlet water from 288 °C to 274 °C); thus, this is the temperature in the recirculation and clean-up piping, the annulus between the shroud and the pressure vessel, and the lower plenum region. In a PWR, the core inlet temperature is about 286 °C, the core outlet temperature is typically 323 °C (ranging from ~316 to 323 °C), nearly 50 °C hotter than most structural components in a BWR. For nickel alloys, this difference (323 vs. 274 °C) leads to a significant increase in crack growth rate of about 14X [7,21]; compared to the 345 °C PWR pressurizer, the difference is about 40X.

### **Improved BWR Nickel-base Weld Metals**

Research has shown that SCC susceptibility is affected by the chromium level, including Cr depletion at the columnar dendrite boundaries of nickel base weld metals. The material parameters that affect chromium depletion include the nominal chromium level, the carbon level, and the concentration of "stabilizing" elements (Nb and Ti) that form non-detrimental carbides in preference to chromium carbide. These factors have been used by the BWR industry to rank materials and guide selection of optimized alloys for new reactors and structural weld overlays. An N-bar parameter has been used to assess susceptibility for Alloy 182 [22], with values below 12 indicating moderate susceptibility:

$$N\text{-bar} = 0.13 \cdot (Nb + Ti) / 2 \cdot C \quad (\text{in weight percent})$$

A more recent measure is the Stress Corrosion Resistance Index (SCRI), which includes chromium level in the assessment [23]. A value below 30 represents significant susceptibility:

$$SCRI = Cr + (Nb + Ta) \cdot 5 + Ti \cdot 10 - 116.5 \cdot C \quad (\text{in weight percent})$$

Higher crack growth rates have also been measured in tests performed to evaluate the effects on SCC susceptibility of other alloying impurities, such as phosphorus, sulphur and silicon, but this may be due to synergistic effects with Cr-depleted boundaries. These elements, especially elevated silicon and lower manganese, adversely affect weldability by leading to a higher potential for hot cracking that could aid initiation and accelerate crack advance.

The PWR industry has shifted to Alloys 52 and 152 weld metal, and Alloy 600 has been replaced with Alloy 690. The BWR industry continues to view Alloy 82 as an optimum choice when fabrication concerns are included in the decision process. This alloy has

been used in Advanced BWRs for 10 years and its selection and good performance reflect the value of automatic welding processes [24] and the ability to perform Alloy 82 welds without re-work. The industry targets specific compositions to achieve high resistance to SCC, with initial carbon levels commonly of 0.01% or less. While the chromium levels are not as high as in Alloy 52, there is 20 years of good component performance in BWRs. Avoiding the use of Alloy 182 – and the associated elements of manual welding, weld repairs, and reduced Cr – has significantly reduced SCC of nickel weld metals.

## References for B.5

- [1] Blanchet, et al., "Historical review of the principal research concerning the phenomena of cracking of nickel base austenitic alloys," Proc. of NACE-5 *Stress Corrosion Cracking and Hydrogen Embrittlement of Iron Base Alloys*, National Association of Corrosion Engineers 1977, pp 1149-1160.
- [2] F. P. Ford, P.L. Andresen, "Development and Use of a Predictive Model of Crack Propagation in 304/316L, A533B/A508 and Inconel 600/182 in 288°C Water," Third Int. Symp. on Degradation of Materials in Nuclear Power Industry, TMS, pp. 789-800, 1988.
- [3] P.L. Andresen, F.P. Ford, "Life Prediction by Mechanistic Modeling and System Monitoring of Environmental Cracking of Fe and Ni Alloys in Aqueous Systems," *Materials Science and Engineering*, A103, pp. 167-183, 1988.
- [4] F.P. Ford, P. L. Andresen, "Corrosion in Nuclear Systems: Environmentally Assisted Cracking in Light Water Reactors," in "Corrosion Mechanisms," Ed. P. Marcus and J. Ouder, Marcel Dekker, pp. 501-546, 1994.
- [5] P.L. Andresen, "Fracture Mechanics Data and Modeling of Environmental Cracking of Nickel-Base Alloys in High Temperature Water," *Corrosion* 47, December 1991, pp. 917-938.
- [6] P.L. Andresen, "Conceptual Similarities and Common Predictive Approaches for SCC in High Temperature Water Systems," Paper 96258, *Corrosion/96*, NACE, 1996.
- [7] P.L. Andresen, et al., "Stress Corrosion Crack Growth Rate Behavior of Ni Alloys 182 and 600 in High Temperature Water," *Corrosion/02*, Paper 02510, NACE, 2002.
- [8] Appendix B6 of this report, "SCC of Alloys 600, 690, 182, 82, 152 and 52 in PWR Primary Water."
- [9] "BWR RPV License Renewal Industry Report, Revision 1," EPRI Report TR-103836, July 1994.
- [10] T.M. Angeliu, et al., "Strain and Microstructure Characterization of Austenitic Stainless Steel Weld HAZs," *Corrosion/2000*, Paper 00186, NACE, 2000.
- [11] P.L. Andresen, et al., "Mechanisms and Kinetics of SCC in Stainless Steels," Proc. Tenth Int. Symp. on Environmental Degradation of Materials in Nuclear Power Systems - Water Reactors, NACE, 2001.
- [12] R.A. Page, "Stress Corrosion Cracking of Alloys 600 and 690 and Weld Metals No. 82 and 182 in High Temperature Water," EPRI NP-2617, September 1982.
- [13] L.G. Ljungberg, "Stress Corrosion Cracking of Alloys 600 and 182 in BWRs," EPRI/SKI Research Project 2293-1, Interim Reports: 1991-1994.
- [14] "Reactor Pressure Vessel Attachment Welds: Degradation Assessment," EPRI-NP-7139-D, Final Report, May 1991.
- [15] H.S. Mehta, R.M. Horn, G.B. Inch, "A Fracture Mechanics Evaluation Of Observed Cracking at a BWR-2 Reactor Pressure Vessel Weld," 2002 ASME PVP Conference, August 4 – 8, 2002, Vancouver, B.C., Canada.
- [16] S. Hettiarachchi, et al., "NobleChem™ Technology for Life Extension of BWRs – Field Experiences," 8th Int. Conf. Of Water Chemistry of Nuclear Reactor Systems, Bournemouth, UK, Oct. 22-26, 2000.



- [17] P.L. Andresen, "Application of Noble Metal Technology for Mitigation of Stress Corrosion Cracking in BWRs," Proc. Seventh International Symposium on Environmental Degradation of Materials in Nuclear Power Systems - Water Reactors, NACE, p.563-578, 1995.
- [18] A. Jensen, et al., "Crack Propagation in Stainless Steels and Nickel Base Alloys in a Commercial Operating BWR," Proc. 7<sup>th</sup> Int. Conf. On Environmental Degradation of Materials in Nuclear Power Plants - Water Reactors, Breckenridge, Colorado, August 1995, NACE, Houston.
- [19] "BWR Vessel and Internals Project, Evaluation of Crack Growth in BWR Bickel Base Austenitic Alloys in RPV Internals (BWRVIP-59)," EPRI Report TR-108710, December 1998.
- [20] P.L. Andresen, et al., "Effects of PWR Primary Water Chemistry and Deaerated Water on SCC," Proc. 12<sup>th</sup> Int. Symp. on Environmental Degradation of Materials in Nuclear Power Systems - Water Reactors," TMS, Snowbird, August 2005.
- [21] R.S Pathania, A. McIlree, J. Hickling, "Overview of Primary Water Cracking of Alloys 182/82 in PWRs," Fontevraud 5th Conference, France, Sept. 23-27, 2002.
- [22] K. Yamauchi, et al., International Conference on Pressure Vessel Technology, New York, NY, ASME, 1984.
- [23] M. Akashi, "Effects of Cr and Nb Contents on the Susceptibility of Alloy 600 Type Ni-base Alloys to Stress Corrosion Cracking in a Simulated BWR Environment," Corrosion/95, Orlando, FL, March 1995.
- [24] Sandusky, T. Okada, T. Saito, "Advanced Boiling Water Reactor Materials Technology," Materials Performance, p.66-71, January 1990.
- [25] P.L. Andresen, P.W. Emigh, M.M. Morra, "SCC of High Strength Ni-base Alloys in High Temperature Water," Paper #04675, Corrosion/04, NACE, 2004.
- [26] D.S. Morton, et al., "The Influence of Dissolved Hydrogen on Nickel Alloy SCC: A Window to Fundamental Insight," Corrosion/2001, Paper 01117, NACE, 2001.

**Table B.5.1 Compositions of Nickel Base Alloys Used in BWRs**

	<b>Alloy 600</b>	<b>Alloy 182</b>	<b>Alloy 82</b>	<b>Alloy X750</b>
Nickel	Bal.	Bal.	Bal.	Bal.
Chromium	14-17	13-17	18-22	15-17
Iron	6-10	≤10.0	≤3.00	8-9
Titanium		≤1.0	≤0.75	2.5-3.0
Aluminum				0.7-1.0
Niobium plus Tantalum		1.0-2.5	2.0-3.0	0.8-1
Carbon	≤0.05	≤0.10	≤0.10	0.05-0.08
Manganese	≤1.0	5.0-9.5	2.5-3.5	0.1
Sulfur	≤0.015	≤0.015	≤0.015	<0.03
Phosphorus		≤0.030	≤0.030	<0.03
Silicon	≤0.5	≤1.0	≤0.50	0.1-0.2
Copper	≤0.5	≤0.50	≤0.50	<0.50
Cobalt	≤0.10	≤0.12	≤0.10	<0.10

**Table B.5.2 BWR Components That Use Nickel Base Alloys**

<b>BWR Components</b>	<b>Nickel Base Alloy Grades Used</b>
BWR Shroud Head Bolts	Alloy 600
Press. Vessel Attachment Pads	Alloy 182
Control Rod Penetrations	Alloy 600
Control Rod Penetration Welds	Alloy 182
Core Shroud Support Welds	Alloy 182
Pressure Vessel Nozzles	Alloys 182 and 82
Safe Ends	Alloy 600
Weld Metal Deposits	Alloys 82 and 182
Jet Pump Beams	Alloy X750
Fuel Rod Spacers	Alloy X750

**Table B.5.3**

**Alloy 82/182 Field Cracking in One Set of BWRs**

Material	Component	Part	BWR Type	First Synch	Find Date	Cause
Alloy 182	Feedwater Sparger	End Bracket	2	Sep-69	Oct-2000	IGSCC
Alloy 82/182	In Core Monitor	Penetration		May-84	Aug-97	Most likely original fabrication weld defects (one possible exception on 08-41).
Alloy 182	RPV Head	Bracket	Non-GE BWR	Jan-81	Jan-95	IGSCC
Alloy 182	RPV Head	Bracket	Non-GE BWR	Jun-80	Jan-95	IGSCC
Alloy 182	Shroud Support	Leg	3	Mar-71	Dec-99	Probable IGSCC

**Alloy 182 Field Cracking in a Second Set of BWRs**

Plant	System	Year of Detection	Location of Indication
E-1	Recirc	1990	Main Loop
E-2	Recirc	1985	Flange
E-2	Core Spray	1999	Brackets
E-3	Recirc	1996	Pipe weld
E-4	Recirc	1997	Pipe weld
E-4	Core Spray	1999	Brackets
E-5	Core Spray	1999	Brackets
E-6	Feedwater	1985	Nozzle
E-6	RPV	1986	Head spring beams
E-6	RPV	1986	Flange
E-6	Feedwater	1997	Nozzle
E-6	RHR	1997	Safe end
E-7	RPV	1985	Head spring beams
E-7	RPV	1990	Flange
E-7	Feedwater	1995	Nozzle
E-8	RPV	1994	Head spring beams
E-8	Core Cooling	1991	Nozzle
E-8	RPV	1995	Head spring beams

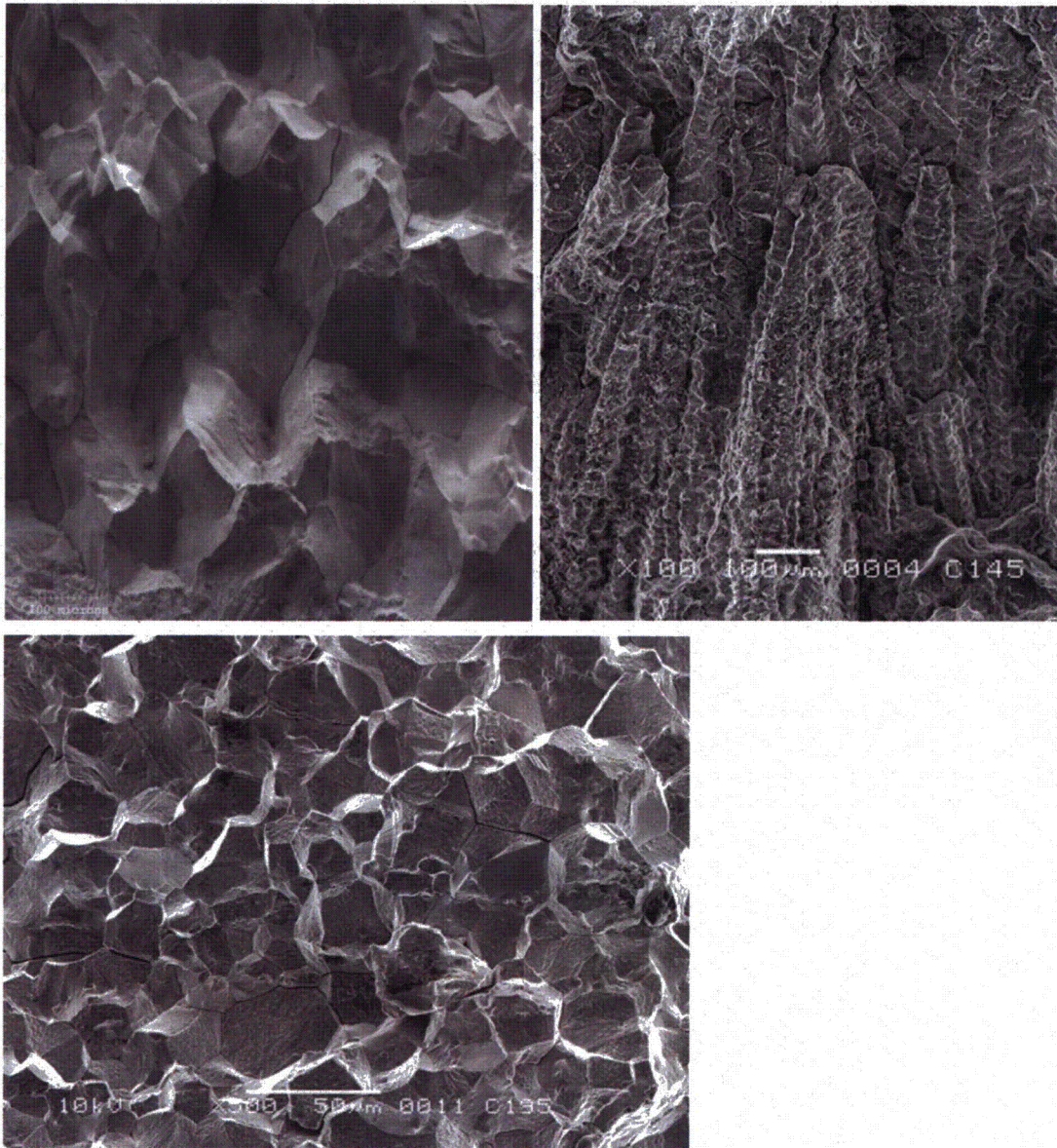


Figure B.5.1. Scanning electron micrographs showing the intergranular fracture morphology of Alloy 600, Alloy 182 weld metal and Alloy X750 when tested in high temperature water. (*© NACE International 2002*)

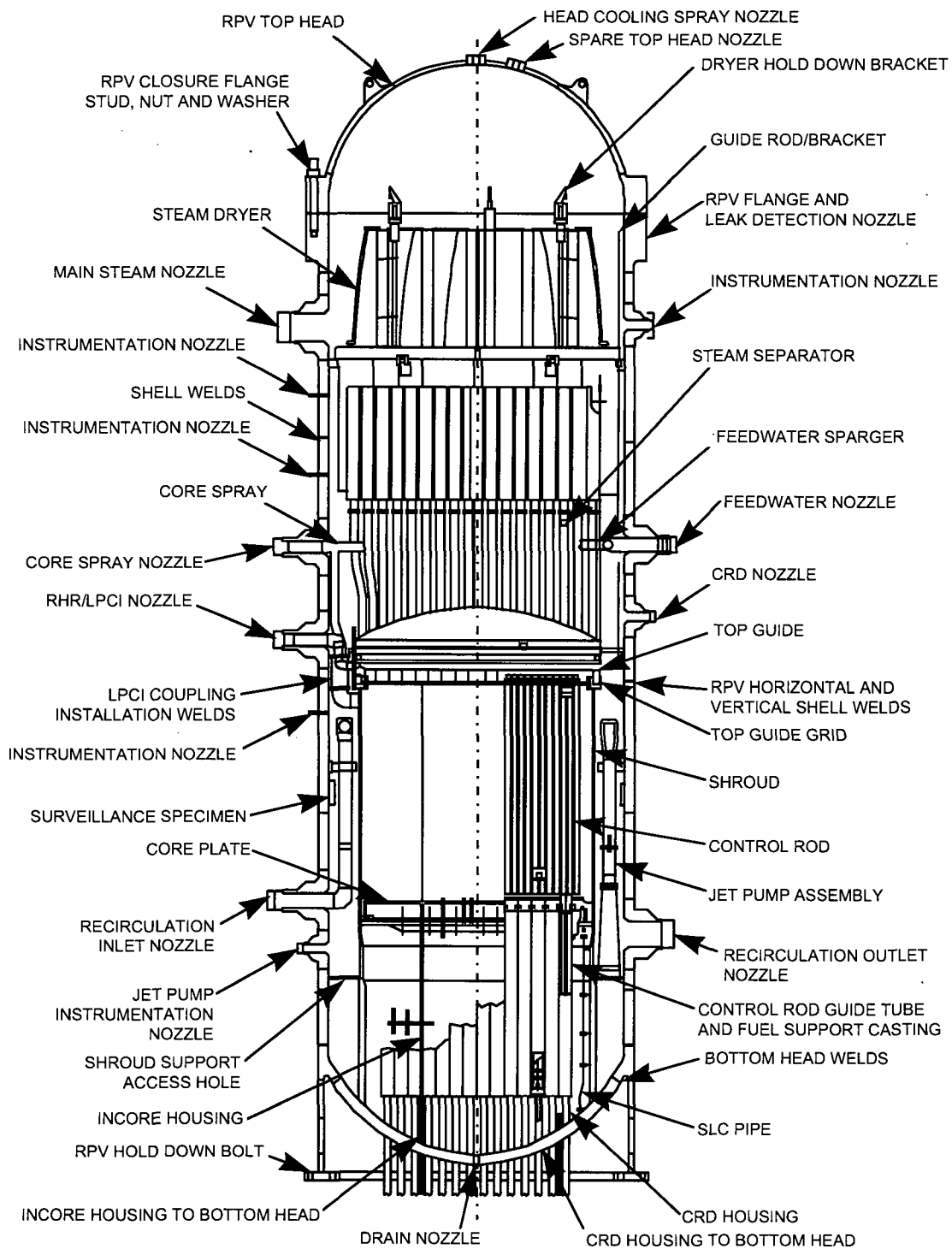


Figure B.5.2. Schematic of typical BWR reactor pressure vessel, nozzles and attachments.

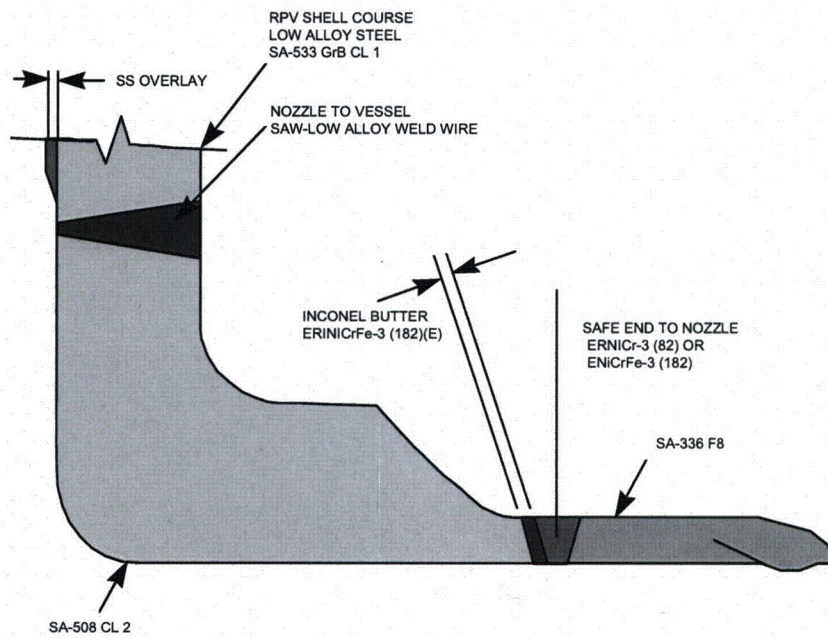
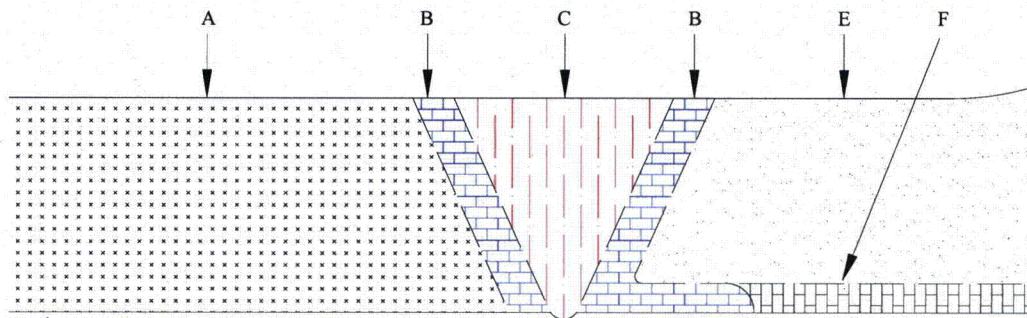


Figure B.5.3. Typical BWR recirculation outlet nozzle, nozzle butter, weld and safe end.



- A) Stainless Steel Safe End
- B) Alloy 182 Weld Butter
- C) Alloy 182 or Alloy 82 Weld Metal
- B) Alloy 182 Weld Butter
- D) Low Alloy Steel Nozzle
- E) E) Low Alloy Steel
- F) Stainless Steel Cladding

Figure B.5.4. Enlargement of safe end to nozzle weld region in BWRs using Alloy 182/82 weld metals.

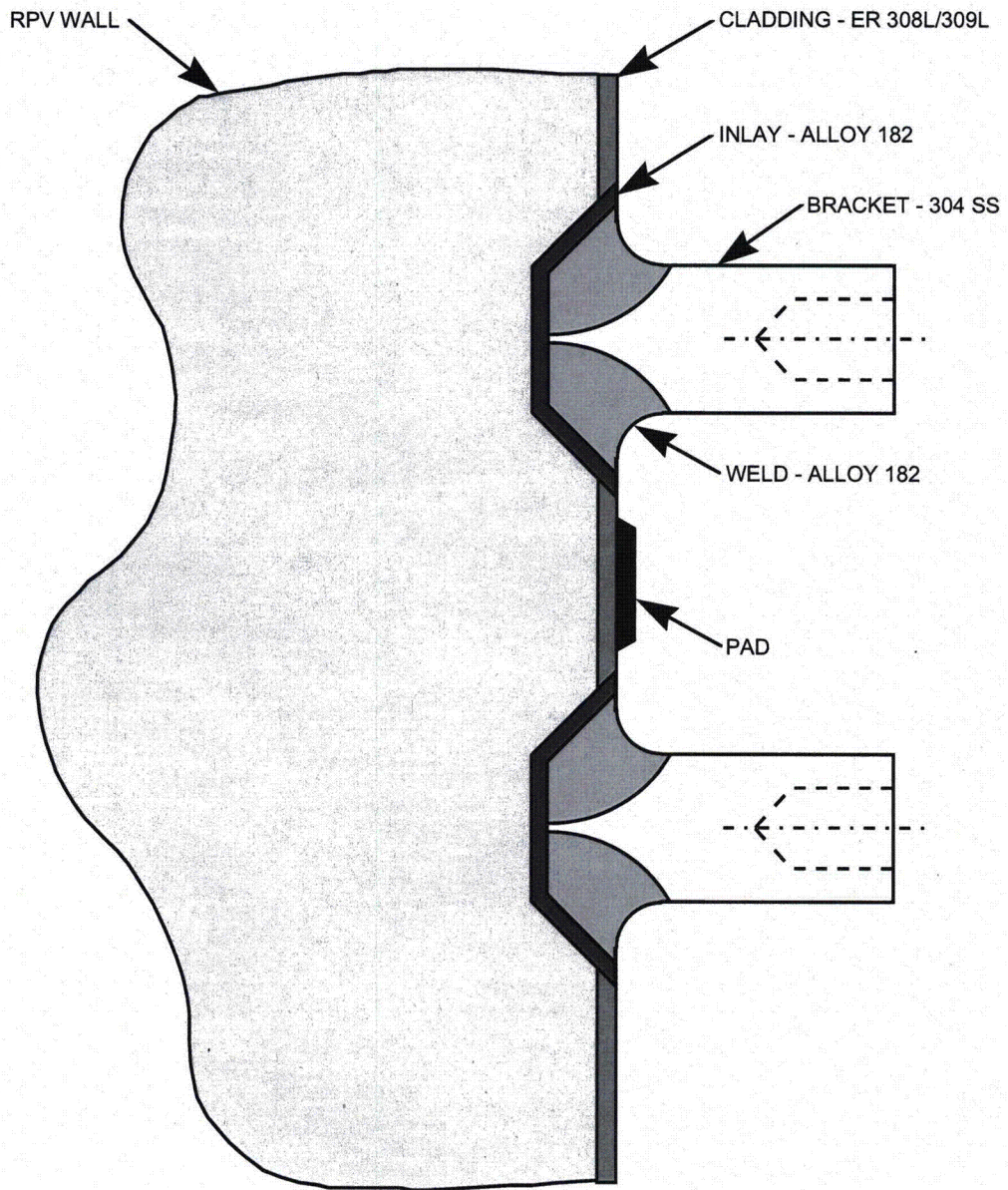


Figure B.5.5. Typical BWR core spray bracket attachment weld configuration. Alloy 182/82 are used.

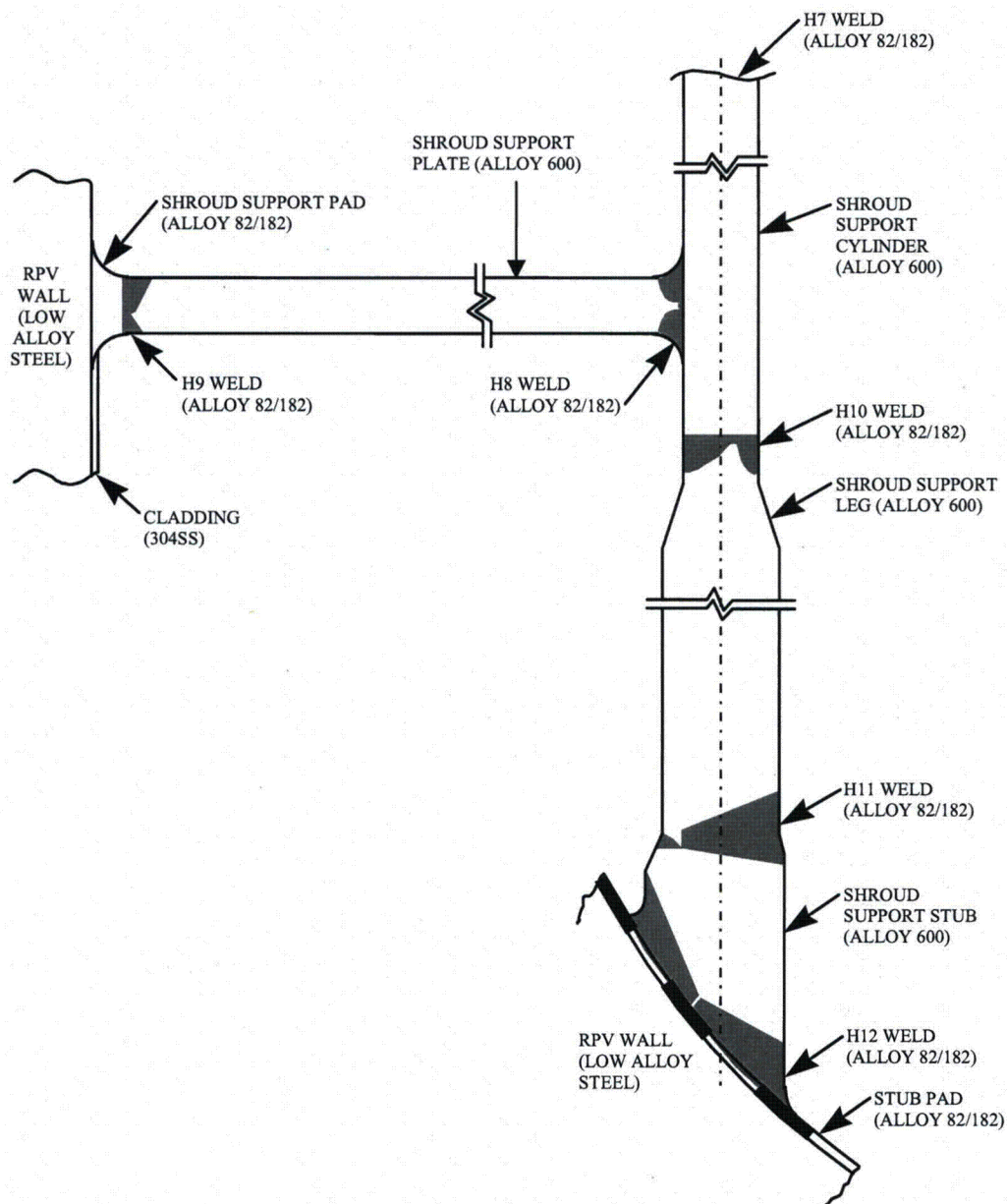


Figure B.5.6. Typical BWR shroud support structure of the leg design. Alloy 182 is used. Also shown are the H9 and H12 welds that join the component to the RPV.



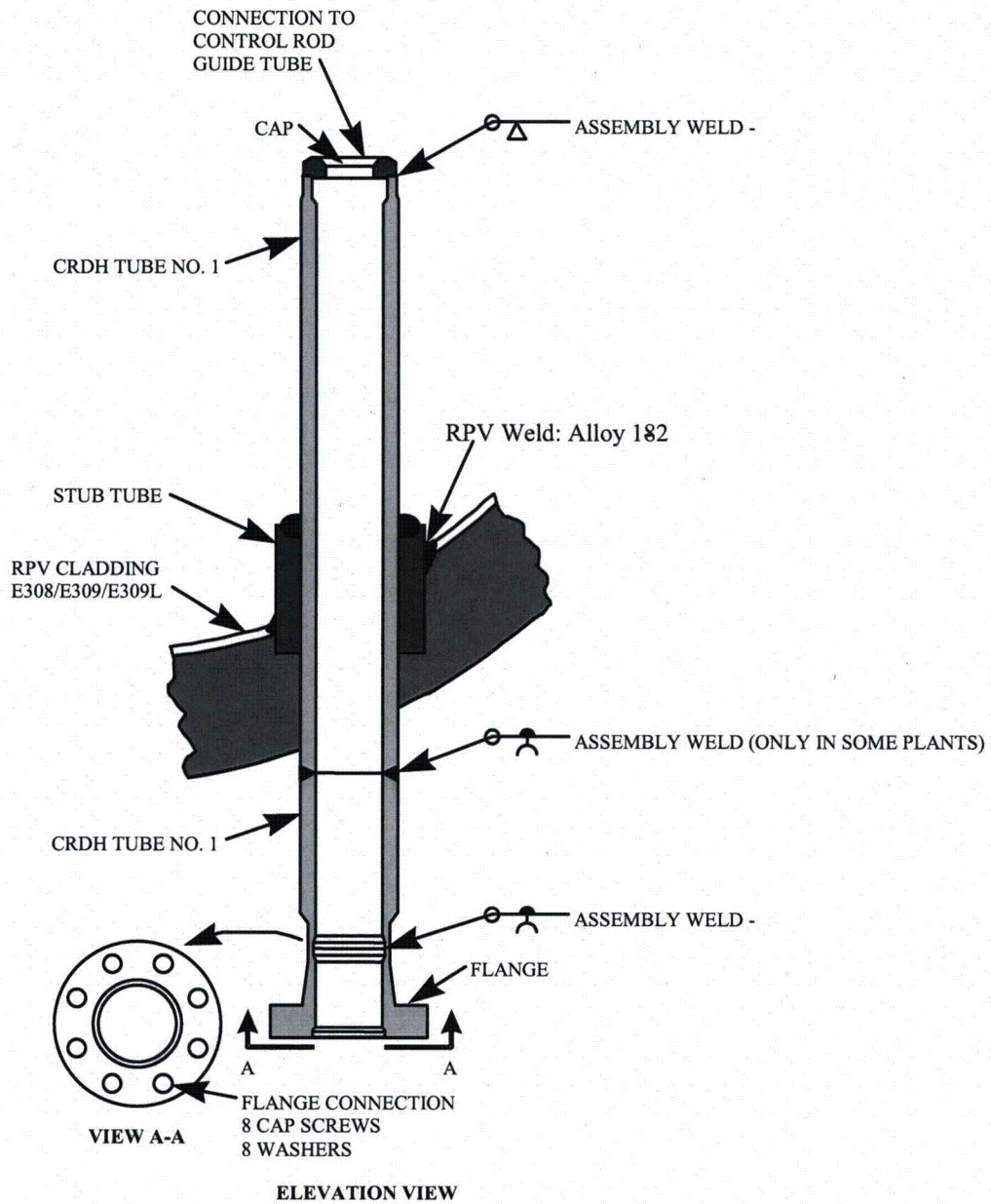
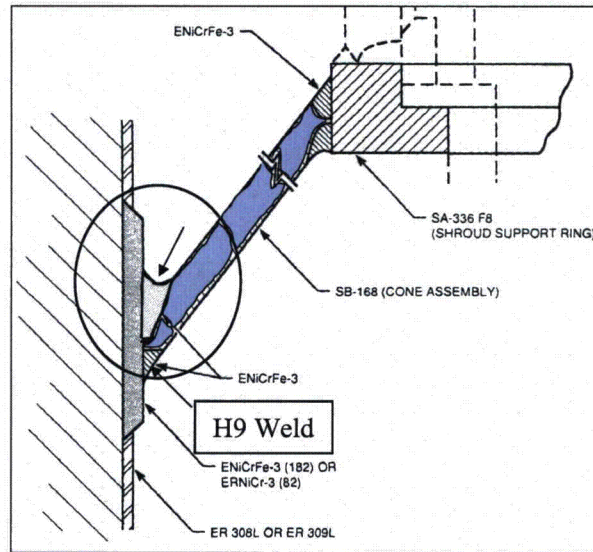
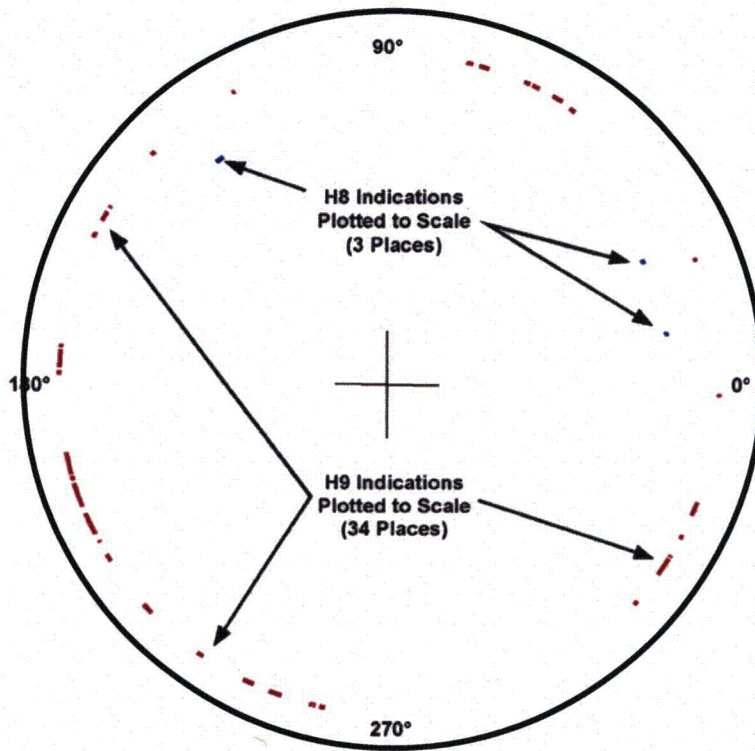


Figure B.5.7. Typical CRD stub tube and CRD housing configurations. Alloy 182 used in stub tube to RPV weld.



(a)



(b)

Figure B.5.8. (a) Cross-section of BWR/2 H9 weld. (b) Schematic of the azimuthal orientation and length of the H8 and H9 indications (around vessel circumference) as determined by UT inspection.

### Creviced Alloy 600 Shroud Head Bolts

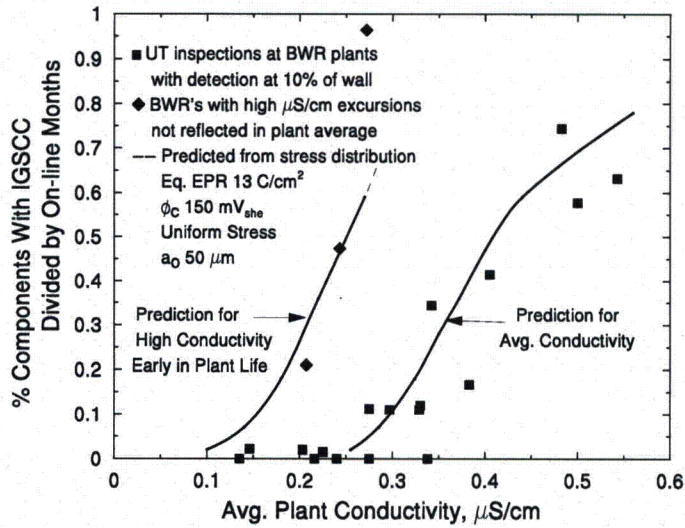


Figure B.5.9. Observation and prediction of the incidence of SCC in Alloy 600 shroud head bolts as a function of average plant conductivity. An unusual population of three bolts showed a much high incidence of SCC because these plants had bad water chemistry early in their life. (© NACE International 2002)

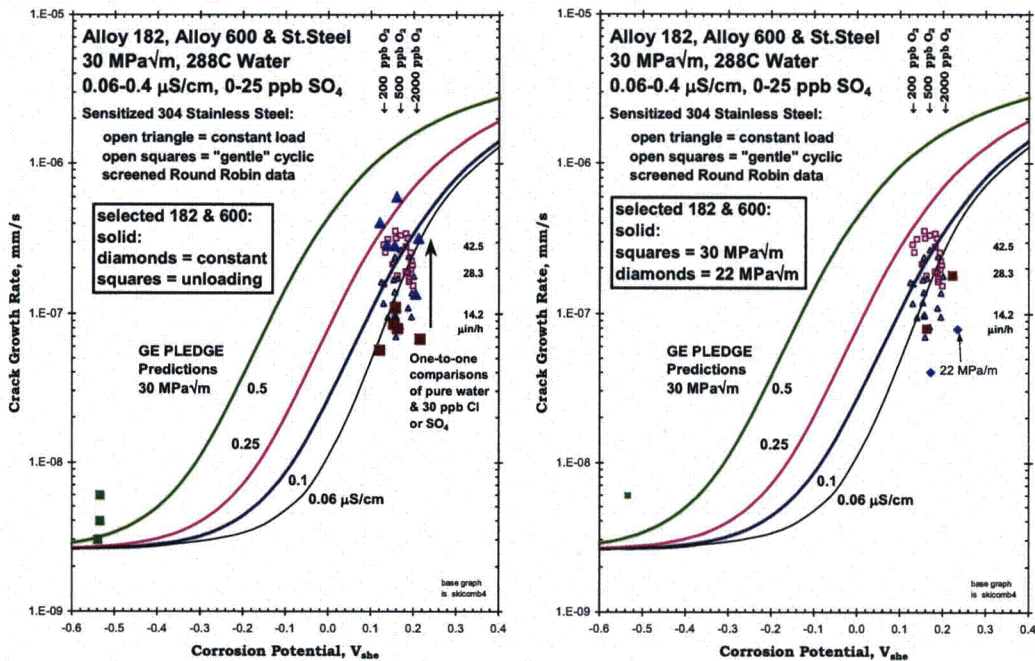


Figure B.5.10. Crack growth rate vs. corrosion potential for Alloy 600 and Alloy 182 weld metal. (Left) The growth rates in high purity water at high corrosion potential fall within the observations for sensitized stainless steel (open symbols), and the effect of low potential or additions of  $6 \times 10^{-7}$  N SO<sub>4</sub> or Cl are consistent with the SCC behavior of sensitized stainless steel. (Right) The effect of corrosion potential and stress intensity factor on the growth rate of Alloy 182 weld metal in near-theoretical purity 288 °C water. (© NACE International 2002)

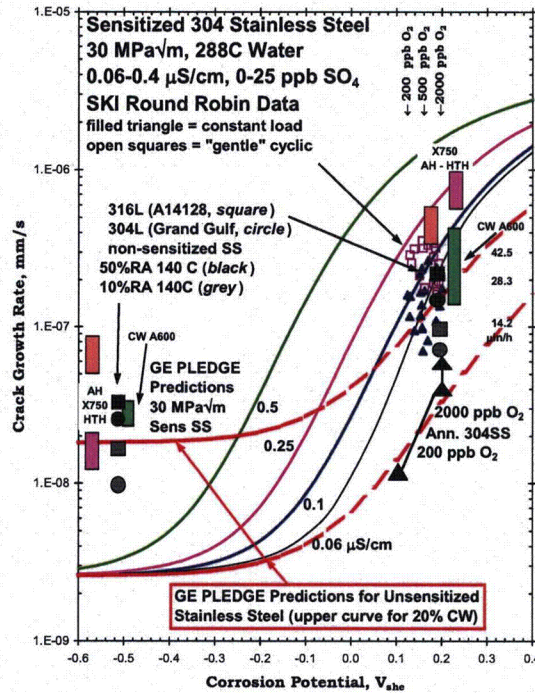


Figure B.5.11. SCC growth rate vs. corrosion potential for stainless steels in various conditions, 20% cold worked Alloy 600, and precipitation hardened Alloy X750 tested in 288 °C high purity water containing 2000 ppb O<sub>2</sub> and 95 – 3000 ppb H<sub>2</sub> [25]. (© 2003 by The American Nuclear Society, La Grange Park, Illinois)

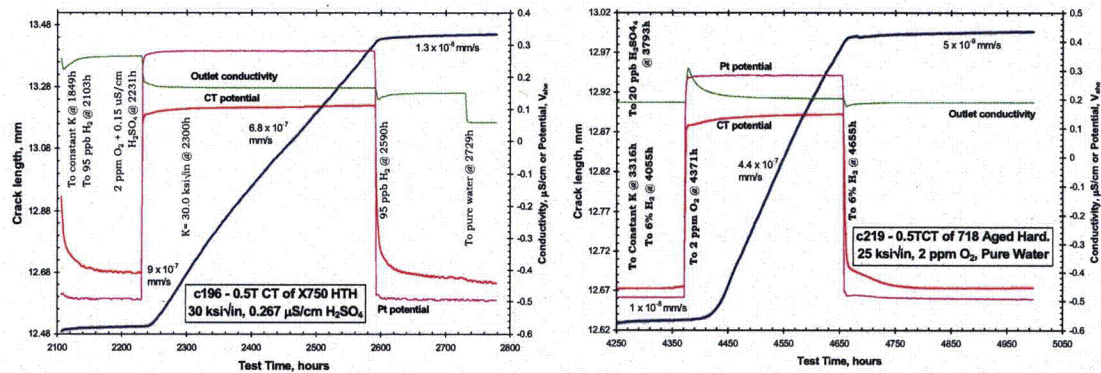


Figure B.5.12. Crack length vs. time for 0.5TCT specimens of Alloy X750 in the HTH condition and Alloy 718 tested in 288 °C water [25]. (© NACE International 2004)

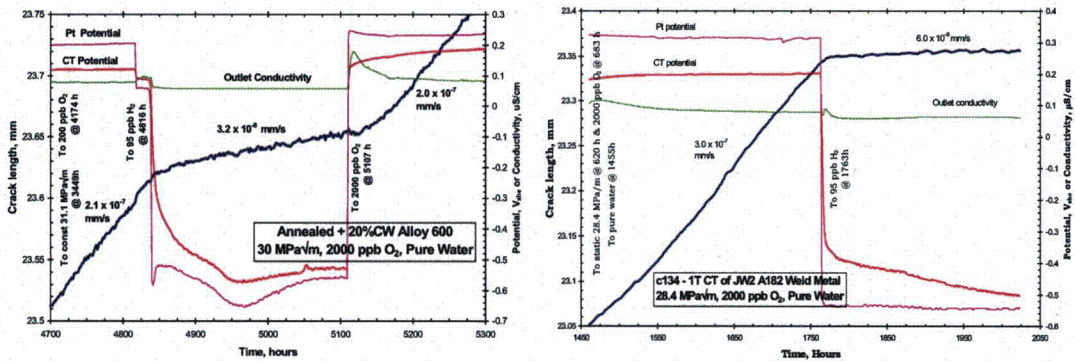


Figure B.5.13. Crack length vs. time for CT specimens of unsensitized Alloy 600 cold worked at 25 °C to 20% RA and Alloy 182 weld metal tested in 288 °C water [7].  
 (© NACE International 2002)

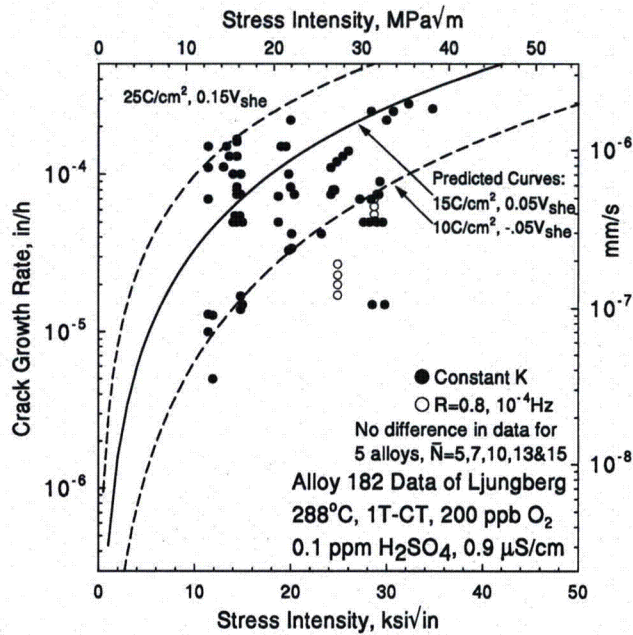


Figure B.5.14. Crack growth rate vs. stress intensity for Alloy 182 weld metal tested in 288 °C water containing 200 ppb O<sub>2</sub> and 100 ppb SO<sub>4</sub> as H<sub>2</sub>SO<sub>4</sub>. The remarkably high growth rates and low dependence on stress intensity are in fact consistent with predictions based on sensitized stainless steel [2-5], which are represented by the lines on the diagram. (© NACE International 2002)

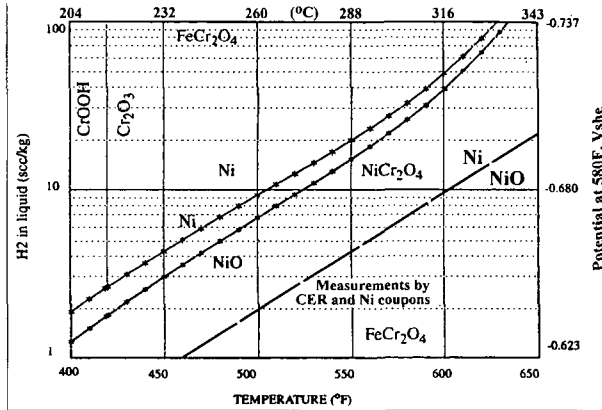
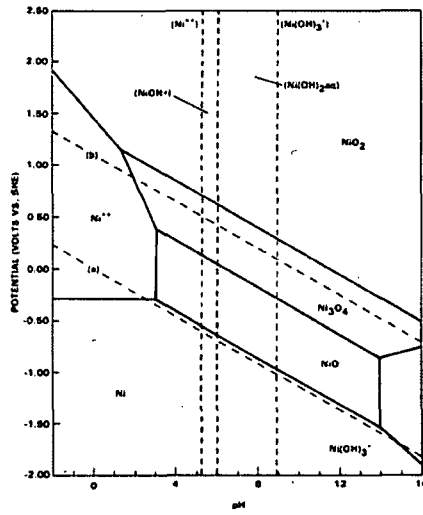


Figure B.5.15. (Left) Pourbaix diagram of the Ni-H<sub>2</sub>O system at 300 °C. (Right) Thermodynamic stability of Ni metal (vs. NiO and various spinels) vs. H<sub>2</sub> fugacity and temperature [6,7,26]. The lower line represents more recent, definitive data. (© NACE International 2002)

**B. 6 "SCC of Alloys 600, 690, 182, 82, 152 and 52 in PWR Primary Water,"**  
by Peter M. Scott

**Introduction**

Nickel base alloys are attractive for PWR primary circuit components because of the close similarity of their coefficients of thermal expansion to that of the low alloy steels used to fabricate the reactor pressure vessel, pressurizer and steam generator shells, as well as their low general corrosion and corrosion product release rates in PWR primary and secondary water. A list of PWR components where Alloys 600 and 690 and their compatible weld metals are used in PWRs is given in Table B.6.1. Typical compositions are shown in Table B.6.2.

**Table B.6.1 PWR Components Fabricated from Nickel Base Alloys**

<b>PWR Components</b>	<b>Nickel Base Alloy Grades Used</b>
Steam generator tubes	Alloys 600 MA & TT, 690TT (& 800)
Steam generator divider plates	Alloys 600 & 690
Upper head penetrations	Alloys 600 & 690
Lower head penetrations	Alloy 600
Core supports	Alloy 600
Pressurizer nozzles	Alloys 600 & 690
Safe ends	Alloy 600
Weld metal deposits	Alloys 82, 182, 52 & 152

The susceptibility of Alloy 600 to Intergranular Stress Corrosion Cracking (IGSCC) in high temperature water was first revealed in laboratory testing in 1957 and then in operational service in PWR primary water from the early 1970s. IGSCC following exposure to the primary side environment is today commonly referred to in the industry as Primary Water Stress Corrosion Cracking (PWSCC). [1,2] Initially, highly cold worked components were affected such as tight U-bends in steam generator tubes and rolled or explosively expanded, cold-worked transitions in diameter of the tubes within the tube sheet[3]. This then became a major cause of steam generator tube cracking in the 1980s, and later, premature steam generator retirement and replacement. PWSCC of pressurizer nozzles and control rod drive mechanism (CRDM) nozzles in the upper heads of PWR reactor pressure vessels followed in the late 1980s and has continued for over a decade [4,5]. CRDM nozzle cracking appeared first in French PWRs in 1991 but was not widely observed elsewhere until the last five years or so.

Apparently interdendritic, but in fact intergranular, stress corrosion cracking (along dendrite "packet" boundaries) of the weld metals Alloys 182 and 82, the former having a composition similar to Alloy 600 (Table B.6.2), has also been observed in recent years in major primary circuit welds of several plants, often after very long periods in service ranging between 17 and 27 years [4,5].

A more detailed description of PWSCC observed in each type of nickel alloy PWR component and the phenomenology of PWSCC in various nickel base alloys is summarized below. A brief description of the methodologies developed to predict and mitigate cracking until, as is often the case, replacement becomes unavoidable, is also

given. When Alloy 600 components are replaced, it is usually by Alloy 690 and its compatible weld metals, Alloys 152 and 52, which have so far proved resistant to PWSCC both in laboratory tests and, to date, after up to 16 years in service. Alloy 800 steam generator tubes have also proved resistant to PWSCC without any known cracking in primary water service.

**Table B.6.2 Some Composition Specifications for Nickel Base Alloys Used in PWRs**

	Alloy 600	Alloy 182	Alloy 82	Alloy 690	Alloy 152	Alloy 52
Nickel	>72.0	Bal.	Bal.	>58.0	Bal.	Bal.
Chromium	14-17	13-17	18-22	28-31	28-31.5	28-31.5
Iron	6-10	≤10.0	≤3.00	7-11	8-12	8-12
Titanium		≤1.0	≤0.75		≤0.50	≤1.0
Aluminum						≤1.10
Niobium plus Tantalum		1.0-2.5	2.0-3.0		1.2-2.2	≤0.10
Molybdenum					≤0.50	≤0.05
Carbon	≤0.05	≤0.10	≤0.10	≤0.04	≤0.045	≤0.040
Manganese	≤1.0	5.0-9.5	2.5-3.5	≤0.50	≤5.0	≤1.0
Sulfur	≤0.015	≤0.015	≤0.015	≤0.015	≤0.008	≤0.008
Phosphorus		≤0.030	≤0.030		≤0.020	≤0.020
Silicon	≤0.5	≤1.0	≤0.50	≤0.50	≤0.65	≤0.50
Copper	≤0.5	≤0.50	≤0.50	≤0.5	≤0.50	≤0.30
Cobalt	≤0.10	≤0.12	≤0.10	≤0.10	≤0.020	≤0.020

#### **Alloy 600 steam generator tubes**

Most PWR steam generators are of the 'recirculating' type although some are 'once-through' where all the secondary water entering the steam generator is transformed into steam. Most in-service PWSCC has occurred in recirculating steam generators. An important difference between the two from the point of view of PWSCC is that the once-through steam generators were subjected to a pre-service stress relief of the whole steam generator at a temperature of about 610 °C (1130 °F). In addition to provoking grain boundary carbide precipitation in Alloy 600, some grain boundary chromium depletion (sensitization) also occurred. The lower strength and grain boundary carbide



precipitation in once-through steam generators tubes has proved to be advantageous for resistance to PWSCC on the primary side, despite the sensitization, although even these steam generators are now being steadily replaced after typically 20 to 25 years service [6]. In one case, however, an accidental ingress of thiosulfate into the once-through steam generators led (predictably) to extensive intergranular attack (IGA) of the sensitized tubes.

PWSCC of Alloy 600 steam generator tubing in the mill annealed (MA) condition became a major degradation mechanism from the 1970s onwards for recirculating steam generators [7]. In 1971, the first confirmed primary side cracking of mill annealed Alloy 600 tubes of recirculating steam generators occurred when leakage at U-bends was experienced in the Obrigheim steam generators after only 2 years of operation [2]. Cracking occurred both in the tight U-bends, mainly on the inner two rows at the apex and at the tangent points as well as in the tube sheet at the transition expansion or roll expansion regions of the tubes. The latter has been responsible for premature steam generator replacement at a number of plants.

The first roll transitions experiencing PWSCC were located on the hot leg side where the temperature is typically around 320 °C (610 °F) and is 30 to 40 °C (55 to 70 °F) hotter than the cold leg inlet at 280 °C (535 °F). Thus, it was clear that temperature had a significant influence on PWSCC, indicating a strongly thermally activated process. The apparent activation energy from fitting the temperature dependence to the Arrhenius equation is rather high (~ 180 kJ/mole) so that a typical temperature difference of 30 °C (55 °F) between hot and cold legs could easily account for a factor of four to five increase in the time to the onset of detectable cracking. Thus, reduction of hot leg temperature has been one possible mitigating action that has been used. Hot leg temperature reductions from 4 to even 10 °C have been applied.

The magnitude of the tensile stresses, particularly residual stress from fabrication, has also had a major impact on the time for detectable PWSCC to develop; only the most highly strained regions of steam generator tubing (that is, row-one and two U-bends, initially, and subsequently larger radius tubes, roll transition regions, expanded regions, and dented areas) have exhibited PWSCC. Consequently, several stress mitigation techniques have been evolved such as local stress relief of first and second row U-bends by resistance or induction heating, and shot peening or rotopeening to induce compressive stresses on the internal surface of roll transitions [8,9]. While peening helps to limit initiation of new cracks, it cannot prevent the growth of existing cracks whose depth is greater than that of the induced compressive layer, typically 100 to 200 µm. Thus, peening has been most effective when most tubes have either no cracks or only very small ones, i.e. when practiced before service or very early in life [9,10].

Material susceptibility, in combination with the factors mentioned above, is also a major factor affecting the occurrence of PWSCC in service. Most PWSCC has occurred in mill annealed tubing. However, it is important to emphasize that there is not a single product called "mill-annealed" Alloy 600 tubing since each tubing manufacturer has employed different production processes. Whereas some mill-annealed tubing has not experienced any PWSCC over extended periods of operation, in other cases it has occurred after only 1 to 2 years of service, particularly at roll transitions. This variability of PWSCC susceptibility is even seen between heats from the same manufacturer in the same steam generator [11]. The variation in susceptibility to PWSCC of the heats of Alloy 600 typically fits approximately a lognormal distribution so that a rather small fraction of Alloy

600 heats may be responsible for a disproportionately high number of tubes affected by primary side PWSCC. The reasons for such variability are only partly understood.

This microstructural aspect of susceptibility to PWSCC has been observed to be strongly affected by the final mill-annealing temperature, which determines whether carbide precipitation occurs predominantly on grain boundaries or intragranularly. The most susceptible microstructures are those produced by low mill-annealing temperatures, typically around 980 °C (1800 °F) that develop fine grain sizes (ASTM 9 to 11), copious quantities of intragranular carbides, and, usually, few if any intergranular carbides [12,13]. Higher mill annealing temperatures in the range of 1040 to 1070 °C (1900 to 1960 °F) avoid undue grain growth and leave enough dissolved carbon so that intergranular carbide precipitation occurs more readily during cooling.

A further development to exploit the apparent advantages of grain boundary carbides for PWSCC resistance was to thermally treat the tubing for ~15 h at 705 °C (1300 °F) after mill annealing. This both increases the density of intergranular carbides in the grain boundary and provides enough time so that most of the carbon in solution is consumed, and the chromium can diffuse to eliminate its depletion profile and thus avoid sensitization [13]. The beneficial influence of grain boundary chromium carbides on primary side PWSCC resistance has been extensively evaluated in laboratory studies and suggests an improvement in life of thermally treated tubing of between 2 and 5 times relative to the mill annealed condition. In fact, primary side PWSCC resistance is improved with or without grain boundary chromium depletion, as also deduced from the generally much better operating experience of Alloy 600 tubing of once-through steam generators [6,12,13]. However, even thermally treated Alloy 600 tubing has cracked in service, although much less frequently than mill annealed Alloy 600. This has usually been attributed to a failure of the thermal treatment to produce the desired intergranular carbide microstructure either due to insufficient carbon or factors such as tube straightening prior to thermal treatment, which has favored carbide precipitation on dislocations instead of grain boundaries.

Steam generator tubes with PWSCC detectable by non-destructive testing have usually been preventively plugged either to avoid leakage or before the crack length reaches some pre-defined conservative fraction of the critical size for ductile rupture. Where depth-based repair criteria are followed, tubes may also have been preventively plugged since cracks could not be reliably depth sized. Sleeving has sometimes been deployed as a repair method in operating PWRs to avoid plugging and maintain the affected tubes in service. The sleeves bridge the damaged area and are attached to sound material beyond the damage. The ends of the sleeves may be expanded hydraulically or explosively and are in most cases sealed by rolling, welding, or brazing [3].

Modern (usually replacement) steam generators have been fabricated using Alloy 690 tubes thermally treated for 5 hours at 715 °C. As well as being highly resistant in severe laboratory tests to PWSCC in PWR primary water compared to either mill annealed or thermally treated Alloy 600, the lead steam generators with thermally treated Alloy 690 tube bundles have, to date, about 16 years of service with no known tube cracking .

### **Thick section Alloy 600 components**

Thick section, forged, Alloy 600 components started to crack in the mid 1980's starting with the hottest components, pressurizer nozzles [11,14]. In France, for example, all pressurizer nozzles were replaced with stainless steel. In 1991, the first cracking of Alloy 600 upper head Control Rod Drive Mechanism (CRDM) nozzles occurred at the Bugey 3 plant in France. At first, it was thought that this could be a special case because of the combination of a stress concentration due to a counter bore in the nozzles just below the level of the J-groove seal weld with the upper head, as well as a relatively high operating temperature that was believed to be closer to that of the hot leg in this first generation French plant. However, the problem spread during the 1990s to CRDM nozzles in other plants with no counter bore, nor with a tapered lower section to the CRDM nozzle, and in upper heads where the temperature was the same as the inlet cold leg temperature [15,16].

Three common features of the cracking of upper head CRDM nozzles were the presence of a significant cold worked layer due to machining or grinding on the internal bore, some distortion or ovalization induced by the fabrication of the J-groove seal welds, and a tendency to occur much more frequently in the outer set-up circles where the angles between the vertical CRDM nozzle and the domed upper head were greatest. The combination of these three features plus the fact that the upper head is stress relieved before the CRDM nozzles are welded in place pointed to high residual stresses being responsible for these premature cracking occurrences .

Although the generic problem of Alloy 600 CRDM nozzle cracking first appeared in France, only sporadic instances of similar cracking were observed in other countries until the beginning of the 21<sup>st</sup> century, since when numerous other incidents have been reported. In some cases, where cracking was allowed to develop to the point of leaking primary water into the crevice between the CRDM nozzle and the upper head, circumferential cracks initiated on the outer surface of the CRDM nozzle at the root of the J-groove seal weld [17]. This latter observation had also been made in 1991 at Bugey 3 but only to a minor extent. No further leaks of primary water due to CRDM nozzle cracking have occurred in France because of an inspection regime adopted to avoid them and a decision taken to replace all upper heads using thermally treated Alloy 690 CRDM nozzles [15,16]. The same strategy has often been adopted elsewhere as more economic than the cost of repairs and repeat inspections. The dangers of allowing primary water leaks to continue over several years so that extensive boric acid deposits accumulated was amply demonstrated by the discovery of very severe corrosion (wastage) of the low alloy steel of the upper head at the Davis Besse plant in 2002 [5,17].

### **Nickel base weld metals**

The history of PWSCC in Alloy 600 and similar nickel base alloys has continued in recent years with the discovery of cracked Alloy 182 welds in several PWRs around the world [17,18]. This has occurred on the primary water side of the J-groove welds that seal the CRDM nozzles in the upper head and also in a few cases in the safe end welds of the reactor pressure vessel or pressurizer. One case has also occurred in the J-weld of a lower head instrumentation penetration [19]. Cracking seems to be significantly exacerbated by the presence of weld defects and of weld repairs made during fabrication, usually to eliminate indications due to hot cracking, or slag inclusions, thus

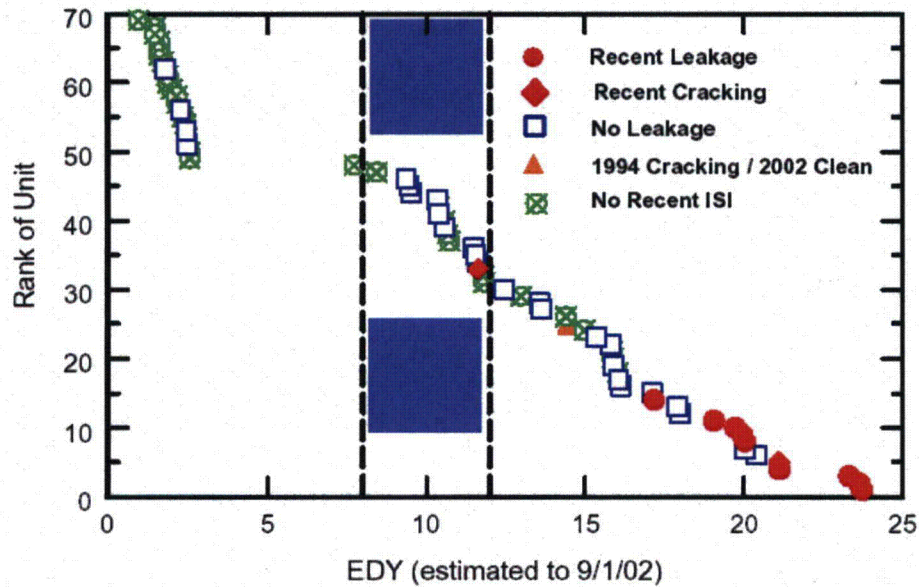
again implicating high residual stress in the cracking observed to date. The cracking has often been described as interdendritic but recent work shows that it is in fact intergranular [20]. Incubation periods before detectable cracking seem to be very long, up to twenty years.

It should be noted that all the nickel base weld metal cracking observed to date has concerned welds that have not experienced the stress relief given to adjacent low alloy steel pressure vessel components [18]. Although the stress relief temperature is clearly not optimized for nickel base alloys (or stainless steels), it has been shown on mockups that the surface residual stress of the welds is very significantly reduced and doubtless imparts greater resistance to PWSCC in PWR primary water.

### **Life prediction**

In spite of the improvements available for new plants or for replacement components equipped with Alloy 690 and welded with Alloys 52 or 152, many Alloy 600 components, either mill annealed, thermally treated or forged remain in service. While most show no sign of cracking in service, it is important to assess component life and endeavor to predict when replacement may become necessary. Prediction methodologies were first developed for steam generator tubes and later extended to pressurizers and upper head CRDM penetrations. Both deterministic and probabilistic methods have been developed [21,22].

Modeling of Alloy 600 component life is often based on the assumption that the time to detectable cracking varies as the inverse fourth power of the stress (including residual stress) above a threshold stress of ~250 MPa with a temperature dependency approximated by the Arrhenius equation. Despite the scatter observed in determinations of apparent activation energy, there is a reasonable consensus that a value of 180 kJ/mole (44 kcal/mole) is adequate for component life estimations. Some approaches to modeling also attempt to include material variability in susceptibility to PWSCC [22,23,24,25]. However, in the case of classification of the susceptibility of CRDM nozzle cracking in US PWRs this aspect has not been taken into account<sup>[17]</sup>. Nevertheless, as can be seen in Figure B.6.1, the plants most at risk from PWSCC of Alloy 600 CRDM nozzles have been correctly identified.



**Figure B.6.1 Equivalent damage years for the upper head CRDM nozzles of US PWRs in September 2002 [17]**

Application of the Weibull distribution to quantify the dispersion in stress corrosion data is well established and has generally been successfully applied to PWSCC in Alloy 600 steam generator tubes and upper head penetrations [21,22]. The dispersion in times to observe detectable cracks arises from the inherent variability in susceptibility of materials to stress corrosion cracking and, in the case of plant components, to uncertainty in the stress and temperature. The Weibull distribution can be fitted to the early observations of PWSCC as a function of operating time and provides an effective tool for predicting the future development of cracking so that informed inspection and repair plans can be formulated [21]. An alternative Monte Carlo simulation approach to improving the stochastic prediction of PWSCC has also been developed in the context of upper head penetration cracking taking into account the inherent dispersion in the input parameters of stress, temperature, activation energy and material susceptibility [22,23,24,25].

Another parameter that can have a dramatic influence on component susceptibility to cracking in service is the quality of the surface finish due to machining, grinding etc. Based on careful characterizations of the thicknesses of cold worked layers and residual stresses left by different machining techniques, a quantitative framework for assessing their impact on component resistance to PWSCC has been developed [14,23,24,25].

Once a stress corrosion crack has been detected by non-destructive examination in a PWR primary circuit component, an essential step in the justification of structural integrity and further operation without repair or replacement of the affected component is an assessment of crack growth during the next few operating cycles. Practical approaches to assessing crack growth by PWSCC in Alloy 600 components have relied on empirical measurements of crack growth rates as a function of crack tip stress intensity,  $K_I$ , as follows [26,27]:

$$\frac{da}{dt} = C.(K_I - 9)^n \quad (K_I \text{ in } MPa\sqrt{m})$$

The values of the coefficients C and n vary for given practical circumstances, but there is a reasonable consensus that the apparent activation energy to be used for adjusting the coefficient C for temperature is ~130 kJ/mole, which is somewhat lower than the value quoted above for overall life prediction, where time to crack initiation usually dominates.

Other variables that are known to influence the rate of crack growth in Alloy 600 are cold work, hydrogen overpressure and possibly pH or lithium hydroxide concentration. Cold work can easily affect the value of the coefficient C by as much as an order of magnitude. Hydrogen overpressure effects are also potentially significant [28]. However, the effect has not been explicitly included in crack growth assessment equations to date, probably because the hydrogen concentration in PWR primary water is controlled within a relatively narrow range. Concerning the possible influence of pH or lithium concentration in PWR primary water on crack growth kinetics, the effect is, at most, small within the range of pH or lithium concentrations permitted by the PWR primary water specification [11,22]. More recent work suggests that the effect of lithium within this range is virtually non-existent [29].

### Summary of laboratory investigations

As early as 1957, laboratory studies of cracking of high-nickel alloys in high-purity water at 350 °C (660 °F) were reported [1,5] although at that time the importance of the corrosion potential as fixed by the hydrogen partial pressure was not understood. During the following years, numerous laboratory tests were performed in different environments to duplicate and explain these observations. Nevertheless, despite considerable experimental efforts, no consensus exists as to the nature of the cracking mechanism [29] and, as noted above, both remedial measures and life modeling have relied on empirical, phenomenological correlations. The essential phenomenological features of primary water PWSCC of Alloy 600 have, nevertheless, been very well characterized, as follows:

- a profound influence of hydrogen partial pressure (or corrosion potential) and observation of maximum susceptibility centered on corrosion potentials near the Ni/NiO stability equilibrium;
- an apparently continuous mechanism of cracking between 300°C sub-cooled water and 400°C superheated steam;
- a high and variable apparent activation energy typically 180 kJ/mole for initiation but with a scatter band of 80 to 220 kJ/mole;
- a strong influence of carbon content and microstructure, particularly a favorable influence of grain boundary carbides and an undesirable effect of cold work;
- a high stress exponent of  $\approx 4$  for lifetime to cracking occurrence.

It can be noted that despite differing opinions about the mechanism of PWSCC of Alloy 600, most recent models incorporate the idea that solid state grain boundary diffusion is rate controlling [30]. Such models provide physically based support for the empirical value of the activation energy, which is typical of solid-state grain boundary diffusion in nickel. Physical support for the fourth power dependency on applied stress comes

mainly from studies of grain boundary sliding (itself dependent on grain boundary diffusion) observed during primary creep in Alloy 600 at temperatures between 325 and 360°C [23,31]. Grain boundary sliding rates are also observed to depend on grain boundary carbide coverage, greater coverage being associated with slower grain boundary sliding rates and higher resistance to PWSCC. However, although grain boundary carbide morphology is a major reason for heat-to-heat variability in susceptibility to PWSCC of Alloy 600 in PWR primary water, it is clear that other metallurgical parameters, albeit poorly characterized or unidentified, must be involved.

Research into PWSCC, particularly of thick-walled components made of Alloy 600 and its weld metals, is ongoing throughout the world and significant progress, both in practical assessment of service life and mitigation measures, as well as in more fundamental understanding, is anticipated within the next few years.

Alloy 690 has been extensively tested in the laboratory in order to quantify its resistance to PWSCC and to estimate the advantage gained relative to Alloy 600 (32). The improvement factor for thermally treated Alloy 690 relative to mill annealed Alloy 600 has been determined to be greater than 26, and greater than 13 relative to thermally treated Alloy 600. These factors have been judged to be sufficient to conclude that cracking is unlikely in 60+ years. The corresponding weld metals, Alloys 152 and 52, have also been tested although to a lesser extent than the base material but nevertheless appear to have similar resistance to Alloy 690.

Some knowledge gaps have been identified apart from an insufficient data base for Alloy 152 and 52 weld metals mentioned above (32). One important gap concerns possible effects of product form and subtle changes of composition and mechanical processing effects on PWSCC resistance since it has proved possible to produce structures that can crack under extremely severe test conditions. A potential concern for susceptibility of weld heat affected zones has also been identified by analogy with known data for Alloy 600 and this could also be extended to the mixing zones with stainless and low alloy steels in bimetallic welds. Little information is available on corrosion fatigue properties of Alloy 690 although these are expected to be similar to those of Alloy 600. Possible low temperature crack propagation during transient conditions encountered during plant cooldown has also been identified as requiring some study.

## References for B. 6

- [1] J. Blanchet, et al., "Historical Review of the Principal Research Concerning the Phenomena of Cracking of Nickel Base Austenitic Alloys," Proceedings of NACE-5 'Stress Corrosion Cracking and Hydrogen Embrittlement of Iron Base Alloys', National Association of Corrosion Engineers 1977, pp 1149-1160.
- [2] H.J. Schenk, "Investigation of Tube Failures in Inconel 600 Steam Generator Tubing at KWO Obrigheim," Materials Performance, Vol 15 (3), 1976, pp 25-33.
- [3] S.J. Green, "Steam Generator Failure or Degradation," Corrosion in the Nuclear Power Industry, ASM Handbook, Volume 13, "Corrosion," 1987, pp 937-945.
- [4] W. Bamford, J. Hall, "A Review of Alloy 600 Cracking in Operating Nuclear Plants: Historical Experience and Future Trends," Proceedings of 11<sup>th</sup> Int. Conference on Environmental Degradation of Materials in Nuclear Power Systems - Water Reactors, Stevenson, American Nuclear Society 2003, pp 1071-1079.
- [5] W.H. Cullen, Jr., T.S. Mintz, "A Survey of Worldwide Experience with the Cracking Susceptibility of Alloy 600 and Associated Welds," Office of Nuclear Regulatory Research, US Nuclear Regulatory Commission, Washington, DC 20555.
- [6] P.A. Sherburne, "OTSG Materials Performance – 25 Years Later," Proceedings of the Fontevraud IV International Symposium, SFEN 1998, pp 529-540.
- [7] D.R. Diercks, W.J. Shack, J. Muscara, "Overview of Steam Generator Tube Degradation and Integrity Issues," Nuclear Engineering and Design, Vol 194, 1999, pp 19-30.
- [8] G. Frederick, P. Hernalsteen, "Generic Preventive Actions for Mitigating MA Inconel 600 Susceptibility to Pure Water Stress Corrosion Cracking," Paper presented at The Specialist Meeting on Steam Generators, Stockholm, Sweden, NEA/CSNI-UNIPeDE, Oct 1984.
- [9] P. Saint-Paul, G. Slama, "Steam Generator Materials Degradation," Proceedings of 5th Int. Symposium on Environmental Degradation of Materials in Nuclear Power Systems - Water Reactors, Monterey, American Nuclear Society 1992, pp 39-49.
- [10] P. Pitner, T. Riffard, "Statistical Evaluation of the Effects of Shot-peening on Stress Corrosion of Alloy 600 in PWR Steam Generators," Proceedings of 6th Int. Symposium on Environmental Degradation of Materials in Nuclear Power Systems - Water Reactors, The Metallurgical Society 1993, pp 707-712.
- [11] P.M. Scott, "Stress Corrosion Cracking in Pressurized Water Reactors - Interpretation, Modeling and Remedies," Corrosion, Vol 56(8), 2000, pp 771-782.
- [12] G. P. Airey, "The Stress Corrosion Cracking (SCC) Performance of Inconel Alloy 600 in Pure and Primary Water Environments," Proceedings of 1st International Symposium on Environmental Degradation of Materials in Nuclear Power Systems- Water Reactors, National Association of Corrosion Engineers, 1984, pp 462-476.
- [13] A.A. Stein, A.R. McIlree, "Relationship of Annealing Temperature and Microstructure to Primary Side Cracking of Alloy 600 Steam Generator Tubing and the Prediction of Stress Corrosion Cracking in Primary Water," Proceedings of 2nd International Symposium on Environmental Degradation of Materials in Nuclear Power Systems-Water Reactors, Monterey, CA, American Nuclear Society 1986, pp 47-51.
- [14] Ph. Berge, "Importance of Surface Preparation for Corrosion Control in Nuclear Power Stations," Materials Performance Vol 36 (11), 1997, p 56.



- [15] F. Champigny, F. Chapelier, C. Amzallag, "Maintenance Strategy of Inconel Components in PWR Primary Systems in France," Proceedings of Conference on Vessel Penetration Inspection, Cracking and Repairs, Gaithersburg, MD, September 29-October 2, 2003.
- [16] P. Chartier, D. Edmond, G. Turluer, "The French Regulatory Experience and Views on Nickel-base Alloy PWSCC Prevention," Proceedings of Conference on Vessel Penetration Inspection, Cracking and Repairs, Gaithersburg, MD, September 29-October 2, 2003.
- [17] A. Hiser, "US Regulatory Experience and Prognosis with RPV Head Degradation and VHP Nozzle Cracking," Proceedings of Conference on Vessel Penetration Inspection, Cracking and Repairs, Gaithersburg, MD, September 29-October 2, 2003.
- [18] C. Amzallag, et al., "Stress Corrosion Life Assessment of 182 and 82 Welds Used in PWR Components," Proceedings of the 10th International Conference on Environmental Degradation of Materials in Nuclear Power Systems – Water Reactors, August 3 to 9, 2001, Lake Tahoe, CA, NACE International 2001.
- [19] S. Thomas, "Bottom Mounted Instrumentation Penetration Condition Resolution," Proceedings of Conference on Vessel Penetration Inspection, Cracking and Repairs, Gaithersburg, MD, September 29-October 2, 2003.
- [20] L.E. Thomas, et al., "High Resolution Analytical Electron Microscopy Characterization of Environmentally Assisted Cracks in Alloy 182 Weldments," Proceedings of 11th International Conference on Environmental Degradation of Materials in Nuclear Power Systems – Water Reactors, Stevenson, Washington, American Nuclear Society 2003, pp 1212-1224.
- [21] R.W. Staehle, et al., "Application of Statistical Distributions to Characterizing and Predicting Corrosion of Tubing in Steam Generators of Pressurized Water Reactors," Proceedings of Life Prediction of Corrodible Structures, ed. R. N. Parkins, (Houston, TX: NACE International, 1994), pp 1374-1439.
- [22] P. Scott and C. Benhamou, "An Overview of Recent Observations and Interpretation of PWSCC in Nickel Base Alloys in PWR Primary Water," Proceedings of 10th Int. Symposium on Environmental Degradation of Materials in Nuclear Power Systems - Water Reactors, Lake Tahoe, NACE International 2001.
- [23] S. LeHong, C. Amzallag, A. Gelpi, "Modeling of Stress Corrosion Crack Initiation on Alloy 600 in Primary Water of PWRs," Proceedings of 9th International Symposium on Environmental Degradation of Materials in Nuclear Power Systems – Water Reactors, Newport Beach, CA, The Metallurgical Society 1999, pp 115-122.
- [24] C. Amzallag, et al., "Stress Corrosion Life Assessment of Alloy 600 Components," Proceedings of 9th International Symposium on Environmental Degradation of Materials in Nuclear Power Systems – Water Reactors, Newport Beach, CA, The Metallurgical Society 1999, pp 243-250.
- [25] C. Amzallag, et al., "Methodology Used to Rank the Stress Corrosion Susceptibility of Alloy 600 PWR Components," Pressure Vessel and Piping Conference, (Seattle: ASME, 2000).
- [26] C. Amzallag, F. Vaillant, "Stress Corrosion Crack Propagation Rates in Reactor Vessel Head Penetrations in Alloy 600," Proceedings of 9th International Symposium on Environmental Degradation of Materials in Nuclear Power Systems

- Water Reactors, Newport Beach, CA, The Metallurgical Society 1999, pp 235-241.
- [27] G. A. White, J. Hickling, L. K. Mathews, "Crack Growth Rates for Evaluating PWSCC of Thick-walled Alloy 600 Material," Proceedings of 11th International Conference on Environmental Degradation of Materials in Nuclear Power Systems – Water Reactors, Stevenson, Washington, American Nuclear Society 2003, pp 166-179
- [28] S. A. Attanasio, J. S. Morton, "Measurements of Nickel/nickel Oxide Transition in Ni-Cr-Fe Alloys and Updated Data and Correlations to Quantify the Effect of Aqueous Hydrogen on Primary Water SCC," Proceedings of 11th International Conference on Environmental Degradation of Materials in Nuclear Power Systems – Water Reactors, Stevenson, Washington, American Nuclear Society 2003, pp 143-154.
- [29] P. M. Scott, P. Combrade, "On the Mechanism of Stress Corrosion Crack Initiation and Growth in Alloy 600 Exposed to PWR Primary Water," Proceedings of 11th International Conference on Environmental Degradation of Materials in Nuclear Power Systems – Water Reactors, Stevenson, Washington, American Nuclear Society 2003, pp 29-35.
- [30] F. Vaillant, et al., "Influence of Chromium Content and Microstructure on Creep and PWSCC Resistance of Nickel Base Alloys," Proceedings of 9th International Symposium on Environmental Degradation of Materials in Nuclear Power Systems – Water Reactors, Newport Beach, CA, The Metallurgical Society 1999), pp 251-258.

## **B.7 "Corrosion of Steam Generator Tubes,"** by Roger W. Staehle

### **Introduction**

The objective of this background paper is to describe the corrosion of tubing materials used in PWR steam generators of LWRs. This tubing includes Alloys 600MA, 600TT, 690TT and 800. The corrosion behavior of these materials has been discussed comprehensively by Staehle and Gorman.<sup>1</sup> This present report emphasizes mainly the initiation stage of SCC since SG tubes are relatively thin compared to thicker sections in pipes and various instrument and control rod housings. Some information on SCC propagation is included. As used in this paper, the term failure means degradation and/or cracking to varying degrees (depending on the context); sometimes such degradation would require tube plugging or repair and other times, failure relates to crack initiation.

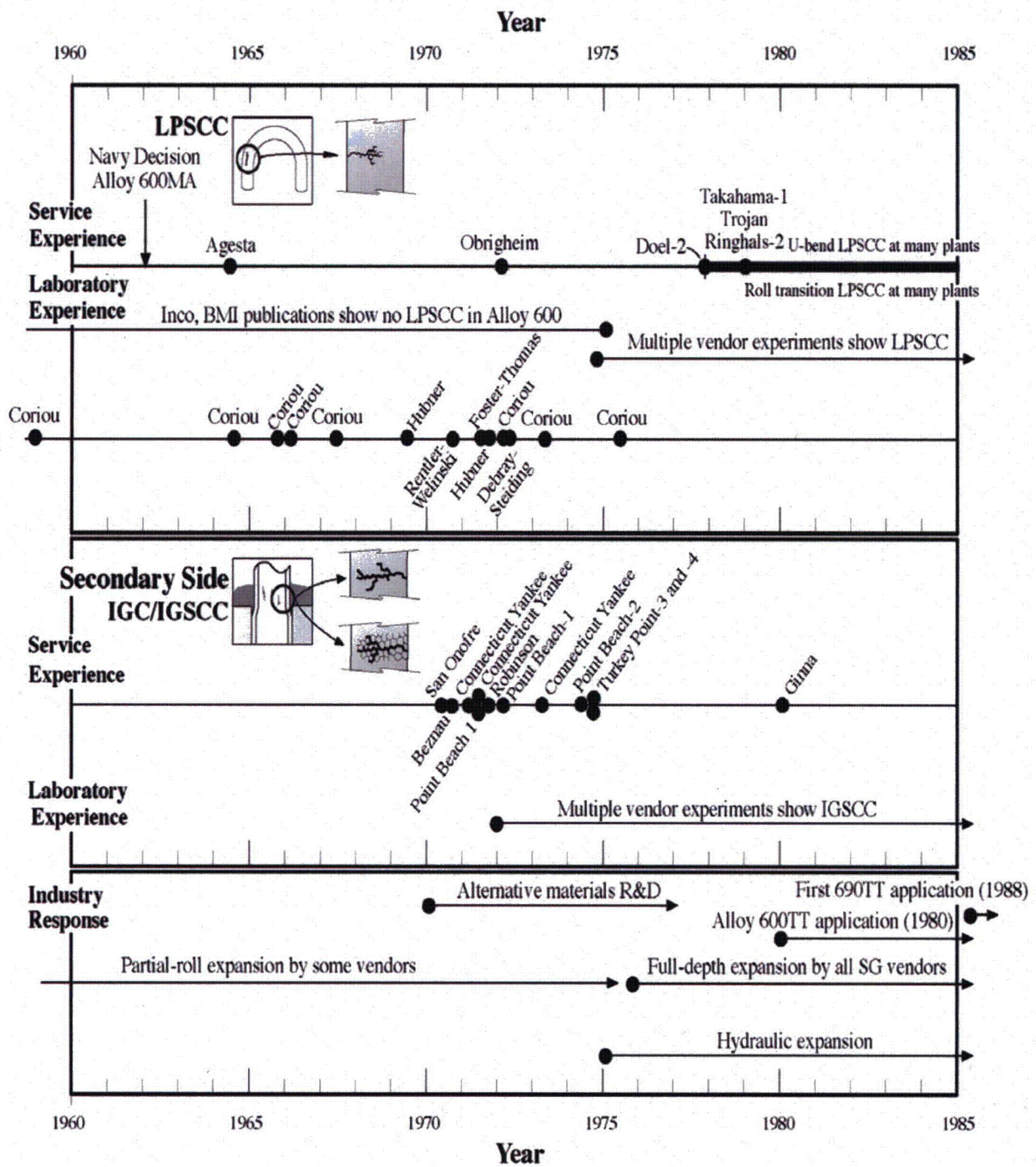
This discussion considers the development and application of Alloy 600MA, Alloy 600TT, Alloy 690TT and Alloy 800, together with the modes of corrosion they sustain and some of the principal dependencies of these modes of corrosion.

The terminology of MA (mill-annealed) and TT (thermal treatment) is used in this discussion. MA for Alloy 600 is heat treated at about 1000°C and for Alloy 690 at about 1070°C. TT for Alloy 600 is heat treated at 700°C for 15 hours and for Alloy 690 at 716°C for 10 hours. A slight variation for MA is given by LTMA (low temperature mill-annealed) and HTMA (high temperature mill-annealed). LTMA is heat treated at 985°C and HTMA at 1010°C.

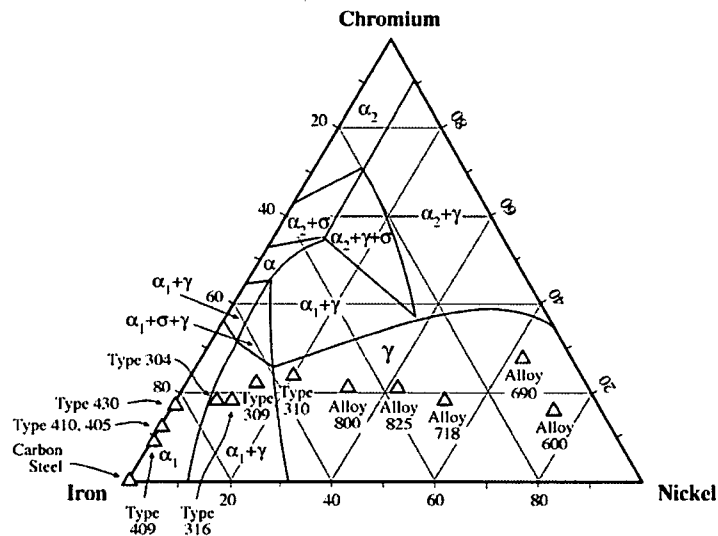
The earliest tubing used in steam generators was the Type 304 stainless steel in the Shippingport plant<sup>2</sup> and noted in Scharfstein et al.<sup>3,4</sup> However, even with the horizontal steam generators used in this application, chlorides and caustic were concentrated at the tube supports and tubesheets thereby producing SCC. In 1962 the Navy program decided to use Alloy 600MA in steam generators, and the subsequent evolution of the use of alloys in LWRs is shown in Figure B.7.1. The Russian designed VVERs followed a different path, continuing to use horizontal austenitic stainless steel tubes terminating at vertical cylindrical collectors. On the whole, these have been reliable in service.

The alloys used for steam generator tubing are nominally single phase with a face centered cubic structure, usually called an "austenitic structure," as shown in the ternary diagram of Figure B.7.2.<sup>5</sup> Chemical compositions of the alloys for SG tubing and for tube supports are given in Table B.7.1.

The choice of the high nickel alloys for replacing the stainless steels for SG tubing was based essentially on the work of Copson and Cheng,<sup>6</sup> who had studied the effect of nickel on the SCC of Fe-Cr-Ni alloys in boiling MgCl<sub>2</sub> solutions as shown in Figure B.7.3a. This work showed that the alloys with nickel concentration exceeding about 40w/o would resist SCC in the concentrated MgCl<sub>2</sub> solutions. By implication, and assuming that the boiling MgCl<sub>2</sub> solutions represented characteristically aggressive solutions generated from seawater or estuarine water ingress at leaking condensers, these results suggested that the high nickel alloys would resist a broad range of stress corrosion cracking. Figure B.7.3b from Berge and Donati<sup>7</sup> shows results from SCC testing of Alloy 600MA in a boric acid solution containing chloride at 100°C; and in contrast, found extensive transgranular SCC in Alloy 600.



**Fig. B.7.1** Service and laboratory experience with LPSCC and IGSCC vs. time. Industry response to these experiences vs. time. From Staehle and Gorman.<sup>1</sup> © NACE International 2003/2004.



**Fig. B.7.2** Alloys of interest to steam generators superimposed on Fe-Cr-Ni ternary diagram for 400°C. Fe-Cr-Ni diagram from Pugh and Nisbet.<sup>5</sup> Reprinted with permission from TMS.

**Table B.7.1** Composition of Alloys Used in Tubing and Tube Supports (maximum w/o, except where noted)

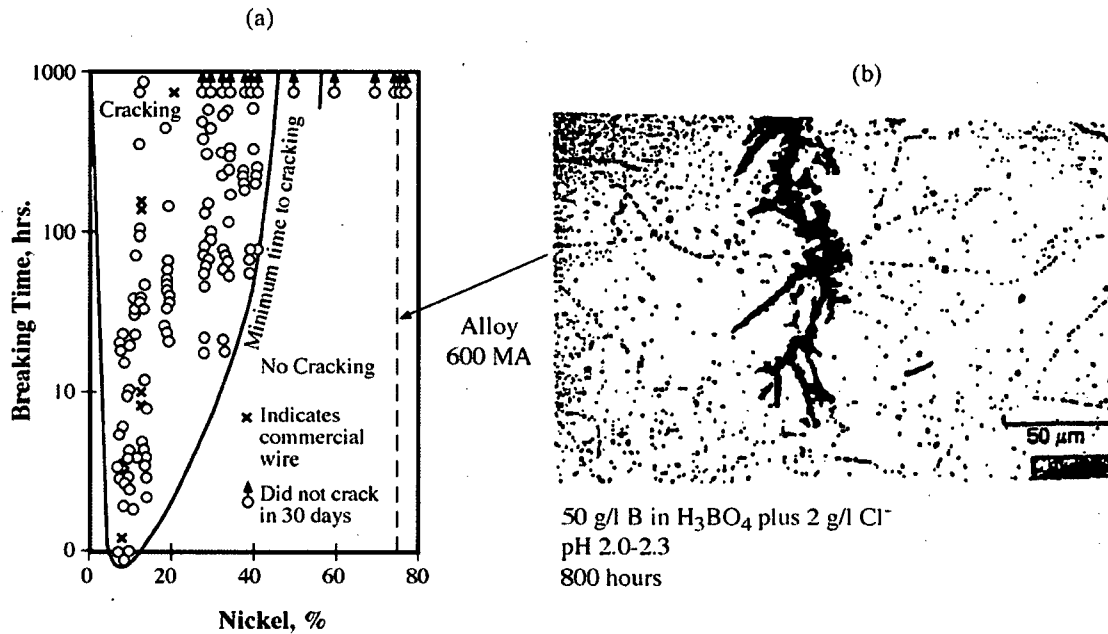
Elem.	Type 304 <sup>[A]</sup>	Type 316 <sup>[A]</sup>	Alloy 600 EPRI Guidelines <sup>[B]</sup>	Alloy 690 EPRI Guidelines <sup>[C]</sup>	Alloy 800 Nuclear Grade <sup>[D]</sup>	Carbon Steel ASTM A285 Gr C <sup>[A]</sup>	Type 405 ASME SA479 <sup>[A]</sup>	Type 409 <sup>[A]</sup>	Type 410 ASME SA479 <sup>[A]</sup>
C	0.08	0.08	0.025-0.05	0.015-0.025	0.03	0.28	0.15	0.08	0.15
Mn	2.00	2.00	1.00 max.	0.50	0.4-1.0	0.90	1.00	1.00	1.00
P	0.045	0.045	0.015	0.015	0.020	0.035	0.040	0.045	0.040
S	0.03	0.03	0.010 max.	0.003	0.015	0.035	0.030	0.045	0.030
Si	1.00	1.00	0.50 max.	0.50	0.3-0.7	-	0.50	1.00	1.00
Cr	18-20	16-18	15.0-17.0	28.5-31.0	20-23	-	11.5-13.0	10.5-11.75	11.5-13.5
Ni	8.0-10.5	10-14	>72	Bal. (>58)	32-35	-	-	0.50	-
Mo	-	2.0-3.0	-	0.2	-	-	-	-	-
Fe	Bal.	Bal.	6.0-10.0	9.0-11.0	Bal.	-	Bal.	Bal.	Bal.
Cu	-	-	0.50 max.	0.10	0.75	-	-	-	-
Co	-	-	0.015 ave.	0.014	0.10	-	-	-	-
Al	-	-	-	0.40	0.15-0.45	-	-	-	-
Ti	-	-	-	0.40	0.60	-	-	6xC-0.75	-
Other	-	-	-	N = 0.050 B = 0.005 Nb = 0.1	Ti/C ≥ 12 Ti/(C+N) ≥ 8 N ≥ 0.03	-	-	-	-

[A] From ASM Handbook.<sup>8</sup>

[B] From EPRI.<sup>9</sup>

[C] From Gorman.<sup>10</sup>

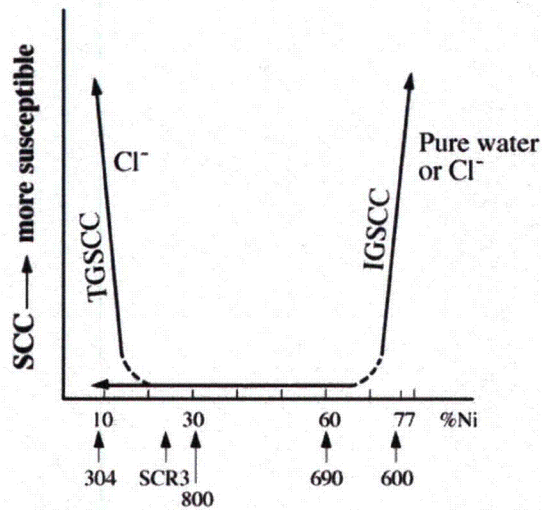
[D] From Stellwag et al.<sup>11</sup>



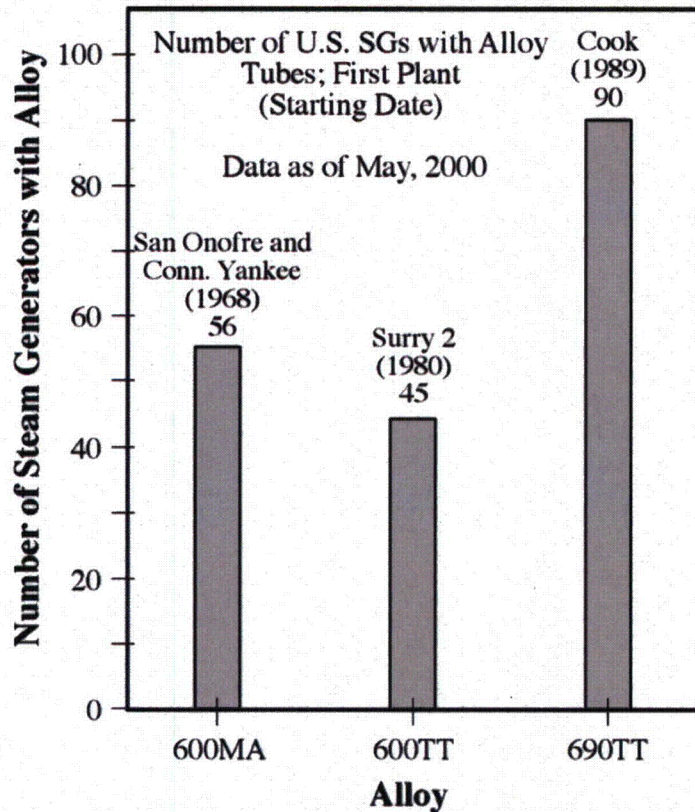
**Fig. B.7.3** (a) Breaking time vs. Ni (in wt.%) for Fe-20Cr-Ni alloys exposed to 42% boiling MgCl<sub>2</sub>. pH of solution is about 4.1. From Copson and Cheng. (b) Photomicrograph of Alloy 600MA exposed at 100°C in a solution containing 50 g/l boron as boric acid and 2 g/l Cl<sup>-</sup>. pH of solution is 2.0 to 2.3. U-bend specimen examined after 800h. From Berge and Donati<sup>7</sup> © 1981 American Nuclear Society.

At about the same time as Copson and Cheng had published the work in Figure B.7.3a, Coriou et al. published their work on the SCC of high nickel alloys which were exposed to 100°C pure water.<sup>12</sup> This 1959 paper, together with subsequent ones, showed conclusively that Alloy 600 would sustain SCC in pure deaerated water. Coriou et al.<sup>13</sup> then published a schematic view shown in Figure B.7.4 indicating that the SCC in pure deaerated water was most aggressive in high nickel alloys while the SCC in chloride solutions was most aggressive in low nickel alloys following Figure B.7.3 from Copson and Cheng. This figure indicated that an optimum material would be in the mid-range of nickel concentration. This observation was the basis for choosing Alloy 800 for some SG tubing as well as indicating that the Alloy 690 composition, to be developed later, would be attractive.

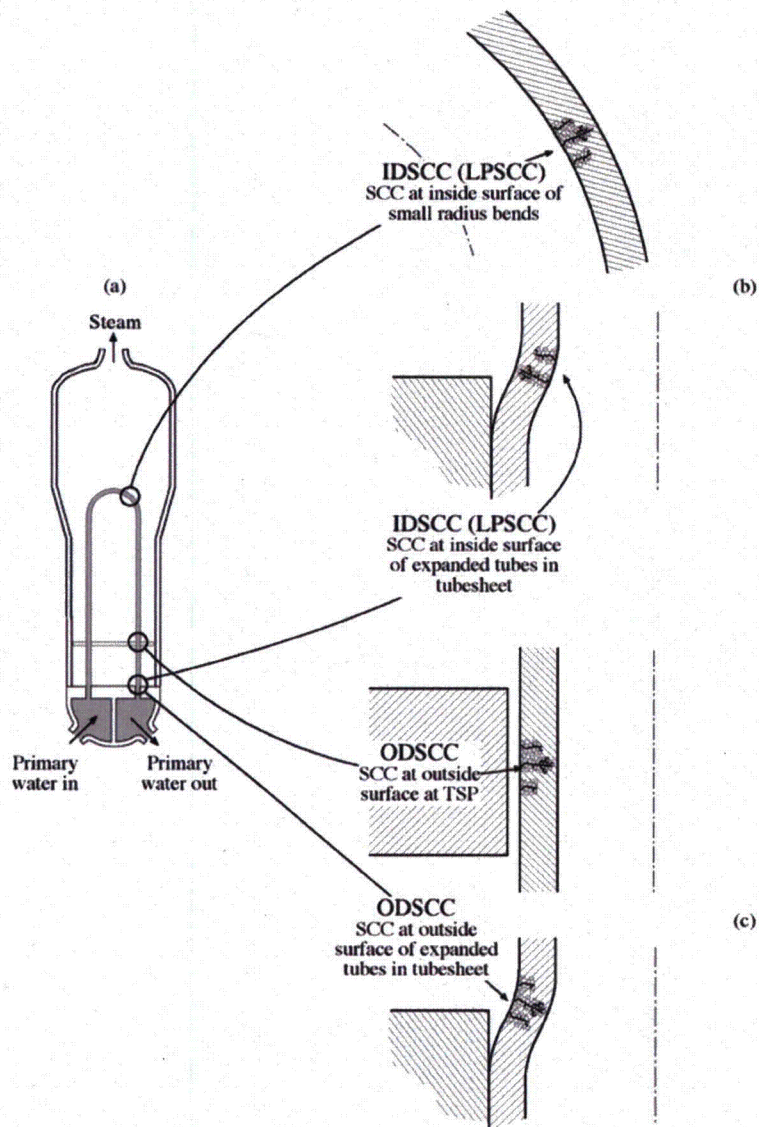
In summary, the chronology of corrosion of tubing in PWR steam generators has been dominated by extensive SCC on both the inside and outside of the Alloy 600 tubes. The application of improved alloys has responded to this corrosion first with Alloy 600TT and then with Alloy 690TT as shown in Figure B.7.5. Today, Alloy 690TT is increasingly used for replacement steam generators because of its improved corrosion resistance; although it should be noted, as shown in Section 4.0, that Alloy 690TT is not immune to SCC. In addition, Alloy 800 has given excellent service, as predicted by Coriou et al. in Figure B.7.4, in operating SGs.



**Fig. B.7.4** Schematic view of SCC intensity vs. Ni concentration for Fe-Cr-Ni alloys in high temperature water for pure deaerated water and chloride-containing water. Important commercial alloys noted. From Coriou et al.<sup>13</sup> © NACE International 1969.



**Fig. B.7.5** Number of U.S. steam generators with various alloy tubing as of May 2000. First plant to use the alloy and start dates noted. Private communication from P. Scott, Framatome and Al McIlree, EPRI. Note that Alloy 800 continues to exhibit excellent performance in international applications.



**Fig. B.7.6** Schematic view of principal location of SCC damage. SCC from the primary side is mostly stress-related and from the secondary side is mostly chemistry related.

Corrosion of Alloy 600 steam generator tubes has occurred both on the inside surface (IDSCC) as well as the outside surface (ODSCC) as shown in Figure B.7.6. On the inside primary surfaces, SCC has occurred mainly at locations of relatively high stresses and high temperatures. These high stresses occur at the tubesheet where the tubes are expanded and at the U-bends, especially the inner U-bends where the radii of curvature are the smallest. SCC on the primary side also occurred during the slow straining associated with "denting." On the outside surfaces, SCC has occurred mainly on surfaces inside heat transfer crevices both at the top of the tubesheet and at tube supports. This corrosion has occurred again mainly at the hottest locations along the tubes; although the stresses at these locations, except at the top of the tubesheet, were nominal being associated with pressure forces and residual stresses due to

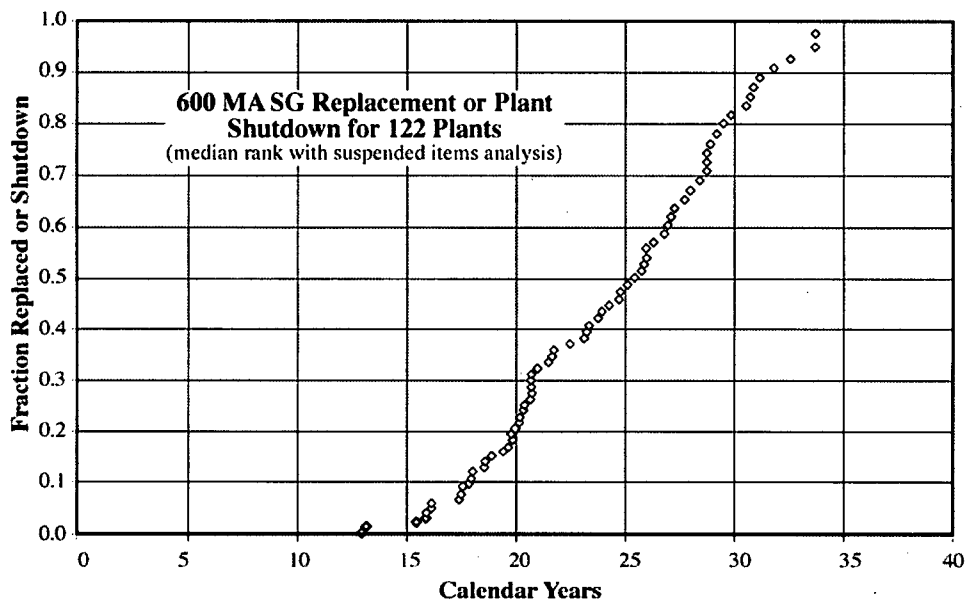


fabrication of the tubes. SCC on the outside surfaces has also occurred in free span locations often associated with scratches.

Much of the corrosion that has occurred in the Alloy 600 tubing of SGs has resulted from erroneous assumptions:

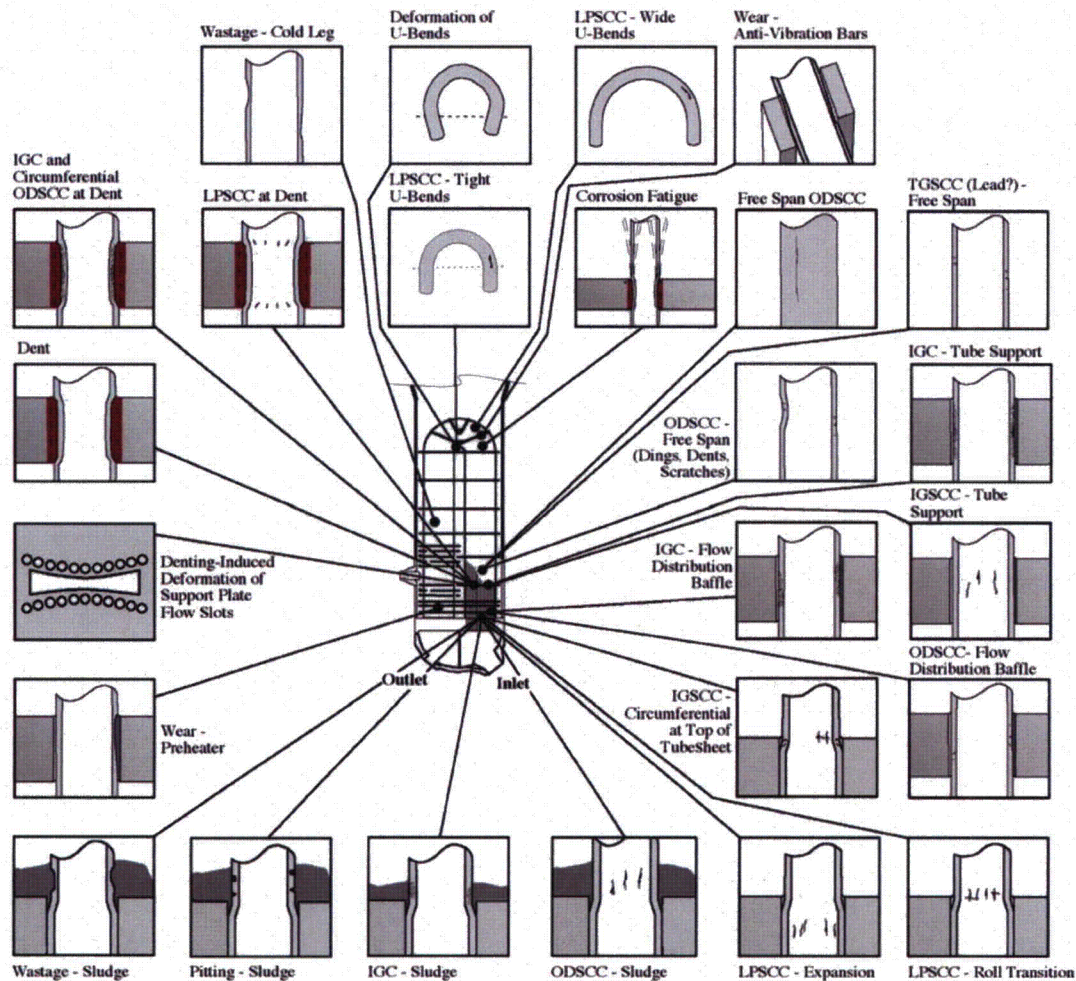
- Assumption that Copson and Cheng's data, Figure B.7.3, were correct as were the implications for adequate performance in other environments.
- Assumption that the Coriou et al. data were not applicable and erroneous.
- Assumption that water chemistry that worked in fossil systems would work on the secondary side of PWR SGs.
- Assumption that significant fouling and hence corrosive concentrations would not occur in drilled hole heat transfer crevices.
- Assumption that residual stresses in expanded regions and in straight tubes were not sufficient to produce SCC.

Figure B.7.7 shows the chronology for the replacement of SGs. These replacements resulted from corrosion degradation.



**Fig. B.7.7** Fraction of replaced or shutdown steam generators vs. calendar years for Alloy 600MA plants in the world. From Dow, Jr.<sup>14</sup> Used by Permission of EPRI.

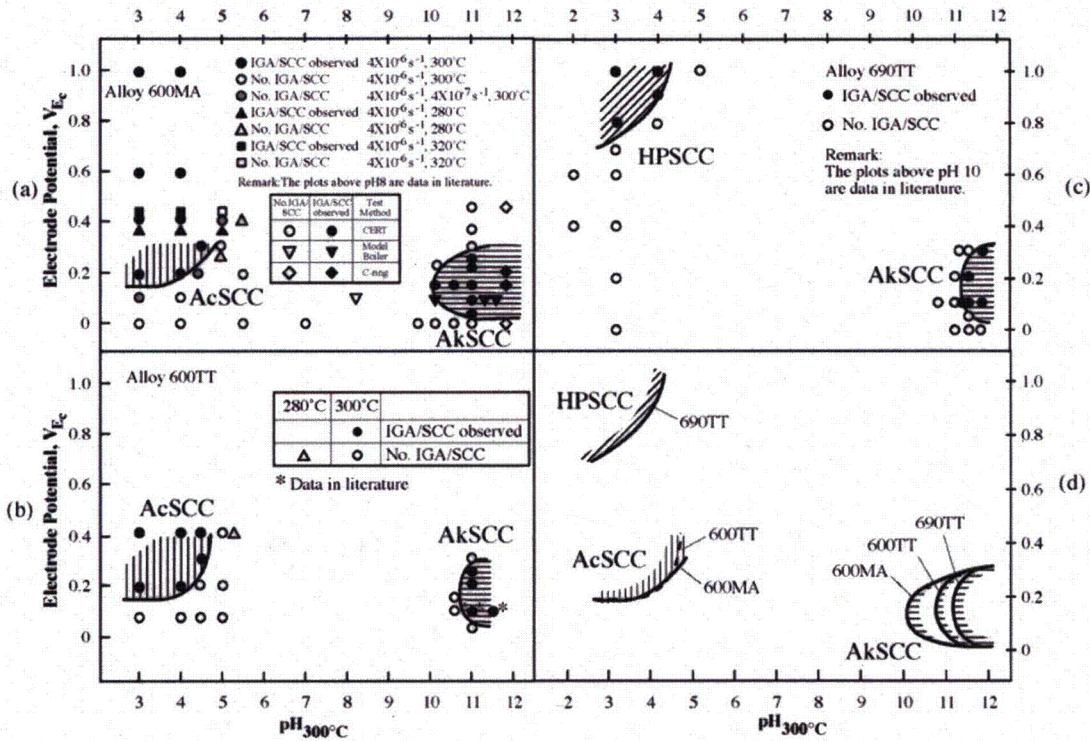
Failures involving multiple modes of corrosion and multiple locations occurred with the combination of Alloy 600MA as it was exposed on both primary and secondary sides. The multiple mode-location cases of degradation with Alloy 600MA and with drilled holes on the secondary side, are summarized in Figure B.7.8. Here, there are 25 mode-location cases of degradation associated with the use of Alloy 600MA.



**Fig. B.7.8** Array of modes of degradation at various locations (mode-location cases) that have occurred in recirculating steam generators using Alloy 600MA at drilled hole tube supports. From Staehle and Gorman.<sup>1</sup> © NACE International 2003/2004.

As these failures, which are shown in Figure B.7.8, evolved, extensive corrosion studies were undertaken both in the laboratory and of failed tubes. These experiments included studies of SCC on the primary side, where there were no crevices, and the secondary side, where there were extensive heat transfer crevices. SCC was identified in regions that were not so surprising based on the past history of SCC in steels and stainless steels. Figure B.7.9 shows the locations of the occurrence of SCC in the framework of the electrochemical variables of pH and potential. The occurrence of such SCC in the acidic, alkaline, low potential and high potential regions corresponds generally with regions where protective films are transiently unstable when broken. The bases for the diagram shown in Figure B.7.9a are described by Staehle and Gorman.<sup>1</sup> In addition to the diagram in Figure B.7.9a that shows the “primary” submodes of SCC, Figure B.7.9b shows the general locations of other submodes of SCC. Again, this diagram has been extensively described by Staehle and co-workers. Also, a similar diagram has been published by Combrade et al.<sup>15,16,17</sup> The term, “submode,” refers to the corrosion mode of SCC, but differentiates occurrences of unique dependencies on the primary variable of

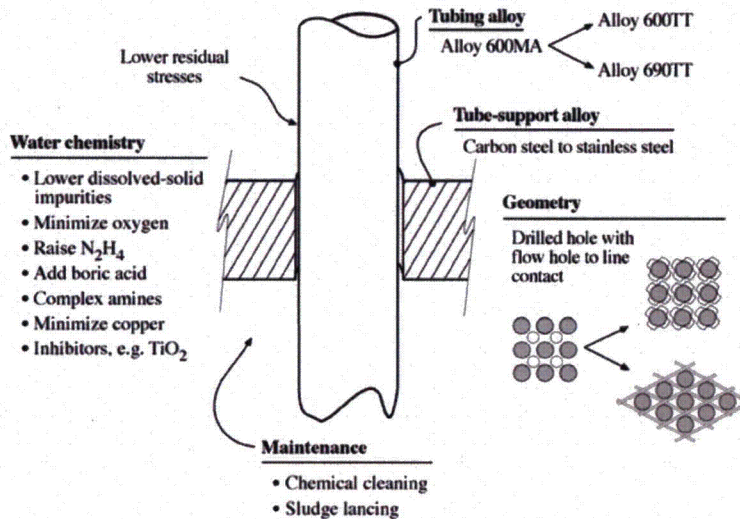




**Fig. B.7.10** IGA/SCC tests results in the range of 180 to 320°C range as a function of electrode potential and pH taken at 300°C for (a) Alloy 600MA, (b) Alloy 600TT, (c) Alloy 690TT. From Ohsaki et al.<sup>18</sup> (d) Comparison of IGA susceptibility among Alloy 600MA, Alloy 600TT, and Alloy 690TT in the range of 280 to 320°C as a function of electrode potential and pH taken at 300°C. From Tsujikawa and Yashima.<sup>19</sup> Permission granted by Canadian Nuclear Society.

### Alloy 600MA - Introduction

Alloy 600MA was the alloy used widely for tubing in SGs of PWRs from 1962 through the mid-1980s in France, Japan, Spain, Sweden and the US. The corrosion that occurred with the use of Alloy 600MA resulted in the replacement of the steam generators as shown in Figure B.7.7. Replaced SGs have primarily been tubed with Alloys 600TT or 690TT with the latter being preferred as indicated in Figure B.7.5. Alloys 600TT and 690TT as well as Alloy 800 have given excellent service as discussed below.


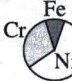
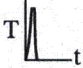
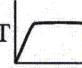


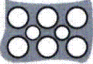





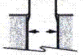
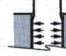






**Fig. B.7.11** Schematic view of changes in maintenance, materials, designs, and water in order to minimize the corrosion of the tubing. From Staehle and Gorman.<sup>1</sup> © NACE International 2003/2004.

During the Alloy 600MA period, corrosion was dominated by two general patterns, mainly of SCC. One was SCC from the ID of the tubes, which was exposed to high purity primary water containing the standard chemical additions of hydrogen, boric acid and lithium hydroxide. The other was SCC and some corrosion from the OD, which was associated mainly with impurity chemicals that were concentrated in the superheated crevices of tube supports and at the top of tubesheets. Figure B.7.6 shows these essential locations, which are discussed below.

The overall chronology of modes of corrosion of Alloy 600 has been described in two different figures as shown in Figure B.7.13. These figures both show the same trends. An early mode of failure was general corrosion associated with phosphate water chemistry in those plants that adopted this secondary water treatment. Following this, IGSCC occurred, which was mainly due to concentrations of alkaline impurities. Next was denting involving the corrosion products from corroding carbon steel tube supports pressing on the tubes to constrict the diameter. Next was an increase in IGSCC on the primary side followed by more IGSCC on the secondary side. These patterns involve mainly the occurrence of corrosion in Alloy 600MA.

Essentially, the evolution of corrosion concerning Alloy 600MA involved mitigating one mode only to find the intensification of another; such was the sensitivity of this alloy to corrosion.

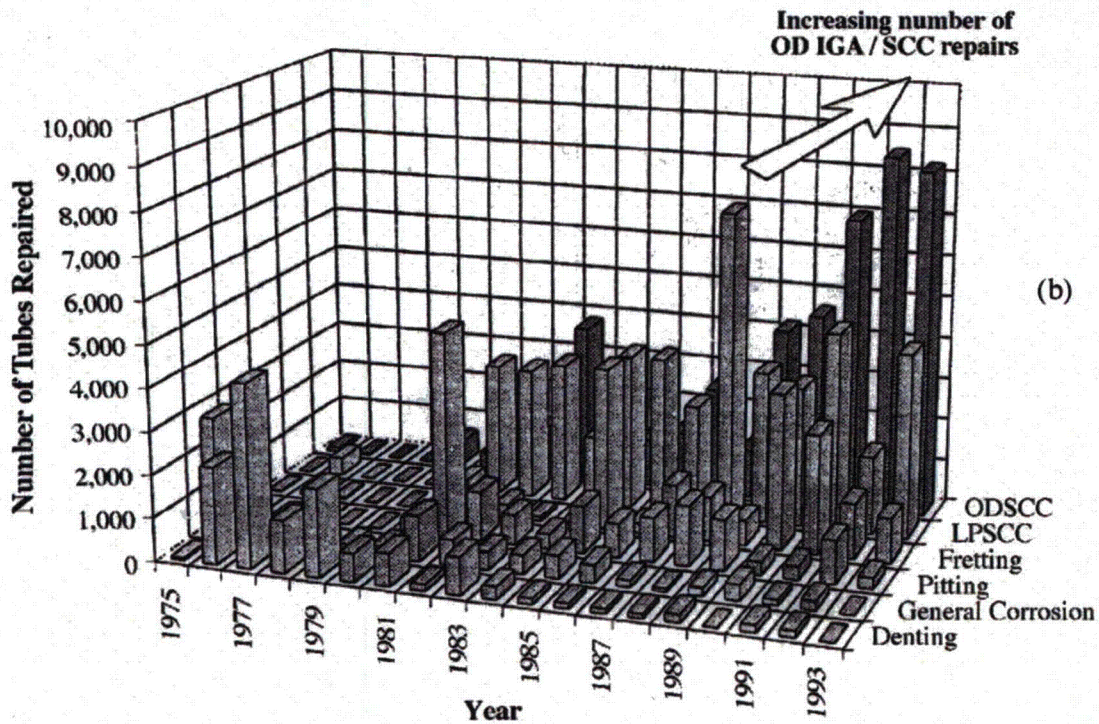
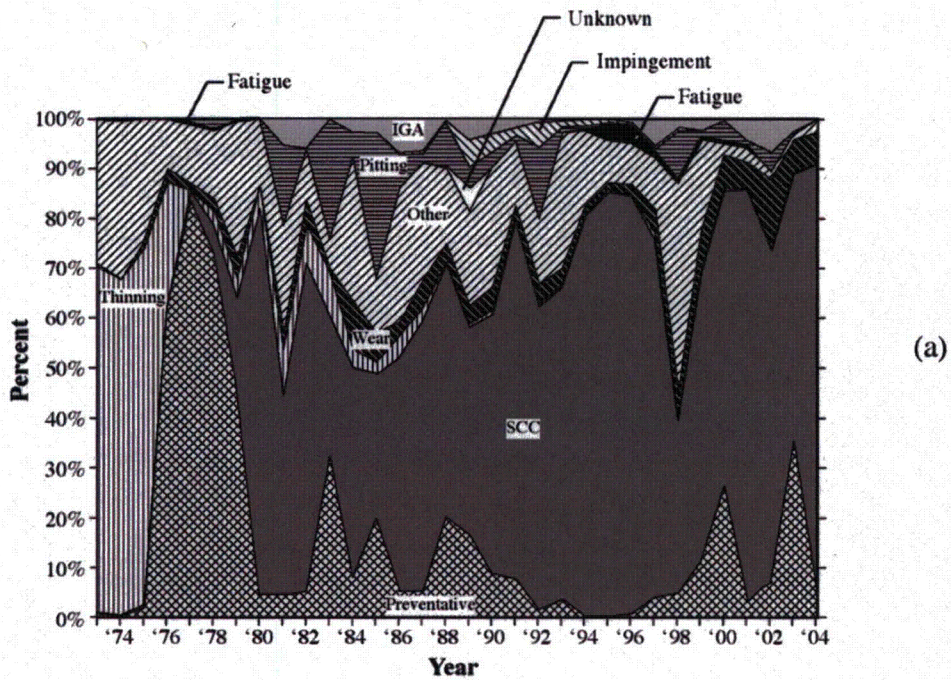
	Model D3, Virgil Summer	Model F
<b>Tube material</b>	Inconel 600MA 	Inconel 600TT or 690TT 
<b>Heat treatment</b>	Low temperature mill anneal (LTMA) 	Thermal treatment (TT) 
<b>Tube support hole</b>	Drilled hole, circular 	Quatrefoil 
<b>Tube support material</b>	Carbon steel 	Stainless steel 
<b>Flow holes</b>	Yes 	None 
<b>U-bend stress relief</b>	None 	Yes 
<b>Tube sheet expansion</b>	Mechanical expansion 	Hydraulic expansion 
<b>Blow down</b>	Original design 	Better location, increased capacity 
<b>Secondary Side Access</b>	Original design 	Improved 

**Fig. B.7.12** Comparison of Models D3 and F from Westinghouse design plants where changes are intended to minimize corrosion of the tubing. From Staehle and Gorman.<sup>1</sup> © NACE International 2003/2004.

### SCC of Alloy 600MA on the ID

SCC on the ID (primary) surfaces of SG tubes is mainly associated with Alloy 600MA, and such SCC has contributed substantially to the failure and widespread replacement of steam generators shown in Figure B.7.7. This section summarizes the main dependencies of SCC on the ID of Alloy 600MA tubes.

Since the SCC on the inside of Alloy 600MA tubes has been associated with the primary side or inside of the tubes, it was initially called "PWSCC" or "Primary Water SCC." This is also interpreted by some as "Pure Water SCC." Both terms however are misleading as they imply that this SCC can occur only on the primary side. A better terminology is "Low Potential SCC (LPSCC)," since this SCC is principally characterized by its occurrence at low electrochemical potentials, as shown in Figure B.7.9, just as some SCC occurs exclusively in the alkaline region and is called AkSCC. Incidentally, as a supporting note here, efforts to reproduce the early work of Coriou failed to identify this SCC, most likely due to the lack of sufficient deaeration of the tests.



**Fig. B.7.13** Chronology of modes of corrosion vs. time mainly for Alloy 600 in drilled hole tube supports. (a) Two dimensional. From Dow, Jr. (b) Three dimensional. From Varrin, Jr.<sup>20</sup> Used by Permission of EPRI.

Principal characteristics of LPSCC in Alloy 600MA are the following according to the seven primary variables that affect aqueous corrosion:

### 1. pH

LPSCC is generally independent of pH over a range from about pH 3 to pH 9 as summarized by Staehle and Gorman.<sup>1</sup>

### 2. Potential

A central feature of LPSCC has been its confinement to low potentials in the general range of the  $H_2O/H_2$  and  $NiO/Ni$  equilibria. There seems to be a tendency for LPSCC to be maximum, both in initiation and propagation, at the  $NiO/Ni$  equilibrium, as shown in Figure B.7.14.<sup>15,21,22</sup> In each figure the location of the  $NiO/Ni$  equilibrium potential is noted; this is an invariant and thermodynamically defined line, not depending on concentration of species in solution. Figure 14a is based on testing of initially smooth specimens; and Figure 14b is based on initially precracked specimens. Thus, the former relates to conditions of initiation and the latter relates to propagation.

### 3. Species

LPSCC has been investigated with respect to concentrations of boric acid and lithium hydroxide as summarized by Staehle and Gorman.<sup>1</sup> Effects of these species are not significant. However, there has been little investigation of effects of chloride, sulfate, or other species over significant ranges of concentration; this lack of breadth impedes connecting LPSCC to domains of chemistry that might be important to the secondary side.

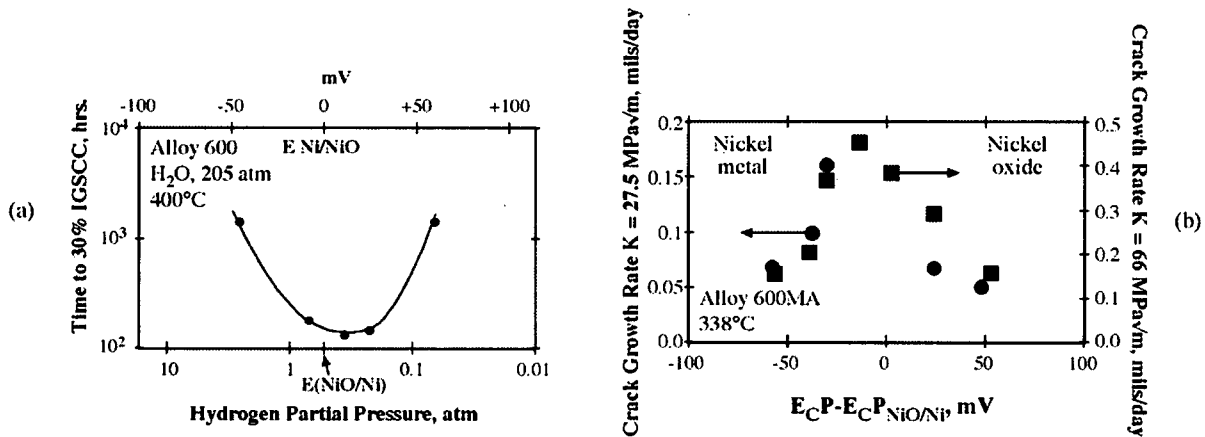
### 4. Alloy composition

Another defining characteristic of LPSCC is its dependence upon alloy composition. With respect to the concentration of chromium, the data from two different investigations in Figure B.7.15<sup>23,24</sup> show that increasing chromium decreases sensitivity to LPSCC. It is noteworthy that Fe-Ni alloys sustain rapid LPSCC and that LPSCC is negligible above 20% Cr, which is relevant to the compositions of Alloy 690 with a Cr content around 30% and Alloy 800.

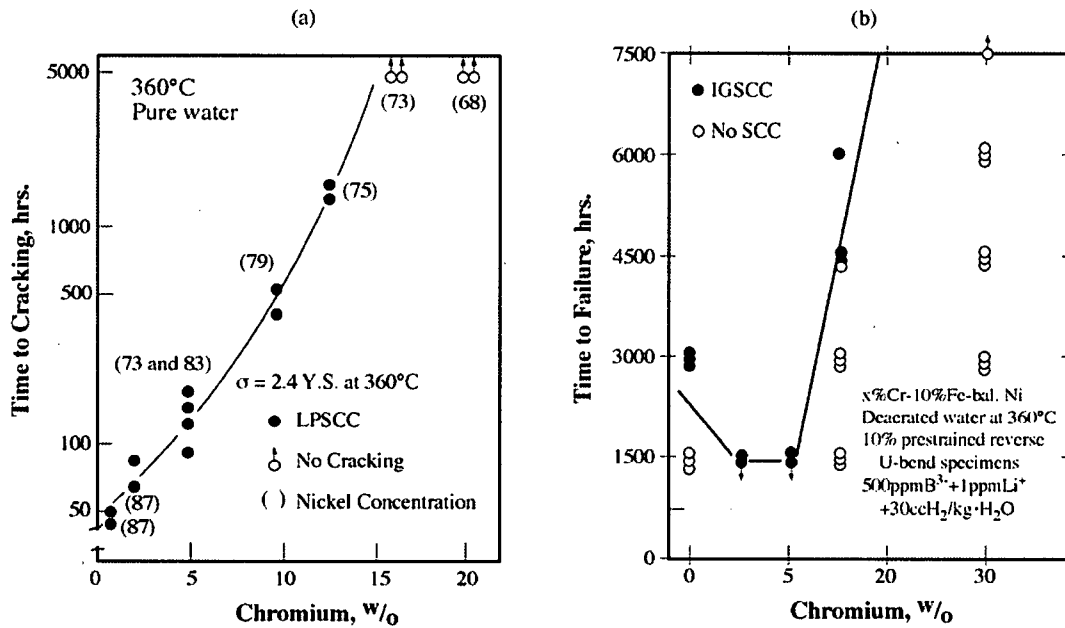
### 5. Alloy structure

LPSCC is generally influenced by the distribution of carbides. As carbides accumulate at grain boundaries, LPSCC is minimized. Figure B.7.16 shows this effect from work by Norring et al.<sup>25</sup> and Cattant et al.<sup>26</sup> A further important result was published by Blanchet et al.<sup>32</sup> where they showed that sensitization greatly reduced the sensitivity to LPSCC as shown in Table B.7.2.





**Fig. B.7.14** (a) Time to 30% IGSCC vs. hydrogen pressure and potential reference to NiO/Ni equilibrium. Experiments at 400°C and 205 atm pressure of steam. Original data from Economy et al.<sup>21</sup> Dependencies recalculated by Scott and Combrade.<sup>15</sup> © 1997 American Nuclear Society. (b) Crack growth rate at two stress intensities vs. potential ( $E_C P$ =electrochemical potential) relative to the NiO/Ni equilibrium potential for Alloy 600MA at 338°C. From Morton et al.<sup>22</sup> © NACE International 1987.



**Fig. B.7.15** (a) Time-to-cracking vs. concentration of Cr for Ni-Cr-Fe alloys exposed in pure water at 2.4 Y.S. at 360°C. From Yonezawa and Onimura.<sup>23</sup> Courtesy of ISIJ. (b) Time-to-failure as concentration of Cr for Fe-Cr-Ni alloys with 10w/o Fe. From Nagano and Kajimura.<sup>24</sup> © NACE International 1995.

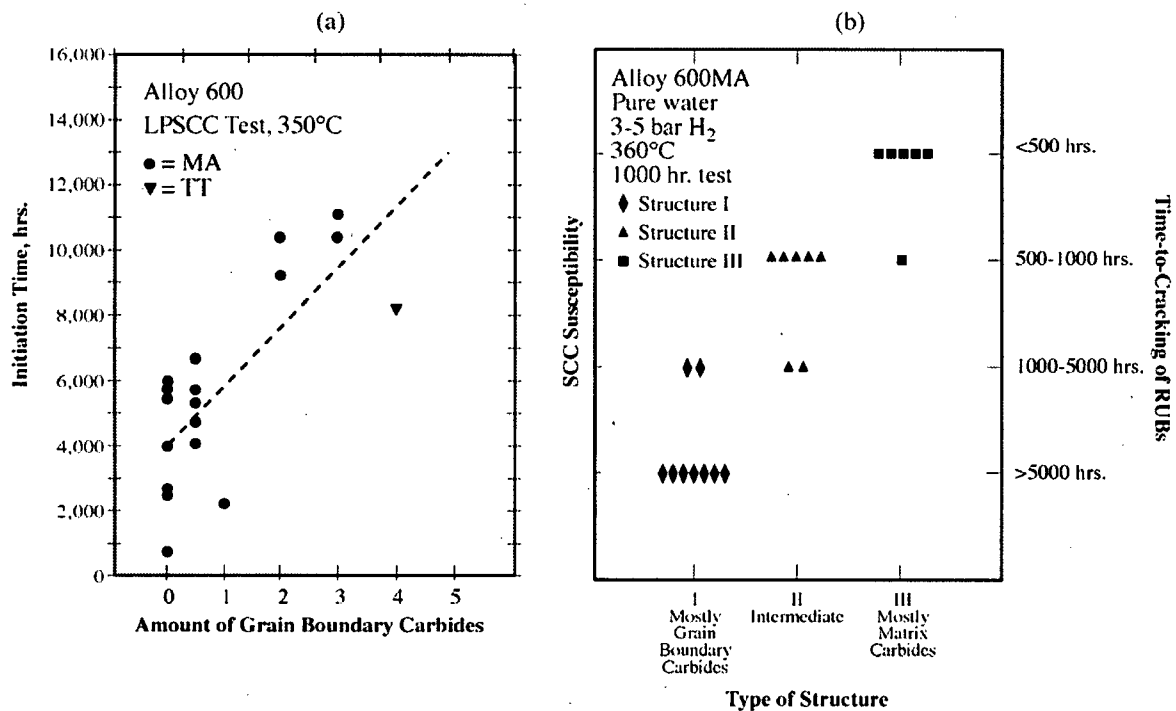
## 6. Temperature

The temperature dependence of LPSCC has been extensively studied, and this work is reviewed by Staehle and Gorman.<sup>1</sup> The most reliable values of the activation energy for initiation seems to be about 40-55 Kcal/mol and for propagation about 30-35 Kcal/mol.

Figure B.7.17 shows some typical data for initiation and propagation from the work of Webb<sup>27</sup> (Figure B.7.17a) and the review by Cassagne et al.<sup>28</sup> (Figure B.7.17b).

## 7. Stress

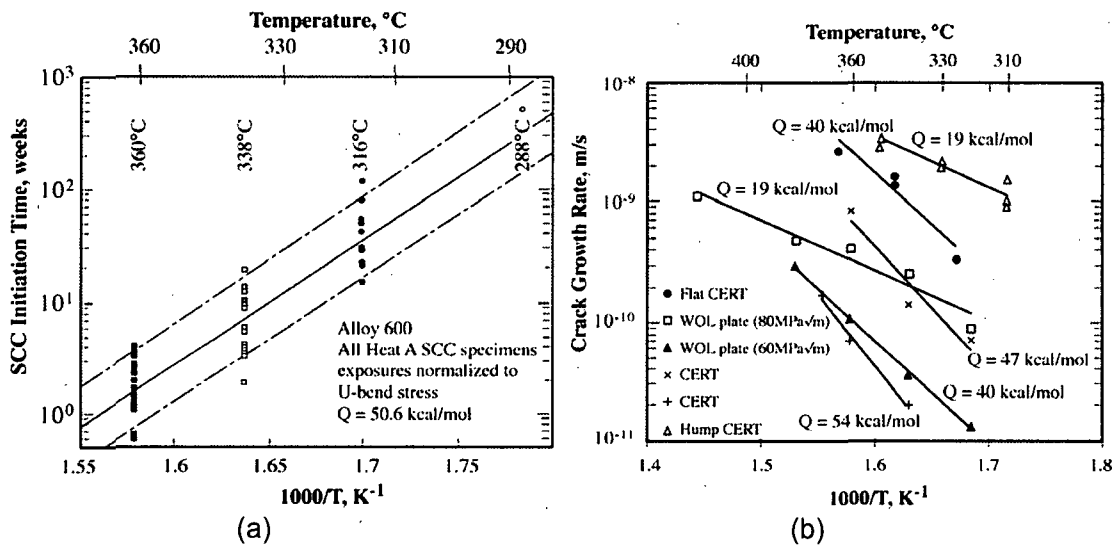
The dependence of LPSCC on stress for Alloy 600MA has also been extensively investigated. Figure B.7.18 shows results from studies of the effects of stress on initiation and propagation, respectively, from Bandy and van Rooyen<sup>33</sup> and Scott.<sup>34</sup> In general, for initiation from smooth specimens the stress required is in the range of the annealed yield stress, with a stress exponent of about 4 as shown in Figure B.7.18a. For propagation, the correlation by Scott has been the most widely used and is shown in Figure B.7.18b.



**Fig. B.7.16** (a) Time-for-initiation vs. extent of grain boundary carbides. From Norring et al.<sup>25</sup> Reprinted with permission from TMS. (b) Relationship between structure and SCC susceptibility. From Gras<sup>29</sup> Reprinted with permission from TMS. Cattant et al.<sup>26</sup>; © 1992 American Nuclear Society. Saint-Paul et al.<sup>30</sup> Courtesy of EDF, and Garriga-Majo et al.<sup>31</sup> © NACE International 1994.

**Table B.7.2<sup>32</sup>** © NACE International 1977  
 Effect of Heat Treatment and Fabrication on Failure at 350°C in Demineralized and Deoxygenated Water. From Blanchet et al.

Metallurgical Condition	Alloy A Alloy 600, C = 0.063 w/o			Alloy B Alloy 600, C = 0.040 w/o			Alloy C Cr 17%, Ni 77%, C = 0.002 w/o	
	As-Received	As-Quenched	Sensitized	As-Received	As-Quenched	Sensitized	As-Received	Sensitized
Determination $\sigma_{max}$ at the outer fiber at 20°C (kg/mm <sup>2</sup> ) ( $\pm 15\%$ )	72	36	72	43	29	43	41	41
Samples cracked after:								
750 hours	0/6	0/3	0/3	0/3	0/2	0/2	6/7	0/5
1500 hours	6/6	0/3	0/3	0/3	0/2	0/2	7/7	3/5
2250 hours	-	0/3	0/3	1/3	0/2	0/2	-	5/5
3000 hours	-	0/3	0/3	2/3	0/2	0/2	-	-
4500 hours	-	1/3	0/3	2/3	0/2	0/2	-	-
8250 hours	-	1/3	0/3	3/3	0/2	0/2	-	-
10000 hours	-	2/3	0/3	-	1/2	0/2	-	-



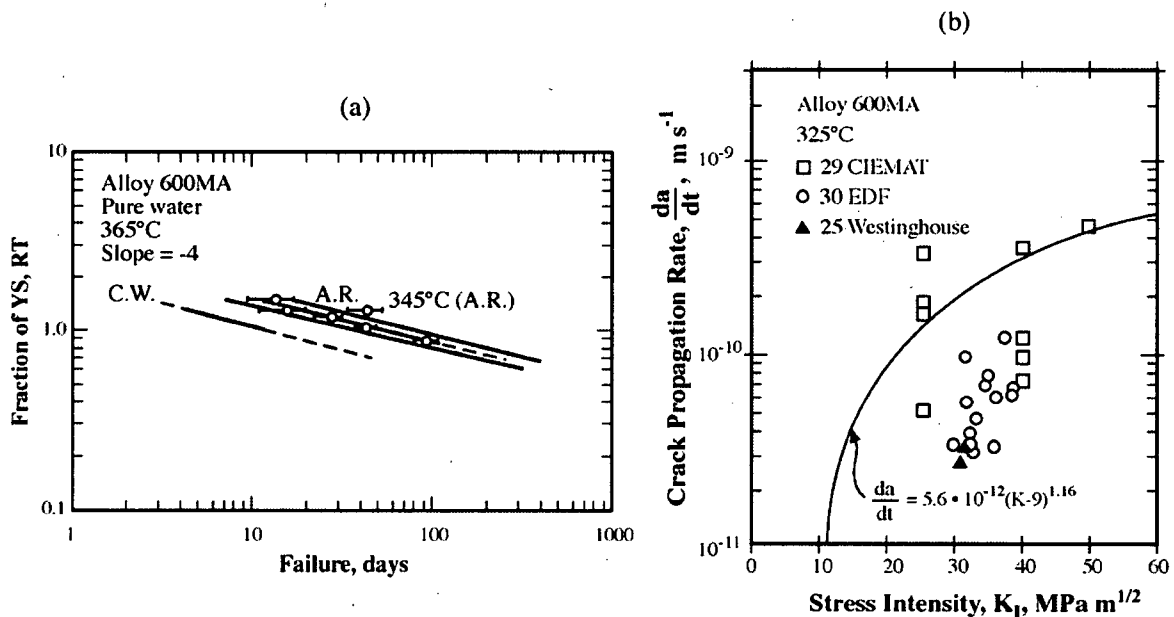
**Fig. B.7.17** (a) SCC initiation time vs. 1000/T for Alloy 600 using U-bend specimens in pure water. From Webb.<sup>27</sup> Reprinted with permission from TMS. (b) Crack growth rate vs. 1000/T for Alloy 600MA from six authors using CERT and WOL type specimens. From Cassagne et al.<sup>28</sup> Courtesy of the European Federation of Corrosion.

## SCC of Alloy 600MA on the OD

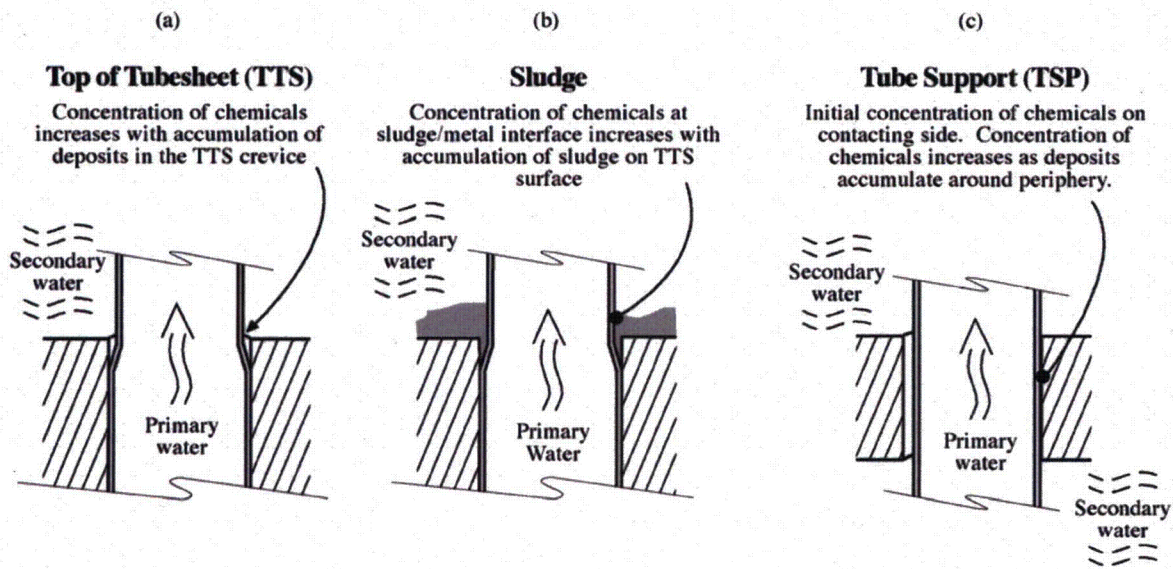
### 1. Geometry, phases, and chemistry

SCC on the OD of SG tubes occurs mainly at locations where impurity chemicals can concentrate due to the local superheat, mainly at tube supports and at the configurational and sludge crevices at the top of tubesheets, as shown in Figure B.7.19. Figure B.7.20<sup>35</sup> shows a schematic view of the complexity and chemistry of these regions of concentration as well the chemicals that typically concentrate and lead to SCC. With time, chemicals accumulate in the heat transfer crevices to produce solids and saturated solutions owing to the superheat. Further, as local transport is stifled by the formation of solids, a steam phase develops. The main intimation here is the complexity of chemical, electrochemical, and physical conditions. Such an array provides many different conditions that can produce corrosion and stress corrosion cracking.

SCC on the OD generally occurs where the superheat is the greatest, and this is mainly on the inlet or hot leg side with the number of affected tubes shown in Figure B.7.21a<sup>36</sup> according to distance from the inlet of the hot side. An indication of the magnitude of concentrations of chemicals in these crevices is given in Figure B.7.21b.<sup>37</sup>



**Fig. B.7.18** (a) Fraction of RT yield stress vs. time-to-failure for Alloy 600MA at 365°C in pure water. Stress exponent about -4. Yield point stresses in the range of 323 to 386 MPa. From Bandy and van Rooyen.<sup>33</sup> (b) Crack propagation rate vs. stress intensity for Alloy 600MA at 325°C. From Scott.<sup>34</sup> © NACE International 1996.



**Fig. B.7.19** Geometries that produce heat transfer crevices involving tubing in steam generators: (a) top of the tubesheet crevice; (b) sludge at the top of the tubesheet; (c) tube support. From Staehle and Gorman.<sup>1</sup> © NACE International 2003/2004.

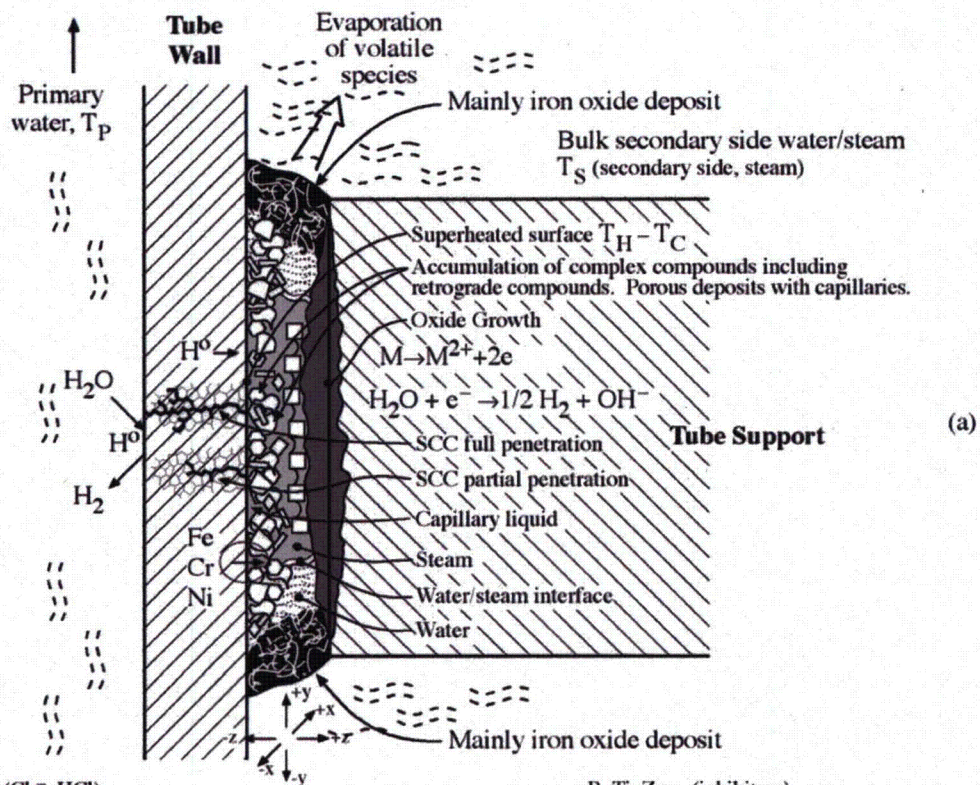
## 2. Surface chemistry--ODSCC is chemistry driven

Some indication of the complexity of the chemistries on the surfaces of tubes is shown in Figure B.7.22, taken from the work of Cattant et al.,<sup>38</sup> where the residual chemistry on the surface of a tube at a tube support region has been analyzed both inside the crevice and outside on the freespan adjacent to the crevice. Figure B.7.23<sup>38</sup> shows the ratio of species inside the crevice to outside on the freespan, indicating that the concentrations, species, and enrichments vary.

## 3. The bulk chemistry

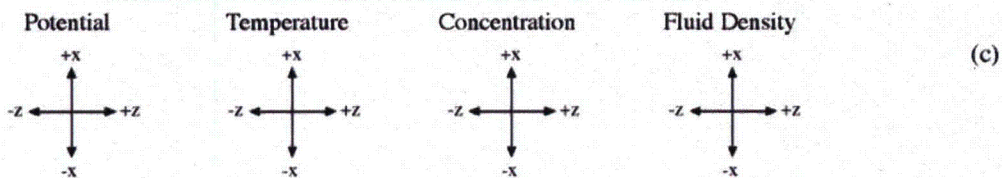
While the chemistries inside the heat transfer crevices provide a variety of possibly corrosive environments, the bulk environment provides important bounding chemistries affecting corrosion:

- a. **Low hydrogen**--The hydrogen concentration on the secondary side is in the range of 1 ppb due to the boiling action removing gases. This low concentration of hydrogen, following the Nernst equation, leads to raising the open circuit potential on the order of 200-250 mV above that on the primary side where there is not boiling and hydrogen is deliberately added at about 3 ppm. A 200-250 mV increase could be sufficient to take the secondary side out of the range of LPSCC.
- b. **Hydrazine (affects potential)**-- $N_2H_4$  is added to the secondary side in concentrations of about 5-100 ppb in order to reduce the oxygen concentration in the recirculating water to <5 ppb. It is also believed by some that additions of  $N_2H_4$  lower the tendency for corrosion to occur in heat transfer crevices. It may also lower the corrosion potential due to the relatively low equilibrium potential for the  $N_2/N_2H_4$  equilibrium. The overall combined effect of low hydrogen and the  $N_2H_4$  on potential is not clear.

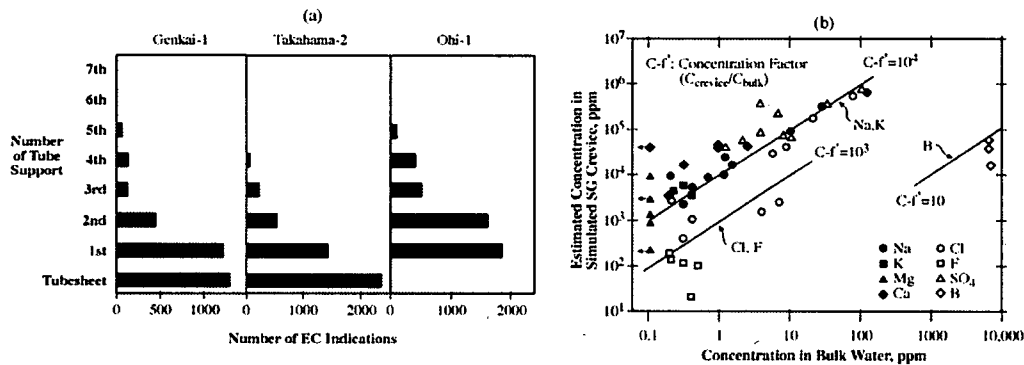


Cl	(Cl <sup>-</sup> , HCl)	B, Ti, Zn	(inhibitors)	(b)
SO <sub>x</sub>	(retrograde compounds plus S <sup>6+</sup> → S <sup>4+</sup> → S <sup>2+</sup> → S <sup>0</sup> → S <sup>2-</sup> )	O <sub>2</sub>	(O <sub>2</sub> , H <sub>2</sub> O, compounds)	
SiO <sub>x</sub>	(SiO <sub>2</sub> , complex compounds)	H <sub>2</sub>	(H <sub>2</sub> , H <sup>+</sup> , H <sup>o</sup> )	
AlO <sub>x</sub>	(Al <sub>2</sub> O <sub>3</sub> , complex compounds)	N <sub>2</sub> H <sub>4</sub>	(N <sub>2</sub> H <sub>4</sub> , NH <sub>3</sub> , N <sub>2</sub> )	
Cu	(Cu <sup>o</sup> , Cu <sup>2+</sup> , CuO)	C	(CO <sub>3</sub> <sup>2-</sup> , organic)	
Pb	(Pb <sup>o</sup> , PbO <sub>x</sub> <sup>±y</sup> )	N	(NO <sub>x</sub> , organic)	
Na, Ca, Mg	(complex compounds)	Fe, Cr, Ni	(Fe <sup>2+</sup> , Cr <sup>3+</sup> , Ni <sup>2+</sup> , complex compounds)	
Na <sub>2</sub> HPO <sub>4</sub>	(retrograde compounds plus H <sub>3</sub> PO <sub>4</sub> )			

#### Gradients



**Fig. B.7.20** Schematic view of heat transfer crevice at a tube support. (a) Geometry. (b) Chemicals that accumulate and transform. (c) Types of gradients inside the heat transfer crevice. From Staehle.<sup>35</sup>



**Fig. B.7.21** (a) Number of indications at successive tube support locations for three plants using Alloy 600MA after about 12 to 15 years service. From Takamatsu et al.<sup>36</sup> © NACE International 1996. (b) Estimated concentration of species in a simulated SG crevice vs. concentration in the bulk water. Various concentration factors shown. From Takamatsu et al.<sup>37</sup> © 1992 American Nuclear Society.

c. Hydrazine (a reductant)--  $N_2H_4$  produces a second effect as it combines with sulfate impurities reducing them to lower valence and ultimately to sulfides. Sulfides are well known to accelerate the entry of hydrogen and to reduce passivity.<sup>39,40,41</sup>

Thus, there are two important environmental influences that affect the occurrence of corrosion on the secondary side. One is the concentration of chemistry inside heat transfer crevices and the other involves the combined effects of low hydrogen and high hydrazine as they interact with the bulk and the crevice chemicals.

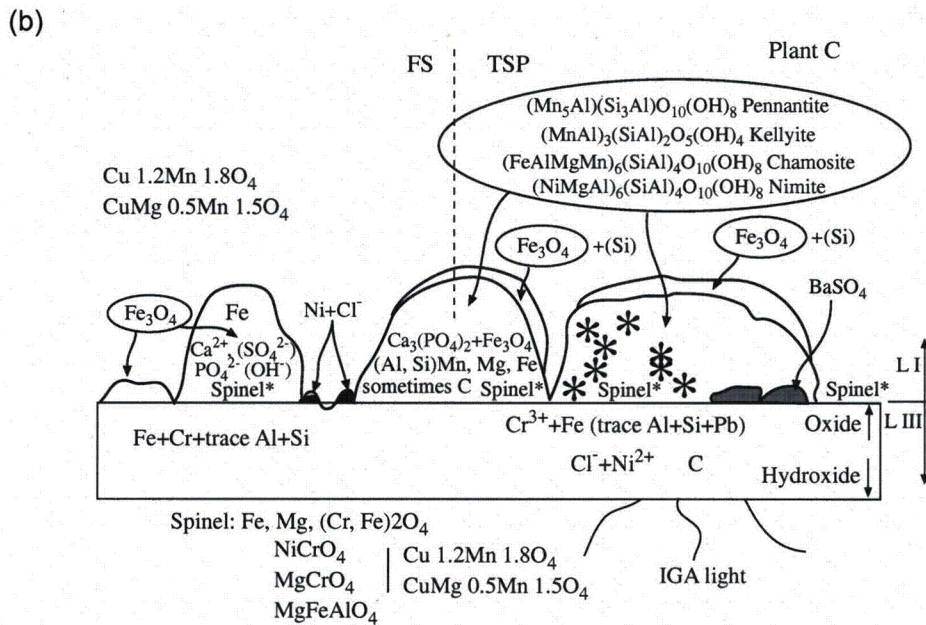
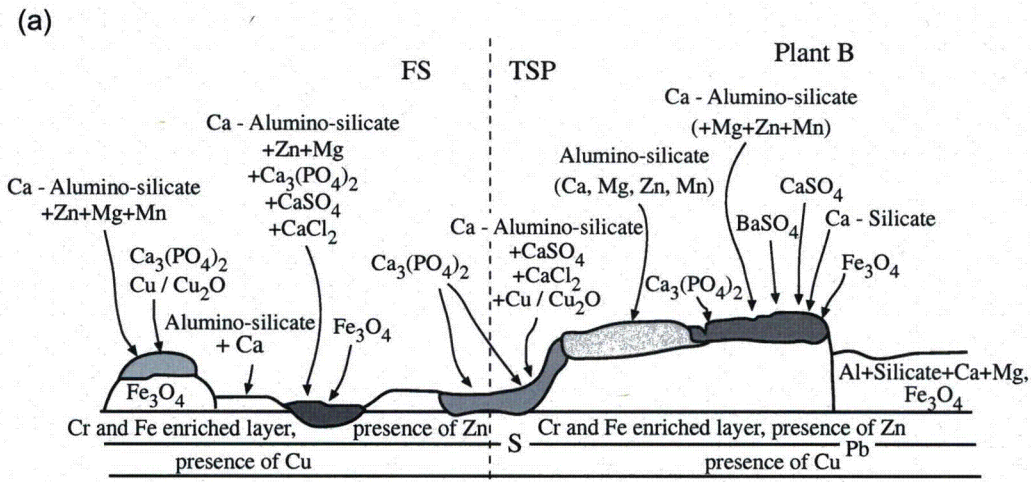
#### 4. Steam phase

Figure B.7.20 suggests that, in addition to the complexity of chemistry, there is also a steam phase in heat transfer crevices. Such local steam conditions and the associated two phase interface have been shown to accelerate SCC in Alloy 600 as reviewed by Staehle and Gorman.<sup>1</sup>

#### 5. Acidic and alkaline chemistries

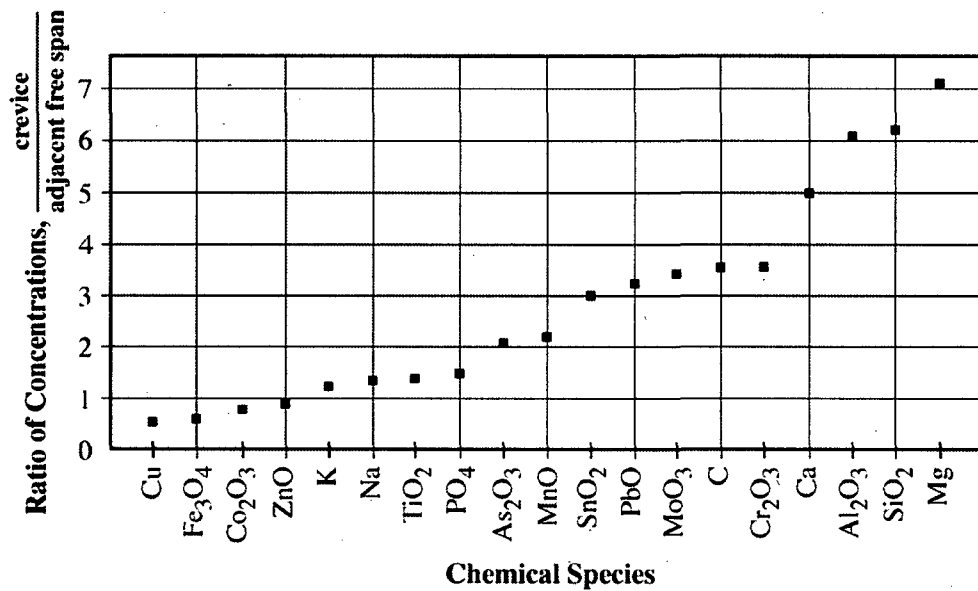
Aside from the LPSCC on the primary side as discussed in Section 2.2 and the possibility of its occurring on the secondary side, both acidic and alkaline environments have been investigated as being possibly related to the SCC that has occurred in the secondary side. The overall view of AcSCC and AkSCC for Alloy 600MA is shown in Figure B.7.9a as well as in Figure B.7.10a.

Figures B.7.24a<sup>42</sup> and 24b<sup>43</sup> show the effect of electrochemical potential on SCC in alkaline environments specifically for Alloys 600MA, 600TT and 690TT. Here, it is clear that the three alloys sustain AkSCC in the same range of potential with Alloys 600TT and 690TT being more resistant. Staehle and Gorman<sup>1</sup> discuss AkSCC and its dependencies extensively.

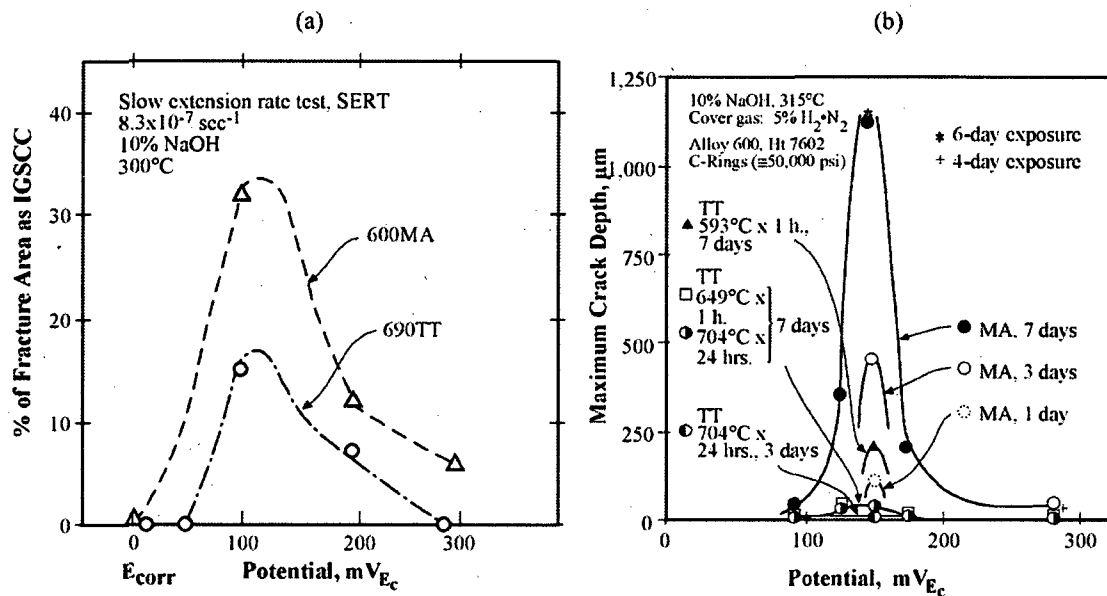


**Fig. B.7.22** (a) Schematic view of the OD of a tube near a TSP showing adjacent regions from inside the TSP and outside on the free surface. The condenser was brass and the water chemistry was morpholine AVT. (b) Schematic view of OD tube surface from TSP 2 showing adjacent regions inside the TSP and outside on the free surface. The condenser was titanium and the water conditioning was NH<sub>3</sub> AVT. The tube was examined after 79,900 hours. From Cattant et al.<sup>38</sup> Courtesy of EDF & Framatome-ANP.





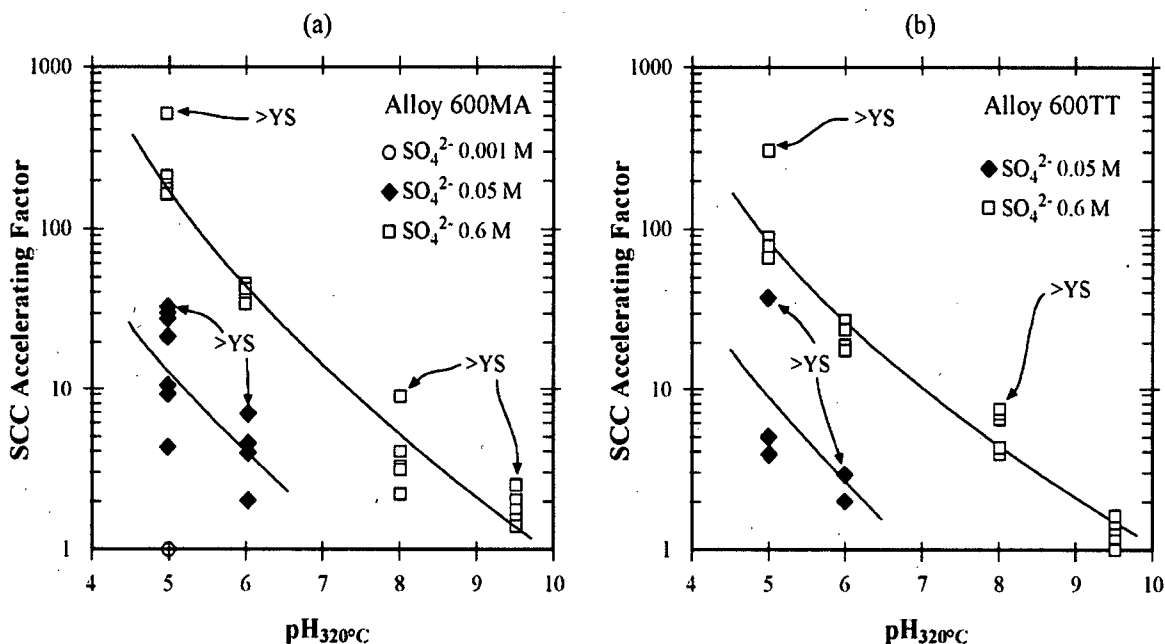
**Fig. B.7.23** Ratio of concentrations of elemental species in deposits from occluded heat transfer crevices vs. those from adjacent free-span surfaces. Species given in ascending order of ratio. Data from 340 pulled tubes. From Cattant et al.<sup>38</sup> Courtesy of EDF & Framatome-ANP.



**Fig. B.7.24** Dependence of IGSCC on applied potential above the deaerated open circuit potential. (a) Percent of fracture area as IGSCC for Alloy 600MA and Alloy 690TT at 300°C as a function of potential in a 10% NaOH solution. From Suzuki.<sup>42</sup> © 1992 American Nuclear Society. (b) Maximum crack depth vs. potential for Alloy 600 exposed in 10% NaOH at 315°C for mill-annealed and various thermal treatments. From Pessall.<sup>43</sup> Reprinted with permission from Elsevier.

Figures B.7.25 and 26 provide insights into AcSCC for Alloys 600MA, 600TT and 690TT and conform also to the patterns noted in Figures B.7.9 and 10. Figure B.7.25<sup>44</sup> shows that the propensity towards AcSCC, when exposed to sulfate anions, decreases with increasing pH, and as expected, continues into the slightly alkaline region for both Alloys 600MA and 600TT.

Figure B.7.26<sup>49</sup> shows the effect of potential on the AcSCC of Alloys 600MA and 690TT also exposed to sulfate anions. Here, the potentials are achieved by adding cupric oxide and by changing the hydrogen concentration. Note in Figure B.7.26c, simply adding copper does not produce significant SCC relative to the CuO. This Figure shows that Alloy 690TT sustains AcSCC but not at normal open circuit potentials; whereas, Alloy 600MA sustains AcSCC regardless of the potentials, although there is an acceleration at pH 4+ at higher potentials.



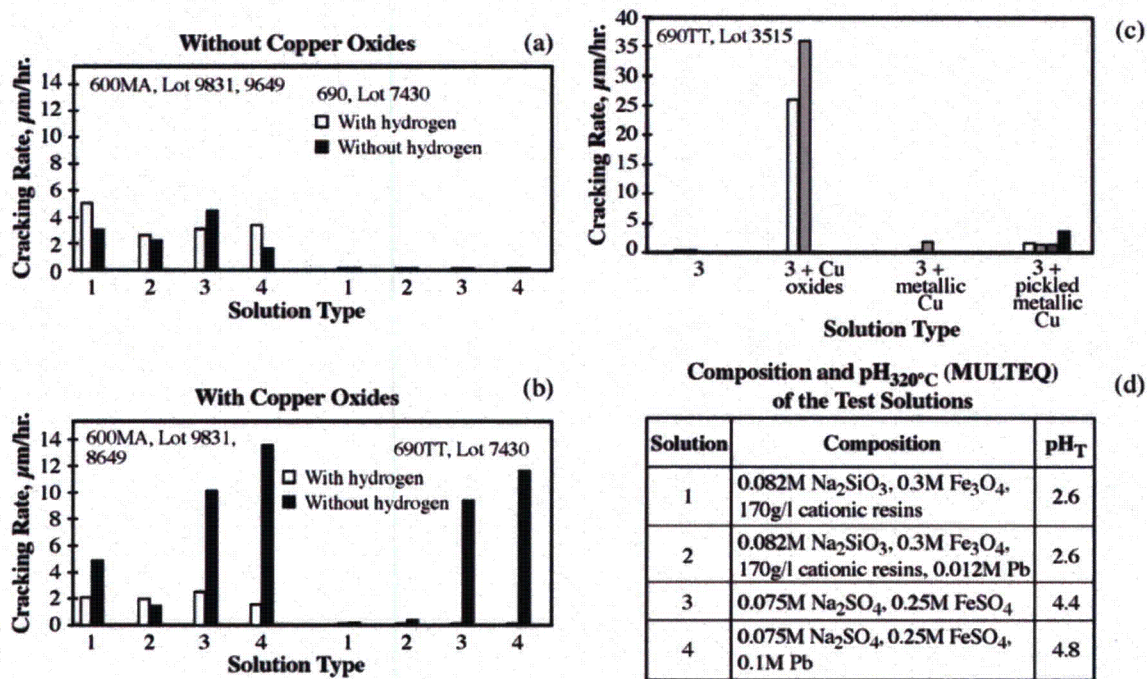
**Fig. B.7.25** SCC accelerating factor vs. pH with different concentrations of SO<sub>4</sub><sup>2-</sup> and with different stresses for (a) Alloy 600MA and (b) Alloy 600TT. Accelerating factor taken from rate of crack initiation at 0.001M (pH<sub>320°C</sub> = 5) being the reference. >YS refers to "two legs touching" condition of the branches of the C-ring; below this stress, specimens were stressed at 0.8 YS and 1.0 YS. From deBouvier et al.<sup>44</sup> Reprinted with permission from TMS.

## 6. Lead chemistries, PbSCC

PbSCC has had varying importance over time. It was first identified as important in the 1965 paper of Copson and Dean<sup>45</sup> and was suggested then as the reason for the SCC observed by Coriou. In this first paper, SCC due to Pb was said to be characteristically TGSCC; since most of the subsequent field observations of SCC exhibited IGSCC, Pb was not considered important, and ODSCC was mainly attributed to AkSCC and to AcSCC.

However, due to the review of Sarver<sup>46</sup> of old work of Copson, it became clear that PbSCC of Alloy 600MA was predominantly IGSCC; whereas, PbSCC of Alloy 600TT, SR (stress relieved), and SN (sensitized) was predominantly TGSCC. This evolution is described by Staehle.<sup>47</sup> Also important are the results from Bruemmer and Thomas,<sup>48</sup> who have shown that as much as 7w/o of Pb occurs in the tips of some SCC taken from SGs. Further, Pb has been observed to concentrate on heat transfer surfaces in many examinations of pulled tubes even where no accidental intrusions of Pb have occurred.

While the proof is not substantial, it is a reasonable speculation that much of the IGSCC on the secondary side, especially after the early concerns about AkSCC and AkIGC, could have been due to Pb.



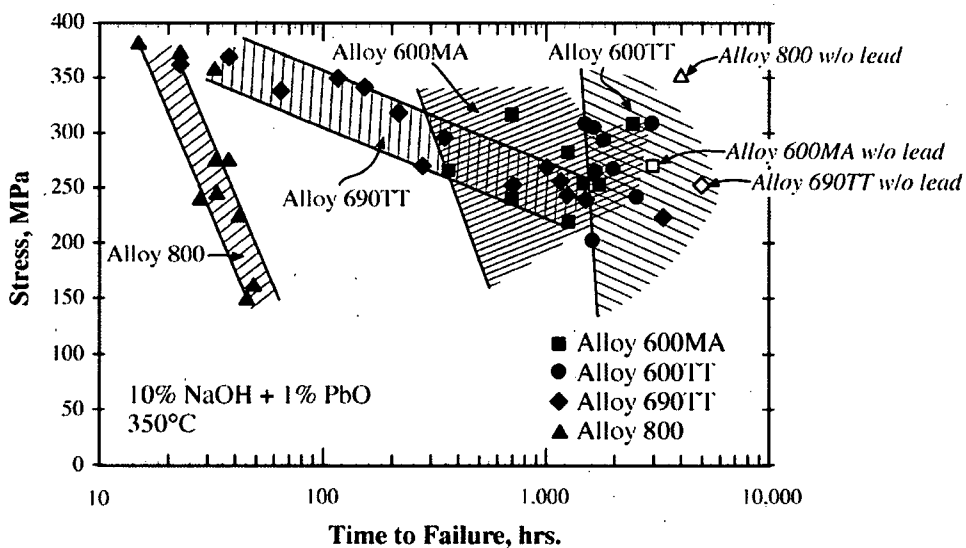
**Fig. B.7.26** (a) Cracking rates for Alloys 600MA and 690TT in acidic solutions without copper oxides with and without 5% H<sub>2</sub> added to argon cover gas in capsules at 320°C. (b) Cracking rates for Alloys 600MA and 690TT in acidic solutions with copper oxides with and without 5% H<sub>2</sub> added to argon cover gas in capsules at 320°C. (c) Cracking rates obtained for Alloy 690TT with solution #3 at 320°C. (d) Compositions of environments. From Pierson and Laire.<sup>49</sup> Courtesy of Laborelec.

The occurrences of PbSCC over the range of pH are shown in Figures B.7.27, 28, and 29. Figure 27<sup>51,52</sup> shows the four alloys in an alkaline solution with and without the presence of Pb. The Pb substantially accelerates the propensity for SCC especially for Alloys 800 and 690TT. At lower pH, which is characteristic of AVT environments, Wright and Mirzai<sup>50</sup> have summarized the results from various authors as a function of Pb concentration as shown in Figure B.7.28. SCC occurs in Alloy 600MA as a function of Pb readily at 1 ppm. However, PbSCC does not seem to occur in Alloy 690TT in this AVT environment. At lower pH in chloride, PbSCC occurs in both Alloys 600MA and 690TT; however, the rate of SCC in Alloy 690TT is lower. At this

lower pH of 4.5 and at 300 ppm Pb, as  $PbCl_2$ , the Alloy 690 sustains SCC and corrodes generally.

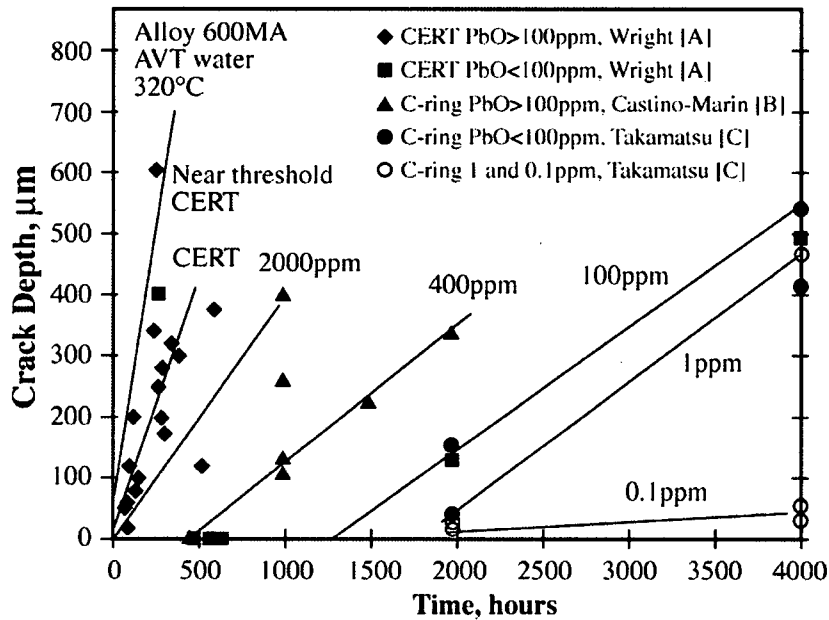
### 7. Low valence sulfur chemistries

Low valences of sulfur-containing anions are important because they can greatly accelerate SCC, at least as shown in the limited work performed to date in alkaline solutions, and because these ions can be produced by the reduction of sulfate ions with hydrazine. Further, from studies at lower temperatures, the lower valence sulfur ions greatly accelerate general corrosion. In particular, the low valence sulfur species accelerate the AkSCC of Alloy 690.

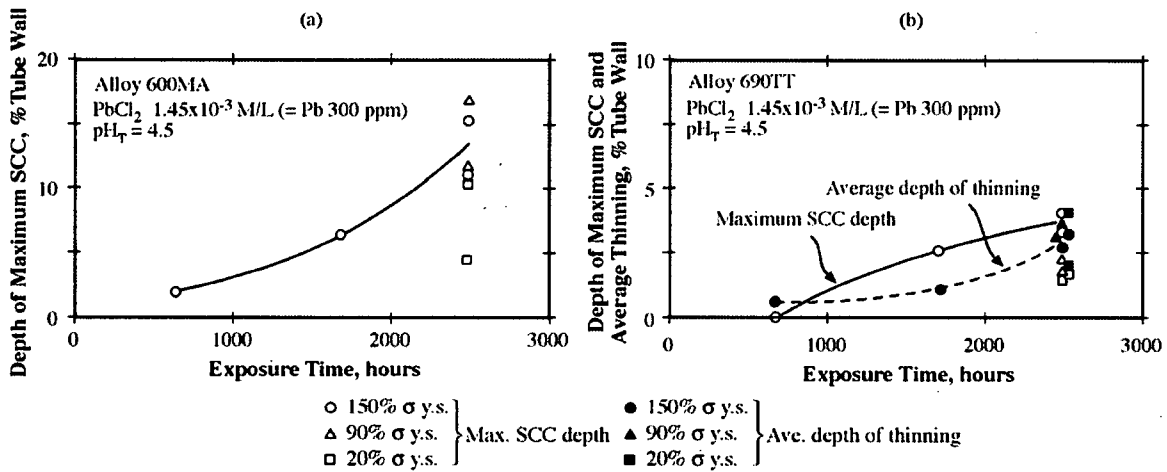


**Fig. B.7.27** Stress vs. time-to-failure of Alloys 600MA and 600TT (two tubes), 690TT (four tubes), and 800 (two tubes) in 10% NaOH + 1% PbO at 350° C. From Vaillant et al.<sup>51</sup> Courtesy of the European Federation of Corrosion. and Rocher et al.<sup>52</sup> Courtesy of EDF & CEA.

Table B.7.3 compares concentrated alkaline solutions with various additions of CuO, PbO,  $S_2O_3^{2-}$ , and  $NaSO_4+FeSO_4$ .



**Fig. B.7.28** Crack depth vs. time data for Alloy 600MA in AVT water at 320°C with various concentrations of PbO. From Wright and Mirzai.<sup>50</sup> Reprinted with permission from TMS. With data from [A] Wright;<sup>53</sup> Reprinted with permission from BNES. [B] Castano-Marín et al.,<sup>54</sup> [C] and Takamatsu et al.<sup>55</sup> © 1997 American Nuclear Society.



**Fig. B.7.29** Depth vs. time for PbSCC at pH<sub>340°C</sub> 4.5 in which various stresses were applied for 2500 hour exposure in water where O<sub>2</sub> < 5 ppb and Pb was added as PbCl<sub>2</sub>. From Sakai et al.<sup>56</sup> © 1992 American Nuclear Society. (a) Alloy 600MA at 1.45 x 10<sup>-3</sup> M/L of PbCl<sub>2</sub>. (b) Alloy 690TT at 1.45 x 10<sup>-3</sup> M/L of PbCl<sub>2</sub>. Maximum SCC depth plus average depth of GC.

**Table B.7.3** Results from Visual Examination of Specimens Exposed\* to Alkaline Solutions at 350°C with Added Species (cracked samples/tested samples). From Briceno and Castano.<sup>57</sup> Used by Permission of EPRI.

Material	10% NaOH	10% NaOH + 0.1M CuO	10% NaOH + 0.1 M PbO	50% NaOH + 5% Na <sub>2</sub> S <sub>2</sub> O <sub>3</sub>	0.75% M Na <sub>2</sub> SO <sub>4</sub> + 0.25% M FeSO <sub>4</sub>	0.75% M Na <sub>2</sub> SO <sub>4</sub> + 0.25% M FeSO <sub>4</sub>
Alloy 800 7-73243	3/3	3/3	4/4	4/4	4/4	0/4 (3/4)**
Alloy 800SP 81373	15/15	15/15	15/15	15/15	15/15	11/15 (15/15)**
Alloy 690TT WF816T	0/15	0/15	15/15	14/14	0/15	1/15
Alloy 690TT 764408	0/15	0/15	15/15	15/15	0/15	0/15
Alloy 600MA 1450	8/9	0/9 (2/9)**	0/9 (3/9)**	2/9	6/9 (8/9)**	9/9

\* 500 hours exposure; C-ring specimens; 2% strain.

\*\* Visual examination after bending the samples.

**Table B.7.4** Results of Cathodic Polarization Scans in 50% NaOH with 5% Additions at 316°C. Courtesy of P. King.<sup>58</sup> Private communication.

5% Addition	Alloy 600		Alloy 690	
	Worst Case	Observations	Worst Case	Observations
Na <sub>2</sub> CO <sub>3</sub>	No difference*	General attack	No difference*	Slight g.b. intrusions
Na <sub>2</sub> S	TT ring	Heavy general attack	MA C-ring	TGSCC
NaHS	No difference	Heavy general attack	MA C-ring	TGSCC
Na <sub>2</sub> S <sub>2</sub> O <sub>3</sub>	No difference	Heavy general attack	MA C-ring	TGSCC
Na <sub>2</sub> SO <sub>4</sub>	No difference	Slight general attack	MA C-ring	Slight g.b. intrusions

\* No difference indicates no substantial difference between ring or C-ring specimens for mill-annealed and thermally-treated condition.

MA - Heat treatment not defined

TT - Mill annealed plus 704°C /16 hrs

TGSCC - Transgranular stress corrosion cracks



In addition to this work directly from operating plants, Figure B.7.31 from the work of Jacko<sup>59</sup> shows that Alloy 600TT is improved relative to Alloy 600MA in about the same proportions as the results in Figure B.7.30. Here, Alloy 690 exhibits no LPSCC.

## 2. Alkaline as AkSCC

In alkaline solutions the propensity for AkSCC in Alloy 600TT is less than Alloy 600MA as shown in Figures B.7.10b and 10d. Figure B.7.32<sup>7</sup> shows that the plateau crack velocity of Alloy 600TT is a 5-10 times less than for Alloy 600MA in 4 and 100 g/l NaOH solutions.

## 3. Acidic as AcSCC

Depending on the data, Alloy 600TT exhibits improvements compared to Alloy 600MA. Figure B.7.33<sup>61</sup> shows significant improvements over a range of acidic pH in sulfate solutions.

## 4. Lead

The work of Miglin and Sarver,<sup>60</sup> which covered a broad range of pH with Pb additions, showed that Alloy 600TT was generally, but not substantially, improved over Alloy 600MA.

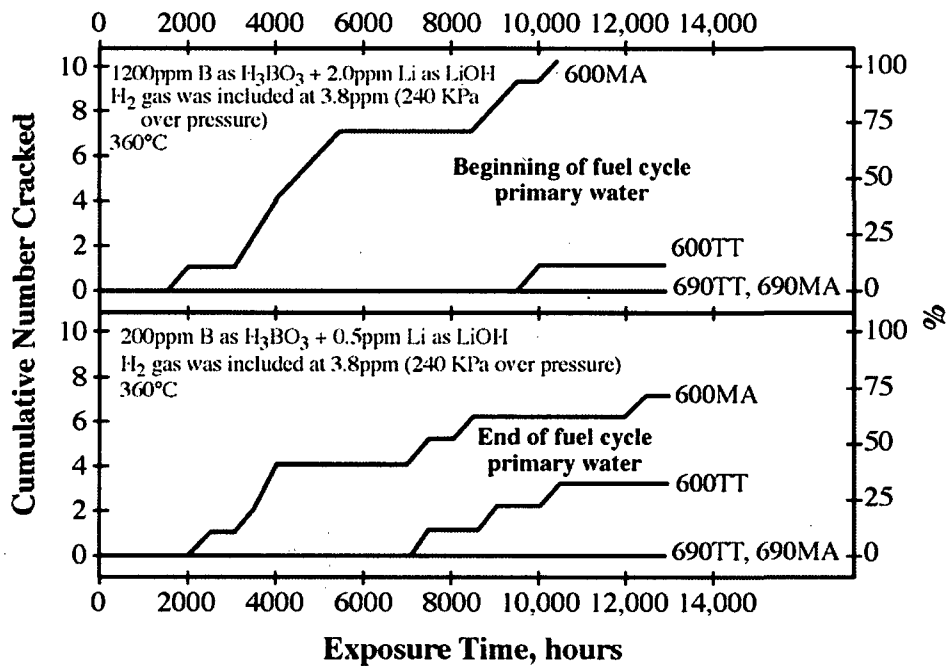


Fig. B.7.31 Cumulative number of Alloy 600 and 690 specimens exposed for 13,000 hours in chemistries typical of the (a) beginning of life and (b) end of life for a fuel cycle. From Jacko.<sup>59</sup> Used by Permission of EPRI.



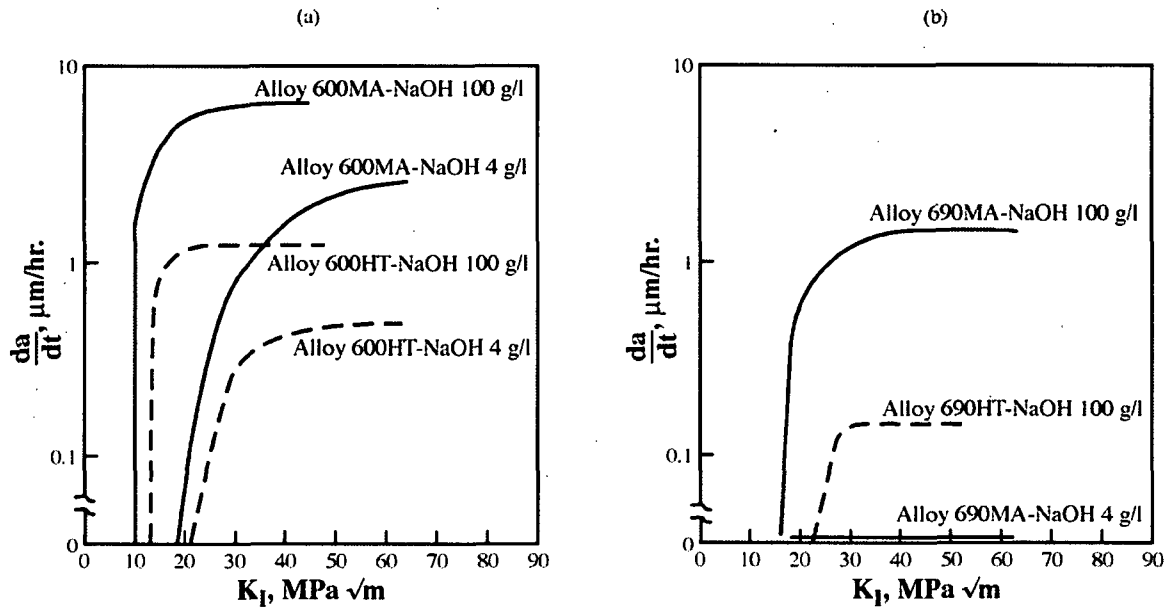


Fig. B.7.32  $da/dt$  vs.  $K$  for Alloys 600 (a) and 690 (b) exposed to various concentrations of NaOH at 350°C with a WOL type specimen. HT corresponds to 700°C for 16 h. From Berge and Donati.<sup>7</sup> © 1981 American Nuclear Society.

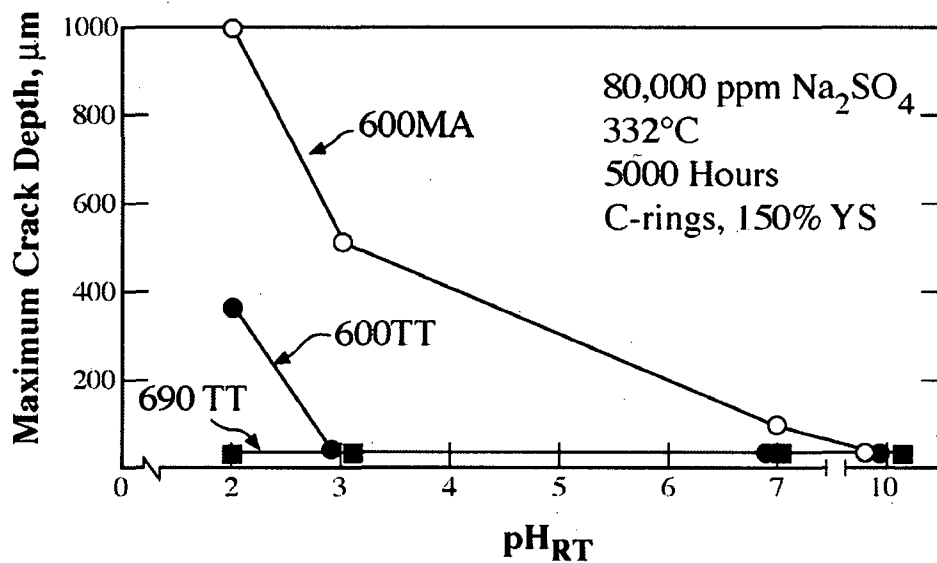
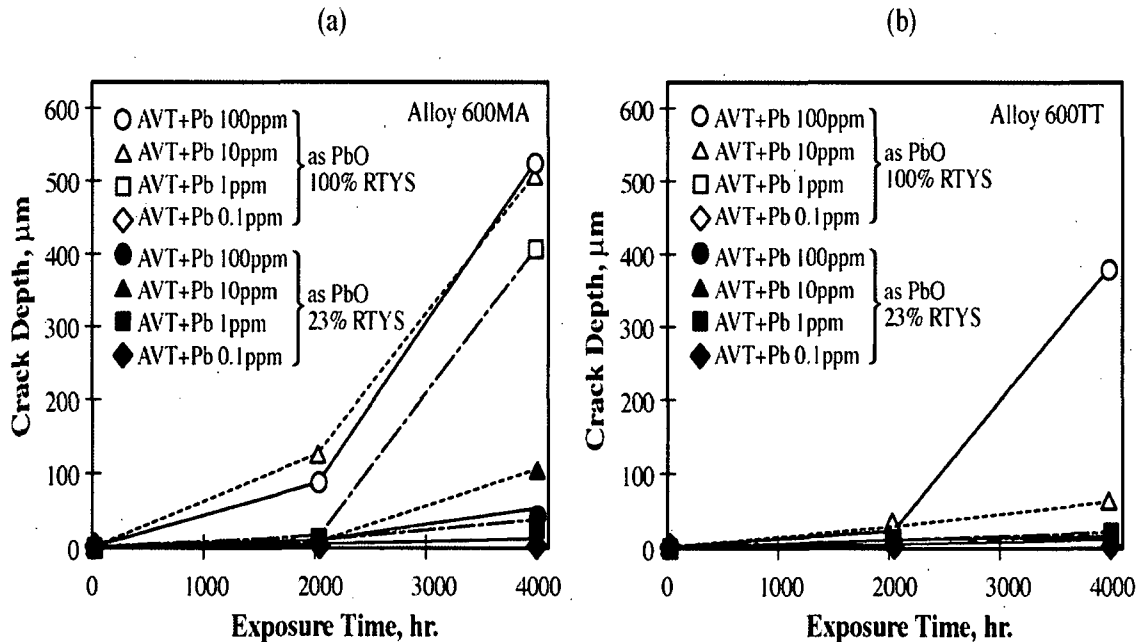


Fig. B.7.33 Maximum crack depth vs. room temperature pH for Alloy 600MA, Alloy 600TT, and Alloy 690TT exposed in acidic sulfate solutions at 332°C for 5000 hours as C-rings stressed to 150% of the yield strength. From Smith et al.<sup>61</sup> © 1986 American Nuclear Society.

Figure B.7.27 shows that Alloy 600TT is improved relative to Alloy 600MA possibly by a factor of five in time-to-failure, but there are no significant differences in the stress threshold.

In AVT environments, as shown in Figure B.7.34,<sup>55</sup> Alloy 600TT is improved, compared to Alloy 600MA, and does not support SCC at such low concentrations of Pb. However, Alloy 600TT is not significantly better at higher concentrations.



**Fig. B.7.34** Crack depth vs. time for various concentrations of Pb at two stresses and for Alloys 600MA and 600TT in deaerated AVT water containing 0.26 ppm  $\text{NH}_3$ +0.1ppm  $\text{N}_2\text{H}_4$ . From Takamatsu et al.<sup>55</sup> © 1997 American Nuclear Society.

## 5. Sulfur

There appear to be no data for the SCC of Alloy 600TT in solutions which contain low valence sulfur.

## Alloy 690 TT

As it became clear that Alloy 600 would undergo degradation and cracking during the service life of steam generators, work had begun, at least by 1970, to develop an improved alloy as reported by Copson et al.<sup>62</sup> and Flint and Weldon.<sup>63</sup> This work involved evaluating alloys in three environments: highly oxygenated environments with double U-bend crevices, lead environments, and alkaline environments. Sensitized and non-sensitized alloys were studied, and a relatively large range of iron and chromium additions to a nickel base were evaluated.

Alloy 690TT is now becoming the standard material for use in SG tubing, where it has so far provided excellent service performance, as well as for welding and for thick sections where substantial corrosion resistance, together with compatibility of the thermal expansion coefficient with adjacent low alloy steel components, is required, as shown in Figure B.7.5.

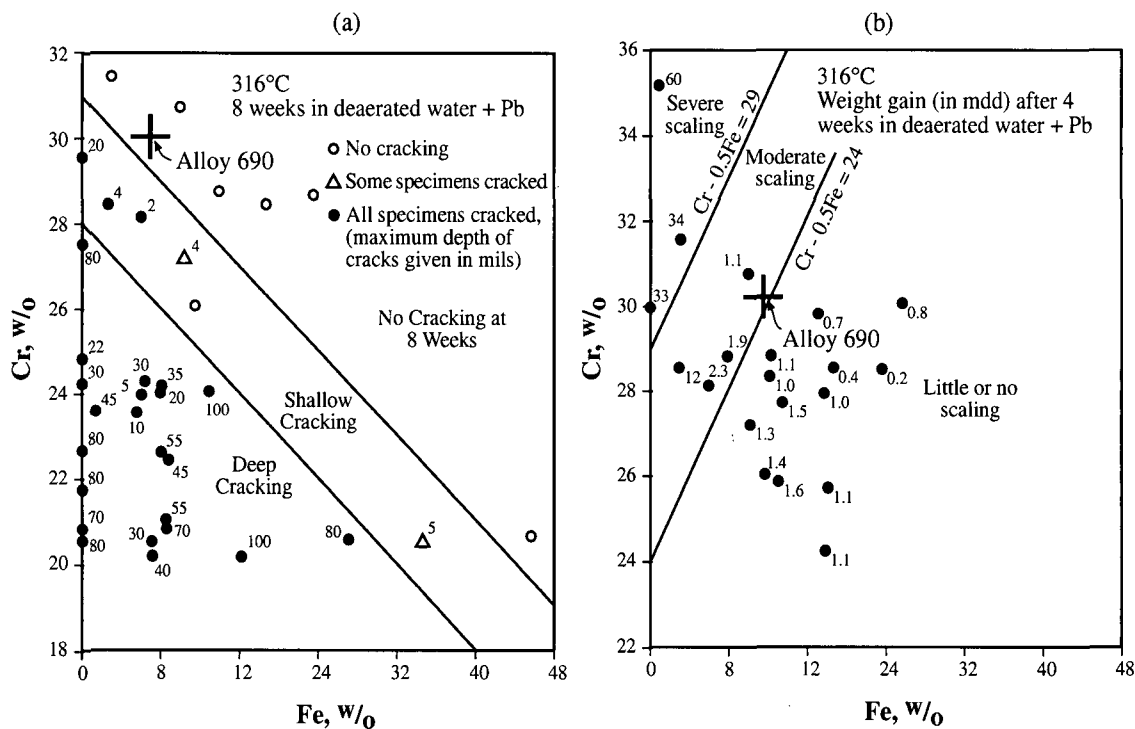
From these early tests, the highly oxygenated solutions were not particularly useful from the point of view of PWR applications, except perhaps for the unknown conditions inside crevices.

However, the testing in the Pb-containing solutions proved to be of great interest in later years as shown in Figure B.7.35.<sup>46</sup>

Figure B.7.35 shows the combined effects of iron and nickel both on the SCC and scaling of alloys exposed to high temperature water containing Pb. Both figures show the locations of the Alloy 690 composition. These results showed that Alloy 690 composition is close to a scaling condition (severe general corrosion) and to SCC in Pb environments. Regardless, the Alloy 690 composition seemed to be an optimum as shown in Figure B.7.35, and the testing in the Pb-containing solutions foresaw, unintentionally, the importance of Pb on the secondary side. In the following years development of these high chromium alloys continued and intensified in the late 1970s and early 1980s.

### 1. Primary water as LPSCC

The improvement of Alloy 690TT over Alloy 600MA, as well as over Alloy 600TT, is shown in Figure B.7.31 where laboratory testing was carried out for about 13,000 hours at 360°C.



**Fig. B.7.35** (a) Maximum depth of SCC of Ni-Cr-Fe alloys after 8 weeks in deaerated water plus Pb at 316°C. (b) Weight gain of Ni-Cr-Fe alloys after 4 weeks in deaerated water plus Pb. From Sarver et al.<sup>46</sup> Used by Permission of EPRI.

### 2. Alkaline as AkSCC

Figure B.7.32 for crack growth rate vs. stress intensity shows that the plateau velocity for Alloy 690 is a factor of 10-100 less than for Alloy 600MA depending on the concentration of NaOH.

The overall mapping of SCC for the three alloys of 600MA, 600TT, and 690TT in Figure B.7.10 shows that Alloy 690TT is improved and the threshold of pH for the onset of AkSCC is higher.

### 3. Acidic as AcSCC

Figure B.7.26 shows that Alloy 690TT at open circuit in sulfate solutions does not sustain AcSCC. This is similar to the pattern for Figure B.7.10. However, with Figure B.7.26 it appears that Alloy 690TT does sustain significant AcSCC, but at potentials that may exceed the normal open circuit range depending on what potentials are actually present in crevices and that results from the very low hydrogen on the secondary side.

### 4. Lead as PbSCC

The extensive work of Miglin and Sarver, which is discussed by Staehle and Gorman<sup>1</sup> and by Staehle,<sup>35</sup> shows that Alloy 690 is improved, in terms of resistance to PbSCC, over both Alloy 600MA and Alloy 600TT until pH 9.9 is reached, at which point the SCC of Alloy 690TT is significant, especially in steam (implying easy vapor phase transport of Pb). Figure B.7.27 reflects this greatly increased sensitivity of Alloy 690 in alkaline solutions.

While Figure B.7.26 shows that sulfates seem to inhibit PbSCC of Alloy 690TT in acidic solutions, Figure B.7.29b shows the Pb as PbCl<sub>2</sub> promotes PbSCC, although at a rate about 1/5 that for Alloy 600MA.

### 5. Sulfur as S<sup>y</sup>SCC

Tables B.7.3 and 4 show that the presence of low valence sulfur either as a -2 (sulfide) or +2 (thiosulfate) increases the susceptibility to S<sup>y</sup>SCC for Alloy 690TT relative to Alloy 600MA.

## **Alloy 800**

Figure B.7.4 from Coriou et al.<sup>13</sup> based on the general trends of his observations, suggests that the composition of Alloy 800 as shown in Figure B.7.2 and Table B.7.1 would resist SCC in both pure water and chloride-containing water, although Copson and Cheng's work in Figure B.7.3 suggests that Alloy 800 is within the domain of chloride SCC. Such SCC of commercial grade Alloy 800 in chloride solutions was also observed by Staehle et al.<sup>64</sup> for commercially available materials at the time.

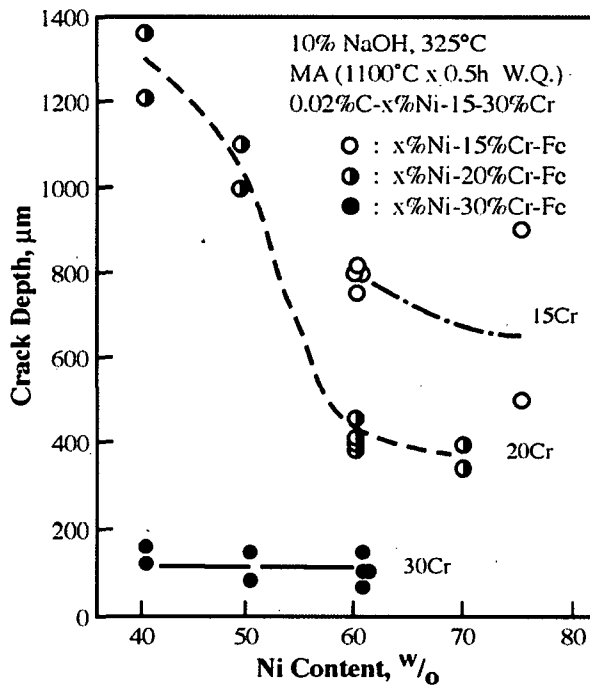
Mainly based on the work of Coriou plus internal work, Siemens chose a controlled version of Alloy 800 for their steam generators, and this alloy has exhibited excellent in-service performance.

### 1. Primary water as LPSCC

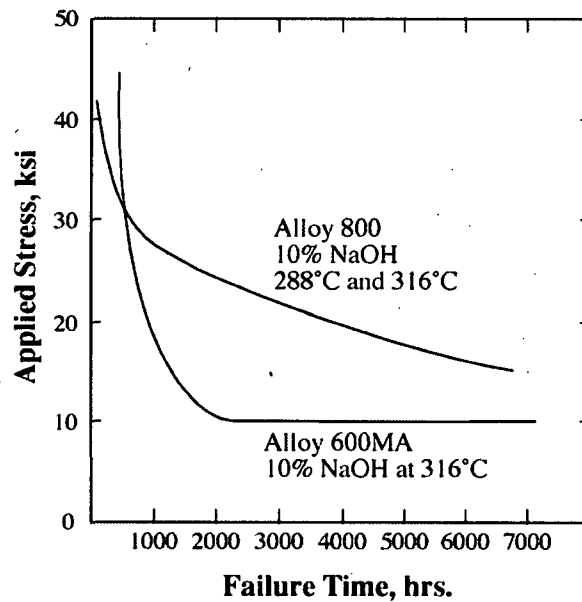
The dependence of LPSCC on nickel concentration was reported by Coriou et al.<sup>65</sup> They showed that the nickel concentration of Alloy 800 was below the Ni concentration that would permit LPSCC. Later Nagano et al.<sup>66</sup> showed that Alloy 800 was equivalent to Alloy 690 as shown in Figure B.7.36.

Since the first observation of Coriou in his schematic assessment in Figure B.7.4, Alloy 800 has remained resistant to LPSCC.

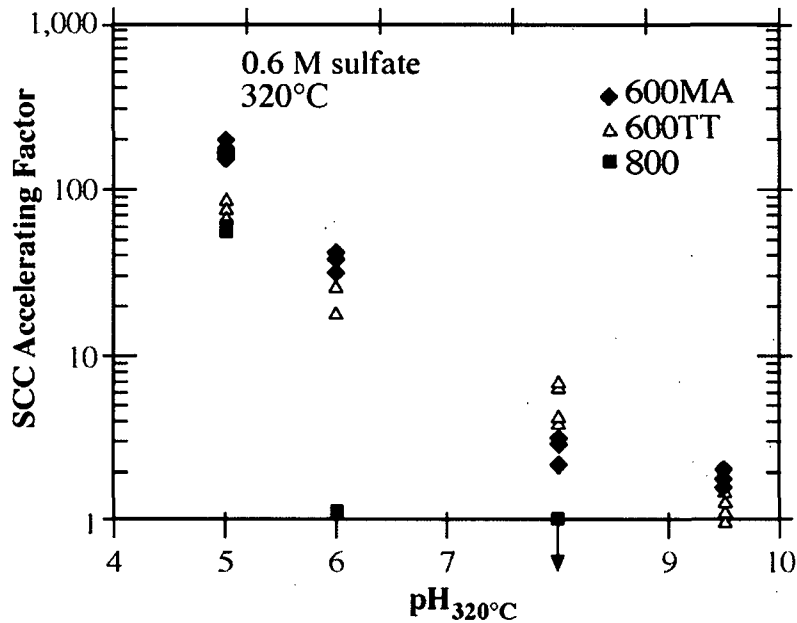




**Fig. B.7.37** Crack depth vs. Ni concentration for Ni-Cr-Fe alloys + 0.02%C exposed in a deaerated 10% NaOH solution at 325°C for 200 hours as single U-bends. Specimens mill annealed. From Nagano et al.<sup>67</sup> Used by Permission of EPRI.



**Fig. B.7.38** Stress vs. time for Alloy 800 in 10% NaOH at 288 and 316°C, and for Alloy 600MA in 10% NaOH at 316°C. From Wilson et al.<sup>68</sup> © 1975 ANS.



**Fig. B.7.39** SCC accelerating factor vs. pH for three alloys in 0.6M sulfate environments at 320°C. Accelerating factor taken from the rate of crack initiation at 0.001M (pH<sub>320°C</sub> =5) being the reference. 150% YS refers to the “two legs touching” condition of the branches of the C-ring; below this stress, specimens were stressed at 0.8 YS and 1.0 YS. From deBouvier et al.<sup>44</sup> Reprinted with permission from TMS.

#### 4. Lead

Alloy 800 seems to be the least resistant of the Alloys 600MA, 600TT, 690TT and 800 in alkaline solutions containing Pb as shown in Figure B.7.27. Despite the relative trends, more recent electrochemical studies by Y. Lu of AECL have shown the standard SG Alloy 800 is generally resistant to PbSCC in alkaline solutions.<sup>69</sup>

#### 5. Sulfur

Table B.7.3 shows that Alloy 800 is similarly prone to SCC in S<sup>y-</sup> SCC (alkaline base) as Alloy 690 in alkaline solutions. There appear to be no other data for other ranges of pH for any of the alloys.

### **Conclusions**

1. The early choice of Alloy 600MA for tubing in PWR steam generators together with drilled hole tube supports, less pure secondary water chemistry, and relatively high residual stresses produced extensive failures of tubing leading to the eventual replacement of many steam generators tubed with Alloy 600MA. This choice of Alloy 600MA was based on a set of assumptions and laboratory testing that turned out not to be valid under the operating conditions of tubes in steam generators.

2. A set of mitigations has reduced, for the present, the rate of SCC on the primary and secondary sides of SG tubes associated with Alloy 600MA. These mitigations have included:

- Using better alloys including Alloy 600TT, Alloy 690TT, and Alloy 800.
- Using line contact tube supports and changing the materials of the tube supports to stainless steel.
- Improving the secondary water chemistry.
- Reducing residual stresses.
- Improved methods of inspection.

3. The potential for secondary-side degradation and cracking still exists:

- Pb and S impurities.
- Acidic crevices, especially with chloride.
- Longer time and significant accumulation of impurities in line contact tube supports.
- Denting and increased stresses at the top of the tubesheet.
- Possible large releases of sequestered lead resulting from subtle changes in water chemistry, perhaps due to a still further increase in purity of the boiler water.
- Nucleation of SCC at locations of dings, dents, and scratches.

### **Acknowledgements**

It is a pleasure to acknowledge Jeffrey Gorman of Dominion Engineering, Robin Jones of EPRI, Yucheng Lu of AECL, Al McIlree of EPRI, Peter Scott of Framatome, and Robert Tapping of AECL for their help in preparing this report. Also, I appreciate the many who contributed to the Staehle and Gorman reference. In my office I appreciate, as usual, the work of Julie Daugherty and John Iig.



## References for B.7

- <sup>1</sup> R.W. Staehle and J.A. Gorman, "Quantitative Assessment of Submodes of Stress Corrosion Cracking on the Secondary Side of Steam Generator Tubing in Pressurized Water Reactors," *Corrosion*, Part 1 Vol. 59 No. 11 November 2003, Part 2 Vol. 60 No. 1 January 2004, Part 3 Vol. 60 No. 2 February 2004, NACE, Houston, Texas.
- <sup>2</sup> The Shippingport Pressurized Water Reactor, prepared for the USAEC, Addison-Wesley Publishing Company, Inc., Reading, Massachusetts, 1958.
- <sup>3</sup> W.F. Brindley, L.R. Scharfstein, and M.A. Golik, "Chloride Stress Corrosion Testing of Type 347 Stainless Steel Steam Generator Tubing," Bettis Technical Review: Reactor Chemistry and Plant Materials, Vol. 1, No. 3, WAPD-BT-3, 1957.
- <sup>4</sup> L.R. Scharfstein and W. Brindley, "Chloride Stress Corrosion Cracking of Austenitic Stainless Steel – Effect of Temperature and pH," *Corrosion* 60, NACE, Houston, Texas, 1958.
- <sup>5</sup> J.W. Pugh and J.D. Nisbet, "A Study of the Iron Chromium Nickel Ternary System," *Journal of Metals* Vol. 188, p. 269, 1950.
- <sup>6</sup> H.R. Copson and C.F. Cheng, "Some Case Histories of Stress Corrosion Cracking of Austenitic Stainless Steels Associated with Chlorides," *Corrosion* Vol. 13, p. 397, 1957.
- <sup>7</sup> Ph. Berge and J.R. Donati, "Materials Requirements for Pressurized Water Reactor Steam Generator Tubing," *Nuclear Technology* Vol. 55, p. 88, 1981.
- <sup>8</sup> ASM Specialty Handbook, Stainless Steels, J.R. Davis, ed., ASM International, Materials Park, 1994.
- <sup>9</sup> "Guidelines for PWR Steam Generator Tubing Specifications and Repair; Volume 1: Specification for Alloy 600 Steam Generator Tubing," EPRI NP-6743, Electric Power Research Institute, 1991.
- <sup>10</sup> J.A. Gorman, "Guidelines for PWR Steam Generator Tubing Specifications and Repair, Volume 2, Revision 1: Guidelines for Procurement of Alloy 690 Steam Generator Tubing," EPRI TR-016743-V2R1, Electric Power Research Institute, 1999.
- <sup>11</sup> B. Stellwag, N. Wieling, and L. Stieding, "Corrosion Resistance of SG Tubing Materials Alloy 800 and Alloy 690 – A Comparative Study," Proceedings of the Second International Symposium on Environmental Degradation of Materials in Nuclear Power Systems – Water Reactors, J.T.A. Roberts, J.R. Weeks, and G.J. Theus, chair, American Nuclear Society, p. 301, 1986.
- <sup>12</sup> H. Coriou, et al., "Corrosion Fissurante Sous Contrainte De L'Inconel D'American Nuclear Society L'eau à Haute Température," Third Colloque De Métallurgie, North Holland Publishing Company, Amsterdam, p. 161, 1960.
- <sup>13</sup> H. Coriou, et al., "Influence of Carbon and Nickel Content on Stress Corrosion Cracking of Austenitic Stainless Alloys in Pure or Chlorinated Water at 350°C," Fundamental Aspects of Stress Corrosion Cracking; NACE-1, R.W. Staehle, A.J. Forty, and D. van Rooyen, eds., NACE, Houston, p. 352, 1969.

- <sup>14</sup> B.L. Dow, Jr., "Steam Generator Progress Report, Revision 14," EPRI TE-106365-R14, Electric Power Research Institute, 1999.
- <sup>15</sup> P.M. Scott and P. Combrade, "On the Mechanisms of Secondary Side PWR Steam Generator Tube Cracking," Proceedings of the Eighth International Symposium on Environmental Degradation of Materials in Nuclear Power Systems -Water Reactors, A.R. McIlree, chair., American Nuclear Society, 1997.
- <sup>16</sup> P. Combrade, et al., "About the Role of Surface Films on Alloy 600 Corrosion in High Temperature Deaerated Environments," Proceedings of the Third International Symposium on Environmental Degradation of Materials in Nuclear Power Systems – Water Reactors, G.J. Theus and J.R. Weeks, eds., TMS, Warrendale, Pennsylvania, 1988.
- <sup>17</sup> P. Combrade, "The Role of Surface Films on the Control of Alloy 600 Corrosion in PWR Reactors – No Results, a Few Comments, a Lot of Questions," Proceedings: Specialist Meeting on Environmental Degradation of Alloy 600; EPRI TR-104898, R.G. Ballinger, A.R. McIlree, and J.P.N. Paine, eds., Electric Power Research Institute, 1994.
- <sup>18</sup> I. Ohsaki, et al., "Study of the Improvement of Steam Generator Tubing and Tube Support Plate Materials," 2nd International Steam Generator and Heat Exchange Conference, D.E. Anderson, ed., Canadian Nuclear Society, 1994.
- <sup>19</sup> S. Tsujikawa and S. Yashima, "Results of Steam Generator Tubing Reliability Test," 2<sup>nd</sup> International Steam Generator and Heat Exchange Conference, D.E. Anderson, ed., Canadian Nuclear Society, 1994.
- <sup>20</sup> R. Varrin Jr., "Characterization of PWR Steam Generator Deposits," EPRI TR-106048, Electric Power Research Institute, 1996.
- <sup>21</sup> Proceedings of the 1987 Workshop on the Mechanism of Primary H<sub>2</sub>O IGSCC; NP-5987-SP, G. Economy, R.J. Jacko, J.A. Begley, and F.W. Pement, eds., Electric Power Research Institute, 1987.
- <sup>22</sup> D.S. Morton, S.A. Attanasio, and G. A. Young, "Primary Water SCC Understanding and Characterization Through Fundamental Testing in the Vicinity of the Nickel/Nickel Oxide Phase Transition," Proceedings of the Tenth International Symposium on Environmental Degradation of Materials in Nuclear Power Systems - Water Reactors, P. Ford, G. Was, and L. Nelson, eds., NACE, 2002.
- <sup>23</sup> T. Yonezawa and K. Onimura, "Effect of Chemical Compositions and Microstructure on the Stress Corrosion Cracking Resistance of Nickel Base Alloys in High Temperature Water," International Conference on Evaluation of Materials Performance in Severe Environments; EVALMAT '89, The Iron and Steel Institute of Japan, 1989.
- <sup>24</sup> H. Nagano and H. Kajimura, "Clarification of Stress Corrosion Cracking Mechanism on Nickel Base Alloys in Steam Generators for their Long Lifetime Assurance," Proceedings of the Seventh International Symposium on Environmental Degradation of Materials in Nuclear Power Systems – Water Reactors, TMS, Warrendale, Pennsylvania, 1995.

- <sup>25</sup> K. Norring, J. Engstrom, and P. Norberg, "Intergranular Stress Corrosion Cracking in Steam Generator Tubing. Testing of Alloy 690 and Alloy 600 Tubes," Proceedings of the Third International Symposium on Environmental Degradation of Materials in Nuclear Power Systems – Water Reactors, G.J. Theus and J.R. Weeks, eds., The Metallurgical Society, Warrendale, Pennsylvania, 1988.
- <sup>26</sup> F. Cattant, et al., "Effectiveness of 700°C Thermal Treatment on Primary Water Stress Corrosion Sensitivity of Alloy 600 Steam Generator Tubes: Laboratory Tests and In Field Experience," Proceedings of the Fifth International Symposium on Environmental Degradation of Materials in Nuclear Power Systems - Water Reactors, American Nuclear Society, 1992.
- <sup>27</sup> G.L. Webb, "Environmental Degradation of Alloy 600 and Welded Filler Metal EN 82 in an Elevated Temperature Aqueous Environment," Proceedings of the Sixth International Symposium on Environmental Degradation of Materials in Nuclear Power Systems-Water Reactors, R.E. Gold and E.P. Simonen, eds., TMS, Warrendale, Pennsylvania, 1993.
- <sup>28</sup> T.B. Cassagne, et al., "The Influence of Mechanical and Environmental Parameters on the Crack Growth Behavior of Alloy 600 in PWR Primary Water," 12th Scandinavian Corrosion Congress & Eurocorr '92, P.J. Tunturi, ed., Corrosion Society of Finland, Helsinki, 1992.
- <sup>29</sup> J.M. Gras, "Stress Corrosion Cracking of Steam Generator Tubing Materials Review and Assessment," Parkins Symposium on Fundamental Aspects of Stress Corrosion Cracking," S.M. Brummer, E.I. Meletis, R.H. Jones, W.W. Gerberich, F.P. Ford and R.W. Staehle, eds., TMS, Warrendale, 1992.
- <sup>30</sup> P. Saint-Paul and G. Zacharie, La Corrosion Sous Contrainte de L'Alliage 600 Dans L'eau, EDF/DER/EMA No. D 729A, Electricite de France, Paris, 1990.
- <sup>31</sup> D. Garriga-Majo, et al., "Prediction of the Stress Corrosion Cracking Resistance of Alloy 600 in Pure/Primary Water," Life Prediction of Corrodible Structures, R.N. Parkins, ed., NACE, 1994.
- <sup>32</sup> H. Blanchet, et al., "Historical Review of the Principal Research Concerning the Phenomena of Cracking of Nickel Base Austenitic Alloys," Stress Corrosion Cracking and Hydrogen Embrittlement of Iron Base Alloys, NACE-5, R.W. Staehle, J. Hochmann, R.D. McCright, and J.E. Slater, eds., NACE, 1977.
- <sup>33</sup> R. Bandy and D. van Rooyen, "Tests with Inconel 600 to Obtain Quantitative Stress Corrosion Cracking Data for Evaluating Service Performance," BNL-NUREG-31814, Brookhaven National Laboratory, 1983.
- <sup>34</sup> P.M. Scott, "Prediction of Alloy 600 Component Failures in PWR Systems," Proceedings of Corrosion '96: Part 1: Life Prediction of Structures Subject to Environmental Degradation," P.L. Andresen and R.N. Parkins, chair., NACE, 1996.
- <sup>35</sup> R.W. Staehle, "Bases for Predicting the Earliest Penetrations Due to SCC for Alloy 600 on the Secondary Side of PWR Steam Generators," NUREG-CR-6737, U.S. Nuclear Regulatory Commission, 2001.
- <sup>36</sup> H. Takamatsu, T. Kitera, and K. Arioka, "Corrosion Experience with the Secondary Side of Steam Generators in Japan," Control of Corrosion on the Secondary Side of Steam Generators,

R.W. Staehle, J.A. Gorman, and A.R. McIlree, eds., NACE, 1996.

<sup>37</sup> H. Takamatsu, et al., "Evaluation of SG Crevice Environment by Directly Sampled Method Using an On-Site Autoclave Facility," Proceedings of the Fifth International Symposium on Environmental Degradation of Materials in Nuclear Power Systems - Water Reactors, American Nuclear Society, 1992.

<sup>38</sup> F. Cattant, et al., "Analyses of Deposits and Underlying Surfaces on the Secondary Side of Pulled Out Tubes From a French Plant," Contribution of Materials Investigation to the Resolution of Problems Encountered in Pressurized Water Reactors; Proceedings of the International Symposium, French Nuclear Energy Society, Paris, 1994.

<sup>39</sup> Z. Fang and R.W. Staehle, "The Effect of Valence of Sulfur on the Passivation of Alloys 600 and 690 at 25° and 95°C," presented at Corrosion '98, Paper No. 272, NACE, 1998.

<sup>40</sup> J. Daret, et al., "Evidence for the Reduction of Sulfates under Representative SG Secondary Side Conditions, and for the Role of Reduced Sulfates on Alloy 600 Tubing Degradation," Proceedings of the Ninth International Conference on Environmental Degradation of Materials in Nuclear Power Systems - Water Reactors, S.M. Bruemmer, F.P. Ford, and G.S. Was, eds., TMS, Warrendale, Pennsylvania, 1999.

<sup>41</sup> O. de Bouvier, et al., "Influence of High Reducing Conditions on IGA/SCC of Alloy 600 in Neutral Sulfate Environments," presented at the 11<sup>th</sup> International Conference on Environmental Degradation of Materials in Nuclear Power Systems - Water Reactors, American Nuclear Society, August 10-14, 2003.

<sup>42</sup> S. Suzuki, "IGA Resistance of TT Alloy 690 and Concentration Behavior of Broached Egg Crate Tube Support Configuration," Proceedings of the Fifth International Symposium on Environmental Degradation of Materials in Nuclear Power Systems -Water Reactors, D.Cubicciotti, chair., American Nuclear Society, 1992.

<sup>43</sup> N. Pessall, "Prediction of Stress Corrosion Cracking in 10% Caustic Soda Solutions at 315°C (600°F)," *Corrosion Science* 20, p. 225, 1980.

<sup>44</sup> O. deBouvier, et al., "Nickel Alloy Stress Corrosion Cracking in Neutral and Lightly Alkaline Sulfate Environments," Proceedings of the Ninth International Conference on Environmental Degradation of Materials in Nuclear Power Systems - Water Reactors, S.M. Bruemmer, F.P. Ford, and G.S. Was, eds., TMS, Warrendale, Pennsylvania, 1999.

<sup>45</sup> H.R. Copson and S.W. Dean, "Effect of Contaminants on Resistance to Stress Corrosion Cracking of Ni-Cr Alloy 600 in Pressurized Water," *Corrosion*, 21, 1965.

<sup>46</sup> J.M. Sarver, "IGSCC of Nickel Alloys in Lead Contaminated High Purity Water," EPRI Workshop on Intergranular Corrosion and Primary Water Stress Corrosion Cracking Mechanisms, EPRI NP-5971, Electric Power Research Institute, 1987.

<sup>47</sup> R.W. Staehle, "Assessment of and Proposal for a Mechanistic Interpretation of the SCC of High Nickel Alloys in Lead-Containing Environments," presented at the 11<sup>th</sup> International Conference on Environmental Degradation of Materials in Nuclear Power Systems - Water Reactors, American Nuclear Society, August 10-14, 2003.

- <sup>48</sup> S.M. Bruemmer and L.E. Thomas, "Insights into Stress Corrosion Cracking Mechanisms from High-Resolution Measurements of Crack-Tip Structures and Compositions," presented at The 2<sup>nd</sup> International Conference on Environment-Induced Cracking of Metals: EICM-2, Banff, Canada, September 19-23, 2004.
- <sup>49</sup> E. Pierson and C. Laire, "The Influence of Copper on the SCC of Alloy 600 and Alloy 690 Steam Generator Tubes," Contribution of Materials Investigation to the Resolution of Problems Encountered in Pressurized Water Reactors; Proceedings of the International Symposium, French Nuclear Energy Society, Paris, 1998.
- <sup>50</sup> M.D. Wright and M. Mirzai, "Lead-Induced SCC Propagation Rates in Alloy 600," Proceedings of the Ninth International Conference on Environmental Degradation of Materials in Nuclear Power Systems -Water Reactors, S.M. Bruemmer, F.P. Ford, and G.S. Was, eds., TMS, Warrendale, Pennsylvania, 1999.
- <sup>51</sup> F. Vaillant, et al., "Influence of Lead on the Secondary Side Cracking of Alloys 600, 690 and 800," Eurocorr'96; Session 1X: Nuclear Corrosion and Protection; Extended Abstracts, F. de Keroulas, chair., Centre Francais de L'Anticorrosion Societe de Chimie Industrielle, Nice, 1996.
- <sup>52</sup> A. Rocher, et al., "Effect of Lead on the OD Degradation of Steam Generator Tubes," Contribution of Materials Investigation to the Resolution of Problems Encountered in Pressurized Water Reactors; Proceedings of the International Symposium, French Nuclear Energy Society, Paris, 1994.
- <sup>53</sup> M.D. Wright, "Establishing Thresholds for Lead Induced Cracking of Steam Generator Tube Alloys," Water Chemistry of Nuclear Reactor Systems 7, British Nuclear Energy Society, 1996.
- <sup>54</sup> M.L. Castano-Marin, D. Gomez-Briceno, and F. Hernandez-Arroyo, "Influence of Lead Contamination on the Stress Corrosion Resistance of Nickel Alloys," Proceedings of the Sixth International Symposium on Environmental Degradation of Materials in Nuclear Power Systems-Water Reactors, R.E. Gold and E.P. Simonen, eds., TMS, Warrendale, Pennsylvania, 1993.
- <sup>55</sup> H. Takamatsu, et al., "Study on Lead-induced Stress Corrosion Cracking of Steam Generator Tubing under AVT Water Chemistry Conditions," Proceedings of the Eighth International Symposium on Environmental Degradation of Materials in Nuclear Power Systems - Water Reactors, American Nuclear Society, 1997.
- <sup>56</sup> T. Sakai, et al., "Lead-induced Stress Corrosion Cracking of Alloy 600 and 690 in High Temperature Water," Proceedings of the Fifth International Symposium on Environmental Degradation of Materials in Nuclear Power Systems - Water Reactors, American Nuclear Society, 1992.
- <sup>57</sup> D. G. Briceno and L. Castano, "Inconel 690TT and Incoloy 800 in S, Cu and Pb Environments," EPRI Workshop on Steam Generator Secondary Side IGA/SCC, Reston, Virginia, 1991.

- <sup>58</sup> Private communication. courtesy of P. King, Babcock and Wilcox, Alliance, Ohio, September 2001.
- <sup>59</sup> R.J. Jacko, "Stress Corrosion Testing of Candidate Steam Generator Materials," Proceedings: Workshop on Thermally Treated Alloy 690 Tubes for Nuclear Steam Generators, C.E. Shoemaker, ed., EPRI NP-4665S SR, Electric Power Research Institute, 1986.
- <sup>60</sup> B.P. Miglin and J.M. Sarver, "Investigation of Lead as a Cause of Stress Corrosion Cracking at Support Plate Intersections," EPRI NP-7367-S, Electric Power Research Institute, 1991.
- <sup>61</sup> K. Smith, et al., "Inconel 690; A Material with Improved Corrosion Resistance for PWR Steam Generator Tubes," Proceedings of the Second International Symposium on Environmental Degradation of Materials in Nuclear Power Systems – Water Reactors, American Nuclear Society, 1986.
- <sup>62</sup> H.R. Copson, D. van Rooyen, and A.R. McIlree, "Stress Corrosion Behavior of Ni-Cr-Fe Alloys in High Temperature Aqueous Solutions," 5th International Congress on Metallic Corrosion, NACE, Tokyo, 1972.
- <sup>63</sup> G.N. Flint and B.A. Weldon, "Some Investigations into the Stress Corrosion Behavior of Fe-Ni-Cr Alloys in High Temperature Water," Direction des Etudes et Recherches, EDF, Ermenonville, France, March 13-17, 1972.
- <sup>64</sup> R.W. Staehle, et al., "Effect of Alloy Composition on Stress Corrosion Cracking of Fe-Cr-Ni Base Alloys," *Corrosion* 26, NACE, 1970.
- <sup>65</sup> H. Coriou, L. Grall, and M. Pelras, "Studies of the Corrosion Resistance of Chromium Nickel Iron Austenitic Alloys with a View to Their Application in the Nuclear Field," 3rd International Congress in Metal Corrosion, M. Kolotyrkin, ed., Swets and Zeitlinger, Amsterdam, 1969.
- <sup>66</sup> H. Nagano, et al., "Development and Manufacturing System of Alloy 690 Tubing for PWR Steam Generators," The Sumitomo Search, No. 40, 1989.
- <sup>67</sup> H. Nagano, et al., "Effect of Alloying Elements and Heat Treatment on the Corrosion Resistance of Alloy 690," Proceedings: Workshop on Thermally Treated Alloy 690 Tubes for Nuclear Steam Generators, EPRI NP-4665S SR, C.E. Shoemaker, ed., Electric Power Research Institute, 1986.
- <sup>68</sup> I.L.W. Wilson, et al., "Caustic Stress Corrosion Behavior of Fe-Ni-Cr Nuclear Steam Generator Tubing Alloys," *Nuclear Technology* 31, p. 70, 1975.
- <sup>69</sup> Private communication, courtesy of Y. Lu, AECL, Chalk River, Ontario, March 2005.